

# **Growth And Study Of Magnetostrictive FeSiBC Thin Films For Device Applications**

**Mannan Ali**

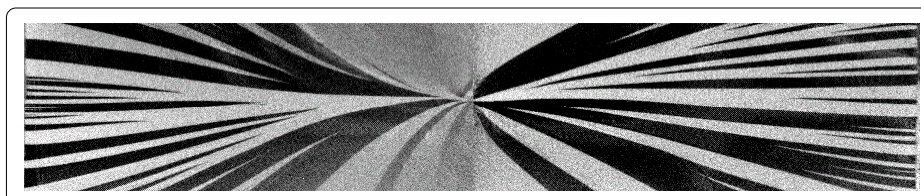


**Department of Physics & Astronomy**

**The University of Sheffield**

**September (1999)**

**A dissertation submitted for the degree of Doctor of Philosophy**



## Abstract

This thesis is concerned with the magnetic properties of magnetostrictive FeSiBC amorphous films based on the METGLAS® 2605SC composition; the films have been produced by RF magnetron sputtering. The ribbon form of the material has excellent magnetic properties, which are ideal for magnetic thin film sensors. The deposition of films is a complex process which is strongly dependent upon many parameters; these are discussed and investigated in detail in this thesis. It has been demonstrated that it is possible to produce FeSiBC films with magnetic properties comparable to those of the original METGLAS® 2605SC ribbon material used as the sputtering target. The magnetic properties were principally investigated using the magneto-optical Kerr effect, with both point hysteresis measurements and domain imaging. These measurements were made using equipment which was constructed during the course of this present work.

A significant, reproducible in-plane radial anisotropy was observed in the as-deposited films, which was attributed to the residual field produced by the magnetron sputter source. The effects of various treatments on the samples were investigated, including the use of forming fields, stress and thermal processing. The deliberate introduction of stress into these materials is found to allow excellent control of both the direction and magnitude of the magnetic anisotropy. A high degree of control is demonstrated in tailoring the anisotropy field, using the technique of stress annealing. The treatments are evaluated for their potential to enable the magnetic anisotropy in magnetostrictive device applications to be controlled.

A simple new technique is described for the measurement of saturation magnetostriction in thin films deposited onto rigid substrates. The method is based on mechanically introducing a small curvature into the substrate. The strain induced anisotropy is measured using the magneto-optical Kerr effect. Quantification of the film strain is obtained using optical interference and stylus measurements; this allows the saturation magnetostriction to be determined. No information about the mechanical properties of the substrate is required and, providing that the Young's modulus of the film is known accurately, the values of magnetostriction obtained are accurate and absolute. It is envisaged that the technique could be applied to a wide variety of films deposited onto commercially important substrates.

The possibility of using magnetostrictive FeSiBC films as Magneto Impedance sensors has also been investigated.

## Publications

- i** “The Use Of Stress For The Control Of Magnetic Anisotropy In Amorphous FeSiBC Thin Films - A Magneto-Optic Study”  
M. Ali, R. Watts, W.J. Karl, M.R.J. Gibbs  
J. Magn. Magn. Mat. 190 (3) 199 (1998).
- ii** “Measurement Of Saturation Magnetostriction Using Novel Strained Substrate Techniques And The Control Of The Magnetic Anisotropy”  
M. Ali & R. Watts  
J. Magn. Magn. Mat. 202 (1) 85 (1999).
- iii** “Magnetic Domains And Transverse Induced Anisotropy In Magnetically Soft CoFeB Amorphous Thin Films”  
D. Garcia, J.L Munoz, G. Kurlyandskaya, M. Vazquez, M. Ali & M.R.J Gibbs,  
IEEE Trans. Magn. 34(4) 1153 (1998).
- iv** “Induced Anisotropy, Magnetic Domain Structure And Magneto impedance effect in CoFeB Amorphous Thin Films”  
D. Garcia, J.L Munoz, G. Kurlyandskaya, M. Vazquez, M. Ali & M.R.J Gibbs  
J. Magn. Magn. Mat. 191 399 (1999).

## Acknowledgements

I thank my supervisor Professor M.R.J. Gibbs for this opportunity and for his assistance through this project. Unfortunately, due to illness, he was not available for periods of this study, and I therefore wish to especially thank Professor Gillian Gehring (2<sup>nd</sup> supervisor), Dr. Harry Blythe, John Bishop and the rest of the departmental staff for providing the time to discuss my work in his absence. This support and supervision was invaluable.

Thanks are also due to the past and present members of the group who have always been there as friends and colleagues. A special mention to Dr. Richard Watts for all his support and helpful discussions. I also thank Michael Cooke, Werner Karl and Dr. Hilary Hatton for all the good times we have experienced along with their helpful discussions about work and life in general.

I thank all the Technical Staff, both in physics and the Central Mechanical Workshop for their expertise and in the preparation of apparatus used during this study. A special thanks must be said to J.C. Newell (John), J. Kelly (JK), R. Nicholson (Dickie), M. Bentley (Martin) and T. Addison (Terry), for their help, expertise and just being good friends.

I also thank the members of departmental office (past and present) for all their assistance and co-operation.

A very special thanks to Maureen Webster not only for her assistance as the physics librarian, but being there as friend.

Finally, I wish to thank my mum and dad for all their encouragement and financial support during the course of this work, and to my two brothers, Nimman and Imran for all their encouragement and their views on the world around us.

## Table of Contents

<b>1.0 Introduction</b>	<b>1</b>
<b>2.0 Magneto Optic Kerr Effect (MOKE)</b>	<b>3</b>
2.1 Introduction	3
2.2 Principles of MOKE	4
2.3 MOKE Magnetometer	9
2.4 MOKE Imaging	22
2.5 Interpretation of the Kerr images	26
2.6 Magnetic measurements through transparent substrates	29
2.7 Conclusions	30
2.8 References	31
<b>3.0 General Experimental Techniques</b>	<b>32</b>
3.1 Thin Film Deposition	32
3.1.1 The sputtering process	32
3.1.2 Radio Frequency Magnetron Sputtering	33
3.1.3 Target and Substrate preparation	35
3.1.4 The deposition procedure	37
3.1.5 Calibration of deposition rate	38
3.2 Inductive magnetometer (MH)	40
3.3 Heat Treatments	42
3.4 X-Ray Diffraction	44
3.5 Magneto Impedance (MI)	45
3.6 Patterning by photolithography	47
3.7 References	48
<b>4.0 Thin Film Deposition</b>	<b>49</b>
4.1 Introduction	49
4.2 Parameters which effect sputter deposited films	50
4.2.1 Pressure	51
4.2.2 Target-substrate separation	53
4.2.3 Sputtering Power	54
4.2.4 Substrate temperature	54
4.2.5 Nature of substrate	55
4.2.6 Target Composition	56
4.2.7 Substrate Biasing	56
4.3 Magnetic properties of thin films	56

<b>4.4 Results and discussions</b>	60
4.4.1 General findings	60
4.4.2 Substrate mounting	61
4.4.3 The effects of pressure	61
4.4.4 Substrate sputter-clean	64
4.4.5 The effects of contamination	65
4.4.6 Substrate biasing	67
4.4.7 Influence of substrate type	68
4.4.8 Thickness dependence	72
4.4.9 X-ray diffraction	73
<b>4.5 Conclusions</b>	74
<b>4.6 References</b>	75

<b>5.0 Magnetic Anisotropy In Amorphous Films</b>	<b>79</b>
---	-----------

<b>5.1 Introduction</b>	79
<b>5.2 Magnetocrystalline Anisotropy</b>	80
<b>5.3 Shape Anisotropy</b>	82
<b>5.4 Magnetostriction and Magnetoelasticity</b>	84
<b>5.5 Magnetic Anisotropy Induced During The Deposition</b>	87
5.5.1 Growth Induced	87
5.5.2 Stress Induced	88
5.5.3 Field Induced	89
<b>5.6 Post-Induced Magnetic Anisotropy</b>	90
5.6.1 Magnetic Annealing	90
5.6.2 Stress Annealing	91
5.6.3 Annealing	92
<b>5.7 Domains in thin films</b>	92
<b>5.8 Results and discussions</b>	
5.8.1 Radial Magnetic anisotropy of the as-deposited films	96
5.8.2 Magnetic Annealing	108
5.8.3 Magnetostriction and Magneotelasticity	109
5.8.3.1 Application of stress	110
5.8.3.2 Strained growth	114
5.8.3.3 Stress annealing	116
5.8.3.4 Strain during measurement	118
5.9 Photolithographically patterned films	121
<b>5.10 Conclusions</b>	123
<b>5.11 References</b>	125

<b>6.0 Magneto Impedance investigation</b>	<b>130</b>
<b>6.1 Introduction</b>	130
<b>6.2 Magneto Impedance</b>	131
6.2.1 Low frequency limit	132
6.2.2 High Frequency limit (<100MHz)	133
<b>6.3 Domain structure and magnetostriction</b>	134
<b>6.4 Sample preparation</b>	136
<b>6.5 Results and Discussions</b>	137
6.5.1 Ribbon samples	137
6.5.2 Thin Film Samples	143
6.5.2.1 FeSiBC amorphous ferromagnetic films	143
6.5.2.2 CoFeB amorphous ferromagnetic films	151
6.5.2.3 Layered FeSiBC amorphous ferromagnetic films with copper	153
<b>6.6 Domain rotational model for the effective transverse susceptibility</b>	159
<b>6.7 Conclusions</b>	164
<b>6.8 Appendix</b>	165
<b>6.9 References</b>	168
<b>7.0 Conclusions and Future work</b>	<b>170</b>
<b>8.0 Access To Thesis (Copyright Notice)</b>	<b>174</b>
<b>9.0 Online Version</b>	<b>175</b>
<b>10.0 Glossary</b>	<b>176</b>

## 1.0 Introduction

In recent years, there has been an explosion in the realisation of incorporating magnetic devices into micro-electro-mechanical-systems, where both the magnetic sensor and its associated electronic operating circuitry are fabricated on a single substrate. This not only allows the miniaturisation of the sensor elements, as dictated by technological demands for smaller and smaller electrical components, but also enables the same micro-fabrication technologies to be used in both the production of the electronic and the magnetic devices. This makes it commercially more attractive due to the reduced costs and the applicability to a wider range of systems.

Magnetic sensors have been utilised for many years now. The advent of the technologies of micro-fabrication and thin film deposition, has allowed the production of more sophisticated magnetic field and stress sensors; these include exotic, three dimensional magnetic sensors; such as, cantilevers, bridges and membrane devices, which have been coated with magnetostrictive films, thus allowing the detection of stress.

There has been extensive research into amorphous materials in melt-spun ribbon form, which exhibit excellent magnetic properties: large saturation magnetostriction, high saturation magnetisation, low anisotropy energies and low coercivity. These factors have made amorphous ribbon materials excellent candidates for sensors and actuator devices. Commercial organisations such as Allied-Signal and Vacuumschmelze now produce a wide selection of melt-spun alloys which are used in a range of applications. Despite their excellent magnetic properties generally, the as-cast melt-spun ribbons suffer from high randomly orientated stresses, which give rise to a complicated domain structure. However, it is well established, that in the stress relieved or magnetically annealed state, they exhibit excellent soft magnetic properties. The disadvantages of these ribbon materials are, that they need to be annealed in an oxygen-free environment to prevent oxidation, some ribbon materials become brittle on annealing, they are difficult to incorporate into sub-millimetre dimensional devices and, most importantly of all, there is no suitable means of bonding such materials onto micro-fabricated structures; the ribbon materials are currently bonded to larger devices using epoxy resin. However, it is found that the optimised domain structure obtained by magnetic annealing is disturbed by the curing epoxy resin, which induces stress into the ribbon.

This thesis is concerned with producing FeSiBC films of similar composition to that of the amorphous METGLAS<sup>®</sup> 2605SC target material ( $\text{Fe}_{81}\text{Si}_{13.5}\text{B}_{13.5}\text{C}_2$ ) which exhibits excellent soft magnetic properties and are ideal for device applications. The films were deposited by RF magnetron sputtering onto commercially important substrates which will, therefore, allow the present/future design of sophisticated devices, and eliminate the problem of bonding the magnetostrictive material to the device.

The chapters within the thesis are generally self-contained, where the literature review, results, discussions and conclusions are presented within the one chapter.

The following chapter (2) is concerned with the construction of a magnetometer and imaging system based on the Magneto Optical Kerr Effect; this was found to be essential for the study and characterisation of the amorphous FeSiBC films. The general principles of the Kerr effect have been discussed, providing the reader with a sufficient insight into the implementation of the Kerr effect, and therefore allowing one to interpret the data from the two techniques presented in this thesis.

Chapter 3 provides a general description of the experimental techniques which have been employed to prepare, analyse and characterise the magnetic films.

Chapter 4 deals with the process of sputter deposition. The deposition technique is discussed and it is shown that the deposition of films by sputtering is a complex process which is strongly dependent on many parameters. Films have been deposited onto commercially important substrates such as GaAs, Si and Si<sub>3</sub>N<sub>4</sub>, which are compatible with the microelectronic fabrication technologies. This may allow the fabrication of both the magnetic sensor and the electronic detection system on the one substrate, making it commercially more attractive. The general magnetic properties of amorphous films deposited by sputtering are also presented.

Chapter 5 is concerned with the magnetic anisotropy of amorphous FeSiBC films which have been deposited by RF magnetron sputtering, mainly at the optimised sputtering parameters. The magnetic properties were investigated principally using the magneto-optical Kerr effect, with both point hysteresis measurements and domain imaging. A significant in-plane anisotropy was observed in the as-deposited films; this has been attributed to the residual field from the magnetron sputtering source. The effects of various treatments on the films are investigated, including the use of forming fields, stress and thermal processing. The treatments are evaluated for their potential to control the anisotropy in magnetostrictive device applications.

A simple new technique is also described for the measurement of the saturation magnetostriction in amorphous thin films deposited onto rigid substrates.

A high degree of control is also demonstrated in tailoring the anisotropy field, using the technique of substrate straining.

Chapter 6 is an investigation into the Magneto Impedance effect in FeSiBC films grown in this study. The objective was to ascertain the potential use of FeSiBC films for Magneto Impedance sensors and to correlate the magnetic properties with that of the impedance responses.

A summary of the conclusions and further work is presented in Chapter 7.

## 2.0 Magneto Optic Kerr Effect (MOKE)

### 2.1 Introduction

Magneto Optical effects in magnetic materials arise due to the optical anisotropy of the materials. The source of this optical anisotropy is the magnetisation  $M$  within surface domains which can be influenced by external forces such as magnetic fields. The optical anisotropy alters the state of linearly polarised light which is reflected off magnetic materials. These effects are generally known as the Magneto-Optical Kerr Effect (MOKE) which were observed by John Kerr in 1887, and are analogous to the Faraday effect where the polarisation of the light is rotated through a transparent material subjected to a magnetic field as observed by Michael Faraday in 1845.

The magneto optical effects are characterised by the Kerr effect being proportional to the magnetisation. This makes it particularly useful in the study of surface magnetism since it is highly sensitive to the magnetisation within the skin depth region, typically 10-20nm in most metals [Bland et al (1989)]. The effect has been utilised to obtain hysteresis loops or domain images and is a relatively simple technique to implement. It has the ability to probe the magnetisation in very small regions of a material, such as wires or patterns [Shearwood et al (1996)], or in real device applications [Karl et al (1999)]. MOKE has emerged as an important technique in the study of surface magnetism. It has been used extensively to characterise magnetic materials, especially in the field of magnetic thin films. The Kerr effect is also the basis of the commercially available magneto optical drives.

Part of this study has been involved with the construction of a MOKE magnetometer and MOKE imaging system, in order that the amorphous ferromagnetic thin films could be studied. The MOKE magnetometer provided information in the form of hysteresis loops, whereas the imaging system provided magnetic information by means of domain images. The two systems were built to overcome the limitations of the Inductive Magnetometer which was designed primarily for studying amorphous, ribbon based materials. The principles of MOKE are discussed here only qualitatively; this account is not intended to be complete and rigorous, but to provide an overview for the reader.

## 2.2 Principles of MOKE

Magneto Optical Kerr effects are generally described macroscopically by dielectric tensor theory [Zak et al (1990)], or the effects can also be described microscopically, where the coupling between the electric field of the light and the magnetisation occurs by the spin-orbit interaction [Daalderop et al (1988)]. In the present work the effects are described less formally, in a pictorial fashion, using the idea of a Lorentz force. To understand the magneto optical Kerr effects, one needs to understand the terminologies associated with the effect, how the state of polarisation of reflected light is dependent upon the initial polarisation and the magneto optical geometry in which it is being used.

Light is a transverse electromagnetic wave which can be manipulated optically into plane, circularly or elliptically polarised light (Fig. 2.1). Generally, the plane of polarisation is the plane which contains the electric field  $E$  and the direction of propagation. However in some texts [Corson & Lorrain (1970)], the definition of plane of polarisation refers to the plane containing the  $B$  field. Any reference to the plane of polarisation in the present work will assume the former definition. If the electric field is polarised in the plane of incidence, it is referred to as  $p$ -polarised light as shown in Figure 2.2. Conversely, if the electric field is polarised perpendicular to the plane of incidence, then it is referred to as  $s$ -polarised light. The plane of incidence is also known as the scattering plane - the plane which contains the incident and reflected light beam. Circularly polarised light can be further referred to as  $L$ -circularly polarised and  $R$ -circularly polarised light, where  $L$  and  $R$  signify the electric field rotating in either a clockwise or an anticlockwise direction with respect to the direction of propagation.

Plane polarised light which is reflected off a metallic surface, is generally elliptically polarised. However if the incident light is either  $p$  or  $s$ -polarised, then the reflected light will still be plane polarised upon reflection ( $p$  or  $s$ ) [Hecht (1989)]. This is because the reflecting surface is a plane of symmetry for the system. This symmetry is destroyed in the situation where plane polarised light is reflected off a magnetised surface. When  $p$ -polarised light is reflected off a magnetic surface, the reflected light has a  $p$ -component as in the ordinary metallic reflection but, in addition, a small  $s$ -component also appears in the beam. In general, this second electric field component is out of phase with the reflected  $p$ -component. This causes the light to become elliptically polarised with its major axis rotated from its initial incident polarisation plane. This magneto optic interaction is shown schematically in Figure 2.3. A similar effect occurs for  $s$ -polarised light. The two effects are known as the Kerr ellipticity and the Kerr rotation. As mentioned earlier, the effects are described macroscopically using dielectric tensor theory. In this theory, plane polarised light is viewed as being

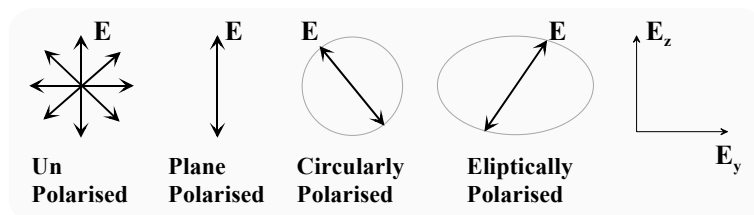


**Figure 2.1:** Polarisation of light.

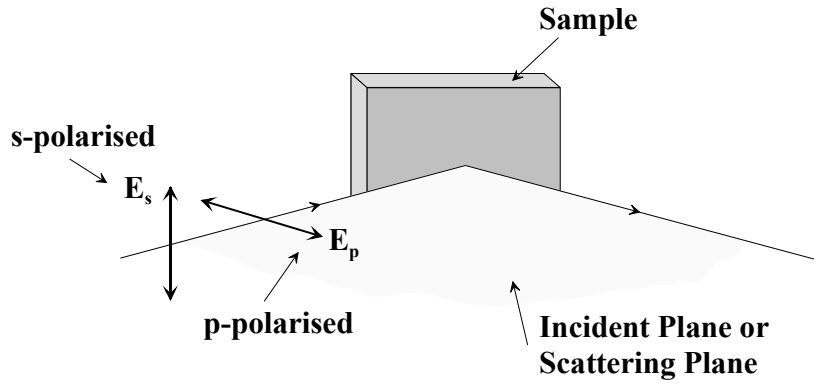


**Figure 2.2:** Illustration of *p*-polarised and *s*-polarised light.

made up of the superposition of two circular components, *L* and *R*-circularly polarised light. The magnetic medium has different refractive indices for these two polarised modes. Therefore the two circular modes travel with different velocities and attenuate differently in the material. Upon reflection from the material, the two modes recombine to produce the Kerr rotation and ellipticity. The macroscopic description of Kerr effects relies on the two modes having different refractive indices within the material. The general form of the dielectric tensor which represents the effects of a magnetic medium is given by [see Zak et al (1990) for details]

$$\epsilon = \epsilon_0 \begin{pmatrix} 1 & -iQ_z & iQ_y \\ iQ_z & 1 & -iQ_x \\ -iQ_y & iQ_x & 1 \end{pmatrix} \quad (2.1)$$

where  $Q_{x,y,z}$  is the Voigt magneto optic constant which describes the magneto optical effect. This Voigt term is to the first order proportional to the magnetisation of the material. It is this complex Voigt term (the off diagonal terms) which generally modifies the polarisation. Basically, what MOKE measures directly, is the magneto optic response of the medium, which is a change in the incident polarisation of the light. This magneto optic response consists of two parts: a change in the polarisation of the in-phase component of the reflected light which gives rise to the rotation, and a change in the polarisation of the out-of-phase component of the reflected light which gives rise to the ellipticity.

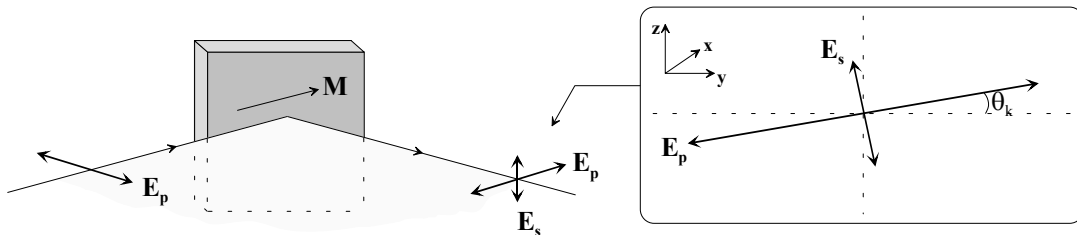


**Figure 2.3:** Reflection of *p*-polarised light of a magnetic sample.

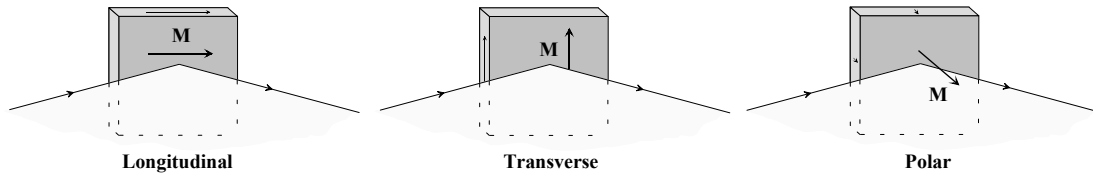


**Figure 2.4:** Longitudinal, transverse and polar Kerr effects.

There are principally three Kerr effects which are classified depending upon the magneto optic geometry being employed. These are shown in Figure 2.4. The effects are dependent on the orientation of the magnetisation with respect to the incident and sample planes. In the longitudinal Kerr effect, the magnetisation is in the plane of the sample and parallel to the incident plane. In the transverse Kerr effect, the magnetisation is also in the plane of the sample, but is perpendicular to the incident plane. In the polar Kerr effect, the magnetisation is perpendicular to the sample plane and is parallel to the plane of incidence. It should be noted the Kerr effect will occur for any arbitrary direction of magnetisation within the sample. Consideration of these three magneto optic geometries simplifies the understanding of the Kerr effect. The longitudinal and transverse Kerr effects are generally used to study the in-plane magnetic anisotropy, whereas the polar configuration is used to study thin films, which exhibit perpendicular anisotropy. The thin films investigated in this study on the whole only exhibited an in-plane magnetic anisotropy and therefore the polar effect was not used. Upon reflection the longitudinal and polar Kerr effects, generally, alter the polarisation of the incident light from plane to elliptically polarised with the major axis rotated (Kerr rotation). In the transverse effect there is no change in the polarisation of the incident light. This is more clearly illustrated in Figure 2.5, where a vector representation using the idea of a Lorentz force indicates how  $p$  and  $s$ -polarised light interact in the three magneto optic geometries. The electric field of the plane polarised light which is incident upon the material, can be thought of as exciting the electrons so that they oscillate parallel to the incident polarisation. This gives rise to the normal component ( $\mathbf{E}_N$ ) of light in the reflected light. The additional Kerr component,  $\mathbf{E}_K$ , arises because of the Lorentz force. The Lorentz force induces a small component which is perpendicular to both the primary motion (normal component) and the direction of the magnetisation. Generally, the two components are not in-phase and it is the superposition of these two components which gives rise to a magnetisation dependent rotation of the polarisation. In the longitudinal and polar Kerr effects (Fig. 2.5a,b),  $p$  or  $s$ -polarised light will generally become elliptically polarised with its major axis rotated (Kerr rotation). This is a consequence of an orthogonal electric field component being induced because of the Lorentz force. The directions of the Lorentz force, and therefore the induced components, are shown by the dashed arrows ( $\mathbf{E}_K$ ). The Kerr effect diminishes as the angle of incidence approaches the normal to the sample plane in the longitudinal effect because either the Lorentz force vanishes ( $p$ -polarised) or points along the direction of the light ( $s$ -polarised). This is not the case for the polar Kerr effect because the magnetisation is out of the sample plane and a Lorentz force always exists at normal incidence. The polar effect is independent of the incident polarisation at normal incidence. The angle of incidence generally tends to be independent of the incident polarisation

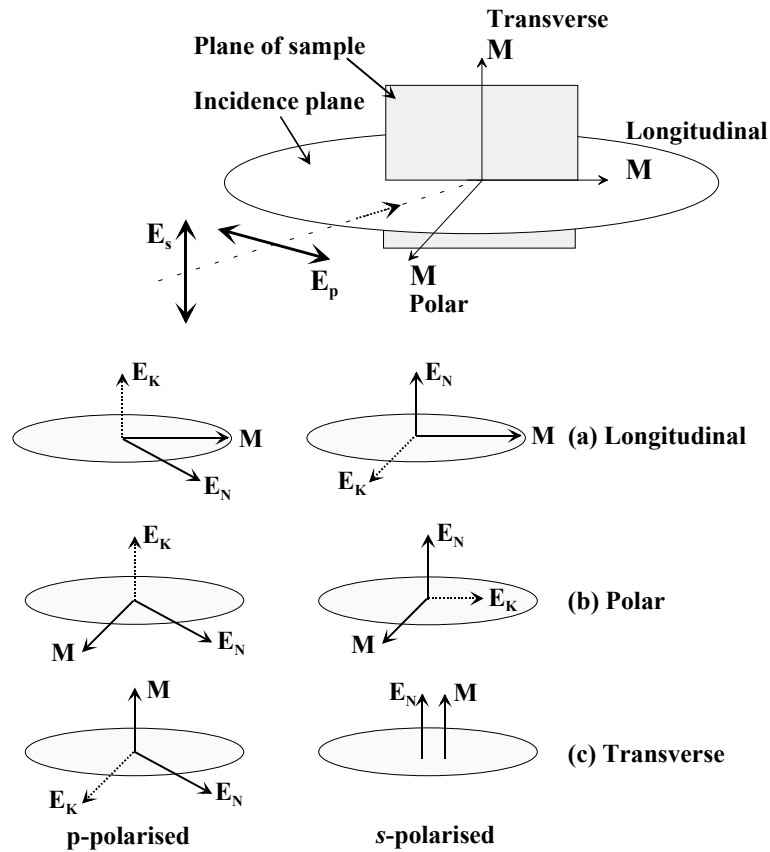


**Figure 2.5:** A schematic representation of the Magneto Optical interaction using the idea of a Lorentz force. The normal component ( $E_N$ ) of light is indicated by the solid lines, the Kerr component ( $E_K$ ) and the direction of the Lorentz force is indicated by the broken lines.

at normal incidence. The angle of incidence generally tends to vary in the range  $5-60^\circ$  depending on the experimental arrangement for the longitudinal and transverse modes. In most instances the angle of incidence is fixed by the constraints of the experimental layout. It has been shown experimentally [Deeter & Sarid (1988)] that the angle of incidence does have a small effect on the magnitude of the Kerr rotation. The polar Kerr effect is usually an order of magnitude larger than the longitudinal Kerr effect. The transverse effect involves no change in polarisation, since there is either no Lorentz force present ( $s$ -polarised) or the induced component ( $p$ -polarised) has the same polarisation as the incident polarisation (Fig. 2.5c). The transverse effect involves a change in the intensity of the light (Kerr reflectivity). The intensity changes are dependent upon the component of magnetisation perpendicular to the plane of incidence. There is no Kerr ellipticity since  $M \times E$  induces a component which is in the plane of incidence. The induced Kerr component and the normal component give rise to a change in the amplitude. One only sees a Kerr rotation if a Lorentz force is present. In general either  $s$  or  $p$ -polarised light is used. This is because any change in the polarisation of the light will be a result of the magnetisation, since in an ideal situation there will be no change in the polarisation of light for either  $s$  or  $p$ -polarised light reflected off a non-magnetic surface.

The above explanation is elegantly summarised by the Kerr Fresnel reflection coefficients [Florczak & Dahlberg (1990)] which have been obtained from applying the Maxwell boundary conditions at the surface of the magnetic films [see Zak et al (1990) for details]. The coefficients for the transverse and longitudinal effects have been listed here for completeness. A more detailed analysis is given in the references cited.

$$r_{pp}^t = \left( \frac{n\beta - \beta'}{n\beta + \beta'} \right) \left( 1 + \frac{in^2 Q \sin 2\theta}{n^2(n^2 \cos^2 \theta - 1) + \sin^2 \theta} \right) \quad (2.2)$$

$$r_{ss}^t = \frac{\beta - n\beta'}{\beta + n\beta'} \quad (2.3)$$

$$r_{ps}^t = r_{sp}^t = 0 \quad (2.4)$$

$$r_{pp}^l = \frac{n\beta - \beta'}{n\beta + \beta'} \quad (2.5)$$

$$r_{ss}^l = \frac{\beta - n\beta'}{\beta + n\beta'} \quad (2.6)$$

$$r_{ps}^l = -r_{sp}^l = \frac{\beta in^2 Q \sin \theta}{n^2 \beta' (n\beta + \beta') (\beta + n\beta')} \quad (2.7)$$

Here,  $\theta$  is the angle of incidence,  $n$  is the index of refraction of the film,  $\beta = \cos \theta$ , and  $\beta' = [1 - \frac{\sin^2 \theta}{n^2}]^{1/2}$ . The term  $r_{sp}^l$  represents the reflection coefficient which relates the incident  $s$ -wave to the reflected  $p$ -wave in the longitudinal effect. From the transverse coefficients, it is clear that the light does not undergo a rotation of its plane of polarisation, since the off-diagonal terms which give rise to the rotation are equal to zero ( $r_{ps}^t = r_{sp}^t = 0$ ). The only quantity which is dependent on the magnetisation is the reflection coefficient relating the incident and reflected  $p$ -polarised light, as shown/explained by Figure 2.5c, whereas the longitudinal coefficients indicate a rotation of the polarisation by the existence of the off diagonal terms ( $r_{ps}^l = -r_{sp}^l \neq 0$ ).

For simplicity and clarity the author has used a pictorial explanation of the Kerr effect for a more qualitative approach here.

### 2.3 MOKE Magnetometer

The MOKE magnetometer characterises materials by providing magnetic information in the form of a hysteresis loop. It relates the magnetisation  $M$ , to the applied magnetic field,  $H$ . The principles of the MOKE magnetometer are based on the Kerr effect as explained in the previous section. Figure 2.6 shows a schematic layout of the MOKE system at Sheffield. The whole system was constructed by the author; this included the computer automation of the equipment and the writing of the associated software. Light was provided by a 15mW He-Ne laser ( $\lambda=633\text{nm}$ ) at an incident angle of  $45^\circ$  to the sample plane. The polarisation of the light beam before reflection was controlled by a Glan Taylor polariser to be either  $p$  or  $s$ -polarised, which was then focused onto the sample by a lens of focal length 30cm. The sampling area was determined by the size of the laser spot; this was approximately  $100\mu\text{m}$  in diameter. The reflected light beam was passed through an analysing Glan Taylor polariser onto a photo-diode, where the reflected intensity was measured. The output signal from the photo-diode was fed into the signal conditioning unit (see later) before being read by the computer by means of an analogue to digital converter (ADC - 12 bit). The software was also interfaced to a programmable voltage controlled bipolar current source (KEPCO BOP 36-12M), by means of a digital to analogue converter (DAC - 14 bit). The KEPCO was used to provide the driving current for the Helmholtz coils, which produced the sweeping magnetic field. The software simultaneously swept the magnetic field and recorded the transmitted intensity as a function of the applied magnetic field. All components were mounted onto an optical table which had anti-vibration cushioning and the MOKE magnetometer was placed in a Faraday room to screen the apparatus from electromagnetic noise. The Faraday room also doubled as dark room which eliminated the problem of the fluctuating ambient light. The samples were mounted onto a non-magnetic holder either by a high temperature vacuum grease, wax or by double sided tape. The holder could be traversed, and this moved the sample in the  $xy$  plane of the magnetic field (Fig. 2.6) by means of two micrometers; it also provided the freedom of rotating the sample through a full  $360^\circ$  in the plane of the magnetic field.

Typical films had coercivities of 30-50 A/m. This meant the applied field had to be stable and uniform across the whole of the film in order for this quantity to be determined accurately. The dimensions indicated for the Helmholtz coils in Figure 2.7 insured that a uniform field was produced over a large volume of space. This is shown in Figure 2.8 where the equation for the field produced by the Helmholtz coil [Jiles 1994] was used to generate the curve to illustrate this. The inset shows that the field strength only varies by 1% over a distance of  $\pm 3.0$  cm from the centre. Measurements taken using a Hall effect magnetometer (Oxford Instruments 5200) indicated no measurable change in the field strength at 100 A/m over a region of  $\pm 2.5\text{cm}$ . The Helmholtz coils also provided ample room for a range of sample dimensions, and the flexibility to enable more exotic holders to be used. Limitations imposed on the sample dimensions by the inductive magnetometer, and its inability to investigate any in-plane magnetic anisotropies are alleviated with MOKE magnetometry.

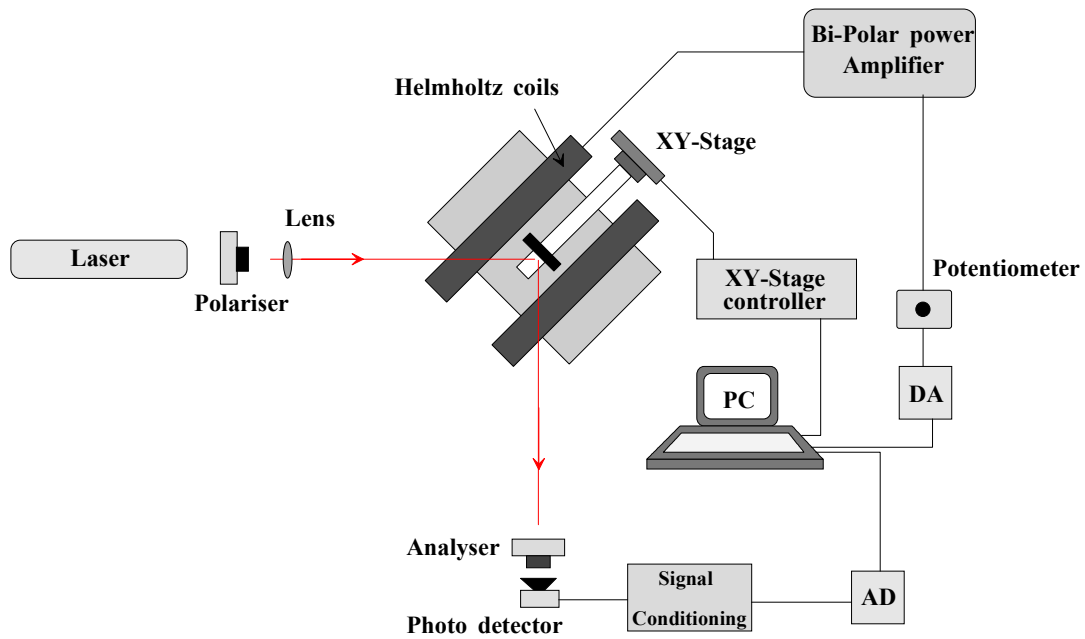


Figure 2.6: Schematic layout of MOKE magnetometer.

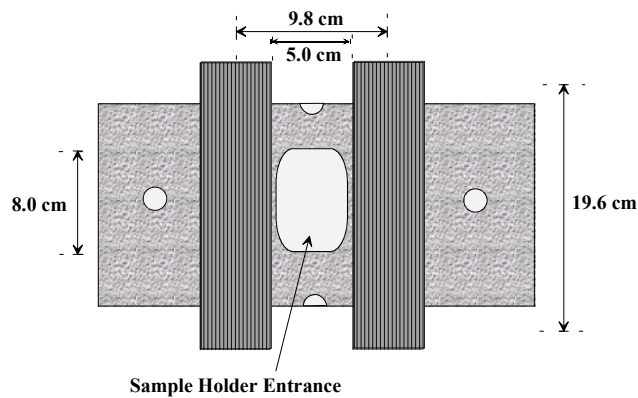


Figure 2.7: Schematic of Helmholtz coils.

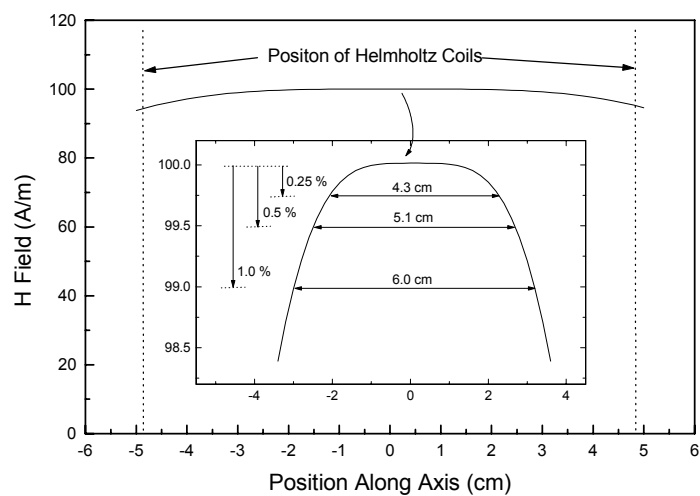
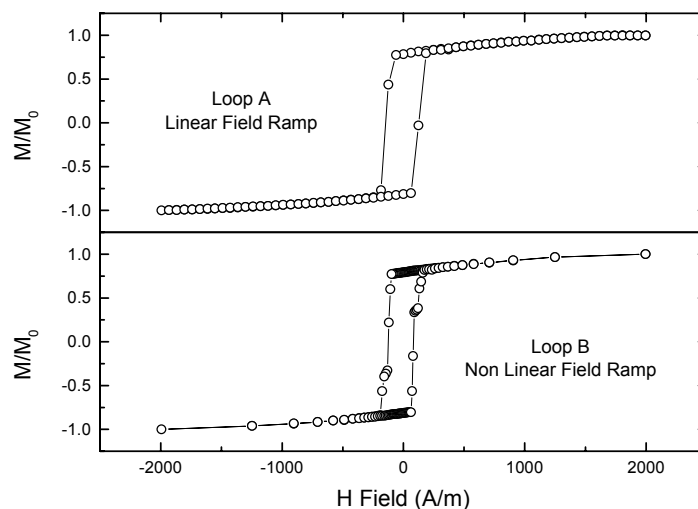
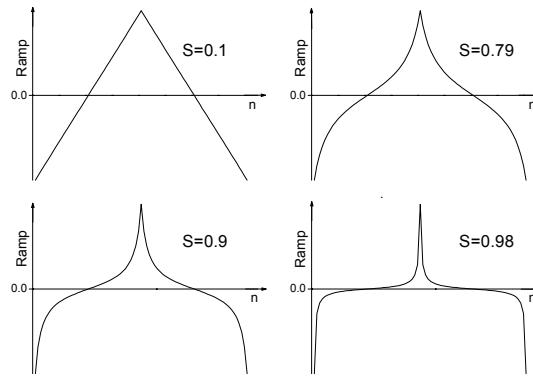


Figure 2.8: Calculated plot of field uniformity produced by the Helmholtz coils.

The Helmholtz coils were designed to generate fields up to 23 kA/m using the KEPCO bipolar power supply. This was so that direct comparisons could also be made with the inductive magnetometer, which had a similar maximum field. Figure 2.7 is an illustration of the Helmholtz coils which were constructed. The coils were mounted onto a cylindrical plastic tube, which had circular apertures bored out for incident and reflected laser beam to pass through. The mounting of the coils on the cylindrical tube ensured that the magnetic field could be orientated easily in either the transverse or longitudinal modes with respect to the incident plane (Fig. 2.2). Each coil consisted of 300 turns of 1.71 mm diameter copper enamel wire. The coils were carefully designed to ensure that they were load matched with the KEPCO power supply to ensure that if needed, the maximum current could be drawn from the supply. Heating effects of the coils were negligible for two reasons. Firstly, the typical field needed to saturate the majority of the FeSiBC films, were of the order of 5kA/m or less. The coils were over engineered to take account of other magnetic thin film systems. These generally required much larger fields to saturate (20 kA/m), and therefore only a quarter of the maximum available current was generally driven through the coils when investigating the FeSiBC films. Secondly, heating of the coils was further reduced by the implementation of a non-linear field ramp, which reduced the amount of time the coils were subjected to a high current. The non-linear field ramps were essential in the measurement of soft amorphous films. This was because the magnetisation in these materials changed rapidly over a small change in the applied field near the origin. Using a linear field ramp (each field point equally spaced) would have meant the sampling rate would decrease in this region where the rate of change of the magnetisation was at its maximum. Figure 2.9 shows two hysteresis loops, one taken using a linear field ramp, and the other using a non-linear field ramp. In both cases, 128 sample points were taken, and each point was equally spaced in time. The general shapes of the two loops were independent of the field ramp. The loop obtained using the linear field ramp illustrates the problem associated with the sampling rate, by only managing to sample one data point as the magnetisation changes rapidly. However, in loop B, the sampling rate is increased in



**Figure 2.9:** Loop A is a hysteresis loop taken using a linear field ramp, whereas the loop B was taken using a non-linear ramp.



**Figure 2.10:** Digital ramps generated using equation 2.8 for a selection of shape factors  $S$ .

this critical region, by decreasing the density of data points taken along the two extreme regions of each arm of the hysteresis loop, where the rate of change of magnetisation is at its minimum. The reduction of the number of points in this region does not influence the shape of the hysteresis loops and therefore no magnetic information is lost, as shown by Figures 2.9 and 2.11. This also had an added benefit of ensuring that the coils were only subjected to the maximum field applied for short periods of time. The increased sampling rate in this region insured that a number of data points could be sampled as the magnetisation changed rapidly, increasing the resolution of the measurement in the critical region. The form of the function which was used to generate the field ramps was a truncated tangent [Squire et al (1988)]

$$F(n) = \tan\left(\frac{2\pi n S}{N} - \frac{\pi S}{2}\right) \quad (0 < S < 1) \quad (2.8)$$

where  $n$  was the data point being taken,  $N$  was the total number of data points being taken in one half of the ( $\pm H$ ) loop, and  $S$  was a user-adjustable shape parameter which determined the shape of the field ramp being generated. Small values of the shape factor  $S$ , produced a ramp which was approximately linear, whereas large values of  $S$  produced a sharply peaked ramp. The shape factor,  $S$ , governed the region of the tangent curve which was used to generate the ramp. Figure 2.10 shows a selection of ramps generated using the tangent function. The second half of the ramp is a mirror image of the first. The ramps were software generated by parameters pre-determined by the user. The software generated ramp in turn produced the corresponding magnetic field ramp via the DAC through the KEPCO power supply; this is shown in Figure 2.6. The use of the potentiometer to control the maximum voltage applied from the DAC to the KEPCO power supply ensured the full scale (all bits) of the DAC was always being utilised. The field ramp was determined by trial and error by varying the shape factor, the total number of points and the maximum field, so that a reasonable number of points were taken in the critical region. This was not always possible for films which were very soft and exhibited very square hysteresis loops. Figure 2.11 shows two hysteresis loops taken from a magnetically soft FeSiBC film. For comparison with Figure 2.9, 128 data points were taken, but this time at a field ramp of 0.9 and a

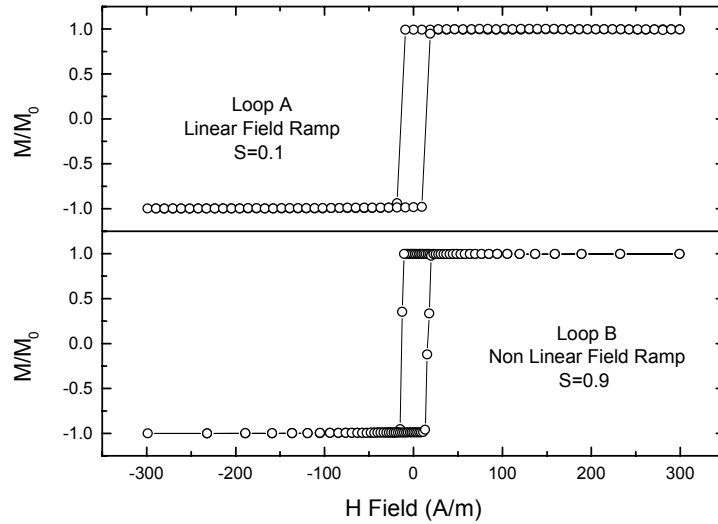


**Figure 2.11:** Two loops obtained using a field ramp of 0.1 and 0.9 from a FeSiBC film which exhibits a very square hysteresis loop.

maximum field of 300 A/m. Using these parameters, it was only possible to sample one or two data points as the magnetisation switched. The resolution of the field step is determined by the shape factor,  $S$ , the total number of data points,  $N$ , the maximum applied field, and the resolution of the DAC. The inset in Figure 2.12 shows the field step between consecutive points using a field ramp of 0.99 and 340 data points, which generates a digital field ramp that approaches the resolution of the 14 bit DAC. The main figure shows the resolution of the field step suffers from bit noise as 5 bits or less is approached. To ensure that the field step did not suffer from any bit noise during the measurements, a maximum shape factor of 0.98 was imposed. This insured that the smallest field step consisted of 7 bits or more. This gave a possible field step resolution of 0.5 A/m at a field of 500 A/m. The field steps were equally spaced in time, and 350ms was allowed for the field to stabilise before each measurement was taken.

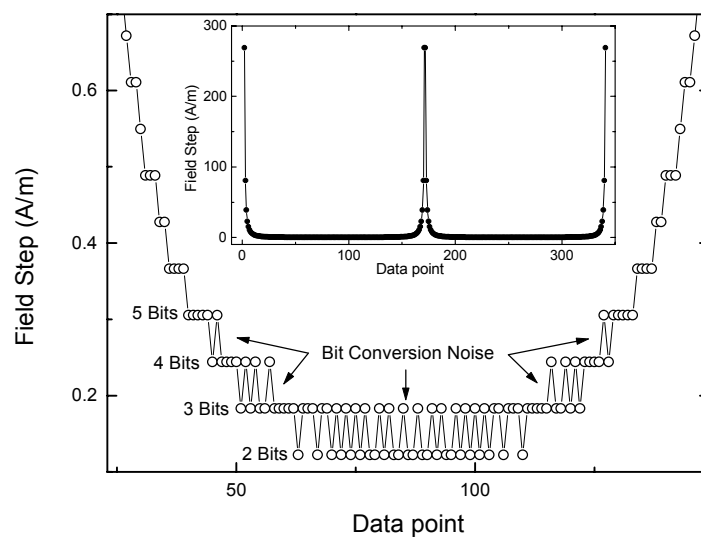


**Figure 2.12:** Resolution of the Digital to Analogue Converter.

Two polarisers are used to detect the changes in the polarisation of the light as shown in Figure 2.6. The system is a low cost arrangement, which is adequately suited for measuring hysteresis loops of thin films by detecting the Kerr rotation. The polariser is used to control the polarisation of the incident light, whereas the analyser is used to produce an intensity variation at the photo detector from changes in the polarisation. The magnitude of the Kerr rotation is typically a fraction of a degree, and this only produces a very small change in the intensity. The analyser is generally set one or two degrees from extinction to detect the Kerr rotation. It may initially seem illogical to operate the analyser at extinction, but we are only interested in the relative change in the intensity due to the Kerr rotation. This will be a maximum when the normal component of reflection is screened out. The intensity of the light after passing through the analyser is given by equation 2.9 where  $I_0$  is the intensity of the reflected light, and  $\theta$  is the angle between the polarisation of  $I_0$  and the pass plane of the analyser.

$$I = I_0 \cos^2 \theta \quad (2.9)$$

The maximum change in the intensity with respect to  $\theta$ , is obtained by differentiation, and this is a maximum when  $\theta=45^\circ$ .

$$\frac{dI}{d\theta} = 2I_0 \cos \theta \sin \theta \quad (2.10)$$

Any changes in the intensity due to the Kerr rotation can be approximated as

$$\Delta I = \frac{dI}{d\theta} K_r \quad (2.11)$$

since the Kerr rotation  $K_r$  is very small compared to  $\theta$ . The relative change in the intensity due to the Kerr rotation can be expressed as

$$\frac{\Delta I}{I} = \frac{dI}{d\theta} \frac{K_r}{I} \quad (2.12)$$

$$\frac{\Delta I}{I} = \frac{2I_0 \cos \theta \sin \theta}{I_0 \cos^2 \theta} K_r \quad (2.13)$$

$$I_{Kerr} = \frac{\Delta I}{I} = 2K_r \tan \theta \quad (2.14)$$

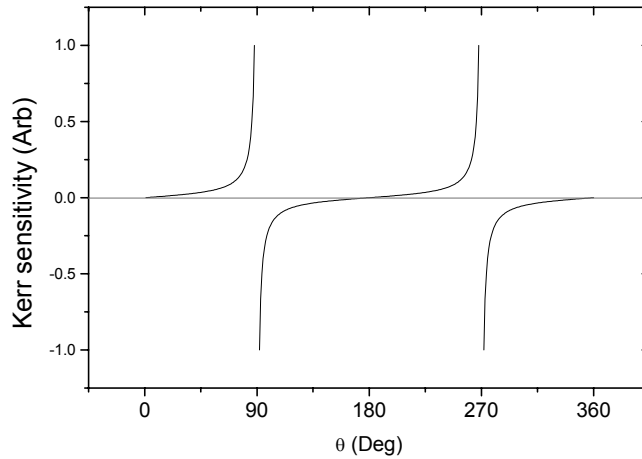


**Figure 2.13:** The dependence of the analyser setting on the Kerr sensitivity as from equation 2.14.

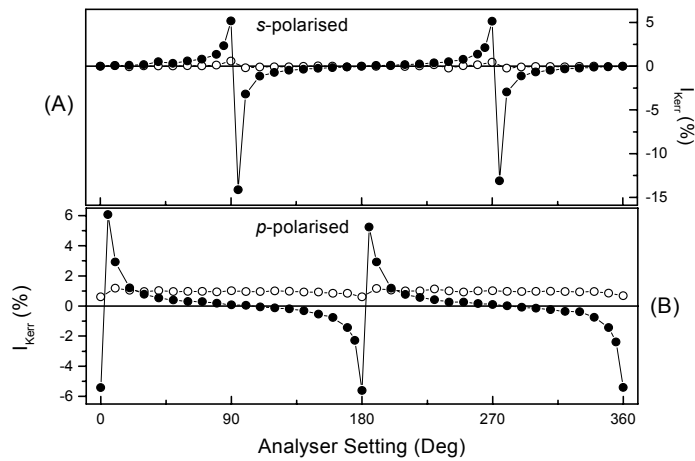


**Figure 2.14:** The dependence of the analyser setting on the Kerr sensitivity for  $s$  and  $p$ -polarised incident light. The solid circles represent the measurements taken in the longitudinal mode and the open circles represent measurements in the transverse mode.  $s$ -polarised is equivalent to  $0^\circ$ , and  $p$ -polarised is equal to  $90^\circ$ .

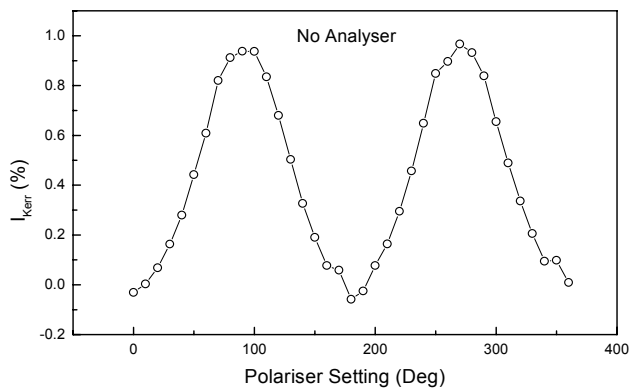


**Figure 2.15:** The dependence of the Kerr sensitivity on the polariser setting for transverse mode with no analyser present.  $s$ -polarised is equivalent to  $0^\circ$  degrees, and  $p$ -polarised is equal to  $90^\circ$  degrees.

Equation 2.14 shows that the maximum relative change in the Kerr intensity, or the Kerr sensitivity, occurs as  $\theta$  approaches  $90^\circ$  as shown in Figure 2.13. The Kerr sensitivity  $\frac{\Delta I}{I}$  is defined [Moog et al (1989)] as the difference in the intensity for a sample magnetised in opposite directions and normalised to the maximum intensity (Eq. 2.15).

$$\frac{\Delta I}{I} = \frac{I_{\max} - I_{\min}}{I_{\max}} \quad (2.15)$$

It should be noted that setting the analyser close to extinction is only applicable to the longitudinal and polar Kerr configurations, where the light undergoes a Kerr rotation. The transverse effect involves a change in the intensity of the light, and one would assume from equation 2.10 that the analyser should be set to  $45^\circ$  to maximise any changes in the intensity. A number of experiments were carried out to experimentally verify how the analyser settings effected the Kerr intensity in both the longitudinal and transverse Kerr modes. Figure 2.14 shows the Kerr sensitivity, as defined in equation 2.15, for *s* and *p*-polarised incident light for varying analyser settings. As predicted by equation 2.14, the maximum Kerr sensitivity occurs as the analyser approaches  $90^\circ$  from the incident polarisation for either *s* or *p*-polarised light in the longitudinal mode. The curves obtained have the form of the tangent function as obtained in Figure 2.13. In contrast, the Kerr sensitivity for *s*-polarised light in the transverse mode is zero for all angles of the analyser setting. This was as expected, since no Kerr effect is seen using *s*-polarised light as shown in Figure 2.5c. There is a slight signal at extinction, but this may be due to the incident polarisation not being perfectly *s*-polarised and therefore some Kerr rotation may be present. The use of *p*-polarised light in the transverse mode (Fig. 2.14b), indicates that the Kerr sensitivity is independent of the analyser setting and is approximately constant. This is because there is no Kerr rotation involved, just a change in the intensity (Fig. 2.5c) and therefore the analyser is not needed for the transverse effect. This is shown in Figure 2.15 where the analyser was removed and the incident polarisation was varied in the transverse mode. The Kerr effect increases from zero to 1% as the polarisation of the incident light changes from *s* to *p*-polarised. The Kerr rotation is much larger in magnitude than the Kerr reflectivity and therefore it is utilised in most MOKE magnetometers. The analyser setting is usually set a few degrees from extinction to compensate for various sources of noise which are present in the system. A detailed theoretical evaluation of the signal to noise ratio for such systems has been carried out by Bland et al (1989). Figure 2.16 shows four hysteresis loops obtained from a sample for different analyser settings. In each case, the loops have been normalised so direct comparisons can be made. As the analyser setting is increased from extinction, the slopes of the loops increase and it seems that an extra signal is appearing. The MOKE loop, taken at an analyser setting of  $30^\circ$ , is totally different to the loop obtained at  $3^\circ$ , which is similar to a loop obtained by the inductive magnetometer. It is important that the analyser is set as close as possible to extinction as high-lighted by these loops, so that only the Kerr rotation is detected. Florczak & Dahlberg (1990) have shown that the

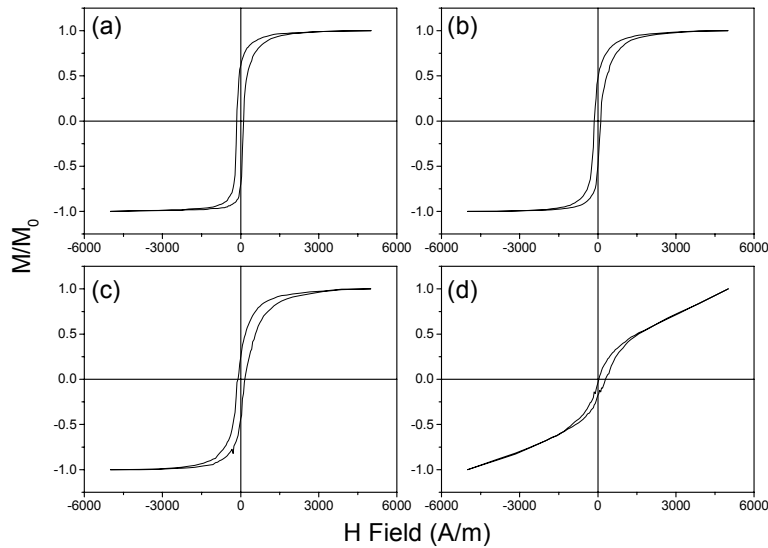


**Figure 2.16:** Hysteresis loops obtained for various analyser settings  $\theta_a$  from extinction. (a)  $\theta_a=3^\circ$ ; (b)  $\theta_a=10^\circ$ ; (c)  $\theta_a=20^\circ$ ; (d)  $\theta_a=30^\circ$ .

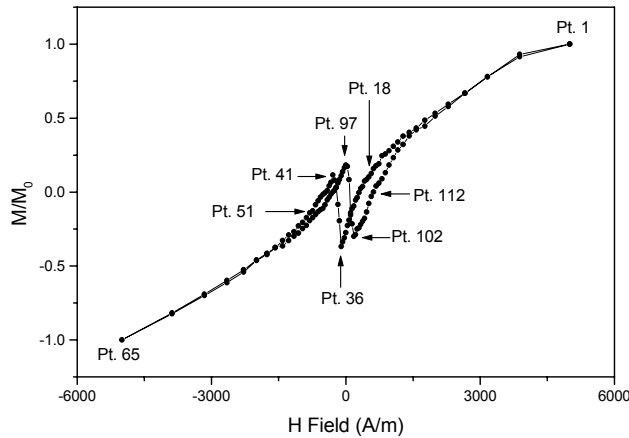


**Figure 2.17:** Hysteresis loop obtained for analyser setting of  $\theta_a=60^\circ$  from extinction. A number of points have been labelled to help visualise not only the crossing of the curve, but also the direction of the magnetisation.

difference in the transverse and longitudinal effects can be utilised to detect specific components of the magnetisation. For analyser angles approaching extinction, the component of magnetisation parallel to the plane of incidence is detected, whereas for analyser angles approaching  $90^\circ$  from extinction, the component of magnetisation perpendicular to the plane of incidence is detected. For intermediate analyser angles, both components are simultaneously detected to varying degrees (Kerr rotation and reflectivity). This can lead to unconventional hysteresis loops as shown in Figure 2.17. For a more detailed analysis one should review the paper by Florczak & Dahlberg (1990) where the technique is extensively discussed. Here we were only concerned with obtaining conventional hysteresis loops for the purposes for characterisation, and the optimum setting for the analyser was found to be  $2.0^\circ$  for the system built in this study.

A silicon photo diode with an active area of  $35\text{mm}^2$  with a low noise amplifier was used to measure the reflected intensity. The large active area of the photo diode removed the need for any precise focusing optics. Typical intensities would correspond to a third of volt, and changes in the intensity due to the Kerr rotation would be approximately 50mV (15%). In order to enhance the detection of these small changes in voltages from the photo diode, the signal was initially conditioned before being read by ADC by the software. The signal conditioning unit consisted of a DC off-set, an amplifier with a number of gain settings, and a number of time constant settings. The amplifier was used to amplify the small signal from the photo diode to approximately three to four volts, ensuring the full resolution of the 12 bit ADC was being utilised by the software when reading the measurements. The signal was electronically cleaned which removed any low frequency signals, any background noise from the photo diode and ambient light. A number of experiments were performed by examining the hysteresis loops at a number of amplifier and time constant settings to ensure that they had no other influence on the magnetic signal being measured. It was established that the drift from the HeNe laser was negligible over the time period required to obtain a hysteresis loop (1 min), once the laser was allowed sufficient time to reach thermal equilibrium with its surrounding environment.

The software which was written by the author to automate the system was user friendly and straight forward to use. The sample was mounted onto the relevant holder and placed into position ensuring the reflected laser beam was passing through the analyser. A number of user-adjustable parameters were available on the menu if need. The main ones were:

**Shape Factor** - Which controlled the distribution of points in the field ramp. ( $0 < S < 1$ )

**Number of points per loop** - Typically 128 points were taken, maximum possible 500.

**Number of loops to average over** - Typically 3 averages were taken, maximum possible 11.

Upon selection for data acquisition, the software generated the corresponding digital ramp from the parameters set by the user. The first point of the digital ramp was triggered; this set the maximum positive field. The user now has the option of setting the maximum field he/she wishes by adjustment of the potentiometer. The voltage set by the potentiometer was constantly measured by the software and the corresponding field was displayed on-screen for the user. Once the field was set, the software then commenced data acquisition by stepping the field ramp, allowing 350ms for the field to stabilise before each measurement was taken. If a number of loops were being taken, the data for each loop was stored until all the required loops were obtained. This was so that each loop could be examined to determine whether the loop had closed, in some instances the loops would fail to close because of drift due to the electronics, especially when the whole system had recently been first turned on. The drift was measured to be small (0.1%) and was found to be linear with time. In this situation, a linear drift correction routine was executed whereby the difference in the initial and final points was divided by the total number of points in the loop and then added/subtracted to each point respectively. This was possible since each point was equally spaced in time. If the loops displayed a visible drift on-screen as the loops were being taken, this implied the sample was moving in the applied field and had to be secured more

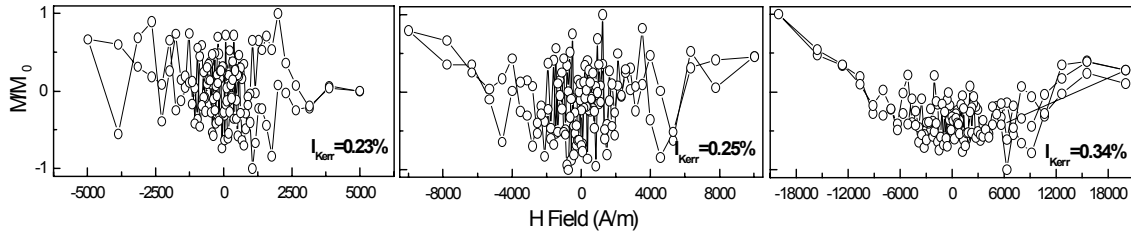


**Figure 2.18:** Hysteresis loops obtained from an aluminium thin film for three different field settings. The loops show no artificial signal which may influence the shape of a hysteresis loop.

firmly. The loops were then normalised before being averaged, and then re normalised between  $\pm 1$ . It was important that the loops were initially normalised before averaging, since any drift in the system would displace each loop, and the averaging would be invalid. The data was displayed on-screen giving the user the option to save the data after examining the loop. The data for the first loop was saved in its measured state along with the averaged/normalised data. The software also calculated a number of magnetic terms, the coercive field  $H_c$ , the anisotropy field  $H_k$ , and the remanence  $R_m$ ; these were also saved.

To ensure the system was measuring a magnetic signal and that no artificial signal was being added to the magnetic signal, a number of measurements were taken using an aluminium thin film which eliminated the magnetic signal from the system. Figure 2.18 shows the data for three loops taken at different fields. From the loops it is clear there is no artificial signal present, just random noise in the system. The Kerr sensitivity is also shown, and can be directly compared to Figures 2.14 and 2.15. The sensitivity to the non-magnetic signal can be assumed to be negligible ( $I_{kerr} < 0.4\%$ ) compared to the sensitivity to the magnetic signal, which is approximately 15%. There was a very small dependence of the electronics on the applied field but this had no real influence, since the effect was only seen at high fields and is negligible. To confirm the reliability of the measurements, a number of samples were measured at York University under the guidance of G. Matauous, where a similar MOKE system existed. The measurements taken at York were comparable to those taken at Sheffield and are shown in Figure 2.19. The signal to noise ratio of the measurements taken at York were not as good, but the general shape of the hysteresis loops were comparable, considering that it was not possible to sample the exact same spot of each sample on the two respective systems.

MOKE is only sensitive to the penetration depth (10-20 nm) and the sampling area of the laser spot of 100 $\mu$ m in diameter, it was therefore important to complement these measurements, by taking bulk measurements using the inductive magnetometer. This ensured that the magnetisation process at the surface region of the sample was representative of the entire film. This was found not to be the case with the as-deposited FeSiBC films, since they exhibited a unique but peculiar magnetic anisotropy (discussed in more detail in Chapter 5) which influenced both the bulk and surface magnetic measurements. Figure 2.20 shows a number of loops obtained by the two respective systems. It should be remembered that the bulk MH-loops are sensitive to the average magnetisation process over the entire sample, whereas MOKE is only sensitive to the magnetisation process sampled by the laser spot. For these reasons alone, one would not expect identical hysteresis loops from the two systems. The bulk

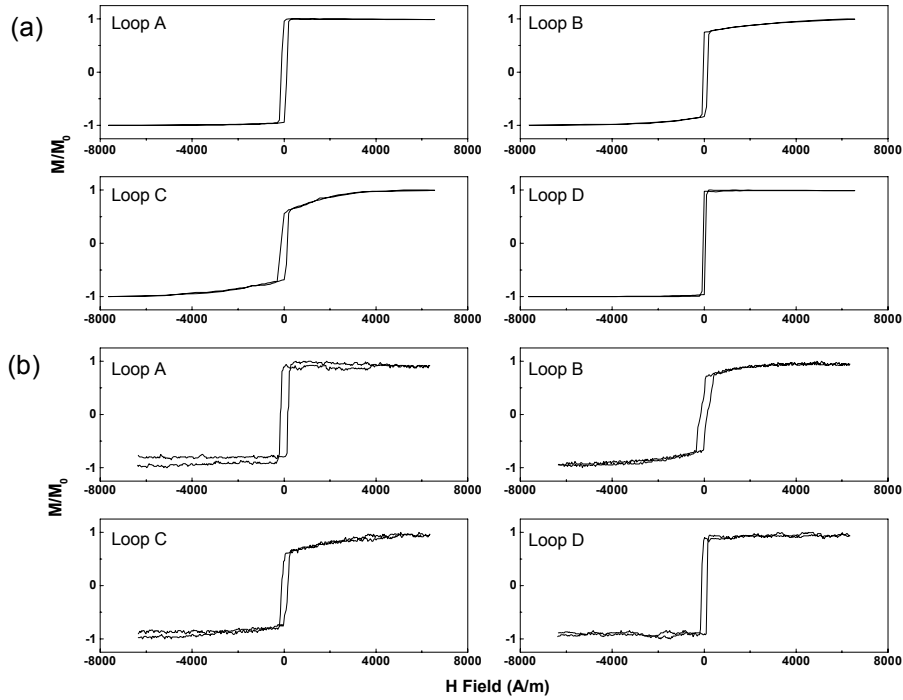


**Figure 2.19:** Comparison of MOKE hysteresis loops taken at York University with those taken at Sheffield. (a) Loops taken at Sheffield. (b) Loops measured at York. The two sets of data obtained indicate that the measurements are comparable and presumably reliable.

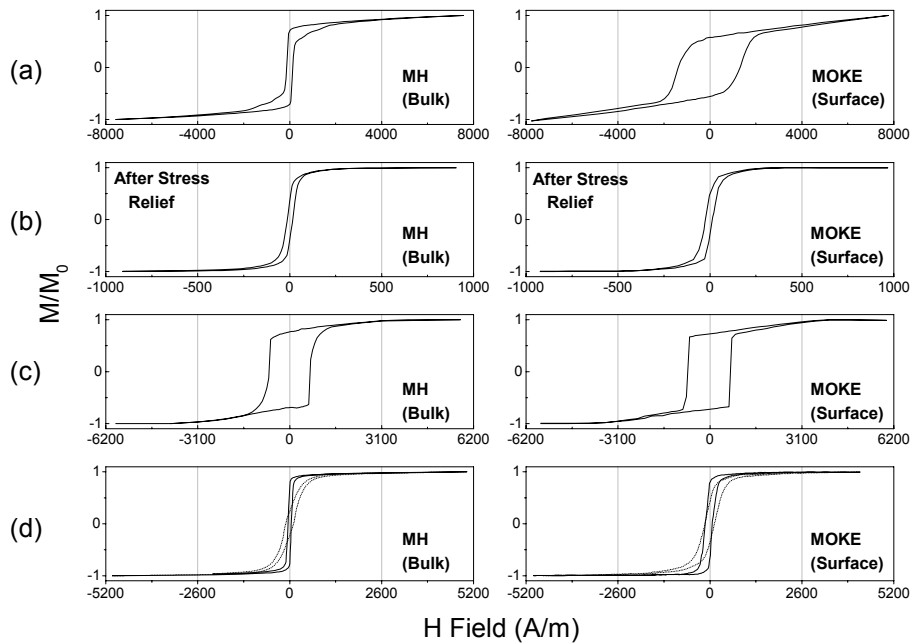


**Figure 2.20:** Comparison of hysteresis loops taken by the inductive magnetometer (MH-bulk) with those obtained by the MOKE magnetometer (Surface). The bulk measurements are sensitive to the average magnetisation process, whereas MOKE is sensitive to the local magnetisation process. (a) Measurements taken from a film which has significant growth induced stresses. The MOKE measurement is sensitive to the local stress induced by the growth. (b) Measurements taken of the sample in (a) after being thermally treated to relieve the stress. The loops are now comparable, indicating that the magnetisation on a local scale are comparable to the entire film. (c) and (d) are further examples of how comparable the loops can be from the two systems. In (d) loops taken at orthogonal directions are shown.

hysteresis loop shown in Figure 2.20a indicates the coercive field is 150 A/m, were as the MOKE loop indicates a significantly higher value. In this sample the differences were attributed to the growth induced stresses which were simply averaged out by the bulk measurement and not by the MOKE measurement. It highlights how misleading the bulk hysteresis loops could have been if no MOKE hysteresis loops were available for comparison. Figure 2.20b is the sample in 2.20a after it has undergone a thermal treatment to relieve the growth induced stresses. Here the bulk and surface loops are now comparable, indicating the surface magnetisation is representative of the entire film. Figures 2.20c and 2.20d are other examples of how comparable the bulk and surface measurements can be.

The MOKE system was capable of measuring the magnetic properties of thin films down to film thickness of 10nm, and there was no minimum sample size restrictions. As long as the laser could be positioned on the magnetic material, it could be investigated. The lower sample volumes do not effect the signal to noise ratio, as they do with inductive magnetometer. The system was not calibrated to give absolute magnetisation values, since the Kerr signal is very sensitive to the precise settings of the polariser/analyser, and also to the surface conditions. Therefore the magnetisation scale was normalised.

## 2.4 MOKE Imaging

The Kerr effect has been used to observe domain structures for many years now, but it was initially considered to be a weak effect and it was thus difficult to obtain satisfactory images, especially from the surface of samples which were not flat and smooth. This led to the magnetic contrast of the images being quite poor for the majority of materials. The arrival of microcomputers, along with digital imaging, overcame such problems by the introduction of digital techniques, where the contrast from the non-magnetic background is digitally subtracted to enhance the magnetic contrast of the domains. The Kerr effect technique allows one to observe the domain magnetisation directly without any ambiguity, and the technique itself does not influence the magnetisation process. It is a non-invasive/destructive technique, compared to the Bitter pattern technique, which tends to spoil (dirty) the surface of the samples. Depending upon the experimental arrangement, there are generally no constraints on the sample dimensions or shape. Most importantly of all, the technique allows the magnetisation process to be observed under the influences of external forces, predominantly magnetic fields.

The experimental layout which was built is shown in Figure 2.21 and is similar to the MOKE magnetometer shown in Figure 2.6. It is a relatively low cost and simple arrangement, but was ideal for obtaining domain images off large areas of thin films. The white light source was provided by a halogen slide projector fitted with an infra red filter, which illuminated an area of 4x4cm. The detection system was an Electrim EDC1000 CCD camera, with a standard 50mm camera lens. The images from the CCD were relayed to a computer through a video card. An additional zoom lens was also available, which allowed imaging of domain structures of fabricated devices as small as 100 $\mu$ m. The resolution of the system allowed domain sizes as small as 100 $\mu$ m to be resolved. Two sets of Helmholtz coils were used to apply a transverse and/or longitudinal field in the plane of the sample, so that one could observe how the domain structure behaved under the influence of the two orthogonal fields. The outer set of coils were of the same specification as those of the MOKE magnetometer which applied the transverse field,

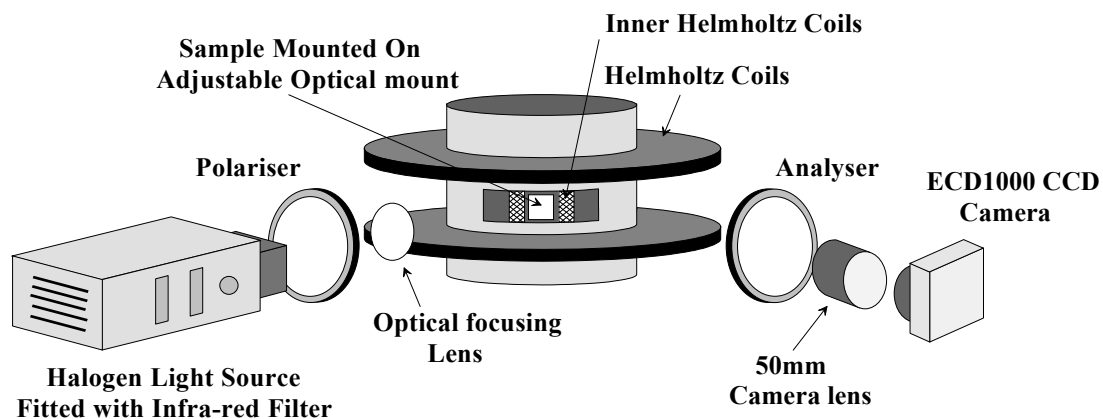


**Figure 2.21:** Schematic layout of MOKE imaging system. Note computer and KEPCO power supply are not shown.

whereas the inner set were designed to provide a longitudinal field of 2kA/m, which was sufficient to saturate the samples along the easy axis. All optical components were mounted onto two optical rails which were housed in a Faraday room to remove the ambient light from the system which was important to maximise the contrast of the images and screen the apparatus from electromagnetic noise. The white light imaging system was configured to detect the changes in the polarisation of the light due to the longitudinal and transverse Kerr Effect, as in the MOKE magnetometer at an incident angle of  $30^\circ$ . The digital imaging of the domains was computer controlled by software written by Dr Richard Watts and the software for controlling the applied fields was written by the author. The samples were mounted onto a non-magnetic holder which provided the freedom to tilt the sample for the purposes of alignment. The samples were secured to the holder either using vacuum grease or double-sided tape depending on the size and nature of the sample.

The Kerr images obtained appear essentially as different shades of grey, which represent the differently magnetised domains. The direction of the magnetisation within the domains governs the direction in which the plane of polarisation of the incident light is rotated. This is shown in Figure 2.22a, where a simple domain structure is shown. The incident light which falls upon the oppositely magnetised domains, is rotated in opposite directions (the rotation is exaggerated). The analyser is adjusted so as to extinguish light being transmitted from domains magnetised to the right, for example. This has the effect of the domain appearing dark on the Kerr image. The light which is reflected off the domain, which is magnetised to the left, is therefore not extinguished and hence appears lighter. Figure 2.22b shows a Kerr image obtained from a FeSiBC film which possesses a uniaxial domain structure.

A digital differencing technique was employed to overcome the problems with the background light, surface imperfections and irregularities which produced a strong non-magnetic contrast which generally masked the magnetic contrast. The process [Schmidt et al (1985)] involved taking a digital reference image of the film in its saturated state, which was then subtracted digitally from the subsequent images which contained the magnetic contrast. Figure 2.23 shows how the digital differencing technique vastly improved the magnetic contrast. The domain structures in Figure 2.23a are just visible

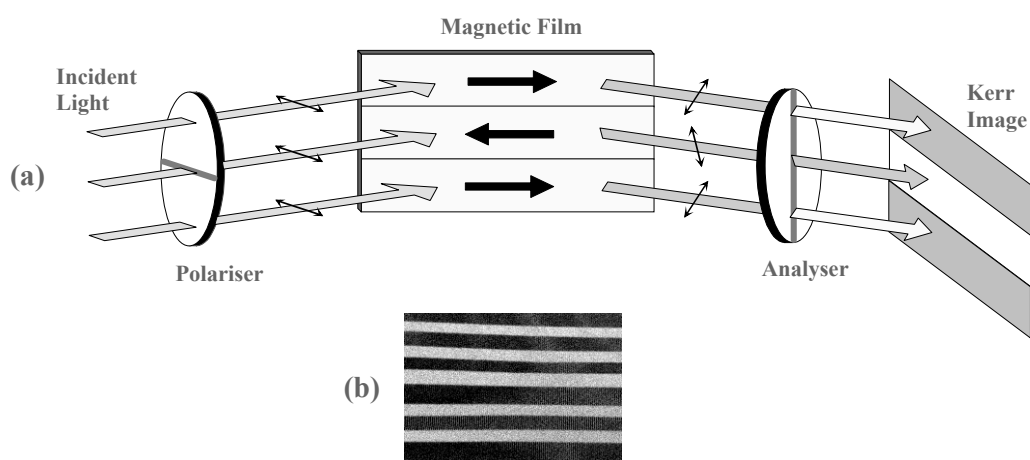


**Figure 2.22:** (a) Domain observation by the Kerr effect. (b) Kerr image obtained from a section of a FeSiBC film which has uniaxial anisotropy.

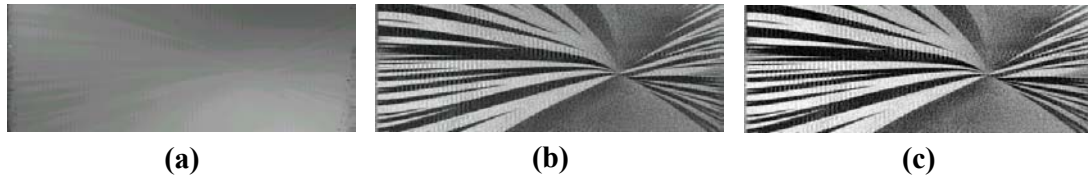


**Figure 2.23:** The domain image obtained from a section of an amorphous as-deposited FeSiBC film. See Chapter 5 for a detailed discussion about the domain structure. (a) a direct image of the film with no digital signal processing, (b) image obtained by subtracting a reference image from image (a), (c) the brightness has been digitally optimised for image (b).

in parts of the image, but are too faint to be satisfactory. Subtraction of the saturated reference image removes the majority of the non-magnetic contrast revealing the domain structure. The magnetic contrast of the resulting image is outstandingly sharp and very clear. Surface blemishes (finger-prints deliberately introduced as a test) at the two edges of the film do not appear, indicating that only the non-magnetic contrast has been removed. The digital difference images can be further improved, if necessary, by averaging, and other digital techniques such as brightness and contrast optimisation. Figure 2.23c represents a brightness optimisation of Figure 2.23b, and there is only a slight improvement, indicating the exposure time is neither too long or too short. It was not always possible to obtain images which did not require any digital enhancement (contrast and brightness optimisation) after the subtraction of the non-magnetic contrast. This was because it was difficult, and time consuming, in the early stages to optimise the reflected light and optics to produce the maximum magnetic contrast. Once the conditions were favourable, it took approximately 20 seconds to take an image, depending on the size of the image. Each image consisted of 20 images, which unless otherwise stated were averaged. The maximum image size was limited to 2.5×1.5cm.

As with all techniques, one needs to be aware of artificial effects which can occur, and which can be misinterpreted as being of a magnetic origin. Figure 2.24 shows how the digital difference technique can produce an artificial effect which appears to be magnetic. Figure 2.24a shows a typical domain image obtained from a section of FeSiBC film. At first glance, it would appear that there are two  $180^\circ$  domain walls producing three domain regions. A more careful inspection reveals that a finer detail domain structure may exist within the main domains. This has been highlighted on both the main image and on the enlarged section of the image (arrows labelled [A]). This apparent fine domain structure only appears in parts of the image and the stripe domains are very uniformly spaced. There are three main reasons why it was thought this fine domain structure was doubtful;

[1] On repeated measurements the fine domain structure was not reproducible at all. It appeared to occur randomly, and not in the same regions of the film, even though the main domain structure was virtually identical.

[2] The stripe domains seem unaffected by the main domain walls and do not alter, even on crossing the domain walls. This is high-lighted by the arrow labelled [B] in Figure 2.24a and by Figure 2.24b where this apparently fine domain structure is unaffected by multiple domains and the direction of the walls. The domains always appeared to be vertical and very uniformly spaced, even after the sample had been rotated by  $45^\circ$ , so the main domain structure was rotated through  $45^\circ$ . This implied that the stripes did

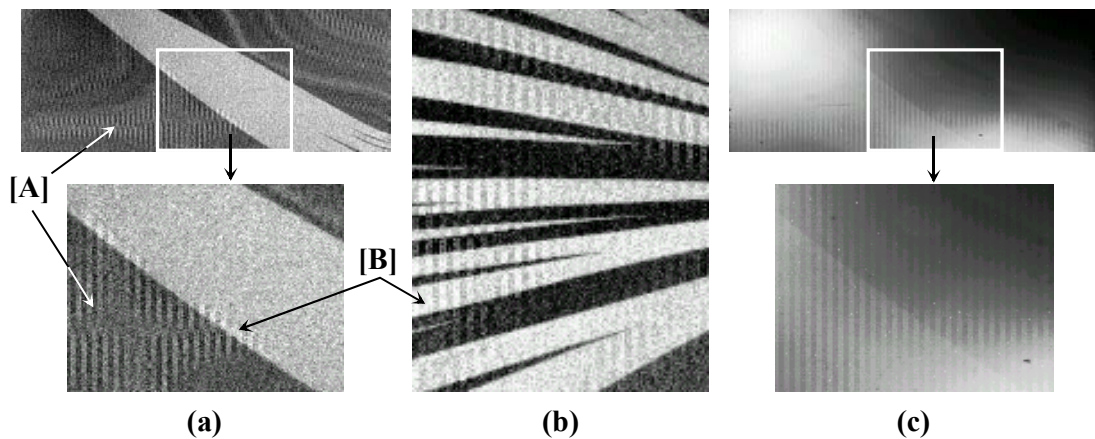


**Figure 2.24:** Artificial effects which can appear in the magnetic Kerr images. The vertical stripe patterns are non-magnetic in origin and are produced by the CCD camera in conjunction with the subtraction of the reference image (see text). (a) An image obtained from a section of an as-deposited FeSiBC film. Notice the vertical stripe pattern in parts of the image, (b) the pattern is unaffected by multiple domains, (c) represents the image of (a) before the reference image was subtracted. Notice the stripe pattern occurs uniformly across the entire image.

not originate from a magnetic effect, or any surface structural effect of the film. If it were a surface structural effect, then rotating the sample would have also rotated the striped pattern.

[3] Figure 2.24c is the identical image of Figure 2.24a, but without the reference image being subtracted. Again, notice the dramatic improvement in the contrast. Close examination reveals that a vertical stripe pattern exists across the entire image. This effect has been attributed to the CCD camera, and only seems to occur under certain light illumination of the CCD camera. The stripe patterns which occur on the difference images are a consequence of the non-magnetic contrast being slightly different to the saturated reference image. This is assumed to be a result of the film moving on the application of the saturation field for the reference image. The samples were held in position either with vacuum grease or double sided tape to prevent any clamping stresses from being introduced (Section 5.931). The movement was not detectable by eye, but it was assumed to be sufficient to cause such an effect. A number of images in this thesis are effected by this effect, and it is important to be aware that this was found to be an artificial effect.

## 2.5 Interpretation of the Kerr images

The Kerr images were obtained using both the longitudinal and transverse Kerr effects. The polar effect had no influence on the two effects, since the magnetisation was confined to the plane of the film because of the large demagnetising field. The longitudinal effect is only sensitive to the components of magnetisation, which lie parallel to the plane of incidence. This meant that any components of magnetisation perpendicular to the plane of incidence did not show any appreciable magnetic contrast. This is shown in Figure 2.25a where a Kerr image was taken from a sample which possessed a well defined uniaxial anisotropy. The easy axis was oriented perpendicular to the plane of incidence and the image was taken using the optical conditions which favoured the longitudinal effect. The image indicates no magnetic contrast in the horizontal axis. A close examination reveals that there is very faint magnetic contrast in the vertical axis (transverse effect). The positions of the domain walls have been marked in order to help the eye to locate the faint contrast. In order to make the Longitudinal Kerr effect sensitive to the vertical component of magnetisation in the film, the plane of incidence of the light needs to be rotated through  $90^\circ$  with respect to the sample. This was not feasible in this case. The other possibility was the rotation of the sample through  $90^\circ$  so that the longitudinal Kerr effect was sensitive to the magnetisation in this direction. This was also not possible in the current experimental arrangement without physically removing the sample from the holder. This led to two problems; the magnetisation, and therefore domain structure, changed on handling the film because of its magnetostrictive nature, and secondly, it was difficult to image the exact same area of the film upon rotation. Both of these problems made it difficult to correlate the two images precisely. These problems are overcome by use of the transverse Kerr effect, where it is not necessary to disturb the sample. Figure 2.25b is the identical Kerr image obtained of the domain pattern in Figure 2.25a, but using the transverse Kerr effect. The Kerr image shows a domain structure one would expect from a thin film possessing a uniaxial anisotropy. On rotating the sample, so that the easy axis is aligned parallel to the plane of incidence, the opposite effect occurs; the domain structure is only revealed by the longitudinal effect and not the transverse effect. The importance of the two effects is highlighted by Figure 2.26,

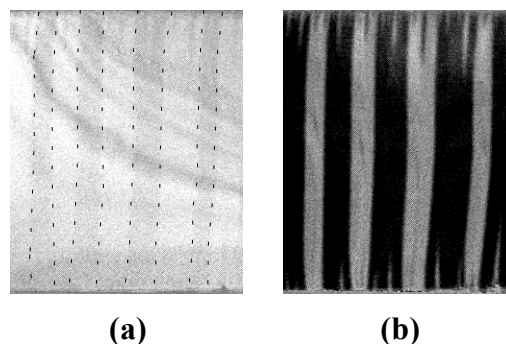


**Figure 2.25:** Kerr images obtained from a FeSiBC film possessing a well defined uniaxial anisotropy. (a) Kerr image obtained using the longitudinal effect - sensitive to the magnetisation in the horizontal axis (b) Kerr image obtained using the transverse Kerr effect -sensitive to the magnetisation in the vertical axis.

where Kerr images were obtained using both effects to reveal the two components of magnetisation. Figure 2.26a shows Kerr images obtained from a FeSiBC film which has been demagnetised and Figure 2.26b are the domain images obtained where an applied field is applied in the direction indicated on the figure. The magneto optical sensitivity has been high-lighted by the arrows for each image. The contrast of the magnetic domains is clearest for the respective magneto optic sensitivity. Together the two images provide a more clear indication of the domain structure, since the individual images do not display all the domain structure. The final image was obtained by the combination of the two images by averaging them. This was a very crude method, but it provided an overall view of the domain structure, even though the grey scale of the averaged image is not quantitative. Quantitative methods have been developed [Rave et al (1987)] to map out the vector magnetisation using the grey (or colour) scale by combination of the two images, but this is a fairly difficult procedure, and requires a very stable system, along with the ability to apply fields in many directions for the purposes of calibration; it is not implemented here.

The domain images obtained using the longitudinal and transverse Kerr effects, provide only an overall view of the domain structure. They do not provide any direct information on the direction of the magnetisation within the domains themselves. For example, the Kerr images obtained in the longitudinal mode, only reveal dark and light regions, which correspond to components of the domain magnetisation magnetised in opposite directions, as shown in Figure 2.26. Any domains which are magnetised in the transverse sense will generally appear equally grey. Thus, we cannot infer directly the direction of the domain magnetisation. Even for simple uniaxial domain structures as shown in Figure 2.22 the dark regions correspond to the magnetisation pointing either to the right or to the left, and therefore the domain images need to be carefully interpreted. For magnetic materials which have a well

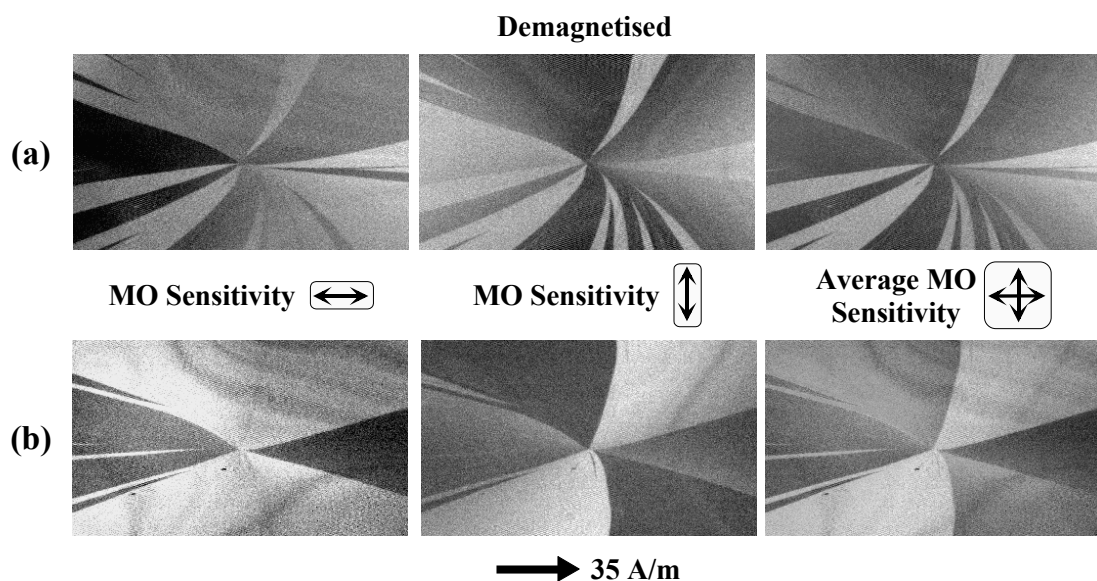


**Figure 2.26:** Domain images obtained from a FeSiBC film possessing a radial anisotropy (Chapter 5). Kerr images obtained using the longitudinal effect (sensitive to the magnetisation in the horizontal axis), and the transverse Kerr effect (sensitive to the magnetisation in the vertical axis). (a) Demagnetised sample. (b) Sample under the influence of an applied field.

defined crystalline structure, the crystalline anisotropy generally dominates the magnetic anisotropy. This simplifies the interpretation of the magnetisation of the domains, since prior knowledge of the magnetisation in such materials allows the determination of the direction of the domain magnetisation for all domains. In materials which do not possess a well defined crystalline structure, such as the amorphous FeSiBC thin films studied here, the interpretation of the resulting domains can be quite complex. In these types of materials the magnetisation is generally determined by random stresses, which tend to vary in magnitude and direction. These stresses are commonly induced during the fabrication process of the material, and therefore the resulting domain structures can be quite complex to interpret. Identification of  $180^\circ$  domain walls, or closure domains at the edges of these samples, can help to piece the domain structure together, but this is not always the case. To establish the direction of magnetisation in a uniaxial domain structure as shown in Figure 2.22, is relatively straightforward. Here, a small magnetic field of known direction is applied along the direction of the domain walls. The favourable domains will grow in size, from which one can then establish if the dark regions correspond to domain magnetisation pointing to the left or right. In more complicated domain structures such as the radial domain structures shown in Figure 2.23 and discussed in Chapter 5, the domain magnetisation no longer points in the x or y directions. Here, MOKE loops are taken at various points on the sample, from which the direction of the domain magnetisation (easy axis) can be determined accurately. Using this information, one can then apply a small magnetic field whose direction is known, along the easy axis for the domain we are interested in, to determine the direction of the domain magnetisation. By this procedure it is possible to map out the domain magnetisation.

## 2.6 Magnetic Measurements Through Transparent Substrates

Magnetic films which were deposited on transparent substrates, allowed the magnetic characterisation of the lower surface of the film, or in the case of multi-layered films the bottom layer to be investigated (see MI chapter). It was found that the magnitude of the field strengths being used had no adverse effects on hysteresis or domain images obtained at the fields being used. Figure 2.27 show a number of MOKE hysteresis loops taken from a FeSiBC film. Hysteresis loops (a) and (b) are the respective loops taken from the upper and lower surface of a 500nm film; which are similar. Loops (c) and (d) were taken from the top surface of a film, but with a glass substrate positioned in front. This allowed the glass substrate to be rotated without disturbing the film, to ascertain if the glass substrates being used were altering the polarisation (Faraday effect) of the laser. It appeared that the glass substrates were not affecting the magnetic measurements. Figure 2.27b are domain images taken from a 750nm FeSiBC film, where images of the upper and lower (through the glass substrate) surfaces are similar. It can therefore be assumed that the magnetic measurements performed through the transparent glass substrates used here are reliable.

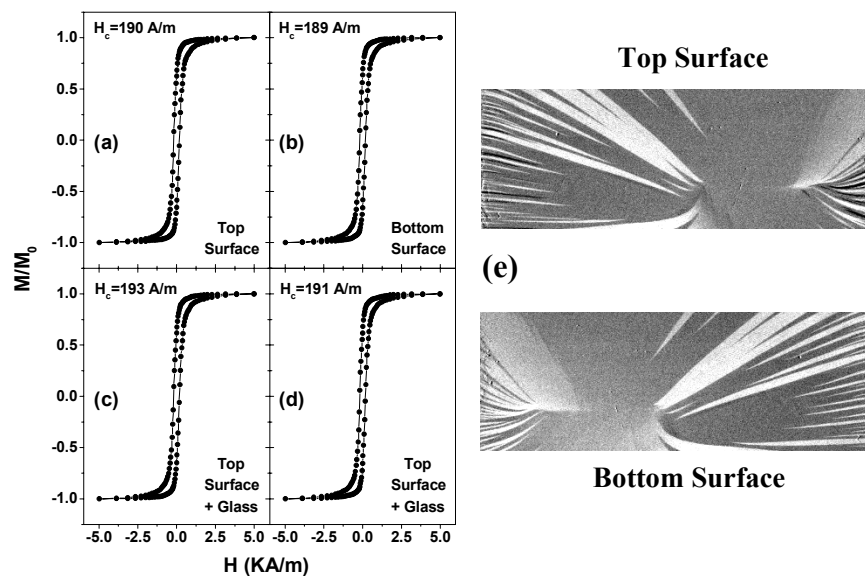


**Figure 2.27:** Magnetic measurements through transparent substrates. (a) Loop obtained from top surface, (b) loop obtained from lower surface through glass substrate (Corning®). Loops (c) and (d) were taken from the top surface of the film, but with a glass substrate positioned in front. The glass substrate in (d) was rotated through  $90^\circ$ . (e) Domain images obtained from the upper and lower surface of a FeSiBC film. Images taken at  $H=15$  A/m.

## 2.7 Conclusions

A magnetometer and a domain imaging system were constructed by the author to characterise magnetic thin films utilising the Magneto Optical Kerr effect (MOKE). The two systems allowed the possibility to fully investigate the in-plane anisotropy present in the amorphous FeSiBC films deposited in this study. The systems were also used by other colleagues within and external to University of Sheffield. The MOKE system built, was also used by Karl et al (1999) to interrogate the changes in the magnetic properties of a micromachined membrane-type pressure sensor. A very similar MOKE magnetometer system was also built by the author on an invitation by the Universidad Del Pais Vasco in Bilboa, Spain [Castano (1998)]. Comparisons of hysteresis loops with measurements done at York University and with bulk hysteresis loops have shown that results can be taken to be reliable.

The general principles of the Kerr effect have been discussed providing the reader with an insight into the implementation of the Kerr effect, and the interpretation of the domain images obtained and shown in the remainder of this study.

## 2.8 References

- Bland et al (1989) “An intensity-stabilised He-Ne laser for measuring small magneto-optic Kerr rotations from ferromagnetic films”, J.A.C. Bland, M.J. Padgett, R.J. Butcher, N. Bett, J. Phys. E. Sci. Inst. (22) 308 (1989).
- Castano (1998) Invited by Professor Fernando Castano (Senior), Department of Chemical-Physics, University of the Basque Country (Universidad Del Pais Vasco), Apto. 644, 48080 Bilbao, Spain, (1998).
- Corson & Lorrain (1970) “Electromagnetic fields and waves”, P. Lorrain, D. Corson (1970), 2<sup>nd</sup> Edition, pp462.
- Daalderop et al (1988) “Theory of the magneto-optical Kerr-effect in NiUSn”, G.H.O. Daalderop, F.M. Mueller, R.C. Abers, A.M. Boring, J. Magn. Mater. (74) 211 (1988).
- Deeter & Sarid (1988) “Magneto-optical characterisation of multilayers by incident-angle analysis”, M.N. Deeter, D. Sarid, IEEE Trans. Magn. MAG-24(6) 2470 (1988).
- Florczak & Dahlberg (1990) “Detecting two magnetisation components by the magneto-optical Kerr effect”, J.M. Florczak, E.D. Dahlberg, J. Appl. Phys. 67 (12) 7520 (1990).
- Hecht (1989) “Hecht Optics - 2<sup>nd</sup> edition”, E. Hecht, A. Zajac, p95 (1989).
- Jiles (1994) “Introduction to magnetism and magnetic materials”, D. Jiles, Chapman & Hall (1994).
- Karl et al (1999) “A micromachined magnetostrictive pressure sensor using magneto-optical interrogation”, W.J. Karl, A.L. Powell, R. Watts, M.R.J. Gibbs, C.R. Whitehouse, Sen. & Act. A \*\* \*\*\* (2000).
- Moog et al (1989) “Thickness and polarisation dependence of the magneto-optic signal from ultrathin ferromagnetic films”, E.R. Moog, C. Liu, S.D. Bader, J. Zak, Phys. Rev. B. 39 (10) 6949 (1989).
- Rave et al (1987) “Quantitative observation of magnetic domains with the magneto-optical Kerr effect”, W. Rave, R. Schafer, A. Hubert, J. Magn. Mater. (65) 7 (1987).
- Schmidt et al (1985) “Enhancement of magneto optical domain observation by digital image processing”, F. Schmidt, W. Rave, A. Hubert, IEEE Trans. Magn. MAG-21(5) 1596 (1985).
- Shearwood et al (1996) “Growth and patterning of amorphous FeSiBC films.”, C. Shearwood, M.R.J. Gibbs, A.D. Mattingley, J. Magn. Mater. (162) 147 (1996).
- Squire et al (1988) “Digital M-H plotter for low-coercivity metallic glasses”, P.T. Squire, S.M. Sheard, C.H. Carter, M.R.J. Gibbs, J. Phys. E. Sci. Instrum. (21) 21167 (1988).
- Zak et al (1990) “Fundamental magneto-optics”, J. Zak, E.R. Moog C. Liu, S.D. Bader, J. Appl. Phys. 68(8) 4203 (1990).

## 3.0 General Experimental Techniques

This chapter describes the process of sputter deposition and the experimental arrangement used to obtain the highly magnetostrictive FeSiBC films used in this study. It also describes the methods used to study the films magnetically and to characterise them, along with the a section on thermal heat treatments employed.

### 3.1 Thin Film Deposition

#### 3.1.1 The sputtering process

The sputtering process consists of the bombardment of the target material by fast moving, heavy, inert gas ions from a plasma. The bombarding ions cause atoms to be ejected from the target material by momentum transfer between the colliding ions and the target atoms. The process is schematically shown in Figure 3.1a, where a number of processes are shown to occur when the ions collide with the target material. Some of the bombarding ions are reflected back and are neutralised, but may still be sufficiently energetic to reach the substrate were the film is being deposited. This can be a source of substrate bombardment (back scattering) which can effect the resulting properties of the film. The majority of the colliding ions tend to induce sputtering by ejecting atoms of the target material by momentum transfer. This is a secondary collision process, as shown schematically in Figure 3.1a. The ejected atoms will have random directions but, as discussed in Chapter 4, the sputtering process can induce texture in the resulting films due to the sputtering conditions. Secondary electrons which are emitted either join the oscillating plasma gas, which cause the continuous ionisation of the gas to sustain the incident ions needed for sputtering, or they liberate their energy in the form of heat on colliding with the substrate or other parts of the chamber. The sputtered target atoms which are deposited at the substrate form the resulting thin film.

The basic processes occurring at the surface of the substrate are shown in Figure 3.1b. The mobility of the incident atoms arriving at the substrate is highly dependent upon the sputtering parameters (pressure and power), the temperature of the substrate, the distance between target and substrate, and the surface

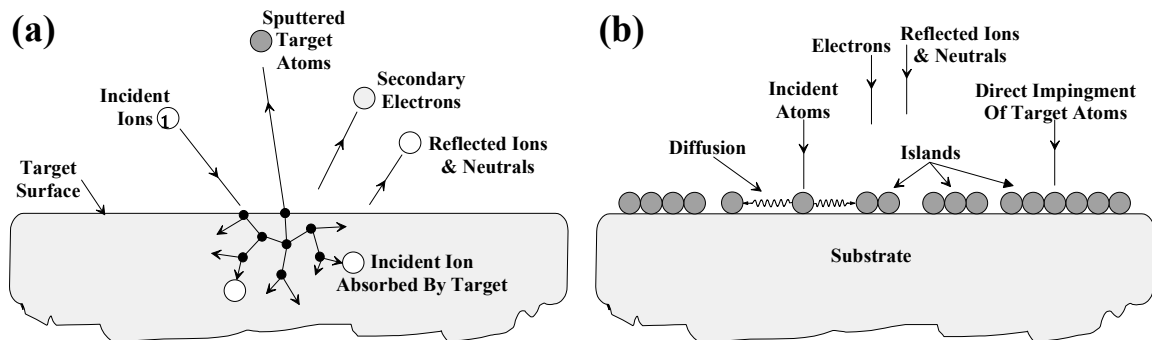


**Figure 3.1:** An illustrative diagram showing the sputtering process at the target (a), and film formation at the substrate (b).

of the substrate itself. Any surface defects or texturing of the substrates can effect the mobility of the incident atoms and will act as a barrier, and this can be reflected in the resulting properties of the film. The incident atoms with sufficient mobility will diffuse to join other incident atoms to form islands which will continue to grow until they coalesce to form a continuous film (see Wagendristel et al (1994) for details). Other species of particles besides the target atoms can also bombard the substrate, which can influence the growth of the film. The neutral reflected atoms and gas particles are particularly difficult to control, as they cannot be manipulated using electric or magnetic fields. These particles can have sufficient energy on arrival at the substrate such that they sputter the film or become incorporated into the film itself. The bombardment of these particles can be controlled by working at pressures where the mean free path of the particles is small compared to the target-substrate separation, or by working at lower sputtering powers. In addition to these neutral particles, the substrate can also suffer bombardment from reflected gas ions. Control of these particles can be achieved by applying a bias to the substrate; this is known as bias sputtering. This effect has been extensively utilised in the study of magnetic films (Chapter 4). All particles impinging on the substrate, including electrons, will liberate energy in the form of heat, increasing the temperature of the substrate which effects the mobility of the target atoms and hence the depositing film.

### 3.1.2 Radio Frequency Magnetron Sputtering

In this study all magnetic films were grown by Radio Frequency (RF) magnetron sputtering using a Nordiko NM2000 system. The system is schematically shown in Figure 3.2. The sputtering system was configured to operate in the sputter-up mode, where the substrates were mounted 6cm directly above the target electrode. The sputter-up configuration had the advantage of not suffering from the problem of eroded target fragments falling on the substrate electrode and thus affecting the depositing film. Both the substrate and target electrodes were 15cm in diameter and were water-cooled. The Nordiko NM2000 consisted of three target electrodes (referred to as 1,2,3) which were mounted on a rotatable carousel. This provided the facility to sputter from three different target materials separately, and therefore allowed the deposition of multi-layered films. A grounded stainless steel shielding plate ensured that only the target below the substrate electrode was being sputtered from. In this study all films were grown using target electrode 1 unless otherwise stated. The importance of this is discussed in Section 5.8.1. The main chamber is attached to a mechanical hoist in order that the vacuum chamber could be lifted clear of the base of the machine to provide access for the mounting of targets and general maintenance. Two Viton seals were used to provide a vacuum seal for the main chamber as shown Figure 3.2. The rotatable shutters were positioned to provide shielding for either the target or substrate from the plasma. This allowed the target or substrate to be sputter-cleaned prior to the deposition of the film. A stainless steel clamping ring was used to secure the target to the copper electrode which ensured good electrical and thermal contact. To prevent sputtering from the clamping ring itself, an over-sized earthing shield was mounted directly above to prevent the plasma from coming into contact with the ring. The earthing shield also prevented the sputtered material from being deposited onto the insulator which isolated the target electrode from ground. Substrates were mounted

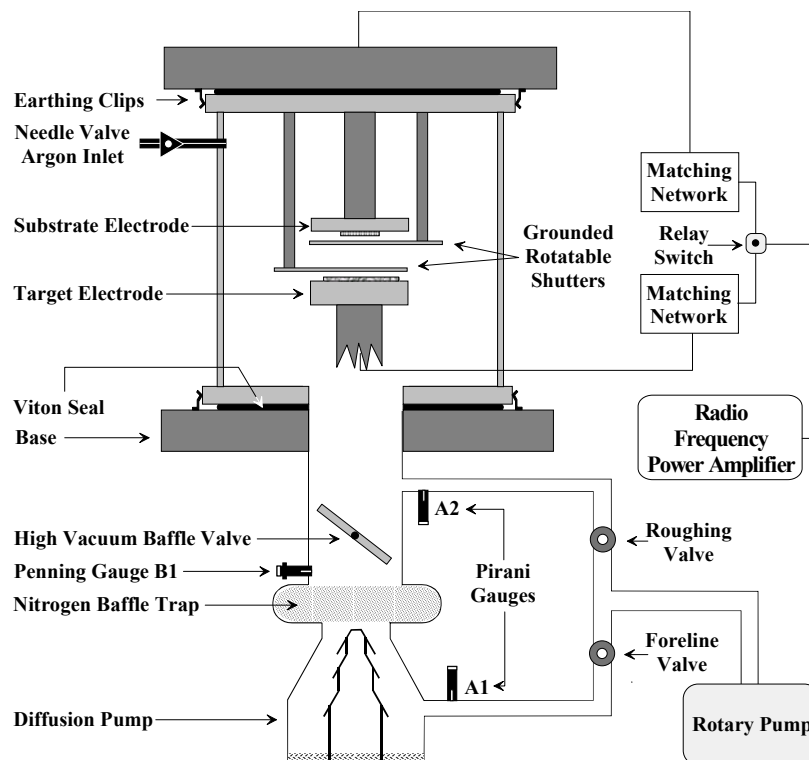


**Figure 3.2:** A schematic representation of the Nordiko NM2000 sputtering system used to sputter deposit the amorphous thin films.

on a removable copper substrate platter which interlocked firmly into the substrate electrode with a copper gasket which insured good thermal and electrical contact.

The power from the RF amplifier could be directed either to the target or the substrate electrode by means of a relay switch through a matching circuit. This allowed the impedance of the power supply and electrode to be matched, so the required power could be delivered efficiently. Directing the power to the substrate electrode allowed the substrates to be sputter etched if needed before the deposition of the film. The sputtering gas used was zero-grade high purity argon (99.99%); the gas flow was controlled by a needle valve and by partially opening the high vacuum baffle valve.

The high vacuum pumping system consisted of a diffusion pump (Balzers DIF 200) which was backed by a mechanical rotary pump (Balzers DUO 030A). A liquid nitrogen trap was situated between the high vacuum baffle valve and the diffusion pump so as to prevent oil or water vapour from entering the chamber. The chamber could be isolated from the pumping system by the high vacuum baffle valve which allowed the chamber to be vented to atmospheric pressure without the requirement of shutting the pumping system down. The baffle valve also allowed the chamber to be gradually exposed to the high vacuum pumping system. This was important since the chamber was only evacuated to a pressure of  $10^{-2}$  mTorr using the mechanical rotary pump, whereas the high vacuum pumping system was in the low  $10^{-8}$  Torr region. Any sudden opening of the high vacuum valve would have resulted in oil vapour passing into the chamber, and disrupting the flow of the diffusion pump. Pneumatic valves were used to isolate or open the rotary pump to either the chamber or the diffusion pump. The chamber pressure was monitored by a Pirani gauge (A2) in the range  $10^2$ - $10^4$  mTorr and by a cold cathode Penning

gauge (B1) in the range  $\sim 10^{-5}$ - $10^{-8}$  Torr. The foreline (backing) pressure for the diffusion pump was monitored using a second Pirani gauge (A1).

All removable items (earthing shields, shutters, etc.) within the chamber were shot-blasted using a fine glass bead prior to the growth of any FeSiBC films. This was to remove any foreign material which had previously been grown in the chamber. The sputtering process deposited material on all surfaces within the chamber, and therefore it could also sputter material back off these surfaces thereby contaminating the films (secondary sputtering). All items were de-greased after shot-blasting and handled with clean-room gloves. The chamber was periodically baked out at  $70^{\circ}\text{C}$  to reduce out-gassing, and hence improve the vacuum. The contaminants within the system were monitored using a residual gas analyser (Balzers QMG64 RGA).

Use of a magnetron source increased the growth rate by ensuring that a high density of electrons exists near the surface of the target. The field from the magnetron forms a race track from where the majority of the material is sputtered. The downside to this is that the target erodes at a much higher rate in these regions, making very little use of the majority of the target. The growth rate is dependent mainly upon the pressure and power at which the films are deposited. The growth rate is also affected by substrate and target separation, but this was always fixed at 6cm. Increasing the sputtering power increases the growth rate and therefore erosion of the target, but it also has the effect of raising the temperature of the target and substrate. Increasing the pressure will also increase the sputtering rate at low pressures, but this will level off and even decrease at higher pressures because the various particles are slowed down by inelastic collisions. The magnetic properties of the films can be highly sensitive to pressure, power and the temperature at which they are deposited.

### 3.1.3 Target and Substrate preparation

The magnetic thin films studied throughout this thesis were sputter deposited from an amorphous METGLAS<sup>®</sup> 2605SC ribbon material of composition  $\text{Fe}_{81}\text{Si}_{3.5}\text{B}_{13.5}\text{C}_2$ . The material was supplied by the Allied Signal Corporation and came in the form of an amorphous melt-spun ribbon 18cm in width. The target used for sputtering consisted of two circular 15cm diameter targets which were carefully cut from the 18cm width melt-spun ribbon. The matt side of each target was lightly cleaned with isopropanol/acetone and immediately dried in a stream of dry nitrogen gas. The two targets were then

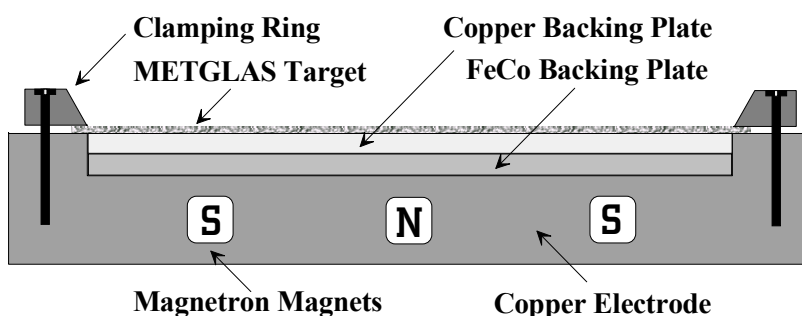


**Figure 3.3:** A diagram of the target electrode illustrating the mounting of the targets.

assembled on target electrode one unless otherwise stated, matt side up as shown in Figure 3.3. A 1mm thick copper and FeCo backing plate was also placed beneath the two METGLAS<sup>®</sup> 2605SC targets. The copper plate was used as a spacer and to protect the electrode and the FeCo disc from the plasma in the instances where the METGLAS<sup>®</sup> 2605SC targets eroded though. Two METGLAS<sup>®</sup> 2605SC targets were used to ensure that any small pinholes in the top target were covered by the target below, thus preventing any sputtering of the copper backing plate. The purpose of the FeCo plate was to increase the sputtering rate, since it increased the density of electrons near the target. The targets were clamped lightly to accommodate for thermal expansion and prevent shattering because of brittleness of the target after being heated during the sputtering process. The top target was changed after approximately 10 hours of growth at 75 watts or when the target shattered or eroded through.

The high quality of the deposited films was maintained by ensuring that the substrates were clean and grease free. This prevented the films from peeling away from the substrate and having imperfections such as pin holes. The glass-based substrates were ultrasonically de-greased, rinsed in acetone/isopropanol and dried in a stream of dry nitrogen gas. Silicon and GaAs substrates are extremely clean on purchase and were only cleaned by a stream of dry nitrogen gas to remove any surface dust particles. Kapton<sup>®</sup> substrates were cleaned in a similar manner to the glass-based substrates. Initially 1cm<sup>2</sup> squared substrates were used. These were glued onto glass slides using a high temperature vacuum compatible glue. The substrates were always glued in the same positions for consistency. The glass slides were then clamped to the copper substrate holder as shown in Figure 3.4a. Further into the study, films were grown on substrates of dimensions up to 7.6cm by 2.6cm. In this case, substrates were mounted on the substrate holder using a picture frame design such that they were only held under their own weight. This eliminated any clamping forces upon the substrate. All substrates were handled with non-magnetic tweezers wherever possible, and using clean-room gloves. The acetone and isopropanol used in the preparation of the substrates were of the analar grade.

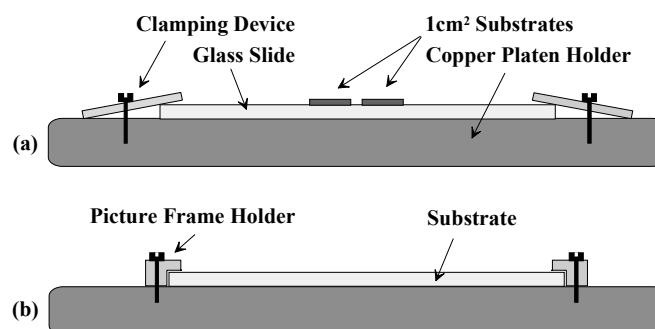


**Figure 3.4:** A diagram representing the two main types of holders used during the sputter deposition of the films in this study.

### 3.1.4 The deposition procedure

The growth of the films commenced once a low base pressure (B1) was established within the chamber in the low  $10^{-7}$  Torr region. The high vacuum baffle valve was reduced to 30%, and a continuous flow of argon was allowed into the chamber via an inlet needle valve. The required pressure (A2) was obtained by careful adjustment of the needle valve which controlled the flow of argon into the chamber precisely. For consistency the baffle valve was always set to 30%, to ensure the same flow-rate of gas through the chamber during each growth. The continuous flow of argon into the chamber ensured that any gas contaminants produced by out-gassing of the chamber were removed. The plasma was ignited by setting the RF power to 20 W and then tuning the matching circuit so that the substrate or target impedance matched that of the power supply (50 Ohms). This was indicated by the reflected power; the smaller the reflected power, the better the match. The argon pressure was momentarily increased until the plasma has ignited using a second argon inlet valve. Once ignited the reflected power was readjusted to zero and the power was increased in steps of 1W to the required value.

During the initial stages of the study, the substrates were pre-sputtered to clean their surface prior to the deposition of the film. This procedure was later abandoned for reasons discussed in Chapter 4. The METGLAS<sup>®</sup> 2605SC ribbon targets were always pre-sputtered for the following reasons:

- [1] It ensured that any contamination or oxidation of the surface of the ribbon targets which may have resulted during the fabrication process was removed, and therefore did not get incorporated into the depositing film.
- [2] It allowed sufficient time for an equilibrium of sputtering particles to be established. At the start of sputtering, the target and surrounding chamber are cold and as the target heats up, the sputtering properties of the target will also change.
- [3] Contamination of the films from secondary sputtering from the surrounding chamber environment is removed, since the chamber is coated with a thin layer of METGLAS<sup>®</sup> during the pre-sputter.
- [4] It allowed an adequate length of time for any substantial out-gassing of the chamber and target to occur and an equilibrium state to be reached. This also allows the pumping system to reach an equilibrium state, which will ensure a constant flow of argon gas through the chamber and hence constant pressure.
- [5] Finally it permitted the whole sputtering system to reach thermal equilibrium before the deposition of the film began.

There were two steps involved in the pre-sputter; the target was initially sputtered at 200 W for 15 minutes to remove any surface oxides and speed up any out-gassing processes (points [1] & [4]), the power was then reduced down to 75 W and sputtered for a further 5 minutes to allow time for the target and surrounding environment to reach thermal equilibrium [points [2],[3] & [5]]. At this stage the substrate shutter which is shielding the substrate from the plasma is rotated to commence the deposition of the film. The pre-sputter times were reduced to 10 and 5 minutes respectively for further growths of the same target. The time of 15 minutes at 200 W was only used for the first growth of each new target.

Upon completion of the deposition, the substrate is shielded from the plasma using the shutter, and the power is decreased to zero in steps of one watt. This procedure was adopted to allow the target to cool gradually, and prevent the target from shattering, increasing the life of the target. The whole system was then allowed to cool for 5 minutes with the flow of argon still on. The continuous flow of argon reduced the possibilities of any contamination from sticking to the cooler film surface from any out-gassing processes. The flow of argon was then turned off and the chamber isolated by closure of the HV baffle valve. The chamber was then vented to atmospheric pressure using dry nitrogen gas which reduces contamination and the substrates removed.

### 3.1.5 Calibration of deposition rate

The deposition rate was determined for each series of films grown at the same growth parameters, or whenever the growth parameters were changed. The deposition rate, for a given set of growth parameters, was determined by masking a standard glass slide with a 1mm strip of Kapton<sup>®</sup>. The Kapton<sup>®</sup> strip was tightly clamped along the length of the slide onto the copper platter using the clamping arrangement shown in Figure 3.4a. A film was then deposited for a fixed period of time and, upon removal of the Kapton<sup>®</sup> strip, a clean step existed to the surface of the un-coated substrate. The profile of this step was determined using a stylus measurement. The DEKTAK profilometer used had a vertical resolution of 1nm. The deposition rate was then determined in nm/minute. It was found that the deposition rate was linear (Fig. 3.5) with time, and provided a simple means of depositing a known thickness. No pre-sputtering of the glass slide was undertaken for the calibration films, since this would have eroded the substrate and therefore affected the determination of the thickness. Thickness measurements were done on the central region of the glass slides, since initially samples were grown on 1cm<sup>2</sup> samples which were mounted to the central region of the glass slides. Measurements performed along the length of the slide revealed that a thickness profile existed along the slide. Figure 3.6 shows there is a 5% decrease in the thickness, as one moves away from the central region of the slide. The film thickness was also monitored on films which were patterned using photo-lithography techniques.

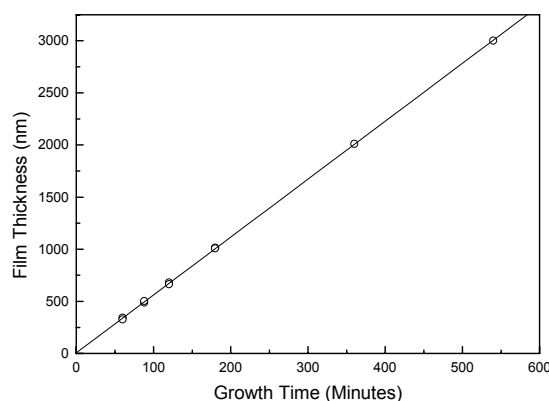
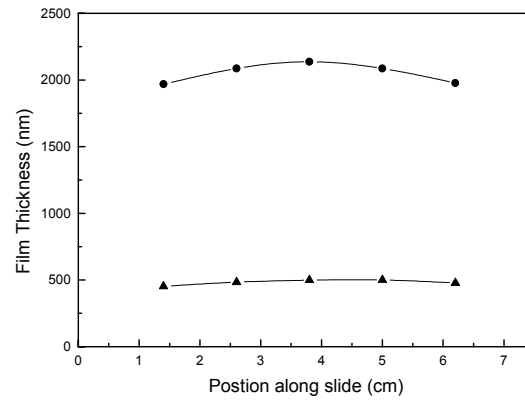


Figure 3.5: Calibration of deposition rate.



**Figure 3.6:** Thickness profiles across the length of two FeSiBC films. Films deposited at an argon pressure of 4mTorr at 75W.

### 3.2 Inductive magnetometer (MH)

The Inductive Magnetometer shown in Figure 3.7 was used to provide bulk magnetic hysteresis loops (referred to as MH loops). The magnetometer is based on a similar design to that which is described by Squire et al (1988). It is an induction method which is dependent on Faraday's law of electromagnetic induction; this states that the voltage  $V$  induced in the search coils is equal to the rate of change of flux linking the coil.

$$V = -NA \frac{dB}{dt} \quad (3.1)$$

Here,  $N$  is the number of coil turns linking the flux,  $A$  is the cross-sectional area of the search coil, and  $B$  is the flux density which is defined as

$$B = \mu_0 M \quad (3.2)$$

From equations 3.1 and 3.2 one finds that the magnetisation,  $M$ , of the sample is proportional to the integral of the induced voltage

$$M = \frac{1}{NA\mu_0} \int V dt \quad (3.3)$$

and this is the basis of the magnetometer described here.

The magnetometer consists of a solenoid one metre in length, in which two identical search coils were positioned 50cm apart along the central axis of the solenoid. The search coils were wired in series opposition through a balance circuit. This ensured that when no sample was present within the search coil  $S_1$ , there was no net signal from the applied field, but the system was still sensitive to changes in

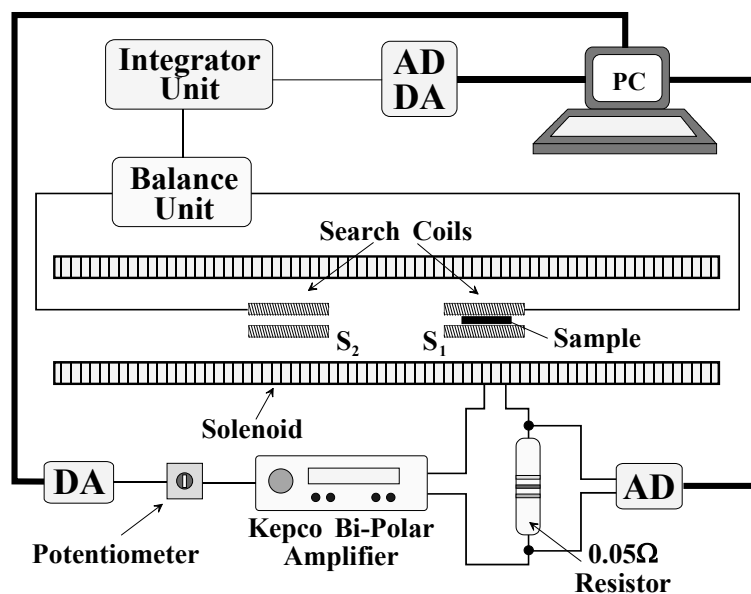


**Figure 3.7:** Schematic diagram of inductive magnetometer used to obtain bulk magnetic hysteresis loops.

the magnetisation. The arrangement allowed the magnetisation of the samples to be measured as a function of magnetic field up to 28kA/m. The signal from the balance unit was integrated digitally before being recorded and stored on the computer. The applied field was software controlled similarly to that of the MOKE magnetometer described in Chapter 2. The digital field ramps were user-adjustable, and a number of user-adjustable parameters were available, as with the MOKE system (see Chapter 2). The magnetic field generated by the KEPCO power amplifier was monitored by measuring the voltage across a standard non-inductive resistor which was in series with the solenoid.

The dimensions of the search coil  $S_1$  allowed sample dimensions of  $1 \times 1 \times 0.15 \text{ cm}$  to be measured in two orthogonal directions. It was not possible to investigate fully any in-plane magnetic anisotropy using this system. This was overcome by the use of the MOKE magnetometer and domain imaging system. The inductive magnetometer was able to provide magnetic information from sample volumes as small as  $1 \times 10^{-11} \text{ m}^3$ . This corresponds to thin films approximately 100nm in thickness. Thicknesses lower than this were found to be more difficult to characterise, but this was overcome by using the MOKE magnetometer which was able to measure sample volumes as small as  $1 \times 10^{-16} \text{ m}^3$  without any difficulty.

The integration unit which was used to integrate the induced voltage was prone to drift linearly with time. This produced hysteresis loops which failed to close and therefore it was mandatory to implement a linear drift routine as described for the MOKE magnetometer in Chapter 2. This was possible because the drift was found to be linear with time [Squire et al (1988)].

It was important that the search coils were carefully balanced so there was no net signal from the applied field with no sample present in the search coil. Otherwise the hysteresis loops would give the impression that the samples could not be saturated. This is shown in Figure 3.8 where a loop was obtained from a sample where the search coils were unbalanced and in the situation where the search coils were correctly balanced.

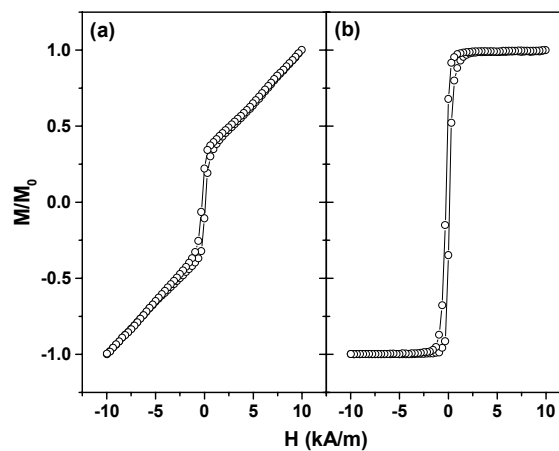


**Figure 3.8:** MH loops obtained from a FeSiBC film with (a) search coils unbalanced and (b) search coils correctly balanced.

### 3.3 Heat Treatments

The heat treatments used to anneal the samples in this study were performed at a temperature of 390°C for 60 minutes in a low vacuum of the order of  $10^{-2}$  Torr. This temperature was found to be sufficient to allow the as-deposited stresses in the films to be relieved, but sufficiently low that crystallisation of the films did not occur. The crystallisation temperature for METGLAS® 2605SC is 480°C [Allied (1995)], and X-ray diffraction analysis of the films revealed no signs of crystallisation after annealing. The annealing process relieves the internal inhomogeneous stresses which can occur during the deposition of the films. This arises mainly as a consequence of the difference in the thermal expansion coefficients between the depositing film and substrate and the dynamics of the sputtering process itself. In highly magnetostrictive materials such as the FeSiBC investigated in this thesis, this can severely affect the magnetic properties by generally increasing the coercive and anisotropy fields. Random stresses can also give rise to complicated domain structures which can make the interpretation of the magnetisation processes difficult. Annealing of the samples has the effect of removing any magnetic anisotropy which may have been induced during the growth process, for instance by stray magnetic fields. In the case of magnetron sputtering as used in this study, it has been shown in Chapter 5 that under certain sputtering conditions the stray field from the magnetron source induces a unique radial anisotropy.

The annealing process was also employed to induce and control the magnetic anisotropy by applying a suitable magnetic field or mechanical stress to the film as discussed in Chapter 5.

The experimental apparatus used to anneal the samples is shown in Figure 3.9. A wire-wound observation furnace was used to heat the samples which were placed inside a Pyrex tube. The low vacuum of  $10^{-2}$  Torr within the tube was maintained by a mechanical rotary pump. The annealing process was performed under a vacuum so as to reduce any oxidation of the films and prevented the surface of the films from being contaminated by impurities in the air. An AC current source, controlled by a Eurotherm temperature controller, was used to maintain the temperature to within  $\pm 1^\circ\text{C}$ . In the situation, where the samples were field annealed, the furnace was positioned between the pole pieces of a water-cooled electromagnet which provided a magnetic field of 0.3T. On completion of the appropriate heat treatment, the samples were allowed to cool gradually to room temperature in a vacuum. Prior to any heat treatments, all films were cleaned to ensure no grease or other impurities were present on their surface; these could have been absorbed into the film during the anneal. It was found that the samples which were deposited onto Kapton® substrates were not suitable under any of the heat treatments. This was due to the large difference in the thermal expansion coefficients of the Kapton® substrate (20ppm/ $^\circ\text{C}$ ) and the METGLAS® 2605SC (4.9ppm/ $^\circ\text{C}$ ) film. The films on Kapton® were found to be highly stressed after annealing and it was not possible to measure their magnetic properties.

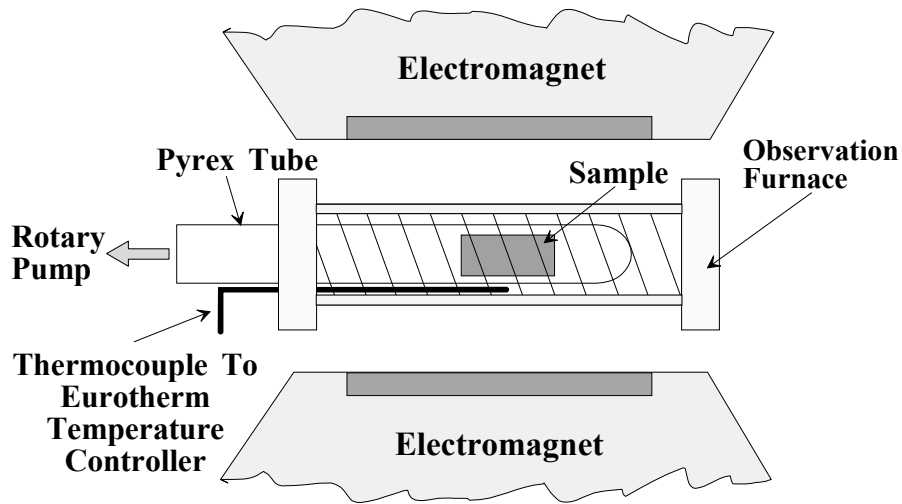


**Figure 3.9:** Apparatus used for thermal treatments of samples. The electromagnet is only present when the samples are magnetically annealed (field annealed).

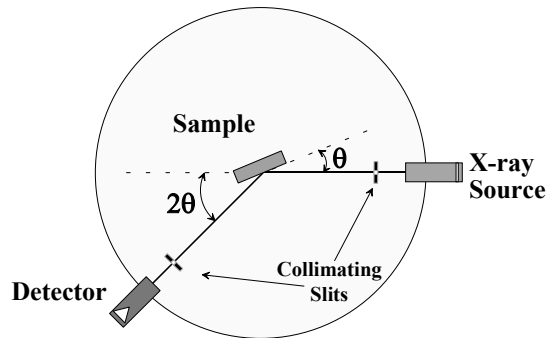


**Figure 3.10:** An illustrative diagram of an X-ray diffractometer.

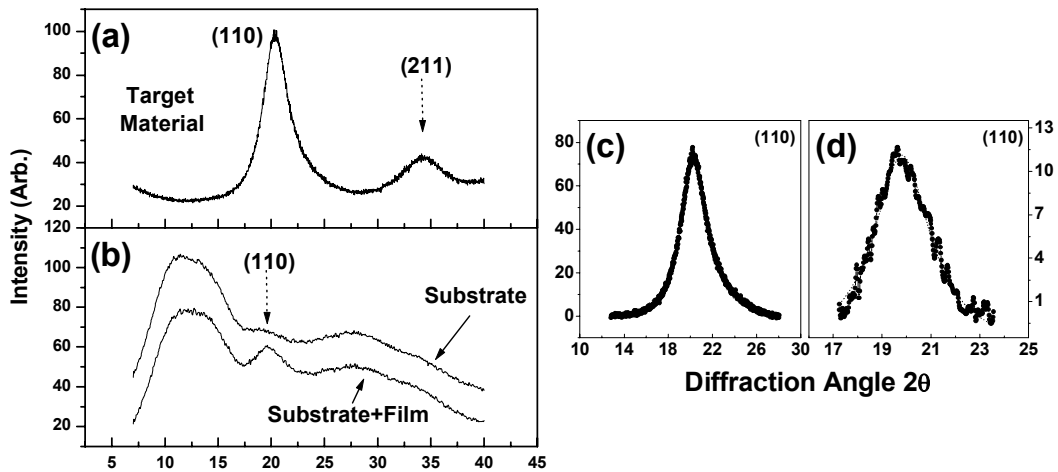


**Figure 3.11:** X-ray diffraction patterns from (a) METGLAS<sup>®</sup> 2605SC ribbon targets. (b) Glass substrate and a 500nm film deposited on a glass substrate (4mT, 75W). (c) Lorentzian fit to the (110) peak from ribbon - FWHM:  $2.9^\circ$ . (d) Lorentzian fit to the (110) peak amorphous film - FWHM:  $3^\circ$

### 3.4 X-Ray Diffraction

X-ray diffraction measurements were performed to ensure that the films deposited by RF magnetron sputtering were amorphous; the analysis was performed using  $\text{MoK}_\alpha$  radiation. A number of samples were also analysed in Madrid using  $\text{CuK}_\alpha$  radiation. The X-ray diffractometer (Philips) was an automated system which operated in the  $\theta$ - $2\theta$  geometry and is shown schematically in Figure 3.10.

The sample, X-ray source and detector are all in the same plane, and collimating slits are positioned in the beam path to ensure a well defined focused beam. The sample holder and detector are mechanically coupled such that a rotation of the sample through an angle  $\theta$  would ensure that the detector would rotate through an angle  $2\theta$ . This ensured that the incident and reflected angles always remained equal. The angular range and step size were software controlled and the recorded data was stored digitally.

The X-ray diffraction patterns obtained using this technique were analysed using the Bragg equation

$$2d_{hkl} \sin \theta = n\lambda \quad (3.4)$$

where  $\lambda$  is the wavelength of the radiation,  $n$  is an integer,  $d_{hkl}$  is the interplanar spacing, and  $\theta$  is the angle between the plane of atoms and the x-ray beam (see Elliot (1984) for details). The interplanar distance between consecutive planes of atoms is a function of the Miller indices ( $h,k,l$ ) and the lattice parameter  $a_l$ . For cubic structures the interplanar spacing  $d_{hkl}$  can be obtained from the following expression

$$d_{hkl} = \frac{a_l}{\sqrt{h^2 + k^2 + l^2}} \quad (3.5)$$

In the case of amorphous materials, there is a distribution of the interplanar spacing because of the random nature of the structure. This leads to much broader peaks in the X-ray diffraction patterns. The amorphous nature of the thin films was compared with the amorphous METGLAS<sup>®</sup> 2605SC ribbon which was used as the target material. Figure 3.11a shows a typical diffraction pattern obtained from a METGLAS<sup>®</sup> 2605SC target ribbon; the peaks have been labelled using the lattice parameter of 0.2866nm for  $\alpha$ -Fe. Figure 3.11b shows a typical X-ray diffraction scan for an amorphous FeSiBC film which has been deposited onto glass. The X-ray scan for the glass substrate alone has also been included for comparison. Figures 3.11c,d, represent the (110) peak to which a Lorentzian fit has been applied to obtain full width half maxima (FWHM). The values obtained for the amorphous films ( $3^\circ$ ) compare well with that of the target material ( $2.9^\circ$ ) which indicates a similar amorphous phase.

### 3.5 Magneto Impedance (MI)

The experimental apparatus used to perform the MI measurements presented in Chapter 6 is shown in Figure 3.12. The MI measurements were performed at the Instituto de Magnetismo Aplicado in Madrid. The system was constructed and maintained at the time of the measurements, by J.P. Sinnecker [J.P. Sinnecker et al (1998)].

The basic principle of the measurement is that a low intensity alternating current is passed through the magnetic sample and the changes in its impedance are measured as a function of applied field (see Chapter 6).

The alternating current was provided by a Hewlett-Packard 38589A spectrum/network analyser, which could deliver a current in the range of 1-100mA up to driving frequencies of 150MHz. At the time of the measurements, frequencies up to 10MHz only were available. To ensure that a constant current was being delivered, the voltage,  $V_R$  across a non-inductive resistor was monitored; this resistor was in series with the sample. The voltages across both the resistor and the sample were measured by the spectrum/network analyser. The samples were orientated so that the magnetic field of the Helmholtz coils was in the plane of the sample and parallel to the current direction. The Helmholtz coils, in conjunction with the KEPCO BOP 50-4M current source, provided a maximum DC field of 10.5kA/m. The measurement system was fully automated using a computer; this swept the magnetic field and recorded the voltage across the sample. At each measurement point, the voltage across the resistor was monitored and recorded, and any changes in the current were then automatically corrected.

The electrical contacts to the samples were made using high purity copper strands which were bonded to the surfaces of the films using silver paint. This was allowed to dry for 24 hours to ensure a good electrical contact. Coaxial cabling was used throughout the apparatus to screen out unwanted signals.

Prior to the performance of any MI measurements it was first established that the current amplitudes which were being used were not causing the films to heat up due to eddy current heating, which would effect the impedance measurements. The impedance of the sample was monitored over a period of 20 minutes at a fixed current. It was found that the current amplitudes were sufficiently small and there appeared to be no measurable changes in the impedance. To verify that no external artificial signals were present in the system, a high purity copper strand was substituted for a magnetic sample; no changes in the impedance were obtained. The system was able to measure impedance ratios as small as 0.1 %.

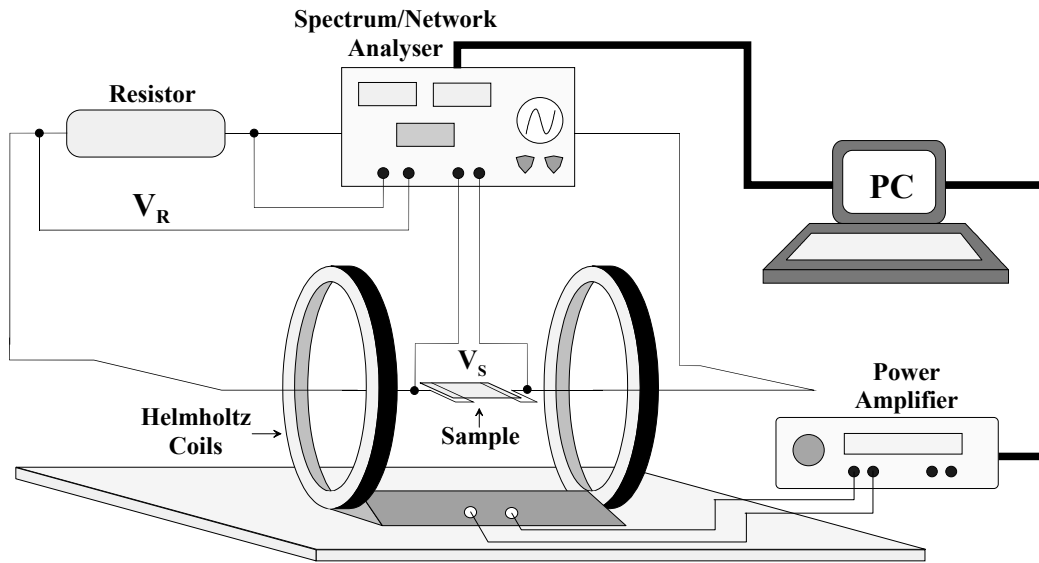


Figure 3.12: An illustration of the MI apparatus used to perform the MI analysis.

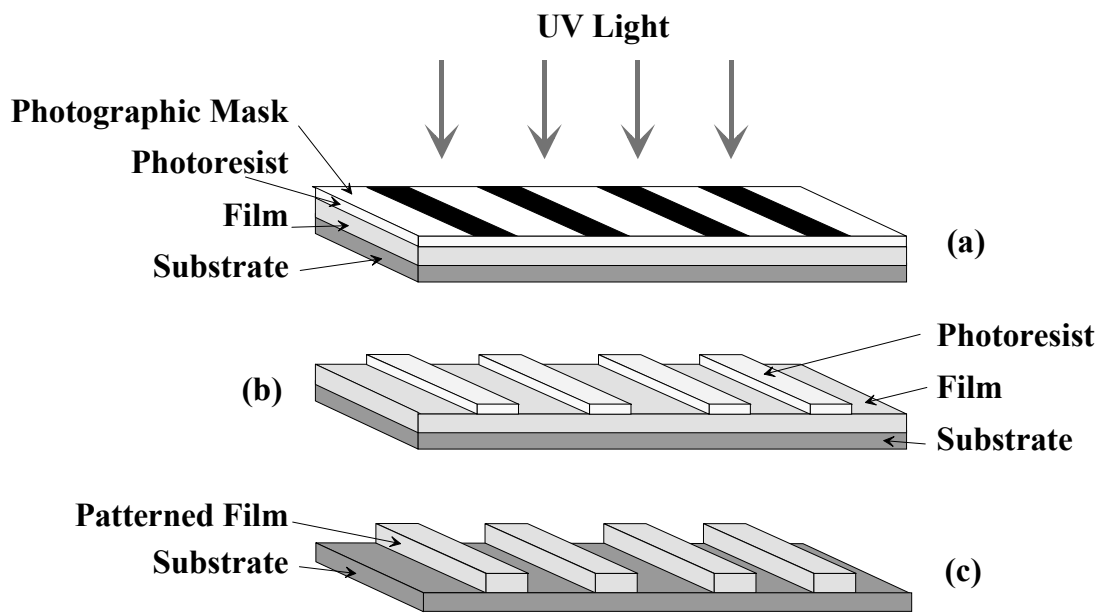


Figure 3.13: Schematic representation of the stages involved in photolithography.

### 3.6 Patterning by photolithography

Photolithography is a technique which is widely used in industry in the manufacture of integrated circuits or semiconductor components. The technique involves transferring a pattern from a photographic mask onto a film so that a pattern can be chemically etched out of the film.

The cleaned film is first coated with an organic photosensitive material known as photoresist. This is allowed to dry and then exposed to UV light through a photographic mask (Fig. 3.13a). The photoresist is developed using a suitable developing agent which removes regions of the photoresist which have de-polymerised due to the expose to the UV light (Fig. 3.13b). The remaining regions of the photoresist act as a barrier during the etching stages. After completion of the etching process, the remaining photoresist is removed using a suitable solvent (Fig. 3.13c) leaving an etched film of the mask.

The films were carefully cleaned by boiling the samples in a solution of trichloroethane. This removed any oily residues and any foreign surface particles. For more stubborn dust particles the surfaces of the films were wiped using cotton buds soaked with trichloroethane. In all instances the films were dried in a stream of dry nitrogen gas. It was important that the surfaces of the films was dust/grease free in order that the photoresist adhered to the surface of the films so as to protect the film beneath. The films were baked at 100<sup>0</sup>C on a hot-plate for 1 minute to ensure no water vapour was present before finally being coated by a few drops of photoresist, with the excess being spun off. The photoresist was also allowed to dry for 1 minute on a hot-plate before being exposed to the UV light through the photographic mask. The resist was developed, exposing regions of the films which were to be etched away. The etchant used was a solution of nitric acid (3 parts of water to 1 part of nitric acid). The etch time was determined by using sacrificial film pieces. On completion of the etching process, the remaining resist was removed using a solvent to reveal the patterned film.

### 3.7 References

- Allied (1995) Manufacturers Data; Allied Signal Corporation (1997).
- Elliott (1984) "Physics of amorphous material", S.R. Elliott, Longman Inc., pp55, (1984).
- Squire et al (1988) "Digital M-H plotter for low-coercivity metallic glasses", P.T Squire, S.M. Sheard, C.H. Carter, M.R.J. Gibbs, J. Phys. E. Sci. Instrum. (21) 1167 (1988).
- Sinnecker et al (1998) "An automated system for measuring the complex impedance and its relaxation in soft magnetic materials", J.P. Sinnecker, M. Knobel, M.L. Sartorelli, J. Schonmaker, F.C.S. Silva, J. de. Phys. IV Vol.8 No.(2). 665 (1998).
- Wagendristel et al (1994) "An introduction to physics and technology of thin films", A. Wagendristel, Y. Wang, World Scientific Publishing, pp31-40, (1994).

## 4.0 Thin Film Deposition

The process of sputter deposition for the production of thin films in an increasing number of applications has increased widely in popularity. This is due to its ease of operation, accurate control of the growth rate (thickness), excellent film adhesion and a high degree of reproducibility of the deposited films.

This chapter is concerned with the deposition and optimisation of the magnetic properties of amorphous FeSiBC thin films which have been sputtered deposited from METGLAS<sup>®</sup> 2605SC (Fe<sub>81</sub>Si<sub>3.5</sub>B<sub>13.5</sub>C<sub>2</sub>) ribbon targets, which were obtained from Allied Signal. The objective of this study was to obtain films which exhibited similar magnetic properties to those of the ribbon material. The results and findings presented here were obtained using radio frequency (RF) magnetron sputter deposition. An overview of sputter deposition of thin films is also presented, in order to highlight the problems of which one needs to be aware in the deposition of amorphous thin films, along with their general properties.

### 4.1 Introduction

Since it was first discovered that melt-spun, amorphous, transition metal-metalloid alloys had excellent soft magnetic properties, there has been a tremendous amount of work done on these materials with a view to optimising their magnetic properties. The properties for Fe, Co and Ni based amorphous melt-spun alloys has been extensively documented [Luborsky (1980)], and commercial organisations such as Allied-Signal and Vacuumschmelze now produce a large range of melt-spun alloys. These are used in a wide variety of modern electrical and electronic applications. See Ref. List (4.1) for further information on types of applications where magnetic materials are used.

Because of their soft magnetic properties melt-spun materials in the form of ribbons and wires (see Chapter 6) have also been exploited as stress and field sensors [Lenz (1990)]. Despite the wide availability of such materials in ribbon or wire form, in their current form they still have a number of disadvantages for modern sensor applications. Generally, the as-cast, melt-spun ribbons suffer from random residual stresses induced during the production stage. This has the effect of degrading the magnetic properties, especially if the material has a large magnetostriction, which is needed for stress-based sensors. This can lead to complex, random domain structures, which complicates both the understanding of the magnetisation process within the material and the output from the sensor itself. Ideally, for stress-based sensors, the domain structure should be orientated perpendicular to the direction of the applied stress to maximise the magnetoelastic effect ( $\lambda_s > 0$ ), or, in the instance of magneto impedance sensors, perpendicular to the applied current (see MI). This problem is overcome by annealing the ribbons in a magnetic field; this reduces the as-cast, random, residual stresses and induces a uniaxial domain structure. In many instances, the ribbon material is usually bonded to a rigid surface, depending on the type of sensor (i.e. Cantilever type sensor [Mitchell et al (1986)]), which can induce extrinsic random stresses because of distortions introduced when the adhesive dries; this can

alter the optimised domain structure previously induced by field annealing. The annealing of some ribbons, such as the METGLAS<sup>®</sup> 2605SC ribbon used in this thesis as the target material, has the undesirable effect of degrading the ductility. In most instances, this not a problem, since the ribbon is usually bonded to a rigid surface, where the stresses transmitted from the rigid surface to the ribbon are relatively small.

However, advances in technology generally mean some form of miniaturisation. Sensors are now being integrated and microfabricated onto commercially important substrates such as silicon and gallium arsenide in such ways that they are compatible with conventional microelectronic fabrication. This allows all the components required for the sensor device to operate to be fabricated on the one substrate. To keep in step with such developing technologies, the potential of these amorphous alloys are now being exploited in thin film magnetic sensors. Magnetic thin films also allow the fabrication of more exotic, three dimensional structural sensors, such as membranes [Karl et al (1999)] and cantilevers [Karl et al (1999a)] on a micron scale. Ribbon materials in their current form would be difficult to incorporate into such small sensor elements. By no means does this mean that magnetic thin films do not pose any problems of their own. The magnetic and structural properties of thin films are strongly dependent upon the deposition process and the parameters under which the film is deposited. Sputtering and evaporation techniques are the two common methods of preparing amorphous magnetic thin films, with the former being the most popular of the two. To achieve device quality thin films with similar magnetic properties to that of the ribbon materials, three main requirements need to be fulfilled: the composition of the film needs to be correct to maintain the required magnetic properties, the microstructure needs be amorphous and, if possible, a uniaxial anisotropy needs to be induced in a given direction. Controlling the composition of the depositing film by vapour deposition is a very difficult process, because of the widely differing melting points and vapour pressures for the different elements. However, sputter deposition tends to preserve the composition of the depositing film [Elliot (1984)] as that of the target alloy, since the sputtering rates tend to vary less widely and this therefore is the more popular method of the two. The very high cooling rates generally ensure the structures of the deposited films are amorphous under most conditions or, at worst, nanocrystalline. The magnetic anisotropy and the methods of controlling the anisotropy in thin films is discussed in the following chapter.

## **4.2 Parameters which effect sputter deposited films**

Sputter deposition is a complex process where there are combinations of sputtering parameters which influence both the magnetic and structural properties of the depositing film. Generally, it is found that one set of sputtering parameters on a given sputtering system cannot be transferred to another system to deposit films with the same magnetic and structural properties. This illustrates how sensitive the films are to the sputtering parameters (see below). It also explains why one finds that similar magnetic films deposited by different researchers are performed under different sputtering conditions. Careful control of the sputtering parameters is essential to prevent the films suffering from residual stresses and

columnar growth (see below) which can severely affect both the magnetic and structural properties. The stresses which deposited films suffer from arise from two contributions: the extrinsic stresses which are brought about by differing thermal expansion coefficients of the film and substrate and the intrinsic stresses which are a result of the sputtering process itself and are discussed below.

The dynamics of the sputtering process have been described in Section 3.1.1, where the basic processes occurring at the target and substrate have been discussed. It is the kinetics of the sputtering process and the mobility of the sputtered atoms at the surface of the substrate which determine the final structural and magnetic properties of the thin film. This process is sensitive to many parameters which need to be carefully controlled in order to deposit films which are unstressed. Factors which influence these processes are listed below.

**4.2.1 Pressure:** The pressure of the sputtering gas is very important, not only does it provide the inert gas ions needed for the sputtering process of the target, but it also acts as a moderator for the ejected atoms from the target. By careful control of the pressure, one can influence both the structural and magnetic properties of the film. At low pressures, the sputtered and reflected neutral atoms have much higher energies than the plasma gas between the target and substrate and arrive at the substrate with super-thermal energies. The sputtered atoms in this situation have a high surface mobility at the substrate. At higher sputtering pressures, the sputtered and reflected neutral atoms, are thermalised [Somekh (1984)] by the plasma gas, due to the increased number of collisions before arriving at the substrate. As a consequence, the sputtered atoms will have a lower surface mobility at the substrate. This will have a significant effect in the growth kinetics of the depositing film and is reflected in the magnetic and structural properties. It is therefore essential that the sputtering pressure is carefully investigated to obtain the optimum magnetic and structural properties.

There have been numerous studies exploring the effects of pressure on sputter deposited films, and it is well established that the pressure has a significant effect on the magnetic properties, mainly through stress [Ref. List (4.2)] and columnar growth [Shimada et al (1981), Leamy et al (1979)]. The as-deposited films tend to suffer from residual stresses if the effects of pressure have not been accounted

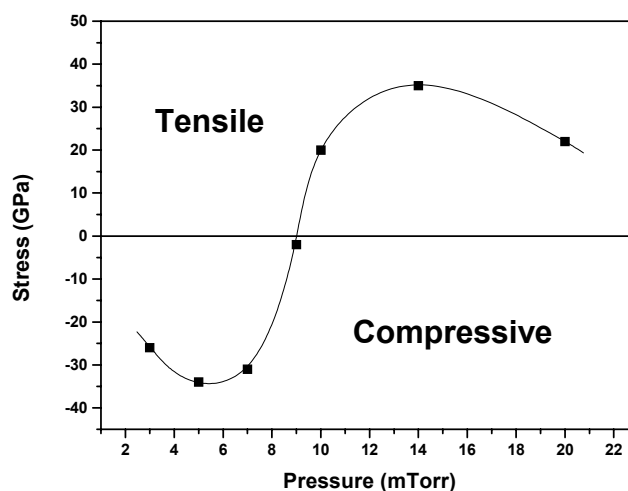


**Figure 4.1:** Stress dependence as function of pressure for Co-based films obtained by RF sputter deposition. [Data obtained from Materne et al (1988)].

for. This generally changes from being a compressive to a tensile stress as the sputtering pressure is increased. An example of such an effect is shown in Figure 4.1, where an investigation of stress in sputter deposited low magnetostrictive Co-based films was performed by Materne et al (1988) as a function of pressure. At low argon pressures, the films were found to be under compressive stress, whilst at higher pressures the stress was found to be tensile. A transition region at approximately 9mTorr existed where the stress changes sign, and the as-deposited films were found to be in a 'stress free' state; this also corresponded to the lowest values of the coercive field (15-30 A/m) as a function of pressure. It is the general consensus that at low pressures, the high surface mobility of the sputtered atoms promotes the formation of dense films which are under compressive stress. The compressive stress is inferred to be due to argon entrapment and lattice distortion caused by energetic incident particles. At higher pressures, the sputtered atoms are less energetic because of the increased scattering. This lowers the surface mobility of the sputtered atoms; it also causes the sputtered atoms to arrive at the substrate at more oblique angles, because of the increased scattering. This can result in the films having a columnar morphology, which induces a tensile stress in the film. The columnar growth is a result of the self-shadowing of the incident atoms by those already incorporated into the growing film [Leamy et al (1979)]. This is obviously controlled by the surface mobility of the sputtered atoms, which in turn is related to the incident energy of the sputtered atoms. As the pressure is further increased to even higher pressures, there is a reduction in tensile stress (Fig. 4.1) in the films, because of the more distinct columnar structure. The more open, columnar morphology is said to prevent the ease with which the stress can be transmitted between the columns [Hudson et al (1996)]. It has also been suggested that the tensile stress at higher pressures may be due to oxygen contamination, since there seems to be a strong correlation between oxygen incorporation and columnar growth morphology developed at high pressures [Leamy et al (1978,1979), Materne et al (1988)]. However, the effect of oxygen on stress is not clearly understood, since there have also been reports that at high pressures, oxygen incorporation leads to compressive stresses [Hoffman (1976), Hudson et al (1996)]. Similar trends due to pressure also occur on other magnetic systems such as FeCoB [Shimada et al (1981)], and FeSiB [Naoue et al (1979)] thin films which have been sputtered deposited. It should be noted that intrinsic stress from sputtering is not only confined to magnetic films and can occur in any sputter

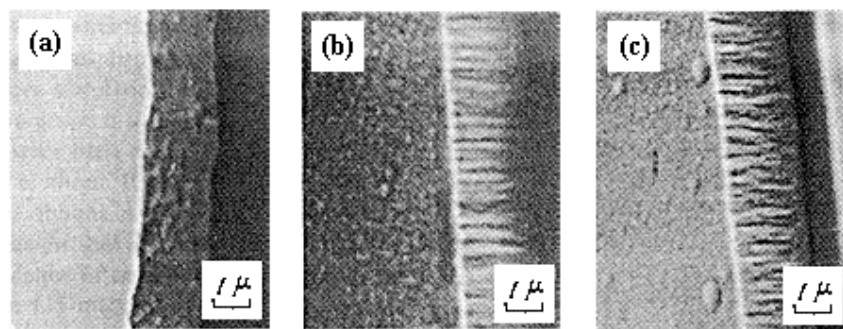


**Figure 4.2:** FeCoB films obtained by RF sputter deposition. Scanning electron microscopy of fractured edges of films deposited at (a) 3mTorr, (b) 50mTorr, and (c) 150mTorr indicating the development of columnar morphology at high pressures. [Data obtained from Shimada et al (1981)].

deposited systems, for example copper [Craig et al (1981)] or tungsten [Vink et al (1993)] films. The morphology of thin films has been summarised by Thornton et al (1974) and Craig et al (1981), where they describe various structure zones, depending on the sputtering pressure and substrate temperature. They infer that the stress and structure of the film is related to the energy of the bombarding particles at the substrate during the sputter deposition. Dense non-columnar films are obtained when the impinging particles (sputtered and reflected neutrals) have high kinetic energies (low pressures), and a distinct columnar texture is developed at low particle energies (high pressures). This is shown in Figure 4.2, where FeCoB thin films were sputter deposited by Shimada et al (1981) at various argon pressures to investigate the magnetic and structural properties. It was found that the columnar texture only appeared at high sputtering pressures ( $>50\text{mTorr}$ ), and the films deposited at low argon pressures ( $<10\text{mTorr}$ ) showed no characteristic structure. These results are in agreement with other studies [Naoe et al (1979), Materne et al (1988)] which also have found that films deposited at low pressures do not have any characteristic columnar morphology. It is well accepted that to obtain good magnetic amorphous films with a high saturation magnetisation and a low coercive field, the sputtering conditions need to be carefully chosen to suppress the formation of columnar growth, which is found to be unfavourable for the soft magnetic properties.

In most sputtering systems, the sputtering gas, usually argon, is allowed to flow continuously through the chamber at a constant pressure; this helps with the removal of any out-gassing impurities which could otherwise build up within the chamber and be incorporated into the depositing film. It is important that the gas flow-rate is not too excessive, since this can lead to the existence of pressure gradients within the chamber and cause non-uniform sputtering of the target, which can be reflected in a non-uniform film thickness.

**4.2.2 Target-substrate separation:** The separation between the target-substrate has a similar effect, as does the sputtering pressure on the growth kinetics. Increasing the separation between the target-substrate has the effect of lowering the mobility of the atoms at the substrate; the reverse is true when the separation between the target-substrate is decreased. This assumes that the sputtering power does not have total dominance over the energy of the particles. A number of studies [Hudson et al (1992,1996)] have been performed to investigate the relationship between the pressure and target-substrate separation. It has been found by Hudson et al that a relationship exists between the pressure  $P$ , the target-substrate separation,  $d$ , and the stress found in the sputter deposited films. It was reported that films deposited at low values of the product,  $Pd$ , produced films which were under a compressive state of stress, whereas films deposited at high values of the product,  $Pd$ , were under a state of tensile stress. It was inferred that the stresses present in the films were related to the energy of the bombarding particles, as discussed above for pressure.

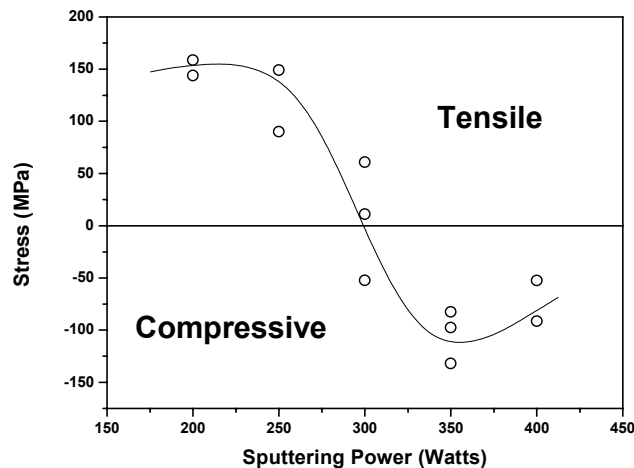


**Figure 4.3:** Stress dependence as function of sputtering power for tungsten films obtained by sputter deposition. [Data obtained from Wagner et al (1974)].

**4.2.3 Sputtering Power:** The sputtering power also has a similar effect to that of the pressure as described above. Figure 4.3 shows the variation in stress for sputter deposited films as the sputtering power is increased. It can be seen that, at low sputtering powers, the film is in a state of tensile stress, whereas the stress state of the films becomes compressive at higher powers. This is due to the increasing kinetic energies of the particles and hence surface mobility. The deposition rate increases linearly with increasing power but, from Figures 4.1 and 4.3, it is clear that to obtain stress-free films, the deposition rate is somewhat restricted by these parameters. The sputtering rate can be increased by use of a magnetron (Section 3.1.3) in conjunction with the target. This produces a denser plasma at the target surface, which increases the deposition rate without increasing the sputtering power. However, the use of low sputtering powers ensures that the system, target and substrate temperature rises are minimised.

**4.2.4 Substrate temperature:** The substrate temperature is very important in controlling the magnetic and structural properties of the depositing film. In the situation where there is a large difference in the thermal expansion coefficients of the depositing film and substrate, it is essential that the substrate temperature is maintained close to room temperature. This will minimise the stresses induced in the film after the deposition, as the film and substrate contract differently on cooling. The temperature of the substrate will also influence the surface mobility of the sputtered atoms, which will therefore control the structure and intrinsic stresses due to the sputtering process. The substrates are usually water-cooled through the substrate platter, but there can still be a significant increase in the temperature of the surface of the substrate, depending on the sputtering conditions, especially if the substrates are poor conductors such as glass, or they are very thick. The low sputtering pressures used during the deposition also means the thermal contact between the substrate and platter is not ideal. The increase in the surface temperature is mainly due to energetic sputtered atoms and secondary electron bombardment of the substrate. Secondary electron bombardment is significantly minimised on magnetron sputtering systems, where the electrons are captured by the magnetic field. Ounadjela et al (1987) have demonstrated that, by applying a DC magnetic field parallel to the substrate at the

substrate platter, it is possible to reduce the substrate temperature by 150<sup>0</sup>C in RF sputter deposition systems. It was inferred that this was due to the reduction of secondary electron bombardment. The only disadvantage with this method is that the magnetic anisotropy of the film is essentially controlled by the applied field.

**4.2.5 Nature of substrate:** The structure and surface condition of the substrate is very important in determining the magnetic and structural properties of the film. It is important to be aware of the thermal expansion coefficients of the substrate and the depositing film. Large differences in the expansion coefficients can cause extrinsic stresses to be introduced into the film, which can influence the magnetic properties such as the anisotropy via the magnetostriction. Any texturing of the substrate can influence texture into the depositing film. The first few layers of the depositing film are expected to conform with the texture, contours and imperfections of the substrate. For thin films, the magnetic properties may be sensitive to scratches or imperfections in the substrate, as will the surface mobility of the atoms since they will need to overcome these obstacles to remain mobile. In the case of amorphous films, the films are deposited onto smooth, amorphous substrates such as glass, or silicon/gallium arsenide substrates which have an amorphous oxide layer. This prevents any possible texturing effects being induced from the substrate. The cleanliness of the substrate surface is important to prevent contamination of the films from oily/greasy residues, which can also cause the films to de-laminate. A number of methods are used to remove surface dust and contamination from the substrates:

[1] Substrates are physically cleaned using degreasing solutions such as isopropanol, using fibre-free cloths in conjunction with dry nitrogen gas.

[2] Ultrasonic agitation in an isopropanol bath.

[3] Ion bombardment of the substrates prior to deposition of the film. This is an effective method of removing any surface contamination. This process is also referred to as pre-sputtering. However, care must be taken to ensure that the surfaces of the substrates do not become roughened in the process, which can affect the magnetic properties by introducing pinning sites for domain walls. The pre-sputter cleaning also increases the temperature of the substrate significantly, compared to the temperature during the deposition. If the deposition of the film commences immediately on completion of the sputter clean, this can cause the first layers of the film to be deposited onto a substrate at a much higher temperature, compared to the rest of the depositing film, thereby placing the lower layers of the film under a compressive state of stress as the substrate equilibrates to the deposition temperature.

The cleaning procedure adopted is dependent upon the type of substrate, and whether or not there are any fabricated devices on the substrates which could be affected.

Another important point about the substrates that one should be aware of, is their thermal and electrical properties. Amorphous films deposited onto good thermal conductors, can be remarkably different to those deposited onto an insulating substrate under identical sputtering conditions. This is usually a result of the much cooler substrate surface, which will affect the surface mobility of the sputtered atoms. It should be remembered that insulating substrates can only be sputter cleaned by RF sputtering, unless an ion gun is added to other types of sputtering systems.

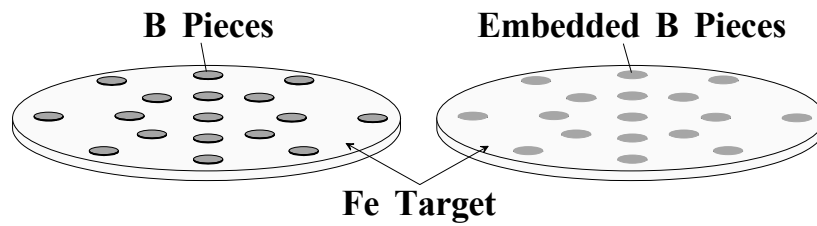


**Figure 4.4:** Target arrangements used in the deposition of metalloid films.

**4.2.6 Target Composition:** The nominal film composition and uniformity of the magnetic properties are determined by the target. It is therefore important that the composition of the target is correct and uniform throughout the target. In most instances, the target consists of a solid disc of the correct composition which has been carefully cast. Other methods involve placing small, circular pieces of various pure elements onto the main circular target [Naoe et al (1979)] or embedding circular pieces [Shimada et al (1979)] into the target as shown in Figure 4.4 at regular intervals. By varying the number of pieces it is possible to control the composition of the film. In more elaborate systems, to overcome the problems with non-uniform compositional targets, the substrate platter is slowly rotated [Aboaf et al (1978)] to ensure the composition is uniform throughout the film.

**4.2.7 Substrate Biasing:** Substrate biasing is usually achieved by applying a negative, or positive, DC potential to the substrate platter. Applying a negative bias to the substrate during the deposition will cause the depositing film to suffer from a bombardment of positive gas ions and is referred to as bias sputtering. This can have the effect of increasing the temperature of the substrate and hence surface mobility of the sputtered atoms. The process can also lead to the incorporation of sputtering gas, giving rise to compressive stresses and it can also be used to control the final composition of the film. A positive bias is applied to minimise the bombardment of the film from positive gas ions, but this can have the effect of increasing secondary electron bombardment of the substrate platter and oxygen incorporation. The effects of substrate biasing have shown that a negative bias produces compressive stresses, whereas a positive bias produces tensile stresses in thin films [Ohkoshi et al (1985), Leamy et al (1979), Wagner et al (1974)].

### 4.3 Magnetic properties of thin films

It has been confirmed by many researchers [Ref. List (4.3 & 4.4)] that it is possible to deposit amorphous magnetostrictive thin films, which have excellent magnetic properties. In most cases, it has been highlighted that the sputtering conditions have a significant effect on the magnetic properties and structure. The magnetic properties in particular have been investigated as a function of sputtering pressure [Ref. List (4.4)], since it is a parameter which is easily controlled and does not generally influence the sputtering process apart from moderating the kinetic energies of the particles arriving at the substrate. Varying the sputtering power for example, increases the sputtering rate, the target temperature, the substrate temperature from the increased electron bombardment, together with the

kinetic energies of the sputtered and reflected particles arriving at the substrate. It is well established that the magnetic properties of deposited films are very sensitive to intrinsic stresses, which can severely affect the magnetic properties such as the coercive field and the anisotropy field. By careful control of the pressure, it has been shown that stresses in the deposited films can be minimised [Materne et al (1988)] to give low coercive field values. The effect of pressure on the coercive field is illustrated in Figure 4.5, for three Fe-based alloys. It can be seen that the coercivity is a strong function of pressure, and clear minima in the coercivity exist in the region of 15-20 mTorr for these magnetic films. The changes in the coercivity are essentially due to variations in the induced stresses in the deposited films as discussed previously. It should be pointed out that Kazama and Heiman et al (1979) have ruled out the possibility that the variation is a result of any compositional changes, since no such changes were found for the FeSiB and FeCCrP films, which displayed similar coercivity trends to the FeC films and which did show some variation in composition as a function of pressure. It was also shown that an obvious correlation existed between the coercivity and the anisotropy field, which seemed to imply that the variations were a consequence of stress. This was confirmed by annealing the samples, which exhibited high coercive ( $>400\text{A/m}$ ) and anisotropy ( $>32\text{kA/m}$ ) fields, to relieve the induced stresses present. The corresponding values for the coercive and anisotropy fields were found to be less than  $80\text{A/m}$  and  $7\text{kA/m}$  respectively. The conclusion that stress was the dominant factor in controlling the magnetic properties was further strengthened by the deposition of CoFeB thin films, which exhibit zero magnetostriction ( $\lambda_s \approx 0$  ppm). The deposited films displayed coercive and anisotropy field values less than  $80\text{A/m}$ , irrespective of the sputtering pressure. The magnetic properties of these films were not sensitive to the induced stresses because of the zero magnetostriction. The effects of stress are found to be more pronounced in highly magnetostrictive materials, than in the zero magnetostrictive materials; this is as one would expect. The pressures at which the soft magnetic properties are obtained usually corresponds to the films being in the most 'stress free' state.

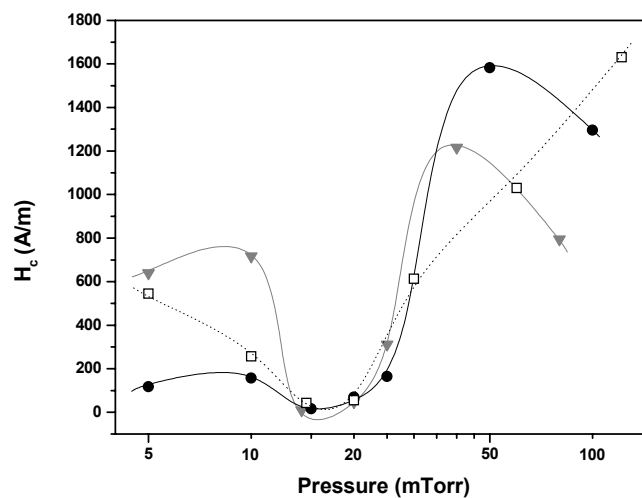


**Figure 4.5:** Coercive field dependence as function of sputtering pressure for films obtained by sputter deposition. Inverted triangles represent FeC ( $\lambda_s=15$  ppm), open squares represent FeSiB ( $\lambda_s=20$  ppm) and solid circles represent FeCrPC ( $\lambda_s=10$  ppm) thin films. [Data obtained from Heiman et al (1979), Kazama et al (1979)].

As discussed earlier, the magnetic properties are dependent upon a number of sputtering parameters and it is important to fully investigate the effects of these parameters on the magnetic properties. Naoe et al (1982) have shown that optimising the sputtering pressure for one magnetic system does not necessarily imply that other magnetic systems will also produce soft magnetic properties at the same pressure. In the instances where stress is a dominant factor in highly magnetostrictive films, the magnetic anisotropy will be generally be determined by the sign (tensile or compressive) and magnitude of the stress present. It has been reported [Ref. List (4.5)] that the magnetisation in the as-deposited magnetostrictive amorphous films can be perpendicular to the plane of the film. This is usually the result of the intrinsic stresses which are induced during the sputtering process, coupling with the magnetisation via the magnetostriction. A perpendicular anisotropy will be induced in positively magnetostrictive films, if large bi-axial compressive stresses exist within the film. Tensile stresses will induce an in-plane magnetic anisotropy. The reverse is true for negatively magnetostrictive films where large bi-axial tensile stresses will result in the magnetisation lying out-of-plane. Heiman et al (1978) and Kazama et al (1978) have shown that the magnetic anisotropy for positively magnetostrictive films is indeed out-of-plane, and is the result of compressive stresses, since deposition of CoFeB ( $\lambda_s \approx 0$  ppm) films, resulted in an in-plane magnetic anisotropy. Similar results are also reported by Kobliska et al (1978). In both cases, the perpendicular anisotropy of the films could be transformed by appropriate annealing to relieve the residual stresses so that the magnetic anisotropy lay in the plane of the film. Perpendicular anisotropy can also be a consequence of columnar morphology, which can appear under certain sputtering conditions, mainly at high sputtering pressures as found by Materne et al (1988). Films of CoZrNb ( $\lambda_s = -0.6$  ppm) were found to possess perpendicular anisotropy at high pressures, where the residual stress was found to be of the tensile form, and the magnetisation was in-plane at low pressures where the stresses in the films were compressive (Fig. 4.1). This is the opposite to what has been discussed for positive magnetostrictive films. On annealing the films, it was found that the films deposited at low pressures, and which were initially in a compressive state, were now in a state of tensile stress, and the films deposited at high pressures were still in a state of tensile stress. The magnetic anisotropy of the films at low pressures was still in-plane and magnetic anisotropy of the films at high pressures was still perpendicular. This indicates that the perpendicular anisotropy at the higher argon pressures is not the result of stress, since all films were in a state of tensile stress after annealing. Scanning electron microscopy of the samples clearly indicated the formation of columnar morphology for films deposited at high pressures, which was absent in the films deposited at low pressures. It was therefore presumed that the columnar structure was the cause of the perpendicular anisotropy, due to shape anisotropy of the columnar structure. Similar findings have also been reported by Shimada et al (1982).

It is well established that the composition of the bulk metal-metalloid amorphous ribbons generally does not deviate much from the 80% transition metal and 20% metalloid composition ratio [Luborsky et al (1979,1980,1980a)], where the optimum magnetic properties are found to occur. The wider compositional ranges possible from sputtering amorphous thin films has also been investigated, and it is

Composition	B <sub>s</sub> (T)	H <sub>c</sub> (A/m)	H <sub>k</sub> (A/m)	λ <sub>s</sub> (ppm)	Ref.
Fe <sub>73</sub> B <sub>27</sub>	1.4	≤8	≤553	50	Kobliska et al (1978)
F <sub>80</sub> B <sub>20</sub>	-	3.2	560	-	Tsunashima et al (1981)
Fe <sub>73</sub> Si <sub>6</sub> B <sub>21</sub>	1.2	≤16	≤474	26	Kobliska et al (1978)
Fe <sub>77</sub> B <sub>23</sub>	1.56	16	1400	-	Gangulee et al (1981)
Fe <sub>70</sub> Si <sub>30</sub>	1.2	≤8	≤395	30	Kobliska et al (1978)

**Table 4.1:** Magnetic properties of Fe-based films obtained by sputter deposition.

generally found that the best magnetic properties are attained at approximate ratios of 80% to 20% metal-metalloid composition. The as-deposited magnetic properties tend to suffer slightly from residual stresses, but appropriate annealing of the films has shown that the magnetic properties are quite comparable to similar compositions of amorphous ribbons. Coercive fields as low as 3 A/m and 4A/m have been obtained for F<sub>80</sub>B<sub>20</sub> and Fe<sub>79</sub>B<sub>16</sub>C<sub>5</sub> films respectively by Tsunashima et al (1981). A number of film compositions along with their magnetic properties are tabulated in Table 4.1.

It is clear from the literature that it is possible to obtain amorphous films with magnetic properties which are comparable to those of the amorphous ribbons, as long the sputtering conditions have been carefully optimised. Annealing of the samples after the deposition can further improve the magnetic properties.

## 4.4 Results and Discussions

### 4.4.1 General findings

The FeSiBC films were deposited from METGLAS<sup>®</sup> 2506SC ribbon targets obtained from Allied Signal using RF magnetron sputtering as described in Chapter 3. The compositions of the film are similar to that of the target material, which is known to display excellent magnetic properties. A number of problems were encountered at the start of the investigation, which had to be addressed. The main problem was the lack of reproducibility of the deposited films, at apparently identical sputtering conditions. It was found that the films had widely different magnetic properties ( $H_c$ ,  $H_k$ ) between consecutive runs. Pressure and power series displayed no obvious trends and they were found to be different every time they were performed. At this stage, the substrates being used were 1cm<sup>2</sup> Corning<sup>®</sup> and standard glass pieces which were glued to a standard glass slide using a high vacuum compatible glue. The slide was then mounted to the substrate platter as shown in Figure 3.4a. For consistency the glass pieces were always glued in the same position. The substrates were cleaned as described in Section 3.1.3, and then sputter cleaned for 1 minute at 5mTorr at a sputtering power of 100W. The variations seen at the fixed power and pressure were obviously due to some other varying parameter, since these two parameters were monitored and found to be very stable during consecutive depositions. It was thought the pre-sputtering of the substrates could be one of the sources of the irreproducibility, since the process does cause the substrates to heat up substantially; also, it has been shown by Mattingley (1997) that the sputtering parameters need to be carefully optimised to ensure that the substrates are not over-etched such that the surfaces become roughened. This can lead to the introduction of pinning sites for domain walls and to inhomogeneous stresses being induced in the film. The pre-sputtering of substrates was stopped since it was not possible to ascertain, at the time, if the cleaning procedure was causing the surfaces of the substrates to be cleaned differently from consecutive depositions. In most instances, the substrates cannot be sputter cleaned if the film is being deposited on to a fabricated substrate containing sensor elements, and therefore soft magnetic properties would be needed without this process. The removal of the sputter cleaning procedure seemed to have no effect, and it was decided that the problem might lie in the actual glueing of the 1cm<sup>2</sup> substrate pieces to the standard glass slides. It was thought that the glue was causing variations in the thermal contact between the 1cm<sup>2</sup> substrate pieces and the glass slide. The changing temperature of the substrate surface will affect the magnetic properties of the film, because of the variations in the surface mobility of the atoms. Films were then deposited onto complete standard glass slides, which were clamped to the substrate platter. The films deposited on the glass slides revealed that the problem was not due to the glue, and it was at this stage that it was noticed that the shape and position of the plasma itself varied between consecutive runs. This indicated that there was an electrical problem with the sputtering system, mainly the earthing around the chamber. The grounded chamber and components within the chamber ensures that the plasma gas is confined over the target area and does not come into contact with any other surface within the chamber. Any deviations in the earthing will give rise to variations in the plasma kinetics. Tests revealed that earthing on the main chamber and the

base of the chamber had become insufficient for the RF environment being used. It was found that the spring earthing clips (see Fig. 3.2) which were positioned around the base of the chamber and which made electrical contact between the base and the main chamber had become defective, and it was no longer sufficient from the point of the RF being used. The two Viton seals essentially electrically isolate the main chamber walls from the rest of the machine (see Fig. 3.2), and these spring earthing clips ground the walls in conjunction with a high density conducting braid which is attached to a single point on the chamber wall. The earthing through the spring clips had become intermittent, as had the earthing to the target and substrate shutters within the chamber. The shutters were earthed through mechanical gears which had become defective because of wear. On rectifying these problems, it was found that the plasma discharge was visibly changed, and was essentially confined over the target. The inconsistency of the magnetic properties of the deposited films at fixed sputtering parameters was also cured. This illustrates how sensitive and complex the sputtering process can be to any sputtering parameter.

#### 4.4.2 Substrate mounting

It was found that clamping the glass slides to the substrate platter, as shown in Figure 3.4a, influenced the magnetic anisotropy of the deposited films. It is shown in the next chapter that it is possible to control the magnitude and direction of the magnetic anisotropy by stressing the slides by mechanical bending. Generally, the glass slides are not perfectly flat, and this therefore induced an uncontrollable amount of stress into the films, at random, when the slides were clamped to the substrate platter. To overcome this problem, the substrates were mounted using a picture frame holder (Fig. 3.4b) which ensured that no clamping forces which could induce any preferential anisotropy existed on the substrates. The holder also ensured the free movement of the substrates, which allowed for any thermal expansion of the substrates during the deposition of the films. It also ensured the consistent positioning of the substrates on the platter.

#### 4.4.3 The effects of pressure

A range of pressure and power investigations were performed, and it was found that films deposited above a sputtering power of 120W had inconsistent magnetic properties between consecutive growths; this was attributed to the high temperature of the substrate platter. It was not possible to monitor the temperature of the substrate platter during the deposition, but it was found that it was too hot to physically touch straight after the deposition of films at high powers (80-90<sup>0</sup>C). The high temperatures cause the films to suffer from stresses as the film and substrate contract differently because of the difference in thermal expansion coefficients (FeSiBC=5.9ppm/<sup>0</sup>C glass=7ppm/<sup>0</sup>C) and also compressive stresses are induced due to the increased mobility of the sputtered atoms and argon incorporation. It was found that a sputtering power of 75W, produced films which were consistent as a function of pressure, and a reasonable deposition rate of ~5.5nm/min was attainable. More importantly the temperature of the substrate was also estimated to be between 40-100<sup>0</sup>C during the deposition at 75W; this was because of the significant decrease in heating from the plasma. This was ascertained by fixing 1cm<sup>2</sup> glass pieces to

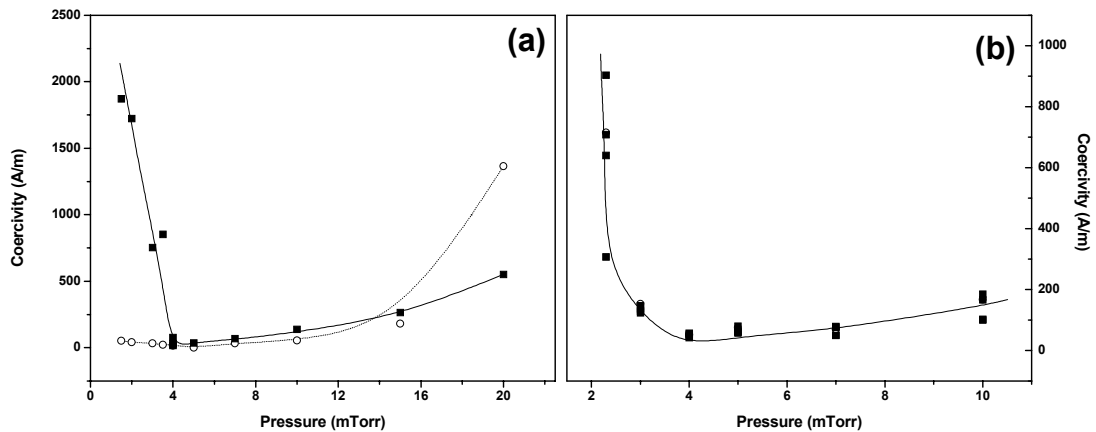


**Figure 4.6:** Pressure dependence on (a) standard glass slides and (b) 1cm<sup>2</sup> Corning<sup>®</sup>. The solid squares represent the as-deposited films, the open circles represent the films after an anneal at 390°C for 1 hour. Both pressure series were performed at 75W, and the respective films thicknesses are 750nm and 330nm. (a) Data obtained using MOKE. (b) Data obtained using MH from 1cm<sup>2</sup> pieces which were glued to a standard slide.

a standard glass slide using wax which has a melting point of 40°C and also by glueing 1cm<sup>2</sup> glass pieces coated with photo-resist (see Section 3.6). It was found that the glass pieces attached with wax fell off within the first few seconds of the deposition, indicating that the temperature was above 40°C, but the photo-resist was intact after the depositions, which implied that the temperature of the substrates was below 100°C. Prolonged heating of the photo-resist at approximately 100°C or above causes the resist to deteriorate -i.e. hard baked; the resist becomes more difficult to remove using a solvent [Karl (1998)]. The measured temperature of the substrate platter immediately (1min) after the deposition was 40-45°C. Figure 4.6 shows the coercivity dependence of the FeSiBC films deposited at 75W as a function of argon pressure on glass slides and 1cm<sup>2</sup> Corning<sup>®</sup> pieces. A clear minimum in the coercivity exists at 4-5mTorr and, as the argon pressure is decreased, there is a sudden increase in the coercivity, whereas there is a gentle increase in the coercivity with increasing pressure. The sudden increase in coercivity below 4mTorr is attributed to the large compressive stresses being induced in the depositing film, this is due to the increased kinetics of the sputtered and reflected particles at the substrate. The sign and the extent of the stress present was monitored by depositing films onto glass cantilevers 50x5x0.1mm<sup>3</sup> which were firmly glued to the glass slides to ensure good thermal contact. If the film side of the cantilever, on removal, bent in a convex form, it indicated that the film was in a state of compressive stress during the deposition; a concave cantilever indicates tensile stresses. The cantilevers were removed by dissolving the glue in acetone. Cantilevers obtained below 4mTorr exhibited large compressive stresses, whereas the cantilevers obtained above 4mTorr appeared to be flat within the experimental limit. It was therefore difficult to determine if the stress was compressive or tensile above 4mTorr, since they appeared to be equally flat as shown in Figure 4.7. The dependence of the coercivity on stress is further strengthened by annealing the films to relieve the stresses induced during the deposition. In all cases, except films grown at 20mTorr, there was a reduction in the coercivity, which was also mirrored by the annealed cantilevers (Fig. 4.7). This indicates that the coercivity is dependent

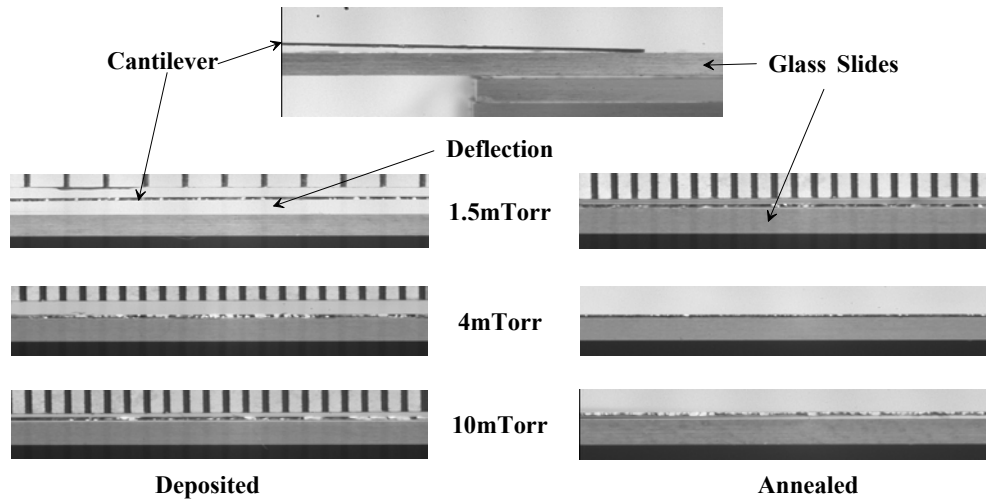


**Figure 4.7:** Glass cantilevers deposited at 75W at the pressures indicted before and after stress relief. Images taken using a Zoom lens in conjunction with a CCD camera. The cantilevers were placed on a glass slide to observe the extent of the stress present by observing the deflection indicated below. No attempt was made in quantifying the stress using this crude method.

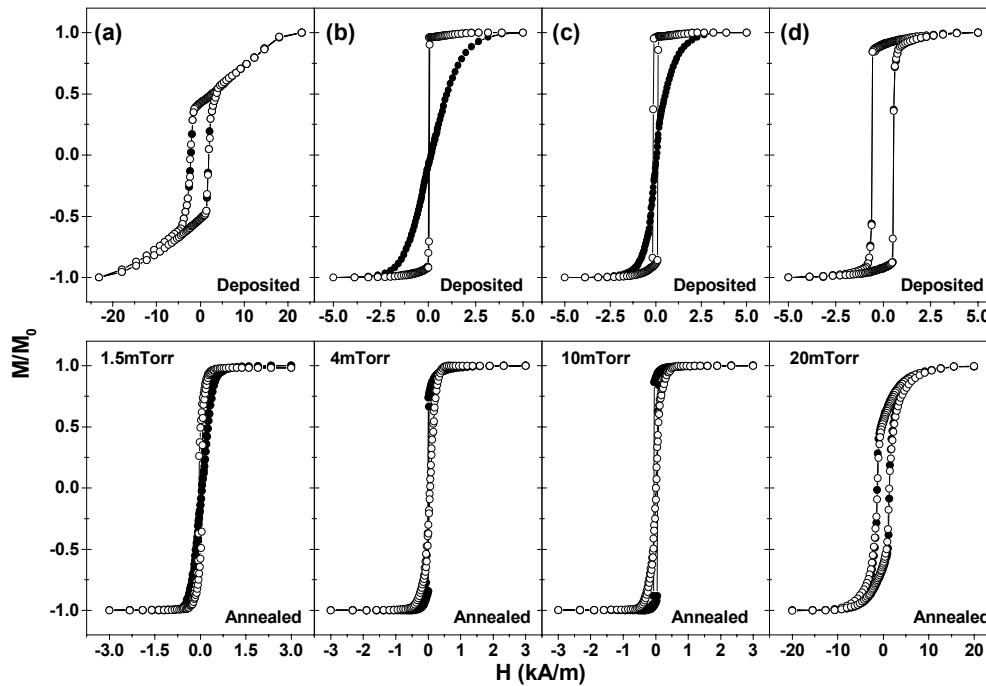


**Figure 4.8:** Orthogonal MOKE loops obtained from a FeSiBC films deposited at 75 watts at the pressures indicated, for the as-deposited state and annealed state. Films were annealed at 390°C for 1 hour for stress relief.

upon the stresses which are induced during the deposition process, as a function of pressure, as reported by other authors [Ref. List (4.4)]. Such large variations, cannot therefore, be a result of changes in the composition as a function of pressure as, shown by Mattingley (1997) and Heiman et al (1978), the compositional variations for these types of alloys are negligible over the pressure range investigated. The reduction in coercivity on annealing indicates that the high initial coercivity is unlikely to be due to the composition or crystallisation, since annealing does not change the composition, and it would induce further crystallisation on annealing, thus increasing the coercivity.

The hysteresis loops for films deposited on glass slides at 1.5, 4, 10, and 20mTorr are shown in Figure 4.8. The magnetic anisotropy in each of the deposited films is very different and it is clear that a uniaxial anisotropy appears to develop strongly in-plane as the sputtering pressure approaches 4mTorr. It should be noted that the anisotropy appears to be uniaxial because of the point hysteresis measurement, but it is shown, and discussed in the next chapter, that the films display a unique, radial magnetic anisotropy distribution [Ali et al (1998)] for films deposited at argon pressures between 4-15mTorr. This has been attributed to the residual field from the magnetron source. Below 4mTorr, the magnetic anisotropy appears to be isotropic in the plane and, from the cantilever measurements, it is known the films are under a state of high bi-axial compressive stress. The bi-axial compressive stress accounts for the isotropic in-plane hysteresis loops, since it is known that high compressive stresses in films can induce the magnetisation to lie out of the plane [Ref. List (4.2)]; this is due to the coupling between the stress and magnetostriction ( $\lambda_s=30\text{ppm}$ ). The annealing of the films deposited below 4mTorr demonstrates that the magnetic anisotropy and the initial coercivity are due to the compressive stresses, since the hysteresis loops for all samples deposited at 15mTorr or below display a similar in-plane magnetic anisotropy after annealing, which relieves the induced stresses. The MOKE hysteresis loops for the films grown at 20mTorr after annealing indicate that the perpendicular anisotropy does not decrease but, on the contrary increases, and therefore indicates the anisotropy and the increase in coercivity are not due to stress. Increases in the stress due to the annealing (thermal mismatch film/substrate) can be neglected because of other samples grown at lower pressures which were annealed at the same parameters. Materne et al (1988) have shown that films deposited at 20mTorr exhibit columnar growth; annealing the films increased both the coercivity and the anisotropy field. The possibility of the occurrence of columnar growth in the FeSiBC films deposited at 20mTorr was not verified at the time, since the results would be of no real interest to this investigation. The aim was to produce soft magnetic films, which would be useful for applications such as sensors. It is assumed that perpendicular anisotropy is a consequence of some form of columnar growth. A similar trend is also observed for films deposited onto Corning<sup>®</sup> glass, where stress dominates the magnetic properties as discussed above. Examples of hysteresis loops on Corning<sup>®</sup> glass will be discussed later.

#### 4.4.4 Substrate sputter-clean

The effects of pre-sputtering glass and Corning<sup>®</sup> substrates was investigated using the parameters which were found to be suitable by Mattingley (1997), since these substrates tend not to be as clean as silicon and GaAs substrates on purchase. It was found that pre-sputtering at 100W for 1 minute showed no improvement in the magnetic properties, and the procedure was not adopted. It should be noted that films presented in this thesis were deposited without a pre-sputter unless stated otherwise. It was found that the stringent cleaning procedure of the substrates as described in Section 3.1.3, ensured the films were of a high quality and did not suffer from any defects such as pinholes.

#### 4.4.5 The effects of contamination

The effects of partial pressure of oxygen on the magnetic properties appeared to have no adverse effects on the FeSiBC films deposited at the sputtering parameters of 75W and 4mTorr, which produced soft magnetic properties for the range of base pressures ( $1-9 \times 10^{-7}$  Torr) investigated. The partial pressure of oxygen in the chamber was monitored using a Residual Gas Analyser (RGA), but there seemed to no significant observable change in the partial pressure ( $\sim 1 \times 10^{-9}$  Torr). The films were not compositionally analysed to establish if oxygen was being incorporated into the films. To increase the partial pressures of atmospheric gases during the deposition, the vacuum of the main chamber was violated by introducing a substantial leak; this was achieved by placing a strand of hair across one of the Viton seals. The high vacuum pumping system was only able to attain a base pressure of  $1.2 \times 10^{-6}$  Torr, compared to the usual base pressure of  $2 \times 10^{-7}$  Torr. The partial pressure of oxygen was found to

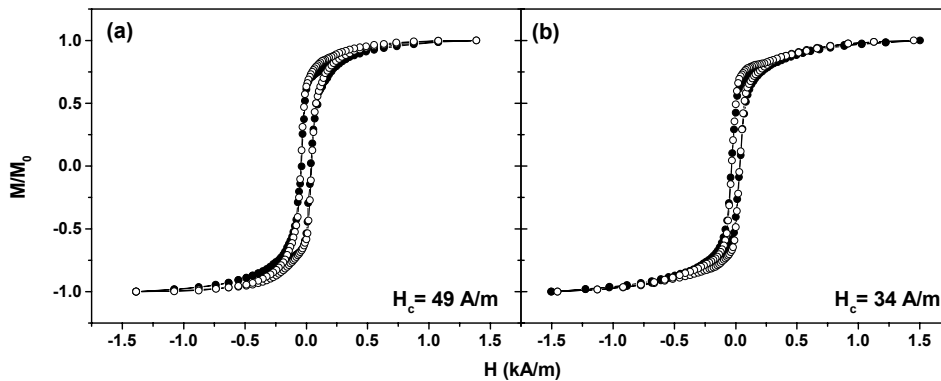


**Figure 4.9:** Orthogonal MH hysteresis loops for FeSiBC films deposited at a sputtering power of 75watts and a pressure of 4mTorr. The base pressure of the system prior to the deposition of each respective film was (a)  $2.2 \times 10^{-7}$  Torr and (b)  $1.2 \times 10^{-6}$  Torr.

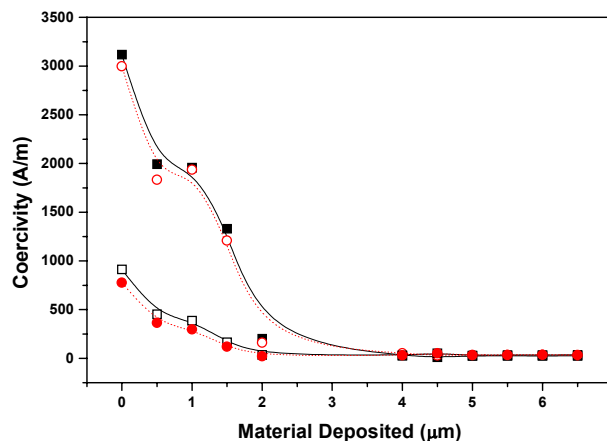


**Figure 4.10:** A series of 500nm thick films grown after the chamber has been cleaned and configured to deposit FeSiBC films. The removable components from within the chamber were shot-blasted using internal facilities within the University of Sheffield. Each point on the curve represents the thickness of FeSiBC deposited since the chamber was first shot-blasted. The solid squares and open circles represent measurements obtained using MOKE and MH magnetometers on the as-deposited films. The open squares and solid circles are the respective measurements obtained after the films have been annealed. Films were annealed at  $390^{\circ}\text{C}$  for 1 hour. (75watts 4mTorr).

increase to approximately  $4 \times 10^{-9}$  Torr because of the introduced leak. The hysteresis loops for this film, and a film deposited at normal base pressures, are shown in Figure 4.9. The two sets of hysteresis loops are similar, which either indicates that the sputtering process is not susceptible to oxygen at these parameters (i.e. not oxidising the sputtered particles), or that any oxygen which is directly being incorporated into the film is insignificant. It is found that the presence of oxygen can lead to high compressive stresses in films [Wagner et al (1974)].

It appears that the FeSiBC films are not sensitive to oxygen. However, Figure 4.10 demonstrates how susceptible they are to organic-based contamination. In the early stages of this work, the internal components of the chamber were shot-blasted using the Central Facility located within the University of Sheffield. Even though the components were thoroughly cleaned after the shot-blasting, it was found that a burn-in period was required where at least  $4\text{-}5\mu\text{m}$  FeSiBC had to be deposited before the films became soft at the established parameters of 75W and 4mTorr. RGA readings before the burn-in period indicated the usual levels of residual gases were present, but also, in addition, a number of other unidentifiable contaminants. These other contaminants were inferred to be organic oil-based, since the shot-blasting facilities used were based in the mechanical workshop, where numerous greasy/oily items were shot-blasted on a daily basis. From Figure 4.10 and 4.11, it is clear that these contaminants have a significant effect on the magnetic properties of the films. The as-deposited films have large coercivities immediately after the cleaning of the chamber; these gradually fall to the expected values as the chamber self-cleans its self by gradually burning and pumping the contaminants away as they out-gas from the contaminated surfaces. RGA readings after deposition of  $4\text{-}5\mu\text{m}$  FeSiBC indicated that the

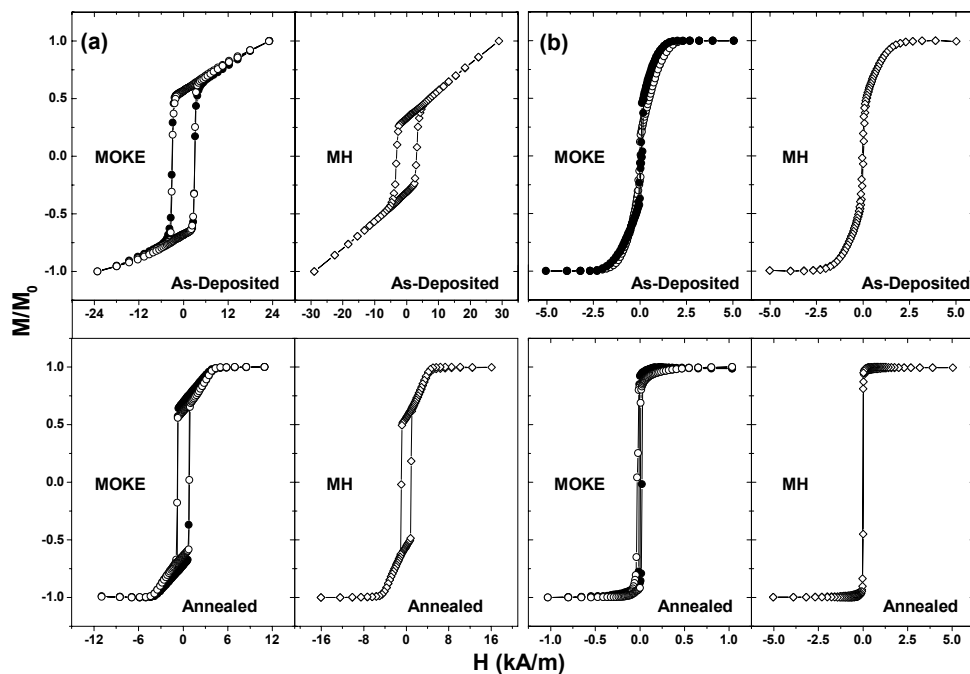


**Figure 4.11:** MOKE and MH hysteresis loops obtained from 500nm thick films as-deposited and annealed. (a) First film deposited after shot-blasting. (b) Film after  $5\mu\text{m}$  of FeSiBC deposition in chamber. Films were annealed at  $390^{\circ}\text{C}$  for 1 hour. Open circles are the transverse loops, the solid circles are the longitudinal loops. (75watts 4mTorr).

contaminants were no longer present. It is inferred that the source of the greasy/oily based contaminants was the internal shot-blasting facility, since subsequent shot-blasting of the chamber components, performed from an external specialist organisation, indicated no such contamination, and no burn-in period was necessary to establish soft films. The annealing of the films appear to indicate that the contamination of the films not only produces a high state of stress in the film but also alters the magnetic properties, since the annealing process does not remove the anisotropy present and produce the expected soft magnetic properties as shown by both the MOKE and MH hysteresis loops shown in Figure 4.11a. It could not be established if the annealed films, which were deposited in a contaminated environment, were still in a state of stress, since no glass cantilevers were coated at the time. The resulting magnetic properties are attributed directly to the incorporation of these contaminants in the film during the deposition, since the magnetic properties of films deposited in a clean environment were soft (Fig. 4.11b). It was also inferred that opening the main chamber to the high vacuum system too quickly, resulted in a similar problem, since films deposited were found to be magnetically harder; it appears this was a result of oil vapour from the diffusion pump entering the chamber due to the sudden change in pressure.

#### 4.4.6 Substrate biasing

It has been shown that it is possible to control both the structural and stress-state of a film during the deposition by applying a DC bias [Wagner et al (1974)] to the substrate. The effect of applying a DC bias to glass substrates was investigated for the FeSiBC films deposited at 75W at 4mTorr, where it is found that the films have excellent soft magnetic properties and are relatively stress free. The effect of applying a DC bias to the substrate was, therefore, not expected to improve the magnetic softness further, because the sputtering parameters were already optimised to produce relatively stress free films.

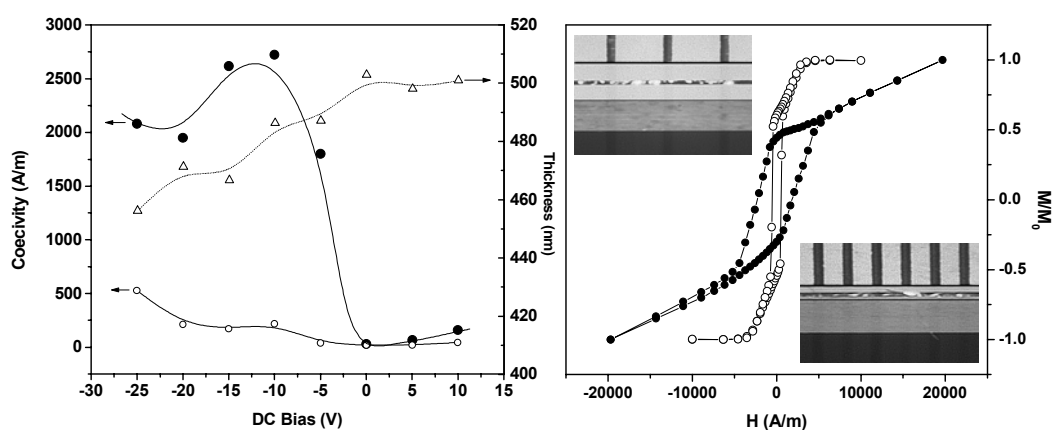


**Figure 4.12:** FeSiBC films deposited at 75W at 4mTorr as function of DC bias applied to the substrate. The as-deposited coercivity are represented by solid circles, the corresponding values after annealing at 390°C for 1 hour are shown by the open circles. The open triangles represent the thickness of the film deposited after a constant deposition time of 90 minutes. MH hysteresis loop for an as-deposited [solid circles] and the annealed [open circles] film grown with a DC bias of -20V are shown. The corresponding images of the cantilever are also included, indicating the film in its deposited state was in a state of compressive stress (Top left hand image).

The DC bias was expected to have a similar effect to that of changes in pressure; this was found to be the case, as shown in Figure 4.12. It should be noted that, even though glass is electrically insulating, the film being deposited on the glass slide will assume the polarity of the bias voltage applied at the onset of the deposition of the film as it makes electrical contact with the sample holder. The application of a DC bias has the effect of changing the kinetic energies of the particles arriving at the substrate, and hence the stress induced in the film. Application of a positive DC bias has the effect of increasing the coercivity only slightly, whereas on the application of a negative DC bias, there was a sudden large increase in the coercivity. The negative bias has the effect of subjecting the film to a positive argon ion bombardment (bias sputtering), which is known to induce compressive stresses into the film because of the increased mobility of the atoms at the substrate, and argon incorporation. The bias sputtering is also assumed to have changed the composition of the deposited films (not compositionally verified) because of the bias sputtering, since annealing of the films did not produce the expected low coercivities and, from the thickness calibrations, it was found that there was reduction in thickness with increasing negative DC bias sputtering. The gentle increase in the coercivity with increasing DC negative bias for the annealed samples, suggests that the coercivity was not only the result of stress, but also to changes in composition and probably the increased argon entrapment in the film. Glass cantilevers which were also deposited simultaneously, indicated that the films were in a state of compressive stress for bias voltages of -5V or below and displayed similar hysteresis loops to those films deposited at low argon pressures and, which indicated a perpendicular anisotropy due to stress. It could not be established with certainty that annealing relieved all the stress, since the cantilevers appeared to be still slightly bowed (Fig. 4.12). Cantilevers deposited at positive biases appeared to be flat. This would seem to suggest that coercivity at negative bias was a result of changes in composition of the film. It was expected that applying a positive bias would have no significant effect, since it prevents the film from being bombarded with positive argon ions and other positive ions. Increases in the temperature of the film due to electron bombardment are assumed also to be small, because of the effect of the magnetron; this traps the energetic electrons being emitted from the target, which therefore prevents them from reaching the film. It appears that applying a DC bias has no advantage, and the films deposited without a DC bias are relatively stress free at the sputtering parameters of 75W and 4mTorr.

#### **4.4.7 Influence of substrate type**

Having ascertained the optimum parameters at which to deposit soft magnetic films onto glass substrates, it is clear that the magnetic properties are highly dependent upon mainly compressive stresses, which can arise in the films due to the kinetic energy of the sputtering process. The stresses can be minimised by careful control of the pressure, or by annealing the films to relieve the stresses present. The effects of the magnetic properties on the more important commercial substrates were investigated to ascertain if there was any significant difference in the sputtering pressure needed to obtain soft FeSiBC films. Films of thickness of 750 nm were deposited simultaneously onto 1cm<sup>2</sup> Corning glass, standard glass, silicon and GaAs substrates. The simultaneous deposition ensured that

the sputtering process was identical, and any differences in the magnetic properties would be a result of the substrate. It should be noted that silicon and GaAs substrates both have an amorphous oxide layer, and therefore no preferential growth should be induced from the texture of the substrate. The four substrates were mounted onto the substrate platter using a picture frame holder, which was especially designed to take account of the different thicknesses of the substrates, and also to ensure that any radial, magnetic anisotropy induced by the field from the magnetron source was similar in each sample (Section 5.8.1). The coercivities of the films from the respective substrates obtained from both MOKE and MH

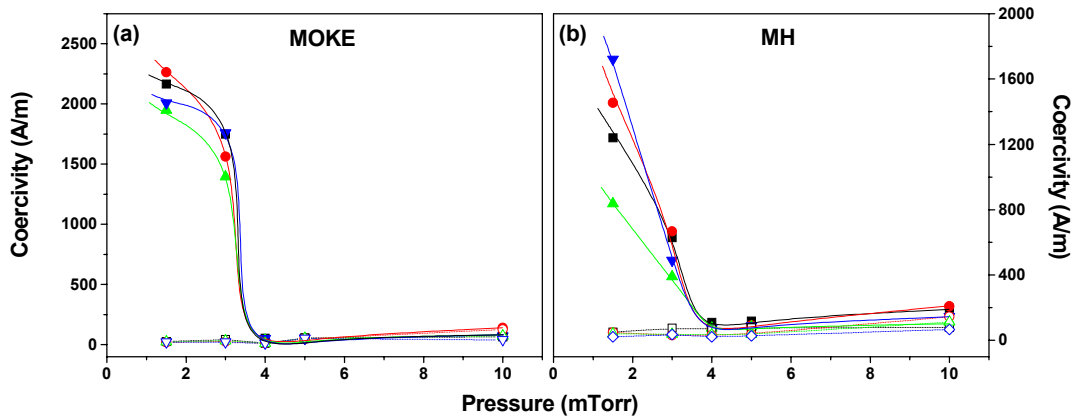


**Figure 4.13:** Pressure dependence on glass[squares], Corning[circles], Si[up-triangle], and GaAs[down-triangle] substrates. The solid symbols represent the as-deposited films, and the open symbols represent the films after an anneal at 390°C for 1 hour for the respective substrates. Films were deposited at 75 watts to a thickness of 750nm. Data obtained using (a) MOKE and (b) MH.

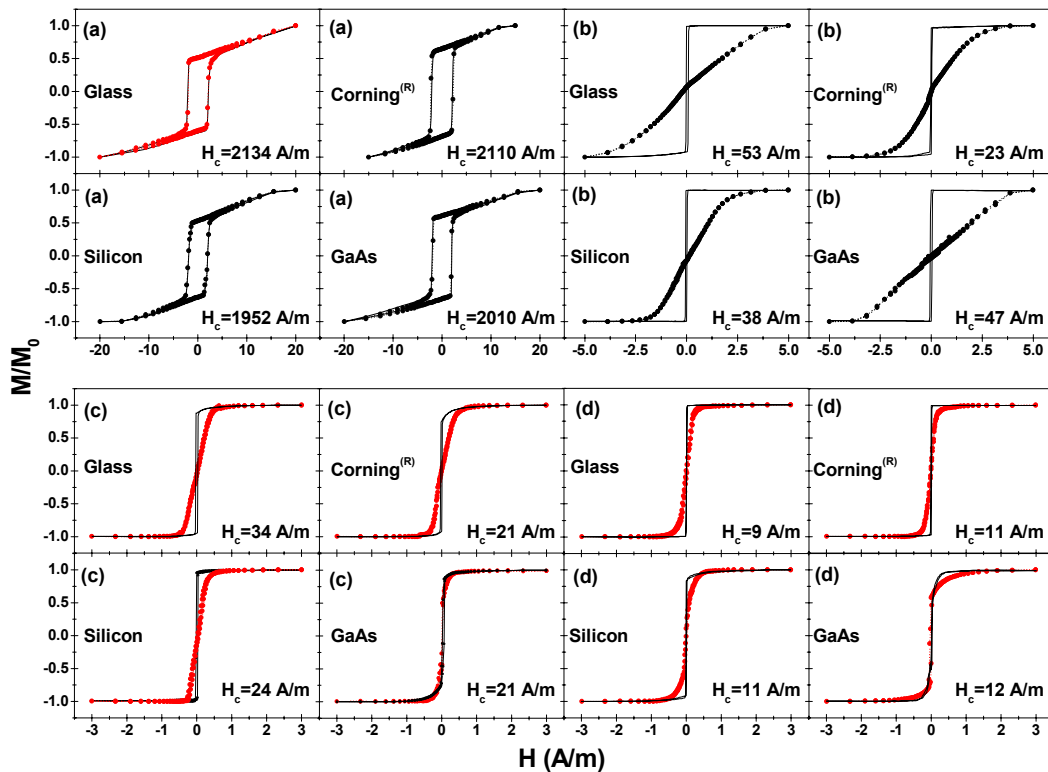


**Figure 4.14:** The as-deposited MOKE hysteresis loops from glass, Corning®, Si, and GaAs substrates deposited at (a) 1.5mTorr, and (b) 4.0mTorr. The corresponding loops after stress relief are shown in (c) and (d). Films were deposited at 75watts to a thickness of 750nm. Annealed at 390°C for 1 hour.

measurements are represented in Figure 4.13 as a function of pressure. It is clear that the coercivity as a function of pressure seems to be independent of the substrates used here; the minimum in the coercivity is obtained at 4mTorr for the as-deposited films where the stress induced from the sputtering process is assumed to be a minimum. Since the sputtering process was identical for each substrate, in order to account for this the mobility of the atoms, and hence temperature of the substrate surface, must also be similar. Annealing of the films on the four substrates relieved any stresses present and yielded similar hysteresis loops, irrespective of the sputtering pressure as is shown in Figure 4.13 and 4.14. It appears that the deposition of films at 4mTorr and at a power of 75W produces the most stress free films, since the temperature of the substrates are relatively low ( $<100^{\circ}\text{C}$ ) and no significant stress results from the small differences in thermal expansion coefficients of the film and substrates. For membrane type sensors, where the magnetostrictive film is deposited onto a flexible diaphragm, the diaphragm usually consists of a flexible substrate such as Kapton<sup>®</sup> or  $\text{Si}_3\text{N}_4$ , both of which have much larger thermal expansion coefficients ( $20\text{ppm}^{\circ}\text{C}$ ) than the rigid substrates (glass, Si, GaAs). It is therefore very important that the depositing film is in a state of minimum stress. A number of films were deposited onto  $20\mu\text{m}$  thick Kapton<sup>®</sup> substrates at 4mTorr at a sputtering power of 75W. The Kapton<sup>®</sup> substrates were wrapped around a standard glass slide and held on the substrate platter using a picture frame holder. The hysteresis loop from a typical film is shown in Figure 4.15a. The slightly higher coercivities of the films are attributed to substrate-induced, random, inhomogeneous stresses which occur because of the increased temperature of the substrate surface. It was, found at times, that the deposited film was under a state of compressive stress (films on Kapton<sup>®</sup> curled cylindrically), and this can only be a result of an increase in the mobility of the atoms at the substrate surface due to increases in temperature. The increase in temperature is a result of the poor thermal contact between the Kapton<sup>®</sup> substrates and the glass slides around which they were wrapped; the hysteresis loops for such a film are shown in Figure 4.15b. To verify that the problem was due to the thermal contact between the Kapton<sup>®</sup> and the glass slide, the Kapton<sup>®</sup> substrates were attached to the glass slides using a high temperature vacuum compatible grease. It appears that the Kapton<sup>®</sup> must be in good thermal contact in order to ensure soft films

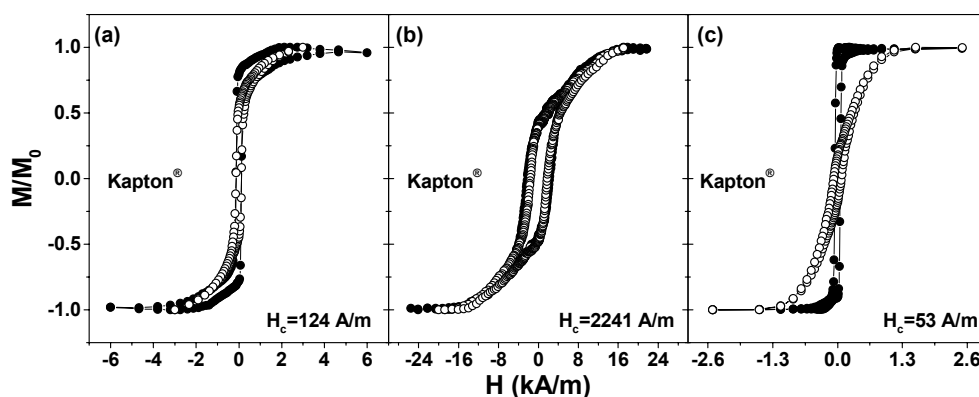


**Figure 4.15:** MH loops from FeSiBC films deposited onto Kapton<sup>®</sup> substrates at 75W at 4mTorr. (a) Kapton<sup>®</sup> wrapped around a glass slide. (b) Kapton<sup>®</sup> wrapped around glass slide, where it is assumed that the thermal contact was not as good as in (a). (c) Kapton<sup>®</sup> substrate attached to the glass slide using a high vacuum compatible grease. It appears that the Kapton<sup>®</sup> must be in good thermal contact in order to ensure soft films.

compatible grease. This ensured that the Kapton<sup>®</sup> was in good thermal contact, and also allowed the Kapton<sup>®</sup> to freely expand in any direction without being constrained by the holder. The films deposited on Kapton<sup>®</sup> in this particular method were found to have comparable coercivities to the rigid substrates as shown by the orthogonal loops in Figure 4.15c; furthermore, the films showed no signs of curling, indicating that they were relatively stress free. It was not possible to anneal such films deposited on Kapton<sup>®</sup>, due to the large difference in the thermal expansion coefficients. Doing so resulted in the film becoming excessively crumpled up, making it useless and impossible to measure the magnetic properties with the magnetic fields available. Also, cleaning off the grease from the reverse side of the substrate was a tedious procedure. However, in general, for small sensors, the diaphragm material (usually Si<sub>3</sub>N<sub>4</sub>), is generally deposited onto either Si or GaAs substrates, upon which the magnetostrictive film is deposited. This eliminates the problem of bonding the membrane to a rigid substrate (see introduction). From the point of the deposition of the magnetic film, this ensures that the Si<sub>3</sub>N<sub>4</sub> is in good thermal contact, and it is also constrained by the rigid substrate. For details on how such membrane sensors are micro-fabricated see Karl et al (1999). Silicon and GaAs substrates coated with Si<sub>3</sub>N<sub>4</sub> and which were prepared by W.J. Karl, were investigated at the deposition parameters of 75W and 4 mTorr. It was found the as-deposited films on such substrates were comparable to those without the Si<sub>3</sub>N<sub>4</sub> present, and were independent of the thickness of the Si<sub>3</sub>N<sub>4</sub> upon which the film was deposited. The hysteresis loops for FeSiBC films deposited onto GaAs and GaAs coated with Si<sub>3</sub>N<sub>4</sub> are shown in Figure 4.16; it can be seen that the loops are comparable. Annealing the films, which were deposited on Si<sub>3</sub>N<sub>4</sub>, had no adverse effects as those films deposited on Kapton<sup>®</sup>. This is the result of the Si<sub>3</sub>N<sub>4</sub> being constrained by the rigid GaAs or silicon substrate.

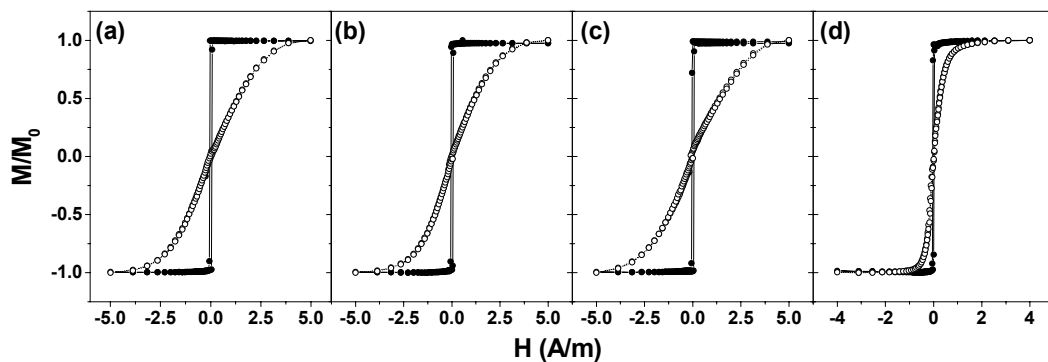


**Figure 4.16:** MOKE loops from FeSiBC films deposited onto 1cm<sup>2</sup> (a) GaAs, (b) GaAs/Si<sub>3</sub>N<sub>4</sub> (250nm) (c) GaAs/Si<sub>3</sub>N<sub>4</sub> (750nm), (d) GaAs/Si<sub>3</sub>N<sub>4</sub> (750nm) annealed at 390<sup>o</sup>C for 1 hour.

#### 4.4.8 Thickness dependence

From the results so far, it is clear that the magnetic properties in the pressure region studied are influenced by stress. It would, therefore, be unreasonable to assume that the stress present in the depositing film would be also dependent on the thickness of the film deposited. Figure 4.17 represents a thickness dependence of the coercivity performed at the sputtering parameters of 75W at 4mTorr on glass and silicon substrates. In order to separate the effect of thickness and stress, the films were annealed to relieve any stress present. By comparing the as-deposited and annealed films, it can be seen that the stress in the films increases slowly with increasing thickness of film because of the increase in coercivity. It was found that annealing films of thicknesses of 50nm or less resulted in the films burning away. Hence, the points for films thickness 40nm or below are missing from the annealed curves. The hysteresis loops for selected film thicknesses are shown in Figure 4.18. On annealing the films, the coercivity appears to obey the inverse thickness law (Fig. 4.17) and the stresses in the thick films are relieved. The films which were annealed on glass below a thickness of 100nm, became magnetically harder and this is assumed to be due to some surface effect. From the hysteresis loops shown for the 50nm film which was annealed (Fig. 4.18d), it can be seen that the loops are very square, and the magnetisation switches rapidly. It is assumed that annealing of the film has introduced stress, or more likely the surface effects have been enhanced because of the high surface to volume ratio of the film, which is pinning the magnetisation.

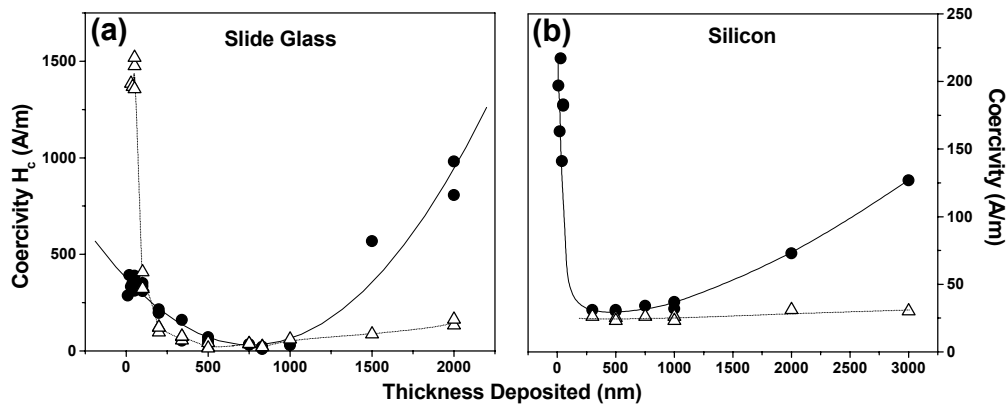


**Figure 4.17:** The coercivity dependence on the thickness of FeSiBC films deposited onto (a) glass and (b) silicon substrates. The solid circles represent the as-deposited films, and the open triangles represent the films after an anneal at 390°C for 1 hour. (75watts 4mTorr).

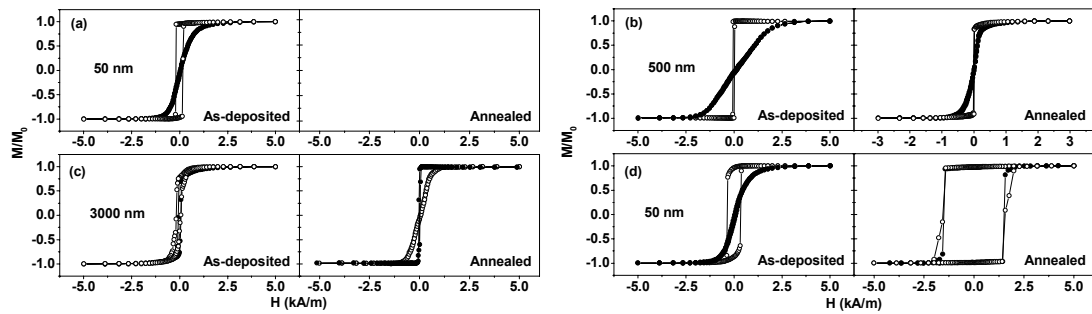


**Figure 4.18:** MOKE hysteresis loops for (a) 50nm, (b) 500nm, and (c) 3000nm films taken from the thickness dependence on silicon substrates. Longitudinal (solid circles) and transverse (open circles) hysteresis loops are shown for the respective as-deposited and annealed films. (75watts 4mTorr). (d) MOKE hysteresis loops from a 50nm film deposited on glass.

#### 4.4.9 X-ray diffraction

X-ray diffraction analysis, as described in Section 3.4, was performed on a range of FeSiBC films deposited at 75W at pressures of 4 and 5 mTorr. The as-deposited and annealed films were found to be amorphous in all instances. A number of films were also deposited onto specially prepared substrates for Transmission Electron Microscopy (TEM) measurements. The diffraction pattern from a selected area of an FeSiBC film is shown in Figure 4.19a, where the image consists of a diffuse halo, typical of amorphous materials. The hysteresis loops for the particular film is also shown in Figure 4.19b, indicating that the film is magnetically soft when taking account of the reduced thickness in film. The FeSiBC film had to be thin in order that the electrons could pass through it and the  $100\mu\text{m}$   $\text{Si}_3\text{N}_4$  window upon which the film was deposited. The deposition of a 30nm film onto Corning<sup>®</sup> produced no unexpected differences and the coercivity was as expected. However, the MOKE hysteresis loops taken from the coated membranes have coercivities which are slightly higher than normal. This is attributed to the  $\text{Si}_3\text{N}_4$  membrane, which is a flexible surface and has a much larger thermal expansion coefficient. The  $\text{Si}_3\text{N}_4$  membrane is also in poor thermal contact with the platter during the deposition. It is therefore inferred that the mismatch between the  $\text{Si}_3\text{N}_4$  and the FeSiBC film, together with a possible increase in temperature, is the cause of stresses to be induced in the film over the membrane. Here the films were deposited on to pre-fabricated membranes.

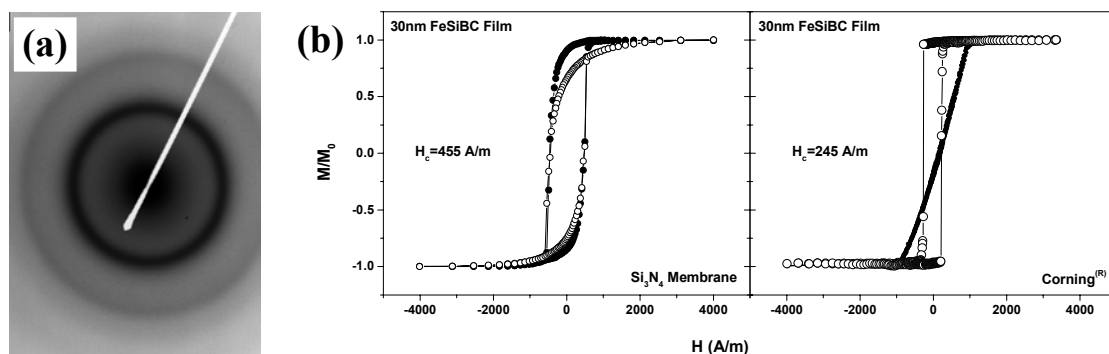


**Figure 4.19:** (a) Diffraction pattern from a 30nm FeSiBC film deposited at 75W at 4mTorr using TEM [Image taken by Kirk (1997)]. (b) Orthogonal MOKE hysteresis loops taken of a  $\text{Si}_3\text{N}_4$  membrane and a  $1\text{cm}^2$  Corning<sup>®</sup> glass coated with 30nm of FeSiBC.

## 4.5 Conclusions

It has been shown that the deposition of films by sputtering is a complex process which is strongly dependent on many parameters. In this investigation, the sputtering process was mainly optimised by careful control of the sputtering pressure, since the sputtering power was chosen to give a reasonable deposition rate of approximately 5.5nm/min, and also to ensure that the temperature of the substrate was below 60°C. This avoided stresses being induced due to the different thermal expansion coefficients of the film and substrate. It was found that the use of a low sputtering power ensured that the sputtering kinetics could be moderated at low argon pressures. Larger sputtering powers would have increased the deposition rates, but this would have meant that larger pressures would have been required to moderate the sputtering process, and this would have increased any possible argon incorporation into the films. It has been demonstrated that once the sputtering conditions have been carefully optimised (75W,4mTorr), it is possible to deposit amorphous FeSiBC films by RF magnetron sputtering, which have excellent soft magnetic properties in the as-deposited state. Films have been deposited onto commercially important substrates such as GaAs, Si and Si<sub>3</sub>N<sub>4</sub>, which are compatible with the microelectronic fabrication technologies. This allows the fabrication of both the magnetic sensor and the electronic detection system on the one substrate, making it more attractive commercially.

Stress due to the sputtering process has been identified as the major factor in controlling the magnetic softness of the deposited films. Any factors which influence the sputtering kinetics will therefore have a direct effect on the stress induced in the films. At the sputtering conditions investigated (75W, 4mTorr) it appeared that the films were insensitive to oxygen contamination, but very sensitive to oil-based contaminants from the cleaning procedure and the diffusion pump. This contamination induced in the films a state of compressive stress, and it was also inferred that it altered the magnetic properties, since it was found that annealing did not produce the soft magnetic properties which were expected.

At the optimised sputtering parameters of 75W and 4mTorr, the as-deposited films had coercivities of ~20-30 A/m; this was further reduced to ~10 A/m on annealing, which compares well with the annealed ribbons of 10 A/m (see MI Chapter). The size of the anisotropy field of the as-deposited films at these parameters is highly dependent on the substrate position and is the topic of discussion of the next chapter.

## 4.6 References

- Ali et al (1998) “The use of stress for the control of magnetic anisotropy in amorphous FeSiBC thin films: a magneto-optic study”, **M. Ali**, R. Watts, W.J. Karl, M.R.J. Gibbs, *J. Magn. Magn. Mater.* 190(3) 199 (1998).
- Abroaf et al (1980) “Magnetic properties of metal-metalloid thin film glasses”, J.A. Aboaf, E. Kloholm, *J. Magn. Magn. Mater.* (15-18) 1385 (1980).
- Abroaf et al (1978) “Properties of transition metal-metalloid ferromagnetic thin films”, J.A. Aboaf, R.J. Kobliska, E. Kloholm, *IEEE Trans. Magn. Mag-14* (5) 941 (1978).
- Baclet et al (1996) “Variation in anisotropy energy versus sputtering gas pressure in ferromagnetic thin films: a magneto-elastic effect.”, Ph. Baclet, G. Perrin, O. Acher, *IEEE Trans. Magn. Mag-35* (5) 4737(1996).
- Craig et al (1981) “Effects of argon pressure and substrate temperature on the structure and properties of sputtered copper films”, S. Craig, G.L. Harding, *J. Vac. Sci. Technol.* 19 (2) 205 (1981).
- Egami et al (1978) “Low field magnetic properties of sputter deposited amorphous Fe<sub>80</sub>B<sub>20</sub>” T. Egami, S.D. Dahlgren, *J. Appl. Phys.* 49 (3) 1703 (1978).
- Elliott (1984) “Physics of amorphous material”, S.R. Elliott, Longman Inc., pp55, (1984).
- Garcia et al (1998) “Magnetic domains and transverse induced anisotropy in magnetically soft CoFeB amorphous thin films.” D. Garcia, J.L. Kurlyandskaya, M. Vazquez, **M. Ali**, M.R.J. Gibbs, *IEEE Trans. Magn. MAG-34* (4) (1998).
- Gangulee et al (1981) “Annealing behaviour of amorphous ferromagnetic Co-Fe-B and Fe-B thin films”, A. Gangulee, J.A. Aboaf, R.J. Kobliska, *J. Appl. Phys.* 52 (4) 2928 (1981).
- Heiman et al (1978) “Low coercivity amorphous magnetic alloy films”, N. Heiman, R.D. Hempstead, N. Kazama, *J. Appl. Phys.* 49 (11) 5663 (1978).
- Hoffman (1976) “Stresses in thin films: the relevance of grain boundaries and impurities”, R.W. Hoffman, *Thin Solid Films* (34) 190 (1976).
- Hudson et al (1996) “Origin of stresses in sputtered elemental and alloy thin films”, C. Hudson, R.E. Somekh, *Vac. Sci. Technol. A* 14 (4) 2169 (1996).
- Hudson et al (1992) “Stresses in UHV planar magnetron sputtered films”, C. Hudson, R.E. Somekh, *Mat. Res. Soc. Symp. Proc.* (239) 145 (1992).
- Jakubovics (1994) “Magnetism and magnetic materials”, J.P. Jakubovics, 2<sup>nd</sup> edition, Cambridge University Press, Cambridge (1994).
- Jiles (1990) “Introduction to magnetism and magnetic materials”, D. Jiles, Chapman & Hall, (1990).

- Kabacoff et al (1986) “Thermal, magnetic and magnetomechanical properties of amorphous magnetron sputtered Fe<sub>78</sub>B<sub>13</sub>Si<sub>9</sub>”, L.T. Kabacoff, H.T. Savage, M. Wun-Fogle, IEEE Trans. MAG-22 (5) 427 (1986).
- Karl (1998) Private communication.
- Karl et al (1999) “A micromachined magnetostrictive pressure sensor using magneto-optical interrogation”, W.J. Karl, A.L. Powell, R. Watts, M.R.J. Gibbs, C.R. Whitehouse, EMSA 98 \*\* \*\*\* (1999).
- Karl et al (1999a) “Magnetostrictive thin-film transducer elements for micro-electro-mechanical systems”, W.J. Karl, R. Watts, A.L. Powell, C.R. Whitehouse, R.B. Yates, M.R.J. Gibbs, Electrochem. Soc. Proc. Vol(98-20) 354 (1999).
- Kazama et al (1978) “Magnetic properties of amorphous FeC thin films”, N. Kazama, N. Heiman, J. Appl. Phys. 49 (3) 1706 (1978).
- Kirk (1997) TEM Images taken By K.J. Kirk at Glasgow (1997).
- Kobliska et al (1978) “Amorphous ferromagnetic thin films”, R.J. Kobliska, J.A. Aboaf, A. Gangulee, J.J. Cuomo, E. Kloholm, Appl. Phys. Lett. 33 (5) 473 (1978).
- Leamy et al (1979) “Microstructure and magnetism in amorphous rare earth transition metal thin films. II. Magnetic anisotropy”, H.J. Leamy, A.G. Dirks, J. Appl. Phys. 50 (4) 2871 (1979).
- Leamy et al (1978) “Microstructure and magnetism in amorphous rare earth transition metal thin films. I. Microstructure”, H.J. Leamy, A.G. Dirks, J. Appl. Phys. 49 (6) 3430 (1978).
- Lenz (1990) “A review of magnetic sensors”, J.E. Lenz, Proc. IEEE Trans. Magn. MAG-78 (6) 973 (1990).
- Luborsky (1980) “Ferromagnetic materials”, edited by E.P. Wohlfarth, Vol.(1), Chapter 6, “Amorphous ferromagnets”, F.E. Luborsky, 451 (1980).
- Luborsky et al (1980) “Preparation and properties of Fe-Si-B-C amorphous alloys”, F.E. Luborsky, J.L. Walter, IEEE Trans. Magn. MAG-16 572 (1980).
- Luborsky et al (1980a) “The Fe-B-C ternary amorphous alloys”, F.E. Luborsky, J.J. Becker, J.L. Walter, D.L. Martin, IEEE Trans. Magn. MAG-16 (3) 521 (1980).
- Luborsky et al (1979) “Formation and magnetic properties of Fe-B-Si amorphous alloys”, F.E. Luborsky, J.J. Becker, J.L. Walter, H.H. Liebermann, IEEE Trans. Magn. MAG-15 1146 (1979).
- Mattingley (1997) “Sputter growth and characterisation of amorphous FeSiBC film”, Ph.D Thesis, University of Sheffield (1997).
- Mattingley et al (1994) “Magnetic and Magnetoelastic Properties of Amorphous Fe-Si-B-C Films”, A.D. Mattingley, C. Shearwood, M.R.J. Gibbs, IEEE Trans. MAG-30 (6) 4806 (1994).

- Materne et al (1988) “Changes in stress and coercivity after annealing of amorphous Co(Zr,Nb) thin films deposited by r.f. sputtering”, A. Materne, H. Moriceau, B. Blanchard, J. Florestan, IEEE Trans. Magn MAG-24 1752 (1988).
- McCurrie (1994) “Ferromagnetic materials - structure and properties”, R.A. McCurrie, Academic press, (1994).
- Mitchell et al (1986) “A new Metglas sensor”, E.E. Mitchell, R. DeMoyer, J. Vranish, IEEE Trans. Ind. Elec. 33 (2) 166 (1986).
- Naoe et al (1982) “Properties of amorphous Co-Ta and Co-W films deposited by rf sputtering”, M. Naoe, H. Kazama, Y. Hoshi, S. Yamanaka, J. Appl. Phys 53 (11) 7846 (1982).
- Naoe et al (1979) “Magnetic properties of amorphous Fe-Si-B films prepared by co-sputtering”, M. Naoe, H. Yamamoto, S. Yamanaka, J. Appl. Phys. 50 (11) 7606 (1979).
- Ohkoshi et al (1985) “Effect of Ar pressure and substrate bias on magnetic properties and microstructure in amorphous TbCo sputtered films”, M. Ohkoshi, M. Harada, T. Tokunaga, S. Honda, T. Kusuda, IEEE Trans. MAG-21 (5) 1635 (1985).
- Ono et al (1993) “Texture, microstructure and magnetic properties of Fe-Co alloy films formed by sputtering at an oblique angle of incidence”, H. Ono, M. Ishida, M. Fujinaga, H. Shishido, H. Inaba, J. Appl. Phys. 74 (8) 5124 (1993).
- Ounadjela et al (1987) “Control of the deposition temperature by the use of a magnetic field in r.f. sputtering”, K. Ounadjela, G. Suran, J. SZtern, Thin Solid Films (151) 397 (1987).
- Ref. List (4.1) McCurrie (1994), Jiles (1990), Jakubovics (1994).
- Ref. List (4.2) Hudson et al (1996), Baclet et al (1996), Hudson et al (1992) Materne et al (1988), Naoe et al (1982), Shimada et al (1981).
- Ref. List (4.3) Ali et al (1998), Garcia et al (1998), Mattingley et al (1994), Kabacoff et al (1986), Tsunashima et al (1981,1979), Aboaf et al (1980,1978), Naoe et al (1979), Egami et al (1978), Kobliska et al (1978).
- Ref. List (4.4) Baclet et al (1996), Ono et al (1993), Materne et al (1988), Ohkoshi et al (1985), Naoe et al (1982), Shimada et al (1982,1981), Kazama et al (1978), Heiman et al (1978).
- Ref. List (4.5) Materne et al (1988), Naoe et al (1979), Kazama et al (1978), Heiman et al (1978), Kobliska et al (1978).
- Shimada et al (1982) “Sputtering of amorphous CoZr and CoHf films with soft magnetic properties”, Y. Shimada, H. Kojima, J. Appl. Phys. 53 (4) 3156 (1982).
- Shimada et al (1981) “Sputtering of FeCo-B amorphous films with soft magnetic properties”, Y. Shimada, T. Hasegawa, H. Kojima, IEEE Trans. Magn. MAG-17(2) 1199 (1981).

- Shimada et al (1979) “Magnetic properties and thermal stability of FeB amorphous films”, Y. Shimada, H. Kojima, J. Appl. Phys. 50 (3) 1541 (1979).
- Somekh (1984) “The thermalization of energetic atoms during the sputtering process”, R.E. Somekh, J. Vac. Sci. Technol. A 2 (3) 1285 (1984).
- Tsunashima et al (1981) “Induced anisotropy and permeability in amorphous Fe-B and Co-Fe-B films”, S. Tsunashima, Y. Machata, S. Uchiyama, IEEE Trans. MAG-17 (6 ) 3073 (1981).
- Tsunashima et al (1979) “Magnetic and magnetoelastic properties of amorphous Fe-Si films”, S. Tsunashima, S. Mitsuya, S. Uchiyama, Jpn. J. Appl. Phys. 18 (8) 1645 (1979).
- Thornton (1974) “Influence of apparatus geometry and deposition conditions on the structure and topography of thick sputtered coatings”, J.A. Thornton, J. Vac. Sci. Technol. 11 (4) 666 (1974).
- Vink et al (1993) “Stress, strain, and microstructure in thin tungsten films deposited by dc magnetron sputtering”, T.J. Vink, W. Walrave, J.L.C. Daams, A.G. Dirks, M.A.J. Somers, K.J.A. van der Aker, J. Appl. Phys. 74 (2) 988 (1993).
- Wagner et al (1974) “Tungsten metallisation for LSI applications”, R.S. Wagner, J. Vac. Sci. Technol. 11(3) 582 (1974).

## 5.0 Magnetic Anisotropy In Amorphous Films

This chapter is concerned with the magnetic anisotropy of amorphous FeSiBC films which have been deposited by RF magnetron sputtering, mainly at the optimised sputtering parameters of 75W and 4mTorr (Chapter 5). The magnetic properties were investigated mainly using the magneto-optical Kerr effect, with both point hysteresis measurements and domain imaging. A significant in-plane anisotropy was observed in the as-deposited films, which has been attributed to the residual field from the magnetron sputtering source. The effects of various treatments on the films are investigated, including the use of forming fields, stress, and thermal processing. The deliberate introduction of stress into these materials is found to allow excellent control of both the direction and magnitude of the magnetic anisotropy. The treatments are evaluated for their potential to control the anisotropy in magnetostrictive device applications.

A simple new technique is also described for the measurement of the saturation magnetostriction in amorphous thin films deposited onto rigid substrates. The method is based on mechanically introducing a small curvature in the substrate either during the deposition (strained growth) or post-deposition. The strain induced anisotropy is measured using the magneto-optical Kerr effect. Quantification of the film strain is obtained using optical interference and stylus measurements; coupled with mechanical finite element modelling, this allowed the saturation magnetostriction to be determined. No information concerning the mechanical properties of the substrate are required and, providing that the Young's modulus and Poisson's ratio of the film are known accurately, the values of magnetostriction obtained are both accurate and absolute. It is envisaged that the technique could be applied to a wide variety of films deposited onto commercially important substrates. Here, it is applied to amorphous FeSiBC films deposited onto glass and silicon substrates. A high degree of control is also demonstrated in tailoring the anisotropy field, by the technique of substrate straining.

### 5.1 Introduction

Most ferromagnetic thin films display a uniaxial anisotropy in plane irrespective of whether they are produced by vapour or sputter deposition techniques. This anisotropy is not always obvious from measurement of bulk hysteresis loops, especially if the film consists of a complex multi-domain structure, where the magnetisation process across the entire film will not proceed by coherent moment rotation, even though each domain structure is uniaxially magnetised. These magnetised domain regions within the film can be seen from domain patterns using, for example, the magneto optical Kerr effect as described in Chapter 2 or point MOKE hysteresis loops if the domains are larger than the sampling area of the laser. The domain images show a tendency for domain walls to lie along preferred directions in the plane of the film. It is well known that the application of a magnetic field during the deposition has the effect of ensuring that the easy axis of magnetisation of the whole film is in the one direction (ie. uniaxial).

The importance of the magnetic anisotropy in magnetostrictive films is becoming increasingly significant, since these magnetically soft, amorphous films are being widely utilised in the production of a new generation of magnetic sensors and actuators [Ref. List (5.1)]. The incorporation of these materials into micro-electromechanical systems requires a good control of the magnetic anisotropy in sensor elements of various aspect ratios and thicknesses. For actuators, the maximum magnetostrictive deflection is obtained when the magnetic moments are rotated coherently through 90°. Such a rotation is conveniently achieved by the application of an external magnetic field along the hard axis of a sample which has a well defined uniaxial anisotropy. It is therefore essential, not only from the point of view of sensor applications, but also from that of understanding the material's magnetic behaviour, that the magnetic anisotropy of the material is understood, since the magnetic anisotropy strongly affects the magnetisation process and therefore the shape of the hysteresis loop, which is widely used to characterise magnetic materials.

## 5.2 Magnetocrystalline Anisotropy

Magnetic materials tend to display a directional dependence of their properties, and this is a consequence of the magnetic anisotropy. The magnetic anisotropy describes the preference of the magnetisation to lie in a particular direction. The magnetic anisotropy in crystalline materials has clearly been demonstrated where certain crystallographic directions are easy directions of magnetisation, whilst others are hard directions. This has been ascertained by the measurement of magnetisation curves. In the absence of any applied external magnetic field the magnetisation prefers to lie along an easy axis, since this minimises the magnetic energy of the system. The easy and hard directions can be distinguished by the magnetic field needed to achieve magnetic saturation. A prime example is a single crystal of Fe, where the  $\langle 100 \rangle$  directions are easy axes of magnetisation, whilst the  $\langle 111 \rangle$  directions are said to be hard axes of magnetisation [Cullity (1972)]. This form of magnetic anisotropy is referred to as the crystal anisotropy, or magnetocrystalline anisotropy, which is intrinsic to the material. The crystal anisotropy originates from the spin-orbit interaction where the electron spin is coupled to the electron orbit. When a magnetic field is applied to rotate the electron spins, it also attempts to reorientate the electron orbit which, however, is strongly coupled to the crystal lattice. The magnetic field or energy needed to rotate the electron spin's (magnetisation) is known as the crystal anisotropy energy, which is the energy needed to overcome the spin-orbit interaction. The expression for the crystal anisotropy energy density for a cubic crystal can be expressed by equation (5.1) [Cullity (1972)]

$$E_a = K_0 + K_1(\alpha_1^2\alpha_2^2 + \alpha_2^2\alpha_3^2 + \alpha_3^2\alpha_1^2) + K_2(\alpha_1^2\alpha_2^2\alpha_3^2) + \dots \quad (5.1)$$

where  $K_0, K_1, K_2 \dots$  are the anisotropy constants, which are material dependent and  $\alpha_i$  are the directional cosines of the angle between the magnetisation and crystal axes. This intrinsic crystal anisotropy is not preserved in amorphous materials, since the crystal field rapidly averages to “zero” on

a macroscopic scale because of the amorphous arrangement of the atoms. On a local scale, it can be assumed that there is some “crystalline” anisotropy because of nearest neighbour interactions, which will be very of a short range, and therefore the average macroscopic crystal anisotropy is close to, or equal to, zero. It should be remembered that ferromagnetism is a result of the exchange energy which is mainly dominated by the interaction between adjacent electron spins and their separations. Instead a number of other (see below) magnetic anisotropies can exist, which are usually induced in some manner, giving rise to a magnetic anisotropy which is uniaxial in direction. This means that there is a single, preferred direction, which for films is usually in the plane of the film. The tendency for the magnetisation to lie along such an easy axis, can be expressed as an anisotropy energy density,  $E_K$ , in a series of powers of  $\sin\theta$ . The expression for the energy density for a uniaxial anisotropy is:

$$E_K = K_{u0} + K_{u1} \sin^2 \theta + K_{u2} \sin^4 \theta + \dots \quad (5.2)$$

where  $\theta$  is the angle between the easy axis, and the direction of the magnetisation  $M_S$ , and  $K_{u0}$ ,  $K_{u1}$ ,  $K_{u2}, \dots$  are the uniaxial anisotropy constants. The first anisotropy constant,  $K_{u0}$ , which is independent of  $\theta$  is usually neglected since it gives no change in  $E_K$  when the direction of the magnetisation changes;  $K_{u2}$  and higher order terms can also be neglected because they are relatively small in comparison to  $K_{u1}$ . This gives the following approximate expression for the uniaxial magnetic anisotropy as

$$E_K = K_u \sin^2 \theta \quad (5.3)$$

where  $K_u$  is the uniaxial anisotropy constant. It can be seen from these expressions that the anisotropy energy is a minimum when the magnetisation lies along an easy axis ( $\theta=0^\circ, 180^\circ$ ), and is a maximum when magnetisation is perpendicular to the easy axis ( $\theta=90^\circ, 270^\circ$ ). The magnitude of the induced anisotropy is usually monitored by measuring the anisotropy constant  $K_u$  or the anisotropy field  $H_K$ , which is related to the anisotropy constant:

$$H_K = \frac{2K_u}{\mu_0 M_S} \quad (5.4)$$

where  $M_S$  is the saturation magnetisation and  $\mu_0$  is the permeability of free space. In this thesis the author has mainly used the anisotropy field when making comparisons of the magnitude of the uniaxial anisotropy present in the FeSiBC films, since the values were obtained from the measured hysteresis loops.

### 5.3 Shape Anisotropy

The shape anisotropy results from the demagnetising fields which occur within a magnetised material. The shape of the sample has the effect of creating directions in which it is easier to magnetise the sample, and this is governed by the demagnetising field,  $H_d$ , which, in the material, points in the opposite direction to the magnetisation and the applied field. For instance, a smaller field is required to magnetise a long cylindrical magnetic rod along its length, because of the smaller demagnetising field, compared to the magnetic field required to magnetise the rod along a diameter. If one thinks in terms of magnetic poles, the strength of the demagnetising field depends upon the separation between these opposite magnetic poles. The poles generated at the ends of a rod are much further apart, giving rise to a small demagnetising field, whereas the magnetic poles will be much closer together when the rod is magnetised across its diameter, thus producing a larger demagnetising field. The demagnetising field depends solely on the magnetisation and the demagnetising factor, and is expressed as

$$H_d = -N_d M \quad (5.5)$$

where  $N_d$  ( $0 \leq N_d \leq 1$ ) is the demagnetising factor which is shape dependent, and  $M$  is the magnetisation. The  $N_d$  term is calculated solely from the geometry of the sample and can only be calculated exactly for an ellipsoid. The energy associated with this demagnetising field can be expressed as follows, and is referred to as the magnetostatic energy density.

$$E_{ms} = \frac{1}{2} \mu_0 N_d M^2 \quad (5.6)$$

The shape anisotropy has an obvious importance in thin films, since there is a significant shape anisotropy because of the thickness of the film. It is well known that the magnetisation usually lies in-plane for a film in the absence of any crystal anisotropy or any other anisotropy which would cause the magnetisation to lie out of plane. In general, a thin film can be approximated by a flat ellipsoid or an oblate spheroid; this allows one to determine approximately the demagnetising factors for a thin film system. The demagnetising factor for an oblate spheroid [Craik (1995)] with the magnetisation in the plane of the film is given by

$$N_d = \frac{1}{2} \left[ \frac{q^2}{(q^2 - 1)^{3/2}} \sin^{-1} \left( \frac{\sqrt{q^2 - 1}}{q} \right) - \frac{1}{q^2 - 1} \right] \quad (5.7)$$

$$q = \frac{d}{t} \quad (5.8)$$

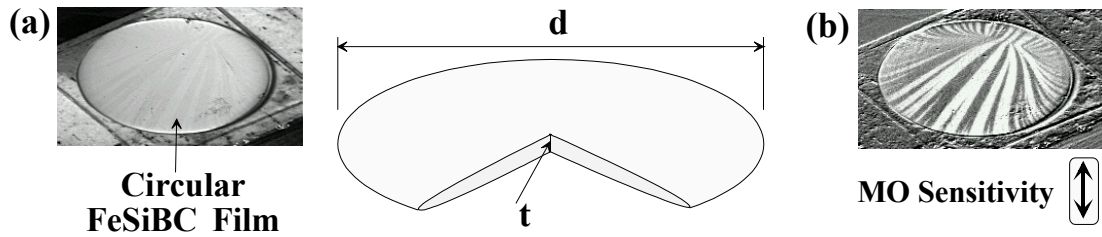


**Figure 5.1:** (a) Illustration of an oblate spheroid, to approximate a thin film. In general thin films tend to be square, or circular. A photograph of a 500nm thick circular FeSiBC film 1cm diameter is also shown, which was deposited onto square glass substrate through a circular mask. (b) Domain image from a circular demagnetised FeSiBC film.

where  $q$  is the ratio of the diameter ( $d$ ) of the spheroid to its thickness ( $t$ ) as shown in Figure 5.1. This is a reasonable approximation for the films which were typically investigated in this thesis; the films were generally either rectangular (mainly square), or circular as shown in Figure 5.1. Using equation (5.6), and the typical values of  $d=1\text{cm}$ ,  $t=500\text{nm}$  the demagnetising factor,  $N_d$ , in the plane of the film is of the order of  $3.9 \times 10^{-5}$ . Essentially, the in-plane demagnetising factor is equal to zero and the demagnetising factor perpendicular to the plane of the film is therefore equal to one ( $N_x + N_y + N_z = 1$ ). Hence the easy-axis is in the plane of the film, whilst the hard axis is perpendicular to the plane of the film. This means that any competing anisotropy, or an applied field, must overcome the demagnetising field which is equal to the magnetisation  $M$  (Eq. 5.5), in order to rotate the magnetisation out of the plane of the film. It is therefore important to be aware of the shape anisotropy in the design process of thin film sensors in situations where the x-y dimensions of the film approach the thickness of the film, since the in-plane demagnetising field will no longer be negligible. The magnetic field,  $H_{int}$ , the sensor will experience in this situation will be

$$H_{int} = H_{appl} - H_d \quad (5.9)$$

where  $H_{appl}$  is the external applied magnetic field. The shape anisotropy can cause the sensor to perform differently compared with measurements made on much larger devices.

Another anisotropy which is related to the shape of the film, is the surface anisotropy. In very thin films ( $<5\text{nm}$ ) the surface or the film/substrate interface can give rise to a significant surface anisotropy [Gradmann (1986), Mattheis et al (1999)]; this can strongly influence the magnetic properties when the surface to volume ratio is comparable with or larger than that of the film thickness. The surface anisotropy is due to the abrupt change in the structural and chemical environment at the surface and can cause the magnetisation to point out of the plane of the film. Most thin film sensors tend to be 100nm or thicker to ensure a good signal to noise ratio.

However, the absence of any shape anisotropy in the plane of the film ( $d \gg t$ ) and/or any significant magnetocrystalline anisotropy in the amorphous films, does not imply that all directions for the magnetisation within the plane of the film are energetically equal, as is shown in Figure 5.1b. In this instance, a circular FeSiBC film deposited in this study was repeatedly demagnetised; it was found

from domain imaging and hysteresis measurements that an approximately uniaxial anisotropy existed across the film, which was always orientated along the same direction. This anisotropy cannot be due to the shape anisotropy, since all directions should be equally magnetisable; therefore it is a result of some other anisotropy (see later).

## 5.4 Magnetostriction and Magnetoelasticity

When the state of magnetisation of a magnetic material is altered by an external magnetic field, it also experiences a change in its physical dimensions, provided that part or all of the magnetisation process occurs by magnetisation rotation as opposed to domain wall displacement. This change in dimension gives rise to a strain which is referred to as the magnetostriction as denoted by  $\lambda$  (Eq. 5.10)

$$\lambda = \frac{\Delta l}{l} \quad (5.10)$$

where  $l$  is the length of the sample before the applied field and  $\Delta l$  is the change in length due to the applied field. The magnetostriction is due to the spin-orbit coupling which is also responsible for the magnetocrystalline anisotropy and they are both intrinsically related [Cullity (1972)]. This type of magnetostriction is known as longitudinal or linear magnetostriction. There are two main sources of magnetostriction, spontaneous magnetostriction which results from the ordering of the magnetic moments at the Curie temperature thus giving rise to a lattice strain, and the field induced magnetostriction, which is a consequence of the domain magnetisation being altered by an external magnetic field and which is due to the rotation of this lattice strain. The magnetostrictive strain  $\lambda$  increases as a function of applied field up to the point of magnetic saturation and is known as the saturation magnetostriction,  $\lambda_s$ . It is defined as the fractional change in length between the demagnetised state and the magnetically saturated state. The magnetostrictive strain can have values which are either positive, negative, or in some cases, nearly zero depending upon the composition of the material; this means that, on application of a magnetic field, a positively magnetostrictive material will elongate in the direction of the applied field, whereas it will contract if it is negatively magnetostrictive. It is found that  $\lambda_s$  is anisotropic for crystalline materials and is therefore defined relative to the crystal axis along which the magnetisation lies. For amorphous materials the magnetostriction is isotropic and a simple expression relates the magnetostrictive strain to the magnetisation as shown in equation (5.11)

$$\lambda(\theta) = \frac{3}{2} \lambda_s \left( \cos^2 \theta - \frac{1}{3} \right) \quad (5.11)$$

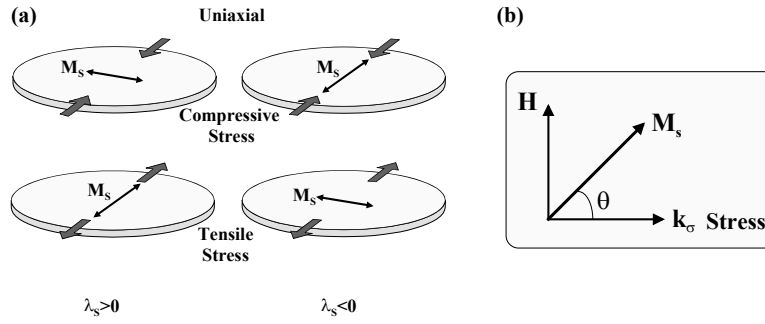


**Figure 5.2:** Illustration of stress induced anisotropy in positive and negative magnetostrictive materials. (a) Anisotropy induced when a uniaxial compressive or tensile stress exists. (b) Diagram illustrating the relationship between the stress and magnetisation.

where  $\theta$ , is the angle between the magnetisation and the direction of measurement. The maximum magnetostrictive strain has the value of  $1.5\lambda_s$  and will occur when the magnetisation is rotated through  $90^\circ$  from magnetic saturation.

An important effect which is related to the magnetostriction is the inverse magnetostrictive or magnetoelastic effect, which deals with the effects of stress on the magnetisation of a magnetic material. In the presence of an external or internal stresses, the magnetisation will couple with the stresses via the magnetostriction to induce preferred directions for the magnetisation. This coupling between the magnetisation is dependent on the sign of  $\lambda_s$  and the stress as is illustrated in Figure 5.2a. For materials with  $\lambda_s > 0$  the magnetisation will rotate so as to lie along the direction of the uniaxial tensile stress, whereas it will lie perpendicular to a uniaxial compressive stress. The reverse is true for materials with  $\lambda_s < 0$  as is shown in Figure 5.2a.

The effect of stress in magnetostrictive materials is to induce a uniaxial magnetoelastic anisotropy. This source of magnetic anisotropy is very important in melt-spun ribbons and deposited films, where random micro-strains occur because of the growth process. This is more significant in melt-spun ribbons where it is unavoidable for stresses to be induced whereas, these growth-induced stresses can be minimised for films formed by sputter deposition as was shown in the previous chapter. If the material possesses a significant magnetostriction, then the magnetic properties are degraded because of the magnetisation coupling with these randomly orientated micro-strains. It should be noted that these randomly oriented strains will in most instances not produce an overall uniaxial anisotropy, unless there is a resultant uniaxial stress. The localised induced uniaxial anisotropies will have the effect of impeding the magnetisation rotation process and domain wall movement, since the applied field will need to overcome the magnetoelastic anisotropy energy  $E_{me}$ . The magnetoelastic energy density for materials with an isotropic magnetostriction is given by equation (5.12)

$$E_{me} = \frac{3}{2} \lambda_s \sigma \sin^2 \theta = K_\sigma \sin^2 \theta \quad (5.12)$$

where  $\theta$  is the angle between the magnetisation and the direction of the stress  $\sigma$ . For materials where the magneto-crystalline anisotropy is not negligible, the direction of the magnetisation  $M_s$  will be controlled by both the magneto-crystalline and magnetoelastic anisotropy. If the crystal anisotropy  $K_I \gg \lambda_s \sigma$ , then the direction of the magnetisation is determined by  $K_I$  and the reverse is true if  $K_I \ll \lambda_s \sigma$ . In amorphous magnetostrictive materials, any magnetoelastic anisotropy will therefore control the direction of the magnetisation. The anisotropy field  $H_k$  associated with this uniaxial magnetoelastic anisotropy can be obtained by assuming a pure moment rotation. If one assumes that a stress  $\sigma$  is applied to a positively magnetostrictive material, then the magnetisation will lie along this stress direction. On application of a magnetic field perpendicular to this induced uniaxial anisotropy, the magnetic energy density of the system can be expressed as

$$E(\theta) = \frac{3}{2} \lambda_s \sigma \sin^2 \theta - \mu_0 M_s H \sin \theta \quad (5.13)$$

where  $\theta$  is the angle between the magnetisation and the stress as shown in Figure 5.2b. The energy of the system must be a minimum at equilibrium

$$\frac{\partial E}{\partial \theta} = 3\lambda_s \sigma \sin \theta \cos \theta - \mu_0 M_s H \cos \theta = 0 \quad (5.14)$$

$$H = \frac{3\lambda_s \sigma \sin \theta}{\mu_0 M_s} \quad (5.15)$$

At the anisotropy field  $H_k = H$ , the magnetisation will lie at angle  $\theta = 90^\circ$ , giving the expression for the anisotropy field in terms of the magnetoelastic anisotropy as

$$H_k = \frac{3\lambda_s \sigma}{\mu_0 M_s} \quad (5.16)$$

## 5.5 Magnetic Anisotropy Induced During The Deposition

### 5.5.1 Growth Induced

As has already been discussed in the previous chapter, the sputtering parameters have a significant effect on the structural and magnetic properties of a depositing film. At high sputtering energies (e.g. low pressures) the films are in a state of high compressive stress, whereas at low sputtering energies (e.g. high pressures), a columnar texture can develop in the depositing film [Shimada et al (1981), Leamy et al (1979)]. The columnar structure is formed by the self-shadowing of the incident atoms by the atoms already incorporated into the growing film. This columnar texture can give rise to a perpendicular anisotropy, because of the shape induced anisotropy of the columns; the magnetisation prefers to lie along the length of the columns because of the lower magnetostatic energy (Eq. (5.5)). The columns, which are formed by the process of columnar growth, are dependent upon the angle at which the impinging atoms arrive at surface of the film. An empirical expression relates the angles of impinging atoms,  $\alpha$ , and the angle,  $\beta$ , at which the columns are formed, by equation (5.17) [Leamy et al (1978)].

$$2 \tan \beta = \tan \alpha \quad (5.17)$$

This is illustrated in Figure 5.3a, where the columnar structure for atoms impinging at  $\alpha=30^\circ$  is shown; in general, the formation of the columnar direction is not equal to the direction of the impinging atoms as expressed by equation (5.17). For the process of sputter deposition, as long as the target area is larger than the substrate area upon which the film is being deposited, then any columnar structure formation tends to be perpendicular. Columnar growth is strongly dependent on the deposition parameters and can develop in both sputter or evaporation deposition techniques. This columnar structure also has the effect of lowering the density of the films because of the more open structure which, in turn, has the effect of lowering saturation magnetisation, besides severely degrading the magnetic properties of the material by inducing a perpendicular anisotropy in thin films.

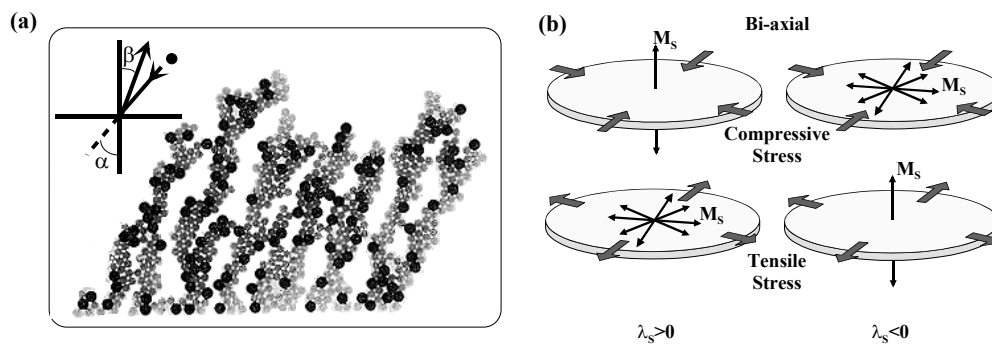


**Figure 5.3:** Columnar structure for impinging atoms at  $\alpha=30^\circ$  to the substrate surface. [Image taken from Leamy et al (1978)]. (b) Anisotropy induced when a biaxial or higher order compressive or tensile stress exists.

For magnetostrictive films the intrinsic stresses induced during the deposition have a strong influence on the magnetic anisotropy. Films deposited at high sputtering kinetics show compressive stresses and no columnar structure formation [Shimada et al (1981)]. As discussed in the previous chapter, the intrinsic compressive stresses can result from any sputtering parameter which will increase the kinetics of the sputtered atoms. The magnetisation will couple with the stresses induced through the magnetostriction to produce a growth induced anisotropy which can be perpendicular to the plane of the film. The direction of the anisotropy induced is dependent upon the sign of the magnetostriction and also the sign and type of the stress (uniaxial, bi-axial, isotropic...) present within the film. This is more clearly illustrated in Figure 5.3b. For a perpendicular anisotropy to be induced in a film, the stresses induced therefore must be at least bi-axial in form to rotate the magnetisation out of the plane of the film as shown by Figure 5.3b. It is unlikely that a film deposited either by sputter or vapour deposition will develop a uniaxial stress direction, because of the random nature of the growth process. The intrinsic stresses which occur will be very random in direction on a local scale, giving rise to stresses which are likely to be isotropic in nature and which can account for the perpendicular anisotropy. It was shown in the previous chapter that FeSiBC films deposited onto glass cantilevers at low pressures, were found to be in a state of bi-axial compressive stress.

### 5.5.2 Stress Induced

Stresses in thin films can also be extrinsically induced due to the differing thermal expansion coefficients of the film and substrate as the film/substrate system cools after the deposition and contracts by different amounts. A film which is deposited onto a substrate which has a larger thermal expansion coefficient will be placed in a state of compressive stress, whereas a substrate with a lower thermal expansion coefficient will place the deposited film in state of tensile stress. If the stress is either bi-axial or isotropic, a uniaxial perpendicular anisotropy may be induced, depending on the sign of the magnetostriction (Fig. 5.3b). For substrates and films with similar expansion coefficients which are deposited at low deposition temperatures, this problem is usually avoided. However, stresses can also result from temperature differences which exist through the film and which cause different parts of the film to expand differently. This is especially important for substrates which are sputter cleaned prior to the deposition. If sufficient time is not allowed for the substrate temperature to cool, then the first few layers of the depositing film will be deposited onto a substrate at significantly increased temperature. This will therefore place the first few layers of the film in a state of stress as the substrate temperature equilibrates to the deposition temperature. This could severely effect the magnetic properties, especially in very thin films.

An alternative novel method of inducing a uniaxial magnetoelastic anisotropy during the deposition is to apply an external mechanical stress to the substrate [Ali et al (1999,1998), Garcia et al (1998)] which will induce a stress of the opposite sign; this is discussed in detail later in this chapter.

### 5.5.3 Field Induced

Inducing a uniaxial anisotropy by the application of a magnetic field parallel to the plane of the depositing film is a widely used technique. It is used in thin film sensors [Lu et al (1997), Morikawa et al (1997)] where it is preferable to align the domain magnetisation in a particular direction during the deposition; this removes the need to magnetically anneal the sensor at a much higher temperature to induce the required magnetic anisotropy. In some instances, depending on the type of sensor, it is not possible to substantially heat the sensor because of the delicate nature of other components which have been pre-fabricated onto the substrate for the operation of the sensor.

The origin of this uniaxial anisotropy is due to the directional ordering of like atom (e.g. Fe-Fe) pairs as described below for magnetic annealing. However, the ordering process in this situation occurs at an accelerated rate, even though the temperature of the depositing film is generally much lower in comparison. This is mainly due to the kinetic energies of the impinging sputtered atoms, which tend to be mobile at the surface of the film. This increased directional ordering is also assumed to be the reason why it is possible to induce much larger anisotropies in the depositing films, compared to conventional magnetic annealing where the directional ordering is not as high.

The magnetic field is usually provided by permanent magnets which are positioned on either side of the substrate or by a horse-shoe type of magnet arrangement. It is usual to shield the magnets by a grounded iron plate which prevents any stray field from the permanent magnets from disturbing the plasma dynamics. The shielding also prevents the magnets themselves from being sputtered. It is important that the applied field is parallel to the substrate surface and to minimise the number of flux lines which intersect (are not parallel to) the surface of the substrate and the plasma discharge. If the applied field is sufficiently large and parallel to the substrate as shown in Figure 5.4, then any secondary electrons on a collision path with the depositing film will be captured by the magnetic field, thus reducing the electron bombardment of the substrate. In the situation where the field lines have a transverse component to the substrate, there is an increase in the density of electrons arriving in the proximity of the substrate, which will therefore increase the likelihood of electron bombardment of the substrate [Ounadjela et al (1987)]. Ounadjela et al (1987) has shown that application of a field parallel to the substrate can reduce the substrate temperature by 150<sup>0</sup>C (see previous chapter). Obviously the application of a magnetic field will alter the sputtering dynamics and the surface mobility of the sputtered atoms; it is important to be aware of this fact. This generally means that the sputtering parameters need to be re-adjusted to account for this change.

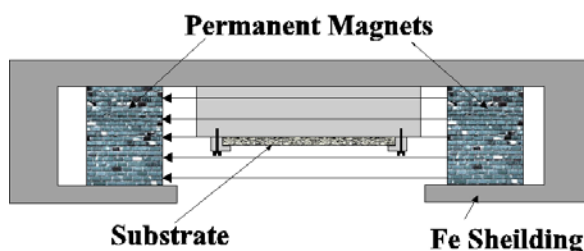


**Figure 5.4:** Schematic arrangement of substrate holder for deposition of films in a magnetic field.

## 5.6 Post-Induced Magnetic Anisotropy

### 5.6.1 Magnetic Annealing

Magnetic field annealing is a well established method for inducing a uniaxial anisotropy in amorphous ribbons or films. It generally involves heating a magnetic sample below the Curie temperature,  $T_c$ , in the presence of a magnetic field which is sufficiently large to saturate the sample so as to ensure that a single domain exists. The origin of this induced magnetic anisotropy has been attributed to the short-range directional ordering of atomic pairs (e.g. Fe-Fe). The high temperature allows atomic diffusion on a local scale so that a preferred orientation minimises the energy of the system of like atomic pairs and aligns them parallel with the magnetic field. This directional order is frozen in place as the sample is allowed to cool in the presence of the magnetic field giving rise to an easy axis direction which is parallel to the magnetic field. The domain structure for such a demagnetised sample displays a strong preference for the domain walls to lie parallel to the induced easy axis. The anisotropy energy for the induced uniaxial anisotropy has the same form as that of equation (5.3). It is found that the anisotropy induced by field annealing is not particularly strong in amorphous ribbons [Lurborsky et al (1977)] or films [Ali et al (1998), Garcia et al (1999)]. Typical induced values of  $K_u$  range from 30-100 J/m<sup>3</sup> ( $H_K=37$ -126 A/m) for the Fe-based ribbon alloys as found by Thomas et al (1992); it is found that the low anisotropy induced is sufficient to develop a well defined domain structure. The uniaxial anisotropy induced by the field annealing is a reversible process; annealing the sample just above the Curie temperature in the absence of a magnetic field, will disorder the atomic pairs. It is important that the sample is fully stress relieved before the field annealing process is undertaken, otherwise the stresses present will not allow a satisfactory field induced anisotropy to develop. The stress relief is commonly carried out at temperatures which are above the Curie temperature, but below the crystallisation temperature. The two steps are commonly performed in a single process, where the sample is first stress relieved at the upper temperature, and then magnetically annealed at the lower temperature for the

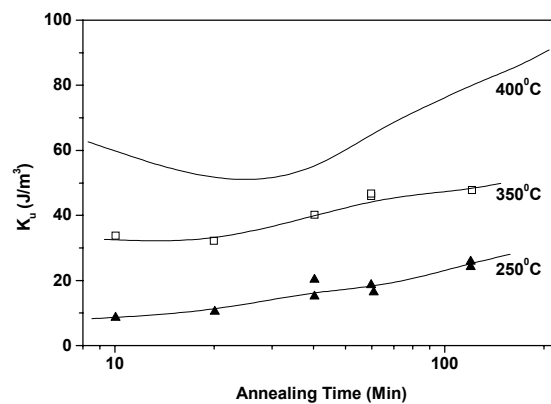


**Figure 5.5:** The development of a uniaxial anisotropy for an amorphous  $Fe_{78}Si_9B_{13}$  ribbon as function of temperature time at different annealing temperatures. Magnetic annealing field 400 kA/m. [Data taken from Thomas et al (1992)].

required time. It has been shown by Thomas et al (1992), that the magnitude of the anisotropy induced in Fe-based materials is dependent upon both the annealing time and the temperature. Figure 5.5 shows the results obtained from an FeSiB composition ribbon, where there is a clear trend shown with both temperature and annealing time.

Careful consideration is also needed when attempting to induce a uniaxial anisotropy in thin film sensors by the process of field annealing. The anisotropy induced by this method is relatively weak, and therefore the desired uniaxial domain structure may not be possible because of a significant contribution from the shape anisotropy due to the reduced lateral dimensions of the thin film sensors it will need to overcome.

In general, the field annealing is carried out under a low vacuum, usually in a wire-wound furnace arrangement similar to that used in this study (Fig. 3.9). However, in the case of amorphous wires, a circumferential anisotropy can be induced by current-annealing the samples using either DC or AC current [Costa-Kramer et al (1995), Dominguez et al (1996)] which optimises the magnetic anisotropy for magneto impedance effects (see MI). Current annealing has also been used to induce a transverse uniaxial anisotropies in ribbon materials [Valenzuela et al (1997)].

### 5.6.2 Stress Annealing

Up to the present time, the effects of external stress on the magnetic properties of materials have been mainly investigated on wires or ribbons [Spano et al (1982)], since it is a relatively straight-forward procedure to apply a tensile stress to such materials. For the same reasons stress annealing at high temperatures to induce a magnetic anisotropy has therefore also been confined to these bulk materials [Ref. List (5.2)]. The technique of stress annealing relies on the inverse magnetostrictive effect, where the magnetisation couples with the applied stress, and therefore the effect is more pronounced in highly magnetostrictive materials. The magnetic sample is placed under a tensile stress and annealed at a temperature below the crystallisation temperature so that the initially stressed sample becomes the zero stress state. On removal of the of the external tensile stress after the annealing, the sample is placed in a

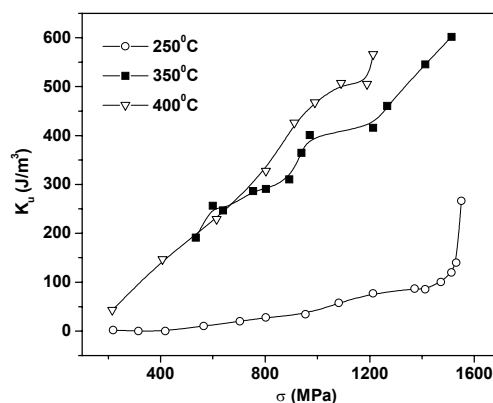


**Figure 5.6:** The development of a uniaxial anisotropy for an amorphous  $\text{Fe}_3\text{Co}_{67}\text{Cr}_3\text{Si}_{15}\text{B}_{12}$  ribbon as function of applied stress by the process of stress annealing at different annealing temperatures. Annealing time 1 hour. [Data taken from Dmitrieva et al (1999)].

state of compressive stress. Depending upon the sign of the magnetostriction of the material, a uniaxial magnetoelastic anisotropy will develop, either parallel or perpendicular to the stress axis. In the case of amorphous wires it is possible to use stress annealing to induce a circumferential anisotropy [Panina et al (1996), Sanchez et al (1996)]. This technique of stress annealing has been extended and applied to amorphous FeSiBC thin films deposited onto relatively ridged substrates [Ali et al (1999,1998)] and is discussed later in this chapter.

Investigations of stress annealing on ribbon samples have shown that the magnitude of the uniaxial anisotropy induced is dependent upon both the temperature and magnitude of the stress applied, and is also reversible; annealing the sample in the absence of any stress reduces the magnitude of the induced anisotropy [Dmitrieva et al (1999)]. The dependence of temperature on stress annealing is shown in Figure 5.6. As one would expect, increasing the annealing temperature accelerates the diffusion process forming a magnetic anisotropy at higher rate for the same annealing period. As with magnetic annealing, it is important that the sample is stress relieved, and therefore the stress annealing is carried out at the same annealing temperatures used to stress relieve the sample.

### 5.6.3 Annealing

The inhomogeneous stresses which are present in films or ribbons have the effect of degrading the magnetic properties of the material, as discussed in the preceding chapter, and therefore a stress relief is usually implemented to relieve these stresses which are carried out at temperatures below the crystallisation temperature. Annealing of a sample also generally has the effect of reducing the induced magnetic anisotropies outlined above.

## 5.7 Domains in thin films

In the absence of any magnetocrystalline anisotropy, the magnetisation will lie in the plane of film because of the large shape anisotropy. There would be no preferred direction for the magnetisation in the plane of the film (assuming  $N_z=1$ ) if no other form of anisotropy was present. However, it is found that films do possess domain structures which are nucleated in order primarily to reduce the magnetostatic energy which is associated with the stray field emanating from the magnetic sample. The domain and domain wall structure in magnetic films are dependent on the minimisation of the total energy of the system which include the anisotropy, exchange, magnetostatic, magnetoelastic and domain wall energies. The effect of the magnetostatic energy is illustrated in Figure 5.7, where the stray field from a uniformly magnetised sample which has a uniaxial anisotropy is shown. In the single domain configuration, there are a large number of free “magnetic poles” at the ends of the film which gives rise to a large stray field or magnetostatic energy. This energy is approximately halved if the single domain splits into two domains which are oppositely magnetised as shown in Figure 5.7b. In this case the opposite “magnetic poles” are now closer in proximity to each other, decreasing the amount of stray field emerging from the sample. Subsequent sub-divisions of the domains as shown in Figure 5.7c

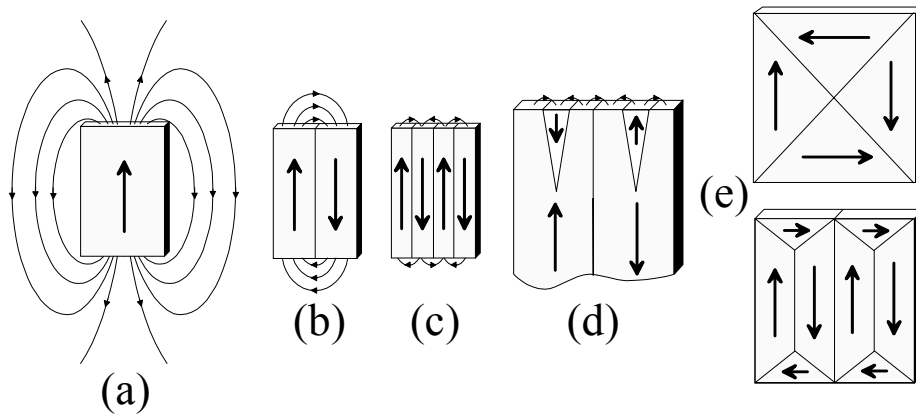


**Figure 5.7:** Illustration of stray magnetic field from a sample with a uniaxial anisotropy with (a) single magnetised domain, (b) two and (c) four domains. (d) Reverse spike domains which can form in a uniaxial domain structure. (e) Flux closure domains which prevent any stray flux from emerging from the sample.

will result in further reductions in the magnetostatic energy. The sub-division of the domains continues until the energy needed to create a new domain wall exceeds the accompanying reduction in the magnetostatic energy. Often a material with a uniaxial anisotropy will form reverse spike domains (Fig. 5.7d) at the edges of the film to introduce “magnetic poles” of the opposite sign at the edges of the film reducing the magnetostatic energy; this occurs without a significant increase in the domain wall energy because of their short length. The domain walls shown in Figures 5.7a-d, are known as  $180^\circ$  walls, since the magnetisation on either side of the wall is anti-parallel, and they occur in virtually all materials. Examples of  $90^\circ$  walls are shown in Figure 5.7e, where the magnetisation direction changes by  $90^\circ$ . In these two examples, there are no free poles and therefore the magnetostatic energy is reduced to zero. These types of domain structures tend to occur in cubic crystals where there are easy axes at  $90^\circ$  to each other. These triangular domains are known as closure domains. It is usual that the second type of domain structure containing both  $180^\circ$  and  $90^\circ$  walls is formed, since it reduces the magnetoelastic energy which is dependent upon the area of the domains. For example, if the magnetostriction of the material is positive, then all domains will distort in the direction of the domain magnetisation. In the case of the domain structures shown in Figure 5.7e this is prevented by the adjoining domains, which therefore introduce strain into the domains. Closure domains tend not to form in films with a uniaxial anisotropy since it involves the magnetisation pointing along a hard axis which is energetically unfavourable. If the anisotropy  $K_u$  induced is relatively small, then closure domains have known to be formed to reduce the magnetostatic energy. One should refer to the text of Hubert et al (1998), where a vast range of domain structures possible in thin films have been presented. It should be noted that when a film is magnetically saturated along an easy axis, the film can still remain as a single domain on removal of the magnetic field. This is due to the in-plane demagnetising fields being essentially zero, especially if the film is relatively large.

The domain walls in films extend through the entire thickness of the film as shown in Figure 2.27e where domain images were taken from the top and bottom surface of an FeSiBC thin film deposited in this study. Domain walls have a finite width where the magnetisation rotates gradually from one domain

direction to the other. The width of a domain wall is dependent upon the exchange energy which prefers the magnetisation to rotate slowly from one orientation to the other leading to wide walls, whereas the anisotropy and demagnetising energies prefer the magnetisation to switch instantly to the opposite direction and therefore prefer narrow walls. An equilibrium between these energies determines the thickness of the domain wall. There are three main types of domain walls which can exist in thin films; these are illustrated in Figure 5.8. The Bloch wall is the same type of wall which appear in bulk materials were the magnetisation rotates out of the plane of the film. A Néel wall is defined by the magnetisation rotating in the plane of the film which reduces the magnetostatic energy of the wall, since the magnetisation is not pointing in an unfavourable directions (out of plane) as with a Bloch wall. A cross-tie wall is defined by a mixture of spins pointing out and in the plane and is identifiable by spike walls which form to ensure flux closure. It is found that in thin films Néel walls have a lower magnetostatic energy than Bloch walls and are therefore more energetically favourable. The energies of different types of walls in thin films are shown in Figure 5.8 as a function of film thickness for a permalloy film. The cross-tie walls appear in between the transition region from Bloch to Néel walls. The widths of the domain walls also vary as a function of film thickness where Bloch walls become narrower and Néel walls become wider with decreasing film thickness.

Knowledge of the domain structure enables a better understanding of the magnetisation and hysteresis process in ferromagnetic materials. On application of an applied field, the domains whose magnetisations are closest to the direction of the applied field will grow at the expense of domains which are not. For example, if a magnetic field is applied vertically along the domain structure shown in Figure 5.7b, the magnetisation process will occur purely by domain wall displacement. However, if

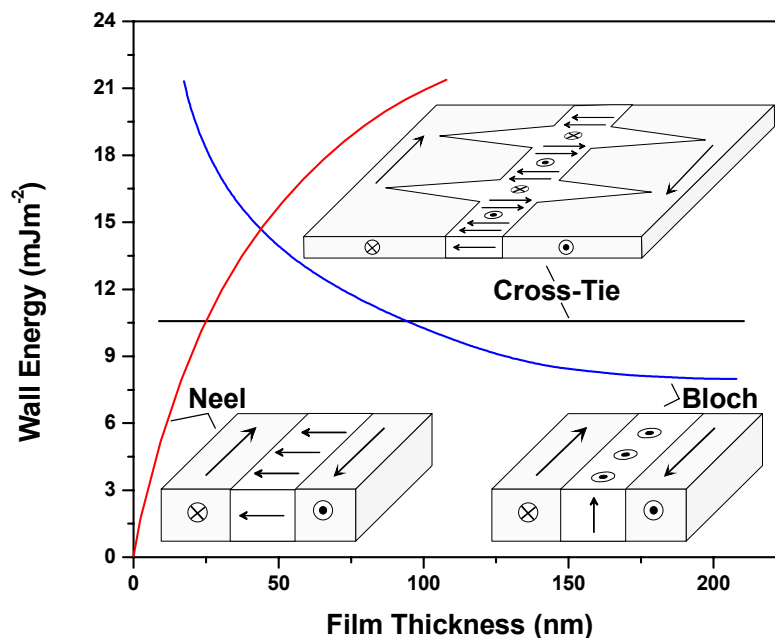


**Figure 5.8:** Comparison of domain wall energies for a Bloch, Néel and Cross-tie wall for a permalloy film as function of film thickness [Data obtained from Prutton (1964)] and illustrative diagrams of the respective domain wall spin configuration.

a small field is applied to the domain structure shown in Figure 5.7e, the domains with the magnetisation parallel with the field will either grow or shrink respectively until there is only one domain with its magnetisation directed along the field and the unfavourable domains where the magnetisation is at  $90^\circ$ . On further increases in the field, the magnetisation process will now occur by domain rotation, where the magnetisation in the unfavourable domains are rotated into the field direction until all the domains are swept out. Usually the magnetisation process is due to both domain wall motion and magnetisation rotation, unless the field is applied either parallel or perpendicular to a material which has a well defined uniaxial anisotropy. In general for sensors, it is preferred that the material possess a uniaxial anisotropy.

In stress sensor applications, for example, a change in magnetic permeability,  $\mu$ , is measured [Arai et al (1994)] as a function of the applied strain,  $\varepsilon$ . In such cases, the effectiveness of the stress sensor is compared by determining a figure of merit (FOM) of the material, which can be defined as

$$FOM = \frac{1}{\mu} \cdot \frac{d\mu}{d\varepsilon} \quad (5.18)$$

Since the permeability is inversely related to the anisotropy field, the FOM may be maximised by careful control over the direction and magnitude of the anisotropy. For maximum sensitivity, a sufficient anisotropy is required to properly define the easy and hard axes, but not to be so large that the relative change in permeability is severely reduced. The maximum FOM obtained for magnetostrictive materials is two orders of magnitude greater than the equivalent FOM for competing piezoresistive materials [Gibbs et al (1997)]; this indicates the potential for excellent highly sensitive devices.

## 5.8 Results and discussions

### 5.8.1 Radial Magnetic anisotropy of the as-deposited films

The as-deposited films display a significant, reproducible anisotropy which is radial about a central point corresponding to the centre of the magnetron sputtering source housing the target [Ali et al (1998)]. Figure 5.9 shows typical domain images obtained from films deposited on two standard (76mm×25mm) substrates which were deposited simultaneously at the optimised sputtering parameters; this figure shows the radially magnetic anisotropy where the easy axis of magnetisation is orientated radially from a central point on the left film. It is generally found that the anisotropy of the as-deposited films is uniaxial, but in this case (Fig. 5.9) it is shown that the induced anisotropy is radial in form when depositing films on large substrates. One should notice that the domains are not exactly continuous in Figure 5.9; the reason for this is, that it was only possible to obtain domain images up to an area of 25×15mm unless otherwise stated, and therefore the domain images shown across larger film surfaces are composite images constructed from individual images taken from the respective areas of the film. An important point emerging from these composite images is that the magnetisation process is reasonably reproducible, since the film had to be physically moved each time a different section of it had to be imaged. This also meant the film had to be magnetically saturated and demagnetised each time in order to obtain a difference image (see MOKE Chapter). The domain images shown in Figure 5.9a,b are continuous in direction from the right to left film, and converge to a central point on the left film. The reproducibility of the magnetisation process was also confirmed by MOKE measurements, where

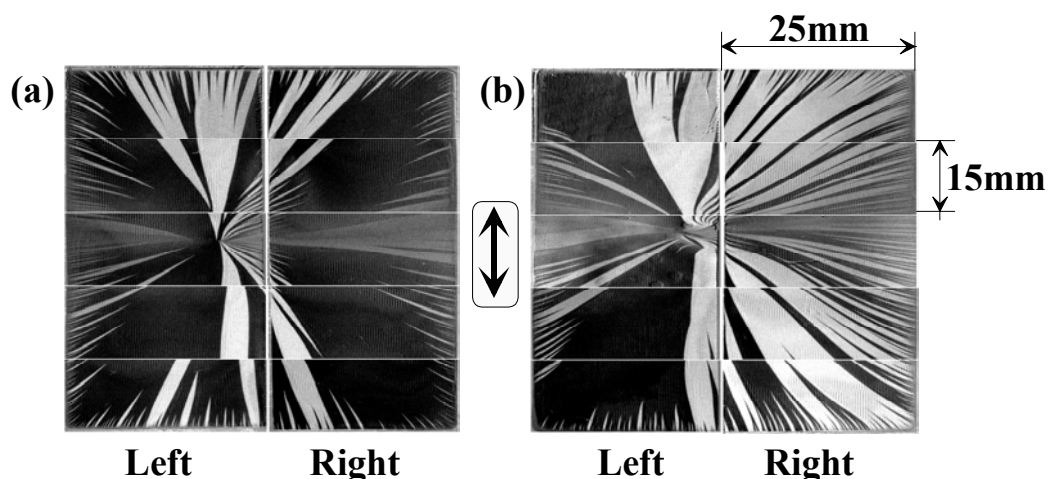


**Figure 5.9:** Typical domain images from as-deposited FeSiBC films displaying a radial induced magnetic anisotropy. The domain images are constructed from composite images (see text), where each image is 25×15mm in dimension. Note the dimension of one slide is 76×25mm. The images were obtained after the film was demagnetised along the length of the film. (a) An FeSiBC film deposited onto two glass slides. (b) An FeSiBC film deposited onto Corning® glass slides. See Figure 5.12, for a further example of the this radial induced magnetic anisotropy. The two films deposited in each growth will be referred to as the left and right films respectively in this study. (Transverse MO sensitivity), (75W,4mTorr).

repeated loops were taken from the same point. The MOKE loops are shown in Figure 5.10 where the loops cannot be distinguished. Domain images have also been included to indicate the reproducibility of the domains and the position at which the loops were taken.

In the early stages of this study it was found that, in the case of the films which were deposited onto  $1\text{cm}^2$  substrates, the magnitude and direction of the anisotropy was influenced by the positioning of the substrate on the substrate platter. The anisotropy of the films appeared to be isotropic in films which

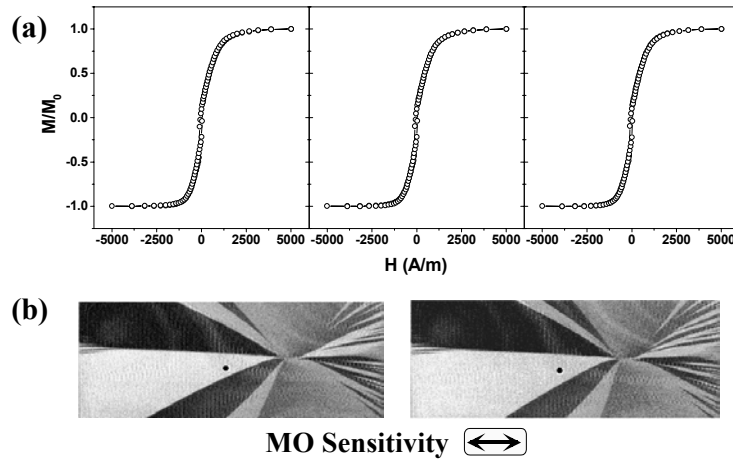


**Figure 5.10:** (a) MOKE loops of an as-deposited film indicating the reproducibility of magnetisation process. Loops taken vertically where the black circular spot indicates the position at which the loops were taken (b) Domain images taken from the central region of the left film. In each case the film was magnetically saturated and the image was taken with an applied field of  $35\text{A/m}$  in the vertical direction.

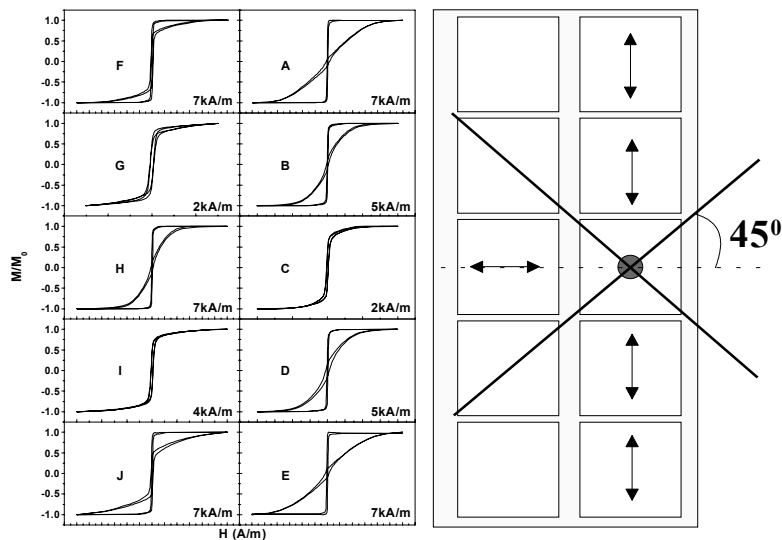


**Figure 5.11:** Orthogonal MH loops obtained from  $1\text{cm}^2$  FeSiBC films which were arranged in the position of the left film. Hysteresis loops from film C, correspond to the sample which is directly above the target and is also indicated by the circular spot. The arrows in the diagram indicate the easy axis as determined from the MH hysteresis loops. The magnitude of the field at which the hysteresis loops were take are shown at the bottom right corner. ( $75\text{W}$ ,  $4\text{mTorr}$ ).

were located directly above the centre of the target and at positions which lay along a line at  $45^\circ$  from the horizontal from position (c) as shown in Figure 5.11. In all other substrate locations, a uniaxial anisotropy appeared to develop in the films. The hysteresis loops were taken using the inductive magnetometer which only allowed measurements to be taken in two orthogonal directions parallel to the square edges of the substrates. This meant if the easy axis lay along a diagonal of the  $1\text{cm}^2$  film, it would appear that the film was isotropic from the hysteresis measurements; this explains the significance of the films appearing isotropic along locations indicated by the solid lines projected at  $45^\circ$  from the horizontal from position (c). It was not until the MOKE magnetometer and MOKE imaging system were constructed (Chapter 2) that the magnetic anisotropy present in the as-deposited films was fully understood.

Films were deposited on substrates with dimensions of  $76\times 50\text{mm}^2$  so that the magnetic anisotropy of the as-deposited films could be fully investigated without the complication of the centre of the radial pattern being effected by the edge of the film. Figure 5.12a shows the central region of the domain structure obtained from one such film. The easy axis was determined from both MOKE hysteresis measurements, which allowed the magnetic anisotropy to be investigated through a full  $360^\circ$  in the plane of the film at any particular point (indicated by the arrows), and by observing domain growth on application of a magnetic field of known direction. It was found that the anisotropy appeared to be isotropic at the centre of the radial pattern, but was uniaxial as one moved away from the central point of the radial pattern in any direction, as also indicated by the domain structure. It should be noted that the domain structure shown in Figure 5.12a is a demagnetised domain pattern obtained by combining images sensitive to the transverse and longitudinal components of the magnetisation (see MOKE

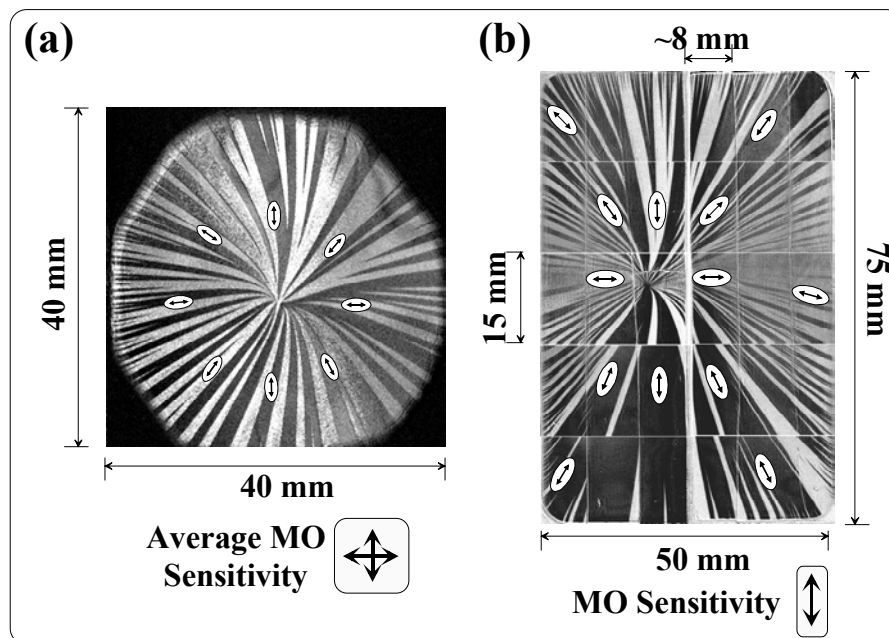


**Figure 5.12:** Radial domain structures from a FeSiBC film deposited on silicon. (a) Domain image from central region of film (b) Domain image from the same film, but with film cut into narrow strips. Note (b) is a composite image of the entire film. The arrows in the two images indicate the direction of the easy axis as determined from MOKE measurements. (75W, 4mTorr)

Chapter). The domain image is very symmetric about the central point and reverse spike domains exist at the edges of the film so as to reduce the magnetostatic energy. The demagnetised domain structure of the same film is shown in Figure 5.12b, where the film had been cut into narrow strips, and the entire film was imaged. This domain image demonstrates that the anisotropy is, indeed, radial in form, since the domains on the individual film strips still converge to the same central point on the left, even though the strips were not in physical contact with one another and hence no magnetic coupling existed. Clearly, a uniaxial domain structure exists on a local scale across the width of the outermost strips, which slowly rotates along the length of the film strips in accordance with the radial anisotropy, whereas the uniaxial anisotropy of the central strips is aligned approximately along the length of the films. MOKE measurements, indicated by the arrows, also confirm the direction of the anisotropy as shown by the domain structure. Further examples of domain images illustrating the radial anisotropy can be seen in Figure 5.34, obtained from patterned films.

The breaking up of the complete film does not affect the radial anisotropy and a further example of this is shown in Figure 5.13, where domain images were obtained from the central region of the narrow films strips in their remanent state after being magnetically saturated along the length and width of the film respectively. The anisotropy induced in the films is sufficiently large and well defined that the domain structure reverts back to the form dictated by the radial anisotropy. The anisotropy is unaffected by the width of the film strips even for the film strip which has a shape aspect ratio of 50:1, but there is an increase in the density of domains per unit area for the narrower films in order to reduce the magnetostatic energy; this behaviour is as one would expect. The magnitude of the uniaxial anisotropy present in the film is found to increase as a function of distance from the centre of the radial pattern. The variation of the anisotropy field along a straight line through the centre of the radial pattern, as measured with MOKE, is shown in Figure 5.14a. At the centre of the pattern the anisotropy field is small and isotropic, but the anisotropy transforms into a well defined uniaxial anisotropy as one moves away from the centre of the pattern with its magnitude increasing linearly. Examples of easy and hard axis loops are shown in Figures 5.14(b,c,d) which indicate a uniaxial anisotropy. On annealing the film,

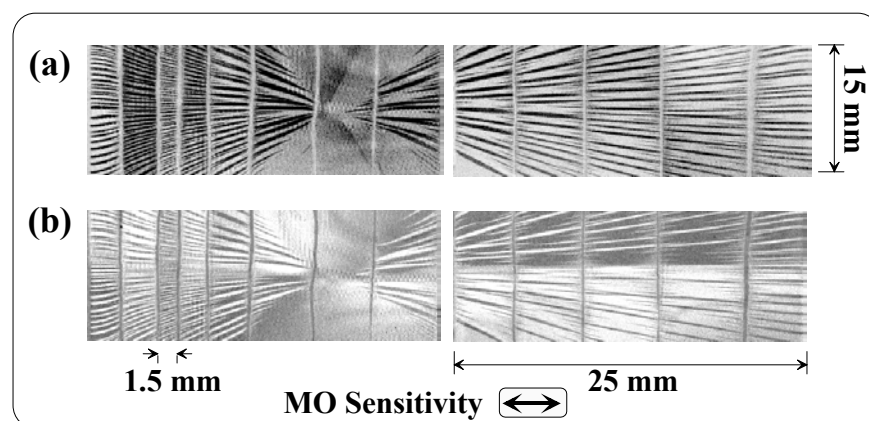


**Figure 5.13:** Radial domain image obtained from the central region of a FeSiBC film which has been cut into various widths. Initial film deposited onto a silicon substrate 76×50 mm. (a) Remanent image after being magnetically saturated across the width of the film strips (b) Remanent image after being magnetically saturated along the length of the film strips. (75W, 4mTorr).

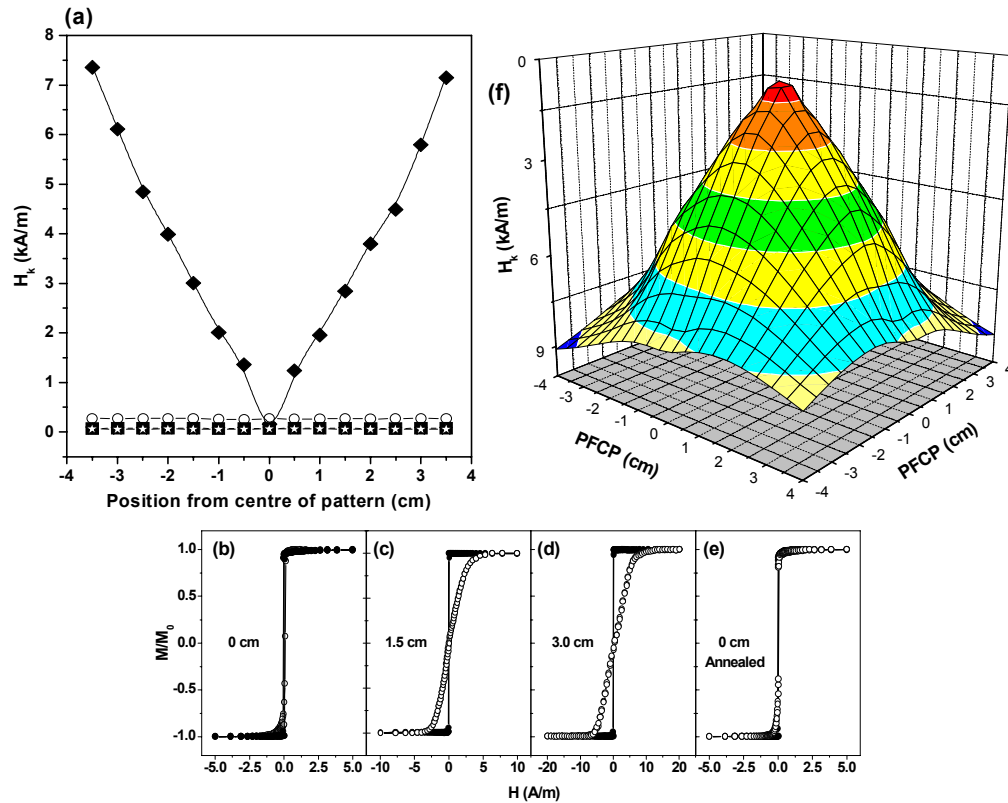


**Figure 5.14:** (a) The variation of the anisotropy field measured along straight line which passes through the centre of the radial domain pattern for a typical FeSiBC film. The solid diamonds represent the hard axis values and the solid squares are the easy axis values for an the as-deposited film. The open circles (hard axis) and the open stars (easy axis) are the respective values (orthogonal measurements) after the film has been annealed (390°C:1hour). (b),(c) and (d) are the MOKE hysteresis loops for positions indicated from the centre of the pattern. (e) are the loops from the film after being annealed from the location where the centre of the radial pattern existed. (f) represents a computed 3d map of the anisotropy field generated from six 2d-line scans as shown in (a) for the as deposited film.

it is found that the radial anisotropy is removed and the film displays no preferential anisotropy (Fig. 5.14e) but is uniform throughout (Fig. 5.14a); this is obviously very important for the mass production of sensors. It would not be economically viable if only one sensor could be coated at time because of the differing magnetic properties due to the position of the sensor on the substrate platter. Obviously, this radial anisotropy could also be utilised to control the direction of the anisotropy and the magnitude of anisotropy field induced in a number of sensors in the one deposition by the careful positioning of the substrates on the substrate platter; the anisotropy field is shown to increase linearly with distance from the centre of the pattern (Fig. 5.14a) and is radially symmetric about the centre as shown by the 3D map of the anisotropy field in Figure 5.14f. The sample or sensors would ideally need to be no larger than 1-2mm<sup>2</sup> in order to ensure that the anisotropy was uniform over the whole film. It is important to be aware of such magnetic anisotropies which can result from sputter deposition, especially in the growth of soft magnetic materials over large areas.

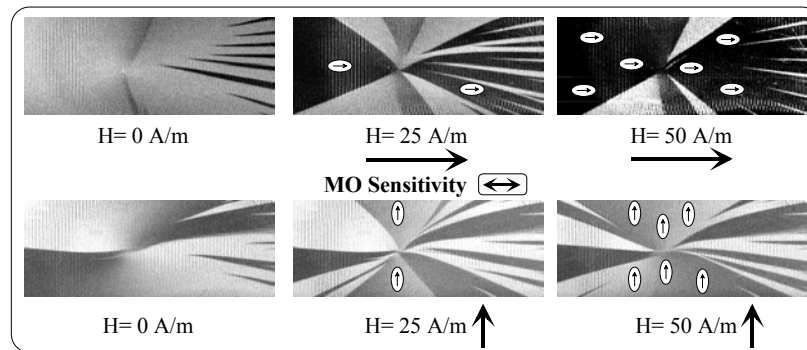


**Figure 5.15:** Domain images taken under the influence of an applied field. The two fields used were orthogonal to each other. (75W, 4mTorr).

Figure 5.15 are domain images taken of the central region of the radial pattern at the applied fields shown. The film was initially saturated in the opposite direction to the applied fields shown in the two sets of images. The application of an applied field in the horizontal or vertical directions illustrates the radial anisotropy present by the growth of favourable domains in the direction of the applied field at the expense of the unfavourable domains. At remanence, the film is not a single domain and some domain structure is present to reduce the magnetic energy of the system. It should be noted that not all the domain structure is visible here, since the MO sensitivity in these images is dependent upon the longitudinal component of the magnetisation. On the images the growth of the favourable domains is illustrated by the arrows. On the onset of an applied field in either direction, the nucleated domains converge to the central point and the favourable domains grow in size at the expense of the others. The reason for the domains to converge to this central point is the strength of the anisotropy and its radial form, which can be clearly seen in Figure 5.14f. The magnitude of the anisotropy is symmetric and decreases radially to a minimum at the central point. Hence, the application of a field in any direction in the plane of the film will always nucleate a domain, which will be parallel to the field and also pass through this central point, since the applied field will always point along an easy axis of magnetisation through this central point as shown by the demagnetised domain image of Figure 5.11a. Domain structures in which the magnetisation points in a non-easy axis will not form at the low fields because of the large anisotropy energy required. Instead, the domains initially converge to this central point in accordance with the radial anisotropy and the applied field to minimise the magnetic energy of the system. Domains with the same domain magnetisation join together at this point, as can be seen from the two sets of images. Since the anisotropy is a minimum at this point, the favourable domains grow in size sweeping radially from this point. At higher fields, the magnetisation process proceeds with both domain wall movement and domain rotation.

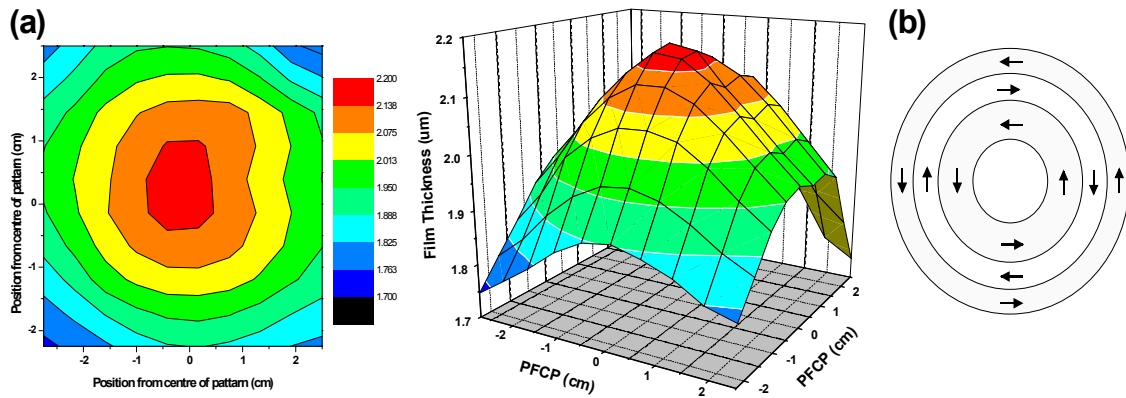


**Figure 5.16:** (a) Computed 3d map of the thickness profile across a FeSiBC film from 2d thickness line scans. PCPP=Position From Centre of Pattern. (75w, 4mTorr, 2µm). (b) A schematic diagram of expected domain structure from such thickness profile.

Ferromagnetism only appears when the sputtered atoms deposit themselves on the substrate, therefore it was believed that this spot on the left film corresponded to the thickest part of the film which would also be the first point where any ferromagnetism would appear. The remainder of the depositing film was then assumed to be influenced by this thus point giving rise to this unique radial anisotropy. A three dimensional thickness map was computed from two dimensional line scans of the thickness profiles (Fig. 3.6) to ascertain the thickest part of the deposited film and the findings for a 2µm film are shown in Figure 5.16a. There is a well defined thickness profile, as one would expect, where the thickest part of the film corresponded to the centre of the magnetron source and the radial spot. However, the magnetic anisotropy from such a thickness profile would not give rise to a radial anisotropy but to an anisotropy which is concentric in form as shown schematically in Figure 5.16b due the shape anisotropy.

Similar radial domain structures can also occur in films which are slowly cooled through their Curie point [Bishop (1998)]; however, this possibility was excluded since it was established that the temperature of the depositing film did not rise above 100°C.

Stress was also considered as a possible source of this anisotropy, because of the mounting of the substrates to the substrate platter. This possibility was eliminated by the use of a picture frame holder, which ensured that the substrates were free to move within the holder, and were only held in position under their own weight. It would be difficult to imagine that such a clamping procedure could repeatedly induce a spherically symmetric bending of the substrate, especially in the instances where two separate substrates were mounted. Stress could also be introduced because of the different thermal expansion coefficients of the substrate and the depositing film. However, it was found that simultaneous growth onto two separate substrates always produced a single spot in the radial anisotropy distribution, which always appeared on the left film corresponding to the centre of the target; the domain patterns were continuous from the right to the left film where they converged as shown in the Figures. Since the thermal contact between the two slides is very poor, this observation is inconsistent with the thermal mis-match or any thermal gradients which may exist across the two slides

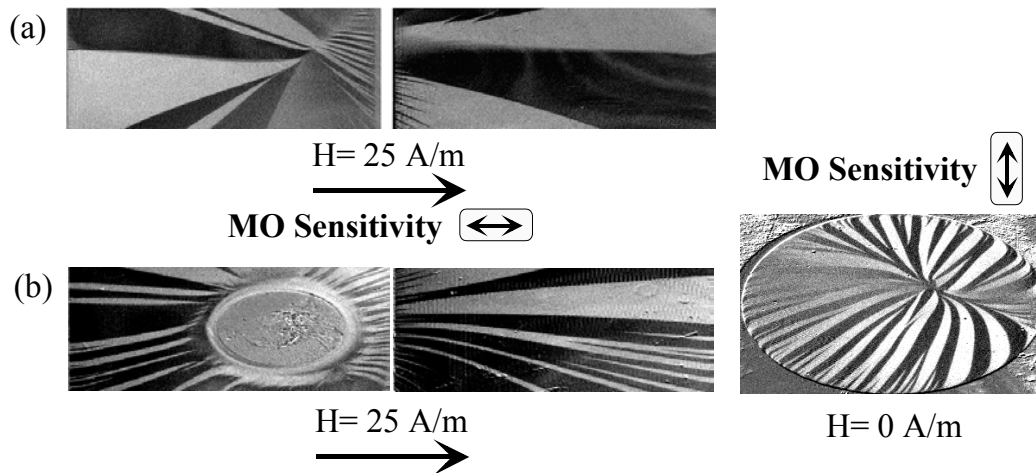


**Figure 5.17:** (a) Domain images taken from the left and right films which were separated by a distance of 5mm and lifted off the substrate platter to ensure isolation of the films during the deposition. Image dimensions 25×15 mm. (b) Domain images from films which were deposited with a cover slip over the central point of the pattern.

and thus being the cause of this radial anisotropy. Another source of stress from which the deposited films can suffer is the growth induced stress from the sputtering process as described earlier. However, in order to minimise this effect the growth conditions have been optimised as investigated in the previous chapter. It is difficult to imagine how the growth induced stresses would be so symmetrical about the same central point and also increase in strength radially from a central point so as to give rise to such a well defined anisotropy distribution as shown in Figure 5.14. Whilst stress free films are difficult to achieve, it is believed (see below) that another anisotropy mechanism dominates.

The above effects also cannot explain why the domain structure of the films deposited onto isolated substrates still display domains which converge to the central point directly above the target (Fig. 5.17a). The substrates were separated and lifted slightly from the substrate platter; this was to ensure that there was no magnetic coupling between the films through the material which was being deposited on the substrate platter, which could give rise to the continuous domains across the films due to the magnetic coupling. Films were also deposited simultaneously onto circular cover slips which were mounted directly over this central point. This was to ascertain whether the centre of the pattern would be effected and move to a new position. The cover slip was mounted in such away that there was no magnetic coupling present between the depositing film on the cover slip and the depositing films on the two glass slides. It is can be seen from Figure 5.17b that the radial anisotropy is still present, the centre of the pattern has not moved and is visible on the cover slip. The anisotropy mechanism which is inducing this radial anisotropy is able to exert its influence in films which are not physically connected to each other. As discussed previously, the morphology of a depositing film can induce a contribution to the anisotropy. Under certain conditions columnar growth, caused by the self shadowing of the depositing atoms can also give rise to an in-plane anisotropy. It has been shown by Leamy et al (1979) that incident atoms arriving at oblique angles to the substrate, will form a film with a columnar structure which is at an oblique angle governed by equation 5.17. This type of columnar growth could explain the radial anisotropy and why the domains appear continuous on isolated substrates, but it is

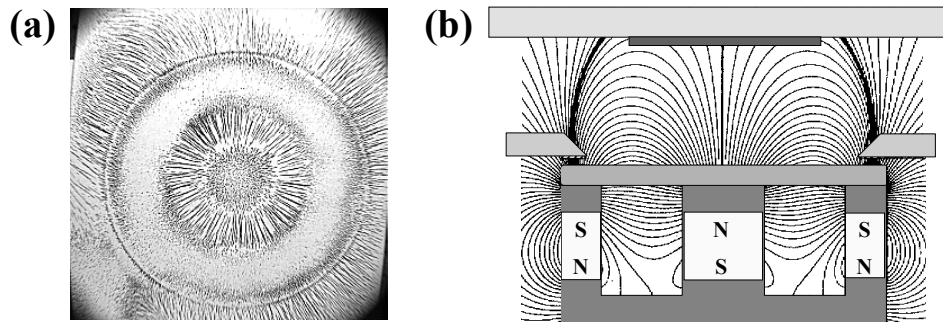


**Figure 5.18:** (a) Magnetic field pattern obtained from the residual magnetron field present at the substrate platter using iron filings from target position one. (b) Schematic illustration of the magnetic field pattern between the target and substrate platter.

very unlikely that such an effect could produce incident atoms with a radial distribution and an increasing angle of incidence as a function distance from the centre. Generally, it is found that the columnar structure induces a uniaxial anisotropy in the films. However, the deposition geometry (15cm diameter target) used in this study and the optimised sputtering parameters at which the film were deposited, preclude such an explanation.

The effects of a forming field during the deposition of magnetic films is a well known method of inducing a uniaxial anisotropy. In this study it was found that a weak residual field from the magnetron source was present at the substrate platter during the deposition of the films; this had a radial symmetry about the centre of the magnetron source. This radial symmetry is shown in Figure 5.18a, where the magnetic field pattern was obtained using iron filings. Figure 5.18b is schematic diagram of the shape of the magnetic field pattern which is likely to be present between the target and substrate platter as a result of the magnetron. The strength of this field at the substrate platter was found to be approximately 500 A/m with the target configuration shown in Figure 3.3. From Figure 5.18a it is apparent that the FeCo backing plate and the METGLAS<sup>®</sup> 2605SC ribbon target were not flux closing all the magnetron field, and there was, therefore, a component of the residual field parallel to the substrate platter. The radial anisotropy present in the as-deposited films was therefore attributed to the variation of the in-plane component of this residual field from the magnetron source. This was further verified by placing weak permanent magnets on either side of the substrates to show that the radial anisotropy could be modified by an additional magnetic field. As discussed earlier, introducing strong magnetic fields near the substrate will dramatically effect the dynamics of the sputtering process, and would therefore have required optimising the sputtering parameters to account for this. However, the radial anisotropy being investigated could have also been effected by these changes in the sputtering parameters. The current system was not designed for housing permanent magnets at the substrate platter, and considerable modifications would have been required to house the magnets ideally, as shown for example in Figure 5.4. This problem was overcome by the use of very weak, flat, bar magnets which produced a measured magnetic field of approximately 800 A/m. The strength of the field is comparable with that of the residual field from the magnetron source and therefore had little influence on the dynamics of the sputtering process occurring at the substrate. Pieces of the METGLAS<sup>®</sup> 2605SC ribbon were cut to

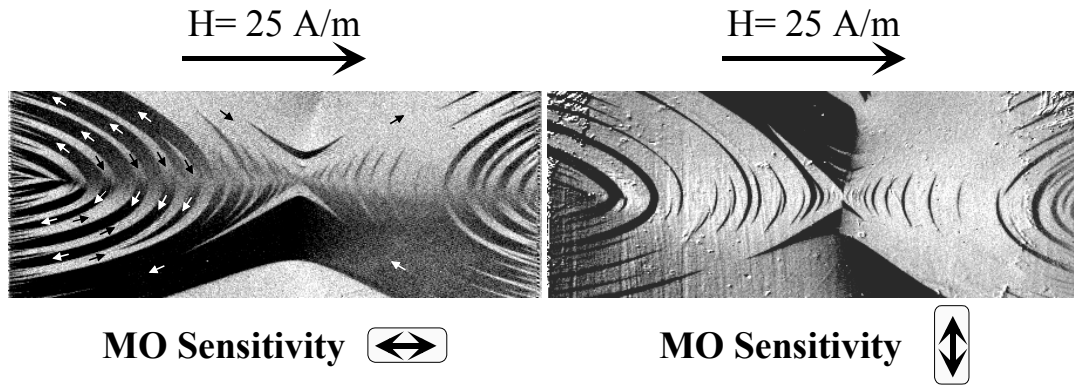


**Figure 5.19:** Domain images taken from an FeSiBC film which was deposited using a forming field provided by two weak bar magnets.

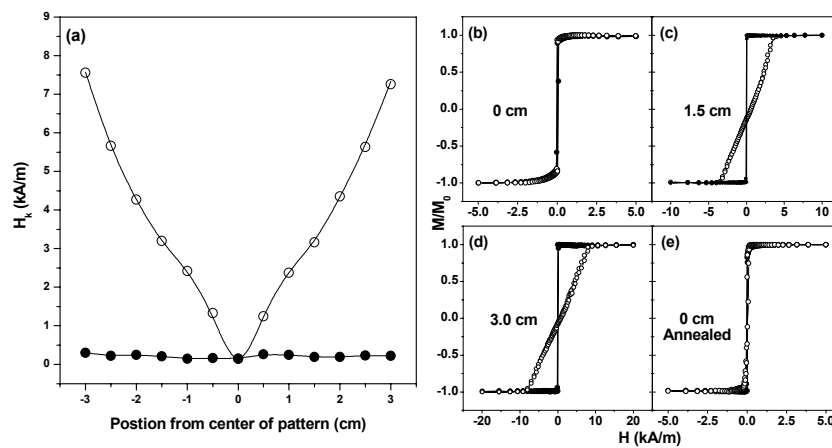


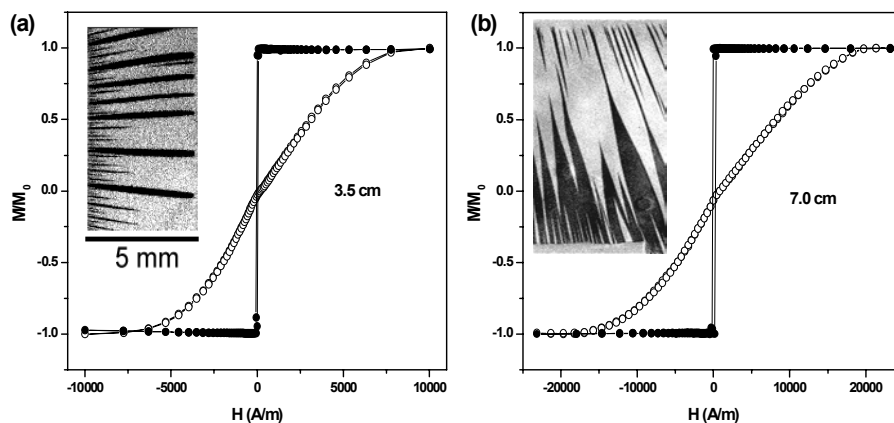
**Figure 5.20:** (a) The variation of the anisotropy field as measured along straight a line which passes through the centre of the radial domain pattern for a FeSiBC film which was deposited in the absence of an FeCo backing plate. The open circles represent the hard axis values and the solid circles are the values after the film has been annealed (390°C:1hour). (b),(c) and (d) are the MOKE hysteresis loops for positions indicated from the centre of the pattern. (e) are the loops from the film after being annealed from the centre.

size and bonded to the top side of the bar magnets which were facing the plasma. This prevented the plasma from actually coming into contact with the magnets, and it also flux closed any magnetic field lines emanating into the plasma. It was found that the positioning of the bar magnets around the substrate did, indeed, modify the radial anisotropy, and one of the more interesting anisotropies induced is shown in Figure 5.19. Here two bar magnets were placed on either side of a glass substrate such that the magnetic field lines from the two magnets parallel to the substrate surface were semi-circular in form. The domain images indicate vividly the form of these magnetic field lines by the presence of semi-circular domains; the domain directions have been indicated by the small arrows. The magnetic softness of the films deposited in the presence of these bar magnets showed no deviations from the standard films which were deposited.

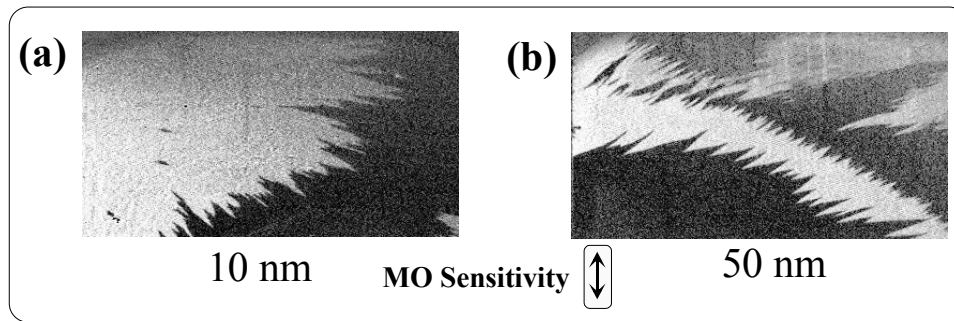
Having ascertained that the radial anisotropy in the films was due to the residual field from the magnetron source, films were deposited in the absence of the FeCo backing plate; this increased the horizontal component of the residual field at the substrate platter to approximately 1kA/m. The magnetic field pattern at the substrate platter obtained by iron filings had a similar appearance to that of

Figure 5.18a. The removal of the FeCo plate halved the deposition rate, so the growth time was doubled so as to maintain the standard film thickness of 500nm. No difference in the magnetic softness was found and the radial anisotropy was still present as shown in Figure 5.20. The profile of the anisotropy field across the film was similar to that found in films deposited with the FeCo backing plate. In the more usual ribbon form of ferromagnets, the introduction of a uniaxial anisotropy by means of magnetic annealing is a well established technique, as demonstrated by Thomas et al (1991). The magnitude of the field strength necessary to achieve a well defined domain structure is of the order of  $5 \times 10^4$  A/m for amorphous ribbons; this is much larger than the stray residual field from the magnetron present at the substrate platter, but is similar to the field (200kA/m) used in this study to magnetically anneal the as-deposited FeSiBC films. This is a consequence of the kinetic energies of the impinging sputtered atoms as they adhere to the substrate. At the surface of the substrate the atoms are highly mobile, allowing the residual field to exert a significant influence. Consequently the directional ordering of like atom pairs is notably larger, whereas in ribbons or films a large field in conjunction with an annealing temperature of the order of the Curie temperature is necessary to provide sufficient mobility of the atoms. The reported [Thomas et al (1991)] hard axis anisotropy fields for METGLAS<sup>®</sup> 2605SC ribbon after optimal field annealing is approximately 100 A/m ( $K_u \sim 80 \text{ Jm}^{-3}$ ), whereas Figure 5.14 shows that  $H_k$  can vary from 150-8000 A/m using the residual forming field present at the platter. It is clear from these results that the introduction of an anisotropy with a forming field produces a well defined anisotropy at significantly lower fields.

It is important therefore to be aware of such anisotropies as can result from magnetron sputter deposition, especially where soft magnetic (300 A/m) materials are being deposited over large areas where the coercive fields of the depositing film are small in comparison with the residual field. By careful positioning of the small substrates on the substrate platter, one can control both the magnitude and direction of the induced uniaxial anisotropy. This is shown in Figure 5.21, where a well defined uniaxial anisotropy is obtained from two as-deposited films positioned 3.5cm and 7cm from the central



**Figure 5.21:** Domain images and respective MOKE loops from as-deposited films. (a) The substrate was positioned 3.5 cm from the central spot along x-axis [Ali et al (1998)]. (b) The substrate was positioned 7 cm from the central spot and rotated through  $15^\circ$ . The easy and hard axis are shown. Domain images taken at remanence ( $H=0$  A/m).



**Figure 5.22:** Domain image from a (a) 10nm and (b) 50nm as deposited FeSiBC film.

spot. The film in Figure 5.21b was also rotated through  $15^{\circ}$  to illustrate that the uniaxial anisotropy can be induced at any direction in the film. The hard axis anisotropy fields induced in the two films were 5kA/m and 15kA/m respectively, significantly larger than the process of field annealing.

The effects on the radial anisotropy of varying the pressure is as one would expect. That is, below about 4mTorr it is completely overcome by the more dominant stress-induced anisotropy, which gives rise to a perpendicular anisotropy. Above 4mTorr the coercivity increases slowly with pressure, and it is found that the radial anisotropy becomes less distinct with increasing pressure. The general findings were that if the as-deposited film had coercive fields larger than approximately 250A/m, then no radial domain structure was visible. No attempt was made to map the anisotropy profiles of these films as in shown Figure 5.14, since they would be of no practical use here because of the larger coercive fields. The domain images from a 10 and 50nm as-deposited film are shown in Figure 5.22, where the film was deposited at the optimised sputtering parameters. These images show that the radial anisotropy is no longer present and some other mechanism dominates. The easy axis coercive fields of these two films were 286 and 311 A/m respectively.

Summarising, the radial anisotropy is due to the horizontal component of the residual field from the magnetron sputtering source. Any other anisotropy mechanism which has a larger influence than the residual field of approximately 500 A/m, will dominate and overcome this radial anisotropy. Annealing the samples without an applied field reduces both the coercive and anisotropy fields to  $\sim 10$  and  $\sim 100$  A/m, respectively. The radial anisotropy in the as-deposited films is destroyed (Fig. 5.14,5.20), and the domains sweep very rapidly through the entire film, making domain imaging very difficult. Small reverse spike domains are visible at the edges of the films. MOKE hysteresis loops have shown that a very weak easy axis lies along the length of the films.

### 5.8.2 Magnetic Annealing

It was found that magnetic annealing with an applied field perpendicular to the length of the films, introduced a weak transverse anisotropy. Typical results are shown in Figure 5.23, where both domain images and MOKE loops confirm that a uniaxial anisotropy has been induced. The domain images shown in Figures 23b,c are the corresponding images after the film was initially magnetically saturated along the hard and easy axis, respectively. Application of a small magnetic field of the order of the coercive field along the easy axis gives rise to a typical uniaxial domain structure where the domains are parallel to the easy axis. It should be noted that the film was a single domain at remanence (not shown) with small reverse spike domains present at its edges. The domain structure, which results from saturating the film along the hard axis, is typical of a film exhibiting anisotropy dispersion, where the easy axis and/or the magnitude of the uniaxial anisotropy constant, deviates slightly from place to place in the film. The domain structure in this case is still uniaxial and approximately parallel to the easy axis, but the domains are significantly narrower ( $\sim 80\mu\text{m}$ - $1\text{mm}$ ) in comparison to the situation when the film was initially saturated along the easy axis ( $\sim 3\text{mm}$ ). It should be noted that the magnitude of the induced anisotropy field obtained by this treatment is significantly lower ( $\sim 300\text{ A/m}$ ) in comparison to what can be achieved by using a forming field, but sufficient to control the domain structure.

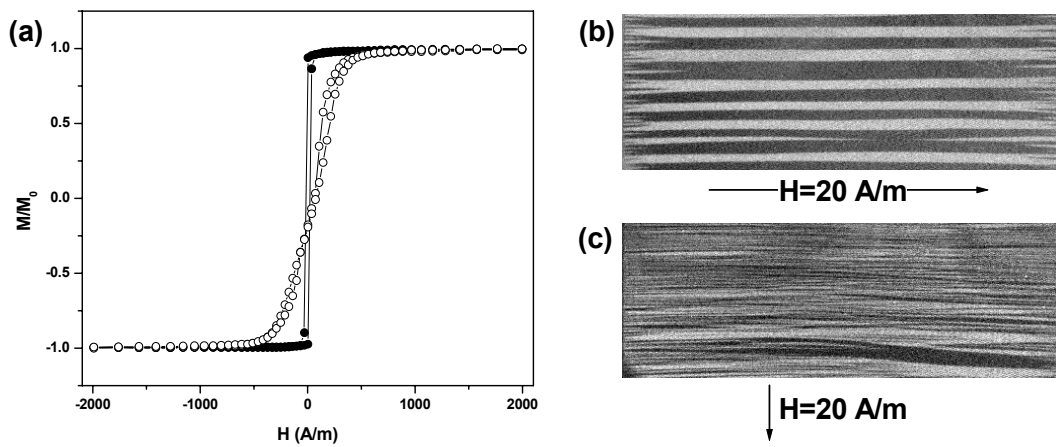


**Figure 5.23:** (a) MOKE hysteresis loops taken from the centre of the area shown. Solid and dashed lines indicate the magnetic field applied along the long and short axes of the sample respectively. The asymmetrical loop shape for the hard is reproducible, and is due to the use of a point probe of magnetisation in films in which domain wall movement is the dominant magnetisation mechanism and very fine domain structure exists. (b) Domain image of a field-annealed film with field applied along the easy axis after being magnetically saturated in the opposite direction. (c) Image obtained after field is applied along the hard direction. ( $15\times 25\text{mm}$ ).

### 5.8.3 Magnetostriction and Magnetoelasticity

The introduction of a uniaxial anisotropy in soft, amorphous magnetic materials is conventionally achieved by the application of a suitable magnetic field, either during the growth process (a forming field) or during subsequent thermal treatment (field annealing) as described above.

An alternative, which is particularly suited to magnetostrictive thin films on flexible substrates, is to use stress [Ali et al (1999,1998)] itself to produce the required anisotropy. From the results and discussions up to this point it, is clear that stress can have a significant effect on the anisotropy. For the case of thin films, if the substrate is deliberately bowed during the deposition then, on release, it will return to its former shape, introducing stress into the film (note that the strain in the film will be opposite to the original substrate strain - if the substrate surface is held under tensile stress during the deposition then the film will be under compressive stress on release of the substrate). It is assumed that the mechanical properties of the film/substrate combination are dominated by those of the substrate. Another alternative is to flex the substrate during thermal processing such that the flexed substrate becomes the zero stress state of the film. The above treatments will be referred to as strained-growth and stress annealing respectively. These methods are assessed as novel alternatives to magnetic field treatments. A simple new technique is also described for the measurement of the saturation magnetostriction [Ali et al (1999)] in amorphous thin films deposited on to rigid substrates; this is also based on mechanically introducing a small curvature in the substrate during or after the deposition.

Magnetostrictive materials in the form of thin films are becoming increasingly important for the development of sensors and actuators. Their incorporation into micro-electromechanical systems allows the production of a new range of devices which, unlike conventional piezoelectric and piezoresistive materials, can be remotely addressed and activated. In addition, these materials offer the possibility of self-test for safety-critical systems and also potential high sensitivity. It is therefore commercially and technologically important that one can investigate the magnetostriction constant of a material on a variety of substrates. Magnetostriction can be determined using either the magnetostrictive [Weber et al (1994)] or inverse magnetostrictive [Narita et al (1980)] effects. In the former case, the mechanical deflection of a cantilever system can be measured as the film magnetisation is rotated. The latter relies on measuring the induced change in anisotropy field as a mechanical stress is applied. The measurement of magnetostriction in thin film samples is not trivial. Techniques such as strain-modulated ferromagnetic resonance [Zuberek et al (1990)] (SM-FMR) and small angle magnetisation rotation [Narita et al (1980)] (SAMR) require thin, flexible substrates. Cantilever measurements can be made on thicker substrates [Klokholm (1976)], but there are difficulties in calibration and in the determination of absolute values of magnetostriction [Watts et al (1999)]. Magnetostriction is often investigated on flexible substrates in which a mechanical load can be applied to produce stress. However, in many cases, the magnetic properties of the films can vary dramatically with the substrate. It was found under certain instances, that thin films grown simultaneously on Corning<sup>®</sup> glass and Kapton<sup>®</sup> (Polyimide substrate) had different magnetic

properties. A further problem with measurement systems in which a known load is applied, is in the calculation of the stress, particularly for the case of multilayer systems. In such cases, the stress in the magnetic layers is dependent on the structure. It is usually assumed that the strain is uniform throughout the thickness of the magnetic material.

Here, a novel new technique for measuring magnetostriction is described for thin films. It is based on mechanically introducing a small curvature into the substrate either during deposition (strained growth), thermal processing (stress annealing) or during the measurement, combined with the Magneto-Optical Kerr Effect (MOKE) to determine the stress induced anisotropy. Quantification of the stress in the magnetic layer gives the ability to determine accurately absolute values of magnetostriction. The technique described is based on a similar method which was first described by Becker and Kersten [Becker et al (1930)] and applied to nickel wires, and then by others to ribbon based materials [Ref. List (5.3)]. Similar methods have also been applied to thin films where the substrate/film are mechanically stressed. However the resulting stress induced anisotropy is obtained from magnetoresistive curves [Baril et al (1999), Markham et al (1989)] or from hysteresis loops obtained by the VSM [Han et al (1997)]. In both instances the magnetisation is monitored over a large area, where it is therefore essential that the strain is also uniform over this area.

Thin films differ from their bulk counterparts not only in their thickness, but also because of surface, substrate and possible texturing effects, which may influence the magnetic properties and hence the magnetostriction. It is therefore important that one should obtain the maximum magnetic information from such films in order to understand them fully.

### 5.8.3.1 Application of stress

An effective method of applying a controlled amount of stress to the FeSiBC films was to mechanically clamp the substrate/film over a knife edge at its two extreme points, as illustrated in Figure 5.24a. The strain in the film depends directly on the radius of curvature induced in the samples, which was determined by optical interferometry and stylus measurements. The optical measurement had the advantage of giving two dimensional information in a single measurement, whereas the stylus measurement gave a quick and accurate measurement of the curvature in a given direction. The results of the two techniques were found to be in good agreement and the stylus method was generally employed for convenience.

Figure 5.24b represents a region of the substrate/film which has been mechanically clamped over the knife edge, inducing a circular arc. The radius of curvature,  $R$ , was determined quickly and accurately from the stylus measurements from the variation of deflection,  $Y$ , with lateral position,  $X$ :

$$R^2 = \left(\frac{X}{2}\right)^2 + H^2 \quad (5.20)$$

Substituting  $H=R-Y$  leads to

$$R = \frac{X^2 + 4Y^2}{8Y} \quad (5.21)$$

A good approximation, when  $X \gg Y$ , is that

$$R = \frac{X^2}{8Y} \quad (5.22)$$

Assuming that the central element of the slide remains unstrained, the tensile strain in the top surface of the substrate is given by the following expression referring to labels shown in Figure 5.24b

$$\varepsilon = \frac{\Delta P}{P} = \frac{\text{Change in surface perimeter}}{\text{Perimeter of unstrained surface}} \quad (5.23)$$

$$\varepsilon = \frac{2\pi(R - F) - 2\pi\left(R - \frac{t}{2} - F\right)}{2\pi\left(R - \frac{t}{2} - F\right)} \quad (5.24)$$

$$\varepsilon = \frac{t}{2R - t - 2F} \quad (5.25)$$

$$\varepsilon = \frac{t}{2R} \quad (R \gg t, R \gg F) \quad (5.26)$$

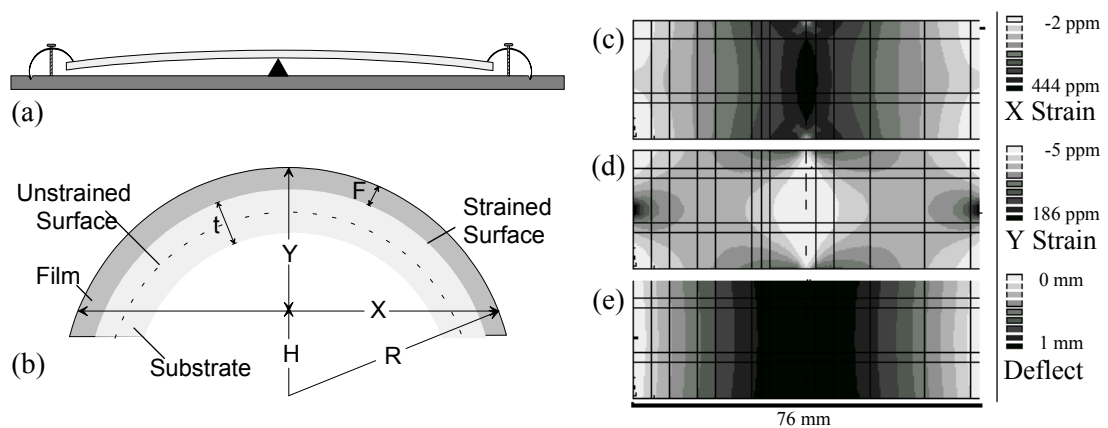


**Figure 5.24:** (a) Schematic of the experimental method used for the introduction of mechanical strain into the film/substrate. (b) Illustrative profile of the radius of curvature from which the radius is calculated using a stylus method. Finite element model of a glass slide clamped tightly over a knife edge. The slide has dimensions of 76 mm x 26 mm x 0.4 mm. (c) and (d) show the magnitude of the strain in the top surface of the slide along the x and y axes respectively, (e) shows the deflection of the slide. [Ali et al (1999)].

where  $t$  is the thickness of the substrate; it is assumed that the thickness of the film is much smaller than that of the substrate which is generally the situation, and was always the case in this study. By this method, the strain is directly measured (on a local scale), and therefore no knowledge of the mechanical properties of the substrate was required as with other techniques simplifying the calculation.

It is realised that a beam or cantilever does not bend into a circular arc, and it has been shown [Joos (1958), Feynman (1964)] that the deflection ( $Y$ ) is proportional to the cube of the length ( $X^3$ ), and not to the square ( $X^2$ ) as for the circular arc (Fig. 5.24b). The strain induced by the clamping process was investigated by three methods: Newton's rings, stylus measurements and numerically. The investigation/measurements of the radius of curvature carried out by the Newton's rings and stylus measurements revealed that a circular arc existed over a small region of the substrate, above the knife edge. This is shown in Figure 5.25a, where a typical Newton's rings interference pattern is shown for a substrate/film under a tensile strain of 707 ppm. Figure 5.25b is a plot of the square of the lateral position ( $X^2$ ) versus the deflection ( $Y$ ); this indicates that the curve, indeed, is circular over a distance of 5 mm. The strain induced anisotropy was measured using MOKE, which had a laser spot size of  $\sim 100\mu\text{m}$  in diameter, and therefore the strain was constant within the sampling area of the laser. This ensured that the measured strain and also the strain induced anisotropy could be directly correlated. The substrates used in this study were found to produce a circular arc over a length scale which was always much greater than the diameter of the laser spot ( $\sim 100\mu\text{m}$ ). Films which are deposited onto substrates such as Kapton<sup>®</sup>, which are too flexible or liable to distort may be studied in this way by first depositing a thin layer of Kapton on a rigid substrate upon which the magnetic film is then deposited. In techniques such as the Small Angle Magnetisation rotation (SAMR) it is assumed that the strain induced is uniform throughout the film. The strain in the film was also numerically modelled using the ANSYS<sup>®</sup> finite element modelling package [Watts (1998)]. This showed that the strain was not constant over the entire slide, but could vary greatly between the central region above the knife edge, compared to the areas near the clamping ends. Figure 5.24c shows the variation of strain with position for the top surface of a glass slide clamped rigidly over such a knife edge. The strain can be

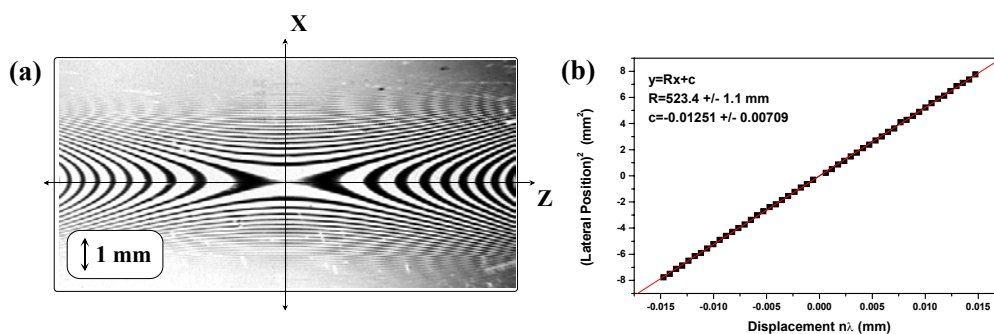


**Figure 5.25:** (a) Newton's ring interference pattern obtained from a glass substrate/film which has been mechanically strained. The image has been enlarged and the scale of the image is shown. The x-axis corresponds to the length, and the z axis is the width of the sample. The y-axis is perpendicular to the page which corresponds to the deflection. (b) The square of the lateral position ( $X^2$ ) is plotted against the deflection from which the radius of curvature is determined for the given image ( $R=X^2/n\lambda$ ). [Ali et al (1999)].

seen to be almost uniaxial in the x-direction over the majority of the area of the slide, but with some edge effects near the clamps and close to the edges on either side of the knife edge. Since the techniques used to measure both the mechanical strain (stylus and interferometric) and the magnetic anisotropy probe the local properties, it can be concluded that, provided the same area is measured in both cases, reliable results can be obtained.

An obvious solution would have been to mechanically clamp the substrate/film over a cylindrical mould as shown in Figure 5.28c. This would have ensured that the strain was uniform across the entire film. However, this would have limited the possible strains available on the range of moulds available. It would have also required the removal of the sample each time, and therefore introducing uncertainty into the exact positioning of the MOKE laser spot each time. This is important when the strain is varied during the measurement (see strain during measurement), since it removes the need to take account of the intrinsic anisotropy present. In situations where the direction and magnitude of the anisotropy varies from position to position, it is therefore important that the same area of the film is sampled each time.

Strain was introduced into the samples in three different ways: by straining the substrate during the deposition, stress annealing and during the measurement. In the first and second cases, the curved substrate becomes the zero strain state for the film. When the substrate is released, it returns elastically to its original flat shape, straining the film in the process. Inducing a strain during the measurement allows a range of strains to be introduced. Measuring the resulting variation of magnetic anisotropy allows the accurate calculation of the magnetostriction.

The saturation magnetostriction constant  $\lambda_s$ , is determined from the variation of the strain induced magnetic anisotropy field,  $H_k$ , with the applied stress,  $\sigma$ , from equation (5.28) [Mattheis et al (1999),

$$\lambda_s = \frac{\mu_0 M_s}{3} (1 + \nu_f) \frac{H_k}{\epsilon Y_m} \quad (5.28)$$

$$\sigma = \epsilon Y_m \quad (5.29)$$

Gudeman (1990)] where  $M_s$  is the saturation magnetisation,  $\epsilon$  is the measured strain,  $Y_m$  and  $\nu_f$  are the Young's modulus and Poisson's ratio of the film, respectively. It should be noted that the factor  $(1 + \nu_f)$  was not included in the analysis in Ali et al (1999), and an erratum has been submitted. Application of stress along the x-axis will also introduce stress in the y and z directions because of the Poisson's ratio of the film [Gehring et al (1999)].

The saturation magnetisation of the material used in this study was assumed to be the same as that of the melt-spun METGLAS<sup>®</sup> 2605SC ribbon which was used as the target material, with  $\mu_0 M_s = 1.61$  T [Allied Signal (1995)]. The stress calculated depended upon the Young's modulus of the film. Unfortunately, such values were not readily available for such amorphous sputtered films and a value of 160 GPa [Allied Signal (1995)] was assumed as for the target ribbon. It should be noted that the strain state and structure of the ribbon and film are likely to be different, with the possibility of

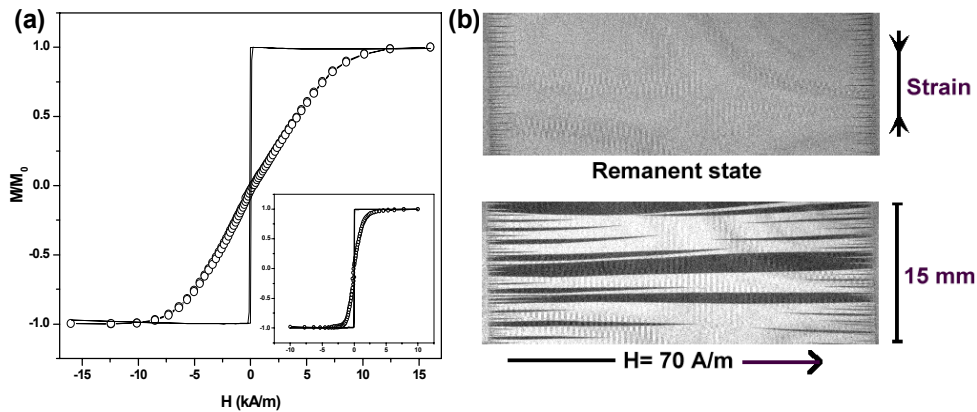


**Figure 5.26:** Strained growth (a) MOKE loops obtained along the easy (solid line) and hard (open circles) axes of magnetisation for a sample deposited while the top surface of the substrate was held under a strain of 562 ppm. The inset shows loops taken in the same directions for an unstrained sample. Comparison gives a strain-induced anisotropy of 5863 A/m. (b) MOKE domain image at remanence and at a field of 70 A/m applied along the easy axis. [Ali et al (1999)].

different mechanical properties. However, evidence from the deflection of FeSiBC thin film membranes under pressure indicate similar values [Karl et al (1999)]. In the present case, the uncertainty in the Young's modulus gives a large systematic error ( $\pm 40$  GPa) which is much greater than the random errors in the measurement of strain and anisotropy. A value for the Poisson's ratio was not available for FeSiBC films nor for the target material from which the films were deposited. It is, however, found that the values for Fe-based metals is approximately 0.3 for films or bulk materials and therefore a value of 0.3 for Fe<sub>80</sub>B<sub>20</sub> ribbon [Kunzi (1983)] was used for FeSiBC films deposited in this study.

### 5.8.3.2 Strained growth

FeSiBC films were produced by straining the substrate during the deposition process, and releasing it afterwards to introduce a strain into the film. The substrate curvature was verified pre- and post-deposition by interferometric and stylus measurements. Such a technique could be used as a simple method for the introduction of a controlled, uniaxial anisotropy for device fabrication. The disadvantage of the strained growth technique is that the strain-induced anisotropy will be added to the intrinsic growth anisotropy which is radial in form in this study. However, since the anisotropy induced during the deposition was found to be constant, it could be subtracted to quantify the magnetostriction measurement. Figure 5.26 shows the hysteresis loops and domain images obtained from a film deposited onto a strained substrate. The hysteresis loops indicate that the film exhibits a well defined uniaxial anisotropy, with no observable opening of the hard axis loop. The domain images confirm the well defined uniaxial anisotropy, with 180° domain walls running parallel to the easy axis. Reverse domain spikes appear at the edges to reduce the demagnetising effect. Subtraction of the intrinsic anisotropy (shown in the inset) yields a magnetostriction constant of  $39.5 \pm 7.5$  ppm, in good agreement with the bulk data [Allied signal (1995)]. The error in this measurement is dominated by that of the

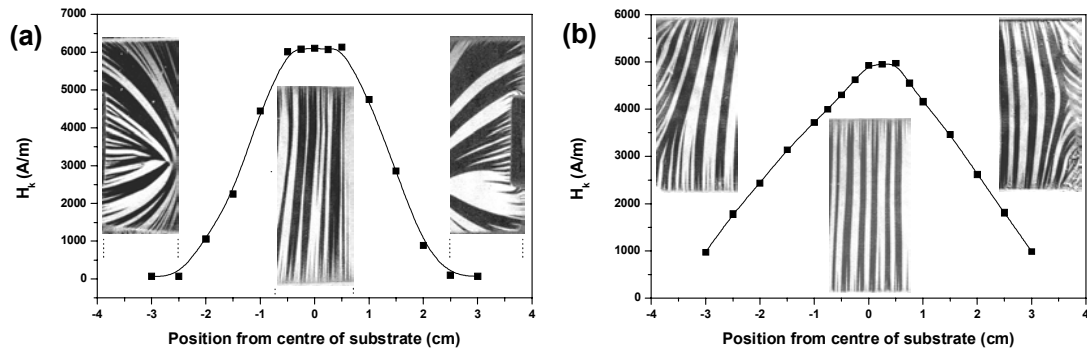


**Figure 5.27:** (a) The variation of the anisotropy field measured for a strained-growth film which was held under a strain of 571 ppm. (b) The variation of the anisotropy field measured for a stress annealed film which was held under a strain of 507 ppm. Domain images were taken at  $H=0$  A/m from the two ends and the central region of the films. Image dimensions  $15 \times 25$  mm.

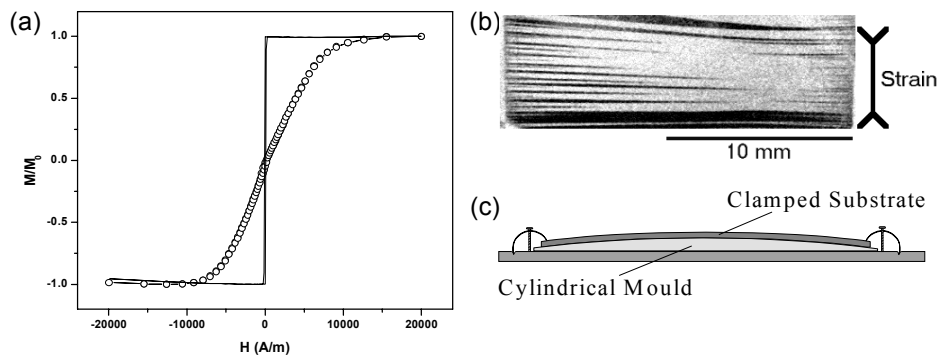


**Figure 5.28:** (a) MOKE hysteresis loops taken from the centre of the domain image in (b). Solid and dashed lines indicate the magnetic field applied along the long and short axes of the sample respectively. (b) Domain image of a sample grown on a strained substrate. On release of the tightly clamped substrate, the film is held under a compressive strain of approximately 675 ppm in the direction indicated. [Ali et al (1999)]. (c) schematic of alternative clamping arrangement to ensure a constant strain across a film.

Young's modulus. Further films grown with varying strains gave similar values. Figure 5.27a shows the variation of the anisotropy field along the length of a typical strained-growth film as measured by MOKE. At the central region of the film the anisotropy is purely uniaxial as expected and the magnitude of the anisotropy decreases along the slide because of the decrease in the strain along the x-axis, as computed and shown in Figure 5.24c. During the deposition, the forming field which is the cause of the radial anisotropy, is the dominate anisotropy since the mechanically strained substrate does not induce any strain in the film until the substrate is allowed to return to its original form. The strain induced anisotropy is a maximum at the centre of the film over the knife edge (assuming that the knife edge is positioned at the centre of the radial anisotropy), where it is found that the radially induced anisotropy in comparison is insignificant on removal of the film. Moving away from the central region, the strain induced anisotropy decreases as the radial anisotropy increases, and the two anisotropies combine to produce a resultant anisotropy which is shown by the domain images taken from the two ends of the film. This shows that the anisotropy is no longer uniaxial across the width of the film. The magnitude of the anisotropy induced in the FeSiBC films by this method of strained growth can be substantially larger than the anisotropy induced by field annealing. Although the

bending which can be applied to the substrates is limited by the elastic limit of the substrate and film, it is sufficient to produce an anisotropy field of 8kA/m in the current experimental arrangement (Fig. 5.28a,b). From a commercial point of view, it would more attractive if the anisotropy field were linear across the entire substrate. This could be achieved by clamping the substrate over a cylindrical mould (Fig. 5.28c) of the required radius so as to induce a constant anisotropy field, instead of a knife edge as used in this study. This would ensure that the radius of curvature were constant along the entire substrate, giving rise to a constant anisotropy field. This is obviously assuming that no growth induced anisotropies are present which vary across the film as found in this study because of the radially induced anisotropy due to the residual field. However, the same clamping arrangement could be used in the technique of stress annealing (see next) which would overcome the problems of the growth induced anisotropies combining with the strain induced anisotropy.

### 5.8.3.3 Stress annealing

Stress annealing is an alternative way to introduce a uniaxial anisotropy. The advantage of stress annealing is that it destroys the intrinsic growth induced anisotropy (radial anisotropy in this case), generally improves the magnetic properties, and provides the means of tailoring the anisotropy field ( $H_K$ ). The problem associated with strained growth was the separation of the substrate from the water-cooled substrate platter. In the vacuum used, there is almost no heat transfer through the residual gas. All transfer of heat is by direct contact conduction or radiation. It was found that a large separation caused the films to become magnetically hard because of the increased temperature which altered the sputtering dynamics at the substrate. This put an upper limit on the induced strain. Stress annealing is immune to such a problem. Figure 5.29a represents the hard axis hysteresis loops taken (i) from an as-deposited film, (ii) the film placed under a tensile strain, (iii) after stress annealing, and (iv) upon removal of the external strain. The intrinsic growth anisotropy (i) competes with that of the stress induced anisotropy (ii), since removal of the external mechanical strain after stress annealing creates a stress induced anisotropy (iv) with a higher anisotropy field. Stress annealing minimises the two dominant anisotropies, leaving only a small material intrinsic anisotropy as shown in Figure 5.29a (iii).

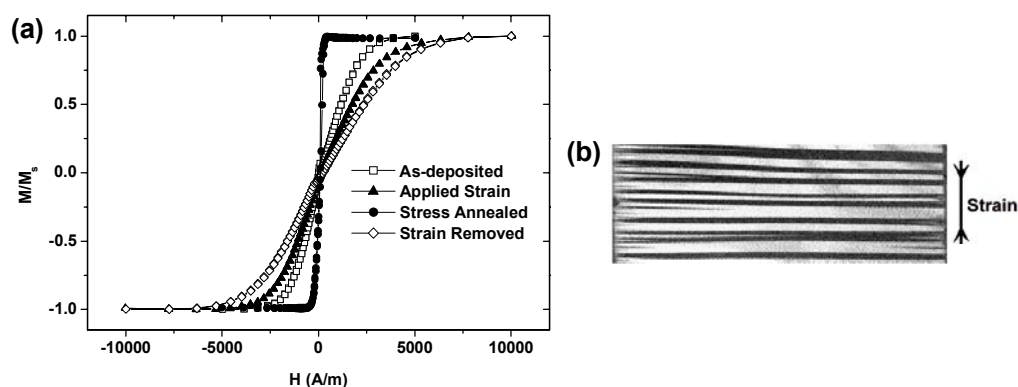


**Figure 5.29:** Stress annealing. (a) Hysteresis loops (i) for an as-deposited film (open squares), (ii) the film placed under an external strain of 507 ppm (solid triangle), (iii) after stress annealing (solid circles), and (iv) upon removal of the strain (open diamond). (b) Domain image at remanence. [Ali et al (1999)].

The annealing temperature causes sufficient atomic mobility to relieve the mechanically induced stress. mechanical strain. A value of  $37.8 \pm 7.3$  ppm is obtained for the magnetostriction constant. Similar values Domain images confirm a uniaxial anisotropy with  $180^\circ$  domain walls upon removal of the external were obtained for other samples using this method. The most beneficial advantage of stress annealing is that it provides the ability to tailor in a specific anisotropy field. This is very important for the fabrication of devices where it is necessary to control the anisotropy field, and hence the permeability. Figure 5.30 shows that the induced anisotropy varies linearly with strain on both glass and silicon substrates, as expected from equation 5.28. In each case, every point was obtained from independently grown films which were then stress annealed. The linearity is due to the strain induced anisotropy which scales linearly, being the dominant anisotropy. Figure 5.30 demonstrates the high level of control which can be achieved in inducing a specific anisotropy field and the reproducibility of the magnetic samples. The magnitude of this induced anisotropy is much larger than an anisotropy induced by field annealing. Domain images have been included to indicate the uniaxial anisotropy. The simplicity of the technique provides the means to induce an in-plane, transverse or longitudinal uniaxial anisotropy which is well defined.

Figure 5.27b shows the variation of the anisotropy field along a film which has been stress annealed. As expected, the anisotropy decreases from the central region. In this case, the anisotropy is still uniaxial across the width of the films, virtually to the ends of the film and there is a distinct difference in the profile of the anisotropy field between stress growth (Fig. 5.27a) and stress annealing. The effect of the stress annealing is two fold: the increased atomic mobility allows the as-deposited stress to be relieved, while zero-field cooling through the Curie point removes the radial anisotropy. On releasing the substrate/film from the mechanical clamp, the anisotropy is essentially due to the strain. This controllable variation of the anisotropy field could be utilised in the development of sensors where a range of anisotropy fields could be induced in a range of devices in the one process. In the situation where a uniform anisotropy field is preferred over a large substrate containing a number of devices, this can be achieved by using the clamping arrangement as shown in Figure 5.28c, which would ensure a constant strain induced anisotropy across the entire substrate.

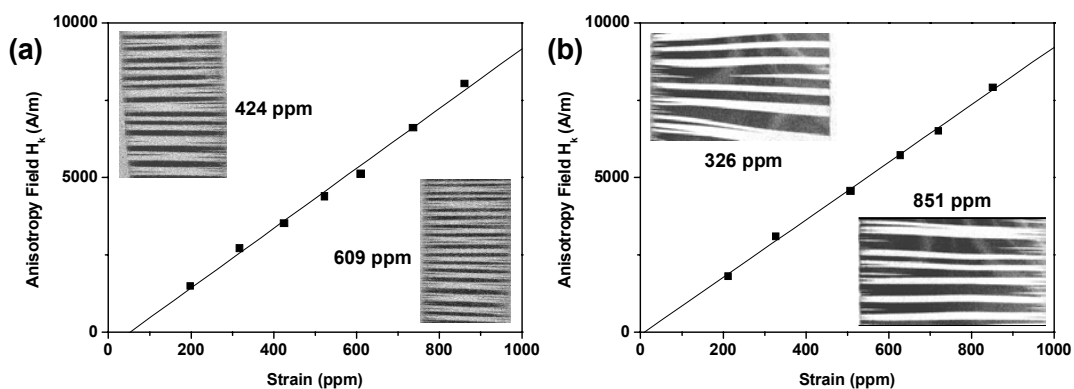


**Figure 5.30:** (a) Induced anisotropy field by stress annealing for films grown on Silicon. Domain images 5 mm by 15 mm at remanence. (b) Induced anisotropy field by stress annealing for films grown on Corning glass. Domain images 25 mm by 15 mm at remanence. In both cases each point was obtained from independent samples. [Ali et al (1999)].

### 5.8.3.4 Strain during measurement

Quantification of the magnetostriction is more conveniently achieved by measuring the variation of the anisotropy field as a function of the strain applied during the measurement. In this way, several independent measurements of magnetostriction can be made from a single film, increasing the level of confidence of the result. It also eliminates the need to take account of the growth induced and/or intrinsic anisotropy. Annealing of the film prior to the measurements effectively destroys the as-deposited anisotropy, making this term quite small.

Figure 5.31 shows the variation of hard-axis MH loop with induced strain for a film grown on a standard microscope slide which was stress relieved. The induced anisotropy varies linearly with strain, as expected. The gradient of the graph of anisotropy versus strain ( $dH_k/d\varepsilon$ ), gives a measurement of magnetostriction using equation 5.28, while the intercept corresponds to the intrinsic anisotropy (for annealed films, this term is usually smaller). It should be noted that it was found that a positive intercept indicated that the easy axis of the film was initially along the direction of the applied strain, whereas a negative intercept implied that the easy axis was perpendicular to the applied strain. Theoretical analysis by Gehring et al (1999a) on the effects of anisotropy on the measurement of magnetostriction in such techniques has shown that, if the anisotropy is either parallel or perpendicular to the applied strain, then  $dH_k/d\varepsilon$ , will always be linear. However, if the anisotropy is at some oblique angle to the applied strain, then the curve will initially be non-linear until the anisotropy induced by the applied strain becomes dominant. In the measurements performed on the FeSiBC films deposited here, the strains applied were always either perpendicular or parallel to the initial anisotropy present in the films and were significantly larger. Prior knowledge of the anisotropy in the films ensured that this was always the situation when these measurements were performed. If situations were a uniaxial anisotropy is not present, it is therefore essential that the strains applied are sufficiently large, in order that  $dH_k/d\varepsilon$  becomes linear. In the predicament where this condition is not satisfied,  $dH_k/d\varepsilon$  will always be lower giving a lower value for the saturation magnetostriction than expected. Further work by Gehring et al (1999a) is expected to account for such effects.

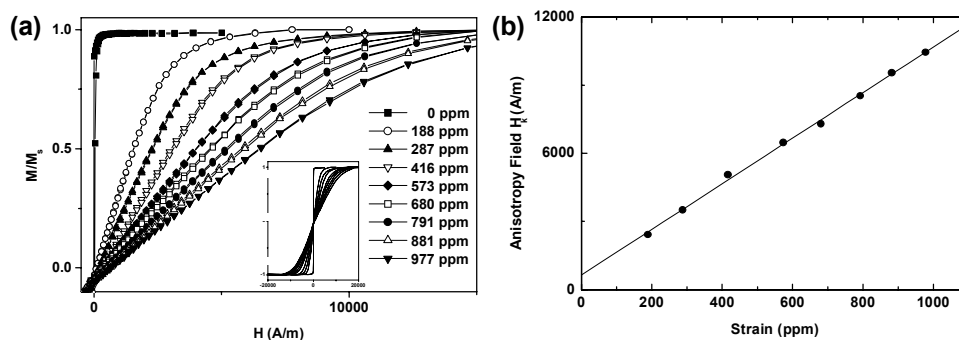


**Figure 5.31:** (a) Hysteresis loops for a FeSiBC film as a function of strain. All loops taken perpendicular to the direction of tensile strain. (b) Corresponding variation of anisotropy field with strain, from which a magnetostriction constant of  $41.6 \pm 7.7$  ppm is determined.

From the gradient of the graph shown in Figure 5.31b, the magnetostriction constant is calculated to be  $41.6 \pm 7.7$  ppm. Similar measurements performed on FeSiBC films grown on silicon and Corning® glass substrates are shown in Figure 5.32. The magnetostriction values calculated from the first two graphs in Figure 5.32 are shown in Table 5.1. Again, the uncertainty in the Young's modulus of the FeSiBC film dominates the error (25%). Repeating these measurements with different samples gave values of  $\lambda_s$  which varied by less than 5%, indicating that the random errors in the measurement are small. The quantity  $\lambda_s Y_m (1 + \nu_f)$  and its associated error have been included in Table 5.1 to indicate how the uncertainty in the Young's modulus ( $Y_m$ ) dominates the error. For systems in which the Young's modulus of the film is well known, values of  $\lambda_s$  which are accurate to within 5% should be possible. Figure 5.32 also shows the technique applied to an FeCo [Cooke (1999)] thin film deposited on glass; as expected the anisotropy field varies linearly with strain. The magnetostriction constant was calculated to be  $92.8 \pm 2$  ppm ( $\nu_f = 0.29$ ), in good agreement with the values obtained by Cooke et al (1999) for films measured by Strain Modulated Ferromagnetic Resonance.

The variation of anisotropy field with strain also shows the potential of such materials for sensor applications. Since the anisotropy field varies by nearly two orders of magnitude over a modest range of strains, the sensitivity of such devices is expected to be high.

The magnetostriction measurements have been gathered in Table 5.1, including values determined from the gradients of the two graphs shown in Figure 5.30. Where films were grown on glass and silicon substrates and then stress annealed to induce different anisotropy fields, the two magnetostriction constants obtained are in good agreement, considering that each point on the graph was obtained from independently grown films. It is apparent from Table 5.1 that the substrate has little or no influence on the value of the magnetostriction constant. This conclusion is confirmed by magnetostriction measurements performed by Mattingley et al (1994), where FeSiBC films grown on Kapton® under similar growth conditions also gave similar values for  $\lambda_s$ , even though the films were magnetically much harder (coercive fields  $\sim 1500$  A/m). The larger coercive fields are due to the stresses introduced by the Kapton® substrate. Experiments [Lachowicz et al (1989)] have shown the saturation magnetostriction does depend upon stress for nearly zero magnetostrictive materials, and therefore the linear dependence between the anisotropy field and stress becomes non-linear. The non-

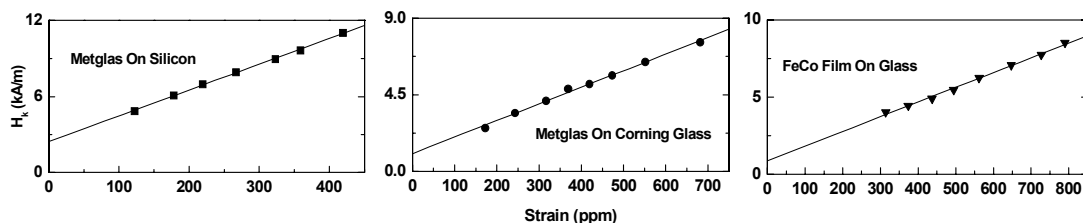


**Figure 5.32:** Variation of anisotropy field with strain. All loops taken perpendicular to the direction of tensile strain. FeSiBC on silicon  $\lambda_s = 39.7 \pm 7.3$  ppm, FeSiBC on Corning® glass  $\lambda_s = 40.1 \pm 7.5$  ppm and FeCo on microscope slide glass  $\lambda_s = 92.8 \pm 1.3$  ppm.

linearity is small and can only be seen in materials possessing nearly zero magnetostriction. The random stresses from the substrate do have a small effect on the value of  $\lambda_s$ , but can be considered to be negligible in highly magnetostrictive materials.

Magnetostriction measurements were also performed on films ( $\geq 500\text{nm}$ ) deposited on silicon substrates which were initially annealed, but there appears to be no thickness dependence in this range (see Table 5.1).

Method	$(1+\nu_f)\lambda_s Y_m$ (MPa)	$\lambda_s$ (ppm)	$H_c$ (A/m)
Strained growth	$5.1 \pm 0.3$	$39.5 \pm 7.5$	60
Stress annealing			
(i) Single measurement	$4.9 \pm 0.3$	$37.8 \pm 7.3$	18
(ii) Corning glass (Fig 5.30a)	$5.0 \pm 0.1$	$38.6 \pm 7.5$	18
(iii) Silicon (Fig 5.30b)	$5.2 \pm 0.2$	$40.1 \pm 7.5$	18
Strain during measurement			
(i) Glass slide	$5.4 \pm 0.1$	$41.6 \pm 7.7$	20
(ii) Corning glass	$5.1 \pm 0.2$	$39.8 \pm 7.3$	52
(iii) Silicon	$5.2 \pm 0.2$	$40.6 \pm 7.5$	18
(iv) $0.5\mu\text{m}$ on Si	$5.1 \pm 0.1$	$39.4 \pm 7.4$	11
(v) $1\mu\text{m}$ on Si	$5.0 \pm 0.1$	$38.7 \pm 7.3$	9
(vi) $2\mu\text{m}$ on Si	$5.1 \pm 0.2$	$39.4 \pm 7.6$	16
(vii) $3\mu\text{m}$ on Si	$5.2 \pm 0.2$	$40.3 \pm 7.5$	18

**Table 5.1:** Typical magnetostriction constants determined for FeSiBC thin films.

## 5.9 Photolithographically patterned films

The micro-fabrication of sensor elements onto commercially important substrates is generally done by the well established technique of photolithography as described in Section 3.7. It is therefore important that the patterned magnetic films retain their excellent magnetic properties and the previously optimised domain structure which has been induced into the film either during the deposition (forming field) or by a subsequent annealing treatment. The domain images from photolithographically patterned FeSiBC films are shown in Figure 5.34. It was found that the process had no significant effect on the magnetic softness of the patterned films. It was also evident from the domain images and MOKE loops obtained from the rectangular patterned films that the in-plane shape anisotropy had no observable influence on the previous anisotropy of the film, besides increasing the density of domains per unit area to reduce the magnetostatic energy. However, on annealing such small dimensional films, the in-plane shape anisotropy does exert some influence as shown in Figure 5.34b, where the easy axis is orientated along the length of the rectangular patterned film as one would expect, whereas the easy axis of the circular films vary. This in-plane shape anisotropy nevertheless is not sufficient to overcome the anisotropy induced by other mechanisms such as field annealing as shown in Figure 5.34c, where a well defined uniaxial domain structure has been induced in the patterned films by a process which has been shown to develop a relatively weak anisotropy in comparison to other techniques. The respective easy and hard axis loops are shown in Figure 5.33. It should be noted that the diameter of the laser spot on the MOKE system is  $\sim 100\mu\text{m}$ , and therefore the asymmetrical loops are due to the movement of many domain walls through the laser spot.

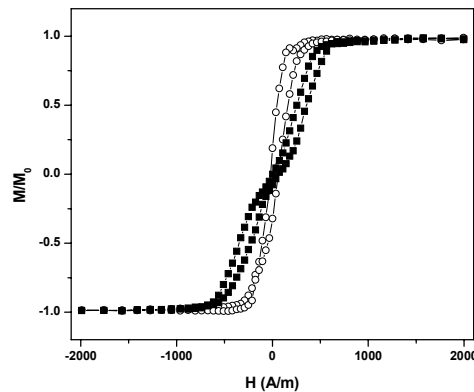


**Figure 5.33:** Easy (open) and hard (solid) axis MOKE hysteresis loops from a Field annealed rectangular film whose dimensions and domain image are shown in Figure 5.34c.

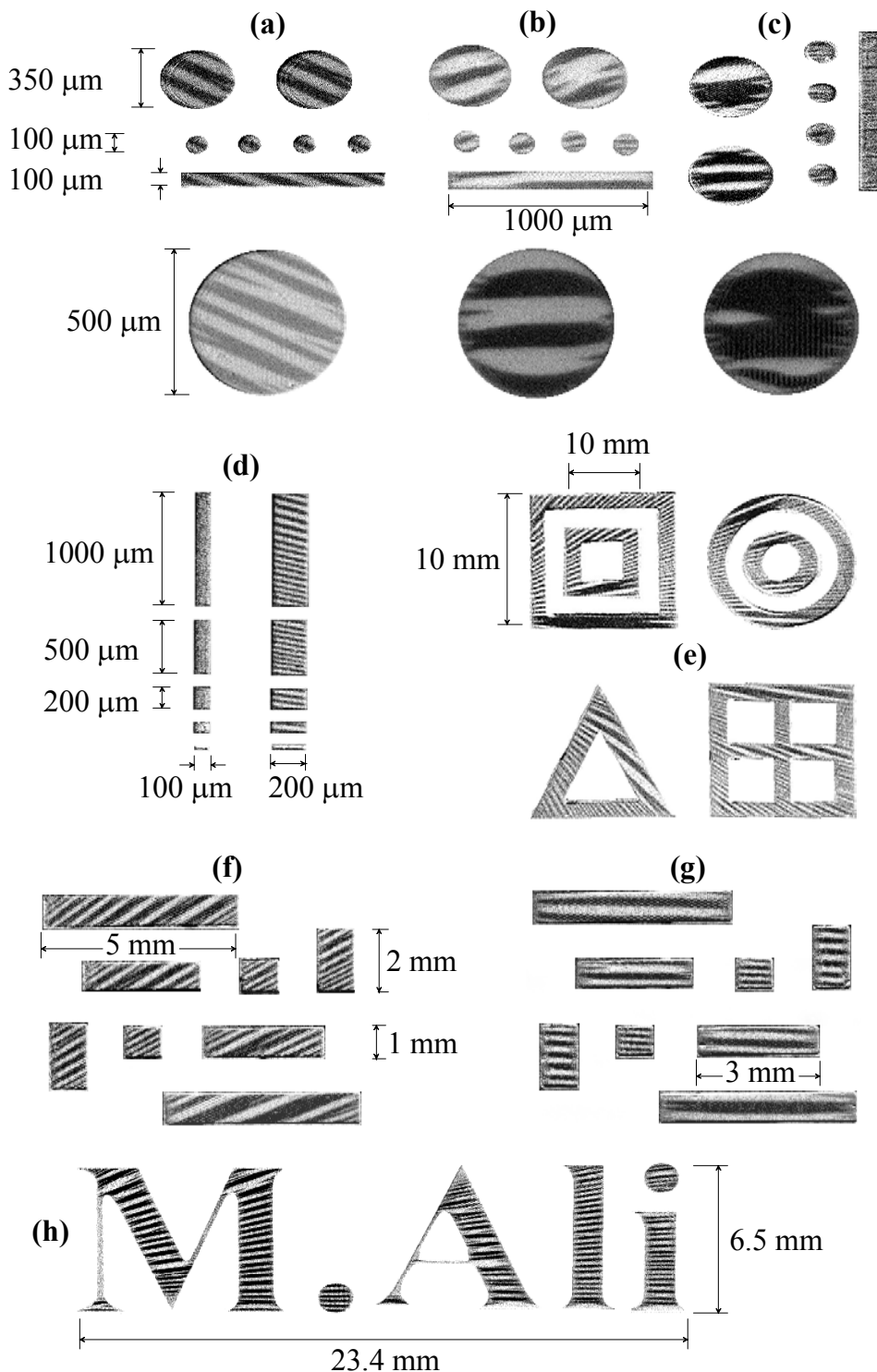


**Figure 5.34:** Domain images from photolithographically patterned 500nm FeSiBC films. Typical dimensions and shapes which are generally utilised in devices are shown in (a-d). (a) as-deposited film, (b) film annealed, (c) film field annealed. (d), (e) and (f) were obtained from as-deposited films. (g) The patterned film in (f) was field annealed. (h) was obtained from an as-deposited film. The width of the window structures in (e) are 1mm in dimension. Horizontal MO sensitivity.

## 5.10 Conclusions

It has been shown that the as-deposited films display a significant, reproducible in-plane anisotropy, which is radial about a central point corresponding to the centre of the magnetron sputtering source. This radial anisotropy has been shown to be a consequence of the small in-plane residual field present at the substrate platter.

The control of magnetic anisotropy in FeSiBC films by various treatments has been described. Field annealing is shown to be capable of producing a small transverse anisotropy. The use of stress induced anisotropy either during the growth or subsequent annealing has been shown to give very a well defined, strong anisotropy whose magnitude can be easily controlled by varying the stress applied.

A new, simple technique for the measurement of magnetostriction in thin films deposited onto fairly rigid thick substrates has been described. It has been applied to amorphous FeSiBC films sputter deposited onto microscope slides, Corning<sup>®</sup> glass and silicon substrates. For these systems, the error in the measurement of magnetostriction is determined almost entirely by the uncertainty in the Young's modulus. The technique has also been applied to an FeCo film deposited by sputtering onto a microscope slide. In both the FeSiBC and FeCo cases the values obtained are in good agreement with expected values.

The technique can be applied to a wide variety of different film/substrate combinations. If the Young's modulus of the film is known to a high accuracy, then the error in the value of  $\lambda_s$  obtained can be less than 5%, which compares well with other methods [Ref. List (5.2)]. Such precise quantitative values could be used to provide sample standards for use with other techniques. The technique is not limited by film thickness, since the Magneto-Optical Kerr Effect can comfortably monitor the magnetisation down to a film thickness of 10nm. It overcomes the problem of non-uniform stresses by correlating the local stress with that of the local anisotropy field. No mechanical properties of the substrate are required, simplifying the calculation of  $\lambda_s$ . There is no special preparation of samples required and the equipment needed to implement the technique is inexpensive and commonly available. This method gives a useful alternative to the conventional techniques and can be applied to films deposited onto moderately thick substrates. This magnetostriction measurement may be applicable to films deposited onto a wide variety of commercially important substrates, for which there may be no alternative techniques.

Since magnetostriction is a fundamental physical property of magnetic materials, it is vital for high precision devices (such as magnetic information storage systems) that accurate quantification of its effects can be obtained.

The values of magnetostriction obtained in this study have been very reproducible from the three different methods used to strain the magnetic films. It has been found that the substrates have no significant influence on  $\lambda_s$ , and the magnetic softness (coercive fields), which is presumed to be caused

by residual strains, also has little influence. These experiments also show that, in these strongly magnetostrictive materials,  $\lambda_s$  is independent of strain for the applied strains and also the residual strains caused by the substrate.

The technique of stress annealing to tailor the anisotropy field has been demonstrated to a high degree of precision on silicon and Corning<sup>®</sup> glass substrates. It provides an excellent means of inducing a given anisotropy field in thin film based sensors. It also provides the means of inducing a well defined uniaxial domain structure, which simplifies the understanding of the magnetic process for device applications.

Photolithographically patterned films display no adverse effects from the process, and it has been shown that the process of field annealing is still able to induce a weak uniaxial anisotropy in films with reduced lateral dimensions.

## 5.11 References

- Ali et al (1998) "The use of stress for the control of magnetic anisotropy in amorphous FeSiBC thin films: a magneto-optic study", **M. Ali**, R. Watts, W.J. Karl, M.R.J. Gibbs, J. Magn. Magn. Mater. 190(3) 199 (1998).
- Ali et al (1999) "Measurement of saturation magnetostriction using novel strained substrate techniques and the control of the magnetic anisotropy", **M. Ali**, R. Watts, W.J. Karl, M.R.J. Gibbs, J. Magn. Magn. Mater. 202(1) 85 (1999).
- Allied Signal (1995) Allied signal data sheets on METGLAS®.
- Arai et al (1994) "A new hybrid device using magnetostrictive amorphous films and piezoelectric substrates", K.I. Arai, C.S. Muranaka, M. Yamaguchi, IEEE Trans. Magn. MAG-30(2) 916 (1994).
- Baril et al (1999) "Magnetostriction in spin valves", L. Baril, B. Gurney, D. Wilhoit, V. Speriosu, J. Appl. Phys. 85(8) 5139 (1999).
- Becker et al (1930) "Die Magnetisierung von Nickeldraht unter starkem zug" . Becker, M. Kersten, Z, Phys. (64) 64 (1930).
- Bishop (1998) Discussions with J.E.L. Bishop, Sheffield University (1998).
- Cooke (1999) I Thank M.D. Cooke for providing the soft FeCo film.
- Cooke et al (1999) "The effect of thermal treatment, composition and substrate on the texture and magnetic properties of the FeCo thin films", M.D. Cooke, L-C. Wang, R. Watts, R. Zuberek, G. Hedon, W.R. Rainforth, G.A. Gehring, To be published JMMM (1999).
- Costa-Kramer et al (1995) "Influence of magnetostriction on magneto-impedance in amorphous soft ferromagnetic wires", J.L Costa-Kramer, K.V Rao, IEEE Trans. Magn. MAG-31(2) 1261 (1995).
- Craik (1995) "Magnetism - principles and applications", D. Craik, Wiley & Sons, p94 (1995).
- Cullity (1972) "Introduction to magnetic materials", B.D. Cullity, Addison-Wesley (1972).
- Dmitrieva et al (1999) "The recovery kinetics of the magnetic anisotropy induced by stress annealing of the amorphous Co-based alloy with low Curie temperature", N.V. Dmitrieva\*, G.V. Kurlyandskaya, V.A. Lukshina, A.P. Potapov, J. Magn. Magn. Mater. (196/197) 320 (1999).
- Dominguez (1996) "Circumferential magnetisation processes in CoFeBSi wires", L. Dominguez, J.M. Blanco, P. Aragonese, J. Gonzalez, R. Valenzuela, M. Vazquez, A. Hernando, J. Appl. Phys. 79(8) 6539 (1996).
- Feynman (1964) "The Feynman lectures on physics", R.P. Feynman, R.B. Leighton, M. Sands, Addison Wesley, Vol(2), ch. 8, pp 38-10 (1964).

- Garcia et al (1998) “Magnetic domains and transverse induced anisotropy in magnetically soft CoFeB amorphous thin films.”, D. Garcia, J.L. Munoz, G. Kurlyandskaya, M. Vazquez, **M. Ali**, M.R.J. Gibbs, IEEE Trans. Magn. MAG-34(4) 1153 (1998).
- Gehring et al (1999) I thank Prof. G.A. Gehring and Dr R. Mattheis for their helpful discussions on this matter.
- Gehring et al (1999a) “\*\*\*\*\*”, G.A. Gehring, M.D. Cooke, **M. Ali**, et al, In preparation (1999).
- Gibbs et al (1997) “Microstructures containing piezomagnetic elements”, M.R.J. Gibbs, R. Watts, W. Karl, A.L. Powell, R.B. Yates, Sensors & Actuators A59 229 (1997).
- Gonzalez et al (1994) “Stress annealing in Fe<sub>73.5</sub>Cu<sub>1</sub>Ta<sub>3</sub>Si<sub>13.5</sub>B<sub>9</sub> amorphous alloy- induced magnetic anisotropy and variation of the magnetostriction constant”, J. Gonzalez, N. Murillo, J.M. Blanco, J.M. Gonzalez, T. Kulik, J. Appl. Phys. 76(2) 1131 (1994).
- Gradmann (1986) “Magnetic surface anisotropies”, U. Gradmann, J. Magn. Magn. Mater. (54/57) 733 (1986).
- Gudeman (1990) “Magnetostriction mapping of soft magnetic films on thick rigid substrates”, C.S. Gudeman, IEEE Trans. Magn. MAG-26(5) 2580 (1990).
- Han et al (1997) “Stress effects on exchange coupling field, coercivity, and uniaxial anisotropy field of NiO/NiFe bilayer thin film for spin valves”, D. Han, J. Zhu, J.H. Judy, J.M. Sivertsen, J. Appl. Phys. 81(8) 4519 (1997).
- Hristoforou et al (1991) “Nonuniformity in amorphous ribbon delay lines after stress and current annealing”, E. Hristoforou, R.E. Reilly, J. Appl. Phys. 69(8) 5008 (1991).
- Hubert et al (1998) “Magnetic Domains - The analysis of magnetic microstructures”, A. Hubert, R. Schafer, Springer pp447-510 (1998).
- Joos (1958) “Theoretical physics”, G. Joos, Blackie, 3<sup>rd</sup> Ed., ch 8, pp 176 (1958).
- Karl et al (1999) “A micromachined magnetostrictive pressure sensor using magneto-optical interrogation”, W.J. Karl, A.L. Powell, R. Watts, M.R.J. Gibbs, C.R. Whitehouse, EMSA 98 \*\* \*\*\* (1999).
- Klokhholm et al (1976) “The measurement of magnetostriction in ferromagnetic thin films”, E. Klokhholm, IEEE Trans. Magn. MAG-12(6) 819 (1976).
- Kunzi (1983) “Glassy metals II”, H.U. Kunzi, Ed. H. Beck & H.J. Guntherodt, springer-verlag, (1983).
- Lachowicz et al (1989) “Unusual behaviour of saturation magnetostriction in metallic glasses”, H.K. Lachowicz and A. Siemko, IEEE Trans. Magn. MAG-25(5) 3605 (1989).
- Leamy et al (1979) “Microstructure and magnetism in amorphous rare earth transition metal thin films. II. Magnetic anisotropy”, H.J. Leamy, A.G. Dirks, J. Appl. Phys. 50 (4) 2871 (1979).

- Leamy et al (1978) "Microstructure and magnetism in amorphous rare earth transition metal thin films. I. Microstructure", H.J. Leamy, A.G. Dirks, J. Appl. Phys. 49 (6) 3430 (1978).
- Lu et al (1997) "Metglas thin film with as-deposited domain alignment for smart sensor and actuator applications", Y. Lu, A. Nathan, Appl. Phys. Lett. 70(4) 526 (1997).
- Luborsky et al (1977) "Magnetic anneal anisotropy in amorphous alloys", F.E. Luborsky, J.L. Walter, IEEE Trans. Mag. MAG-13(2) 953 (1977).
- Luborsky et al (1975) "Magnetic annealing of amorphous alloys", F.E. Luborsky, J.J. Becker, R.O. McCary, IEEE Trans. Magn. MAG-11(6) 1644 (1975).
- Markham et al (1989) "Magnetoresistive measurement of magnetostriction in permalloy", D. Markham, N. Smith, IEEE Trans. Magn. MAG-25 (5) 4198 (1989).
- Mattingley et al (1994) "Magnetic and Magnetoelastic Properties of Amorphous Fe-Si-B-C Films", A.D. Mattingley, C. Shearwood, M.R.J. Gibbs, IEEE Trans. Magn. MAG-30 (6) 4806 (1994).
- Mattheis et al (1999) "Interface governed magnetostriction in ultra thin CoFe films", R. Mattheis, J. Langer, S. Senz, MRS Proceedings [in press] (1999).
- Mitra et al (1991) "Influence of stress and stress-flash annealing on the magnetic-properties of amorphous Fe<sub>77.5</sub>Si<sub>7.5</sub>B<sub>15</sub> wire", A. Mitra, M. Vazquez, K. Mandal, S.K. Ghatak, J. Appl. Phys. 70(8) 4455 (1991).
- Morikawa et al (1997) "Giant magneto-impedance effect in layered thin films", T Morikawa, Y. Nishibe, H. Yamadera, Y. Nonomura, M. Takeuchi, Y. Taga, IEEE Trans. Magn. MAG-33(5) 4367 (1997).
- Narita et al(1980) "Measurement of saturation magnetostriction of a thin amorphous ribbon by means of small angle magnetisation rotation", K. Narita, J. Yamasaki, H. Fukunaga, IEEE Trans. Magn. MAG-16(2) 435 (1980).
- Nielson et al (1985) "Experiments concerning the origin of stress anneal induced anisotropy in metallic glass ribbons", O.V. Nielson, A. Hernando, V. Madurga, J.M. Gonzalez, J. Magn. Magn. Mater. (46) 341 (1985).
- Nielson et al (1980) "Magnetic-anisotropy in Co<sub>71</sub>Mo<sub>2</sub>Si<sub>15</sub>B<sub>10</sub> and (Co<sub>0.98</sub>Fe<sub>0.11</sub>)<sub>72</sub>Mo<sub>3</sub>Si<sub>15</sub>B<sub>10</sub> metallic glasses, induced by stress annealing", O.V. Nielson, H.J.V. Nielson, J. Magn. Magn. Mater. 22 (1) 21 (1980).
- O'Dell (1981) "Magnetostriction measurements on amorphous ribbons by the Becker-Kersten method.", T.H. O'Dell, Phys. Stat. Sol. (a) 68 221 (1981).
- Ounadjela et al (1987) "Control of the deposition temperature by the use of a magnetic field in r.f. sputtering", K. Ounadjela, G. Suran, J. SZtern, Thin Solid Films (151) 397 (1987).

- Panina et al (1996) "Effect of magnetic structure on giant magneto-impedance in Co-rich amorphous alloys", L.V. Panina, K. Mohri, J. Magn. Magn. Mater. (157/158) 137 (1996).
- Prutton (1964) "Thin ferromagnetic films", M. Prutton, Butterworths, pp52 (1964).
- Ref. List (5.1) Romankiw et al (1999), Lu et al (1997), Wallace (1993,1993a).
- Ref. List (5.2) Dmitrieva et al (1999), Gonzalez et al (1994), Hristoforou et al (1991), Mitra et al (1991), Nielson et al (1985,1980), Luborsky et al (1975).
- Ref. List (5.3) Lachowicz et al (1989), Spano et al (1982), O'Dell (1981).
- Ref. List (5.4) Tam et al (1989), Wenda et al (1987), Narita et al (1980).
- Romankiw et al (1999) "Magnetic materials, processes and devices five", L.T. Romankiw, S. Kronselb, C.H. Ahn, Electrochemical Society Proceedings Vol. 98-20 (1999).
- Sanchez et al (1996) "Effects of creep-induced anisotropy on circumferential magnetisation in non-magnetostrictive wires", M.L. Sanchez, R. Valenzuela, M. Vazquez, A. Hernando, J. Magn. Magn. Mater (163) 132 (1996).
- Shimada et al (1981) "Sputtering of FeCo-B amorphous films with soft magnetic properties", Y. Shimada, T. Hasegawa, H. Kojima, IEEE Trans. Magn. MAG-17(2) 1199 (1981).
- Spano et al (1982) "Magnetostriction and magnetic anisotropy of field annealed METGLAS<sup>®</sup> 2605SC alloys via dc M-H loop measurements under stress", M.L. Spano, K.B. Hathaway, H.T. Savage, J. Appl. Phys. 53(3) 2667 (1982).
- Tam et al (1989) "A new high precision optical technique to measure magnetostriction of a thin magnetic film deposited on a substrate", A.C. Tam, H. Schroeder, IEEE Trans. Magn. MAG-35(3) 2692 (1989).
- Thomas et al (1992) "Anisotropy and magnetostriction in metallic glasses", A.P. Thomas, M.R.J. Gibbs, J. Magn. Magn. Mater. (103) 97 (1992).
- Thomas (1991) "Magnetostriction in transition - metalloid metallic glasses", A.P. Thomas, Ph.D. Thesis, University of Bath, (1991).
- Valenzuela et al (1997) "Current annealing and magnetoimpedance in CoFeBSi amorphous ribbons", R. Valenzuela, J. Gonzalez, E. Amano, IEEE Trans. Magn. MAG-33(5) 3925 (1997).
- Watts (1998) in conjunction with Dr R. Watts.
- Watts et al (1999) To be published (1999).
- Wallace (1993) "Magnetoelastic thin films of amorphous alloys, sputtered onto silicon wafers", J.L. Wallace, J. Appl. Phys. 73(10) 5360 (1993).
- Wallace (1993a) "Applications of sputtered thin films of magnetoelastic amorphous alloys", J.L. Wallace, Mat. & Design 14(5) 285 (1993).

- Weber et al (1994) “UHV cantilever beam technique for quantitative measurements of magnetisation, magnetostriction, and intrinsic stress of ultrathin magnetic films”, M. Weber, R. Koch, K.H. Rieder, Phys. Rev. Let. 73(8) 116 (1994).
- Wenda et al (1987) “Measurement of the saturation magnetostriction of a thin amorphous film by means of small angle magnetisation oscillation”, J. Wenda, H. Jankowski, A. Kulak, Thin Solid Films. 148 1 (1987).
- Zuberek et al (1990) “Investigations of magnetostriction in  $\text{Co}_{0.86}\text{Ti}_{0.14}$  amorphous thin films”, R. Zuberek, H. Szymczak, G. Suran, K. Ounadjela, Thin Solid Films (188) 1 (1990).

## 6.0 Magneto Impedance investigation

### 6.1 Introduction

In recent years there has been a considerable upsurge of interest in the Magneto Impedance (MI) effect, found in soft, amorphous, ferromagnetic materials. The MI effect consists of large changes in the high frequency impedance  $Z$ , found in nearly zero magnetostrictive Fe/Co based alloys in the form of melt-spun wires and ribbons. The majority of the research performed has been focused on soft amorphous cobalt based alloys, in the form of wires and ribbons, even though the effect can be observed in a wide variety of materials, as the MI effect has been found to have the largest values in these materials. The intensive research into the MI effect is a result of its technological importance in the field of sensor applications [Vazquez et al (1996)]. A number of authors have shown the effect to have great potential for magnetic sensor applications [Panina et al (1994), Mohri et al (1995), Atkinson et al (1998)]. MI effects have been found to be more field sensitive than the well established giant magneto-resistance (GMR) effects found in GMR materials. These latter materials generally require large fields to obtain a GMR response of a few percent, whereas the MI materials can produce responses of a few hundreds of a percent in very small fields of the order likely to be encountered in practice. It has also been reported [Sinnecker et al (1998)] that under certain conditions the MI effect does not exhibit hysteresis effects, as is the case with GMR materials; hysteresis is undesirable for sensor applications.

The drive for magnetic sensors to become miniaturised has now increased with fresh technological demands. In these systems, sensors are now being incorporated onto commercially important substrate materials such as silicon and gallium arsenide. The advantage of this arrangement is that the sensor, and its electrical detection/analysing circuitry, can be fabricated on the same substrate. In order to make such sensor devices, it is necessary to deposit the magnetic material in the form of a thin film. It would be difficult to incorporate existing favourable MI materials into such devices in their current form of ribbons or wires. Here a different approach to the MI effect is undertaken. Magnetic amorphous films and multi-layered films produced by sputter deposition have been investigated for their potential use as MI materials in sensors. There has been only limited research done on the MI effect in thin films in comparison to their bulk counterparts [Morikawa et al (1995), Panina et al (1995)]. Morikawa and co-workers have shown, by using multi-layered films, that it is possible to increase the MI effect in thin films compared to single layered films, thereby increasing their usefulness as sensor materials. The objective of this preliminary study into the MI effect, is to ascertain the potential use of FeSiBC films for MI sensors, and to correlate the magnetic properties with the impedance responses.

Part of this work was supported by the British Council and the Spanish Ministerio de Education y Ciencia under the Acciones Integradas program (HB95-0013).

## 6.2 Magneto Impedance

When a magnetic material carrying a low intensity, high frequency (up to 100MHz) alternating current is subjected to an external magnetic field, it exhibits a sharp change in its electrical impedance as shown in Figure 6.1a. This effect is known as the magneto impedance (MI) or the giant magneto impedance (GMI) effect. The external magnetic field is generally applied along the direction of the current flow as shown Figure 6.1b. The two MI curves shown in Figure 6.1a have been labelled as having been obtained at a low and high frequency. It can be seen from these two curves that the frequency of the applied current also has an effect on the form of the MI curve. The changes in the impedance are a consequence of changes in the interaction between the magnetisation of the material and the alternating magnetic field generated by the current. These changes occur due to the externally applied magnetic field. The key to understanding the MI effect is the effective permeability ( $\mu_{\text{eff}}$ ) or effective susceptibility ( $\chi_{\text{eff}}$ ) [ $\mu_{\text{eff}} = \chi_{\text{eff}} + 1$ ] of the magnetic material. The magnetic field dependence of the impedance is controlled by the ability of the magnetisation to respond to the magnetic field generated by the current. This is governed by the effective susceptibility of the material in the direction of the field produced by the current. The application of the external field simply alters this effective susceptibility, which leads to the changes in the impedance. The impedance maxima shown in Figure 6.1a correspond to a maximum in the effective susceptibility. For the impedance curve obtained at low frequency, the effective susceptibility is a maximum when no external field exists, but decreases on the application of a field. This is not the case for the curve obtained at the higher frequency. Here the effective susceptibility increases to a maximum on the application of a small applied field, before decreasing with further increases of the field. The effective susceptibility is, in each case, influenced by two different magnetisation processes. The effective susceptibility in the low frequency case is dominated by reversible domain wall movement, whereas in the high frequency case, it is dominated by

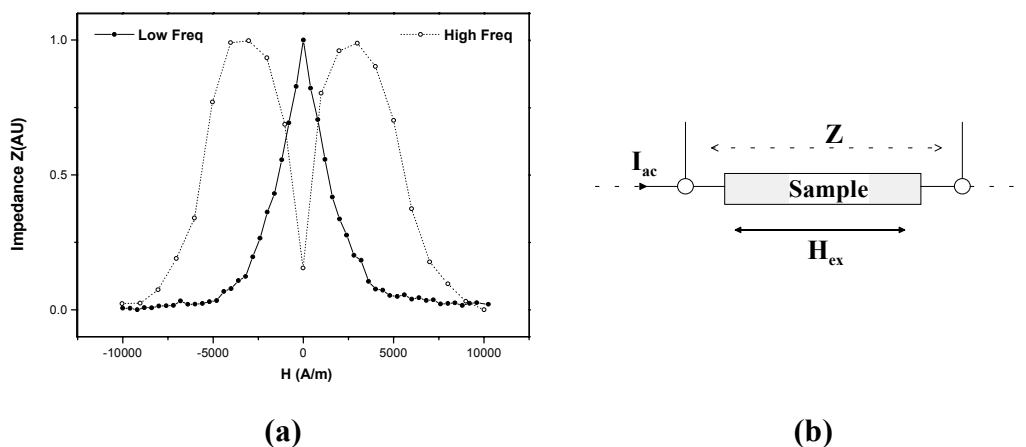


**Figure 6.1:** (a) Typical MI curves obtained from a FeSiBC film at two different current frequencies (labelled as low and high) as a function of applied magnetic field. Note the two curves have been normalised. (b) Illustration of basic impedance measurement.

domain rotation (rotation of the magnetisation). For the high frequency MI curve, the two maxima can correspond to the anisotropy field of the sample obtained along the length of the sample. At sufficiently high frequencies, the skin effect (see below) can dramatically effect the impedance of the material, which is also dependent on the effective susceptibility. It is therefore possible to separate the MI effect at high and low frequencies.

It is generally accepted that when one refers to the giant magneto impedance (GMI) effect, it usually means that a skin effect is present which gives rise to much larger impedance changes. Whereas at low frequencies, where the influence of the skin depth is weak or non-existent, it is termed the MI effect, or more correctly the magneto inductive effect.

### 6.2.1 Low frequency limit

At relatively low frequencies, where the influence of the skin effect is negligible, the MI effect is due to changes in the reactance. In this situation the alternating current generates a magnetic driving field, which causes domain wall movement (oscillation), which in turn dominates the effective susceptibility. The changing magnetisation induces an additional voltage contribution,  $V_L$ , which adds to the ohmic voltage due to the current [Mohri et al (1992), Velazquez et al (1994)].

$$V_L \propto \frac{dM}{dt} \quad (6.1)$$

This additional induced voltage is termed the magneto-inductive voltage. The larger the effective susceptibility, the larger will be the change in the magneto-inductive voltage. On application of an external magnetic field, the changing magnetisation due to domain wall movement is suppressed and the magnetisation is rotated towards the applied field. This has the effect of decreasing the effective susceptibility, since the component of magnetisation which can interact with the alternating magnetic field generated by the current has been reduced. This leads to a fall in the magneto-inductive voltage, giving rise to the magnetic dependence of the impedance. This type of MI effect is relatively small compared to the GMI effect; the largest effect is found in cobalt based amorphous wires [Mohri et al (1992)].

### 6.2.2 High Frequency limit (<100MHz)

The GMI effect has been explained in terms of classical electrodynamics [Beach et al (1994), Panina et al (1994)] as an interaction between the magnetic field created by the current and the magnetisation. At high frequencies the GMI effect is mainly due to changes in the resistive component of the impedance, since it is dominated by the skin effect. This causes the current to flow near the surface of the material, reducing the effective cross-sectional area of the material, leading to an increase in the resistive component of the impedance.

A mathematical description of the skin effect has been obtained from classical electrodynamics. For a conductor carrying a sinusoidal alternating current, the penetration or skin depth,  $\delta$ , is given by the well known expression

$$\delta = \left( \frac{\rho}{\mu_0 \chi_{\text{eff}} \pi f} \right)^{1/2} \quad (6.2)$$

where  $f$  is the frequency of the current,  $\rho$  is the resistivity of the material, and  $\chi_{\text{eff}}$  is the susceptibility. The susceptibility is the effective susceptibility in the case of GMI effect. It has been shown that for a thin film the impedance  $Z$  is related to the skin depth through the following expression [Panina et al (1995)]

$$Z = R_{dc} \cdot jkt \coth(jkt)$$
$$k = \frac{1+j}{\delta} \quad (6.3)$$

where  $R_{dc}$  is the dc resistance, and  $t$  the thickness of the conductor. It follows from expressions (6.2) and (6.3), that the impedance of a magnetic conductor again is dependent upon the effective susceptibility, through the skin depth. Here the effective susceptibility arises from two contributions: domain wall movement and oscillation of the domain magnetisation. At low frequencies, the domain wall movement dominates the susceptibility, whereas at higher frequencies the domain wall movement is strongly damped by microscopic eddy currents [Panina et al (1996)], and the magnetisation rotation contribution becomes dominant. Generally, this process results in a complex effective susceptibility [Panina et al (1996)]. The damping of the domain wall movement at high frequencies reduces the hysteresis effect, which is generally the source of the magnetic hysteresis. For successful sensor applications, it is vital that no hysteresis is present and therefore magnetisation rotation is usually preferable.

### 6.3 Domain structure and magnetostriction

From the description of the MI effect so far, it is clear that the effect is controlled by the effective susceptibility. The magnitude of the susceptibility is controlled by the magnetic anisotropy of the material. For amorphous materials the intrinsic magnetic anisotropy is usually very small, and generally the magnetic anisotropy is extrinsically induced. This could be due to structural defects, strains/stresses introduced during the production of the material, or that of post production heat treatments, such as magnetic field annealing. Typically, the magnetic anisotropy for melt spun ribbons and wires is dominated by the stresses induced by the melt-spinning process. This is usually also the case with sputter deposited magnetic thin films, but not always, as shown by the radially induced magnetic anisotropy in the FeSiBC films discussed in Chapter 5, where it is inferred that the stresses induced during the deposition were negligible. It has been shown in Chapter 5, that the magnetic anisotropy, and therefore the domain structure, can be extrinsically controlled by various heat treatments. To obtain a significant MI effect, it has been generally found by many authors that the material should possess a domain structure in which the domain walls are perpendicular to the current direction. This ensures that the oscillating field generated by the current lies in an easy axis for the magnetisation. This should therefore maximise the effective susceptibility of the system.

There have been numerous investigations [Panina et al (1996), Tejedor et al (1996), Rao et al (1994)] of how the domain structure influences the MI effect. The nature of the magnetic anisotropy has been found to be especially critical in the case of amorphous wires [Costa-Kramer et al (1995), Panina et al (1996)]. Depending upon the sign of the magnetostriction, the amorphous wires which are produced by ejecting the melt into a continuous flow of rotating water, solidifies rapidly developing mainly a tensile radial stress distribution. This leads to two different domain structures being induced in the wire (Fig. 6.2). It is now generally accepted that the domain structures which result for the as-cast wires are

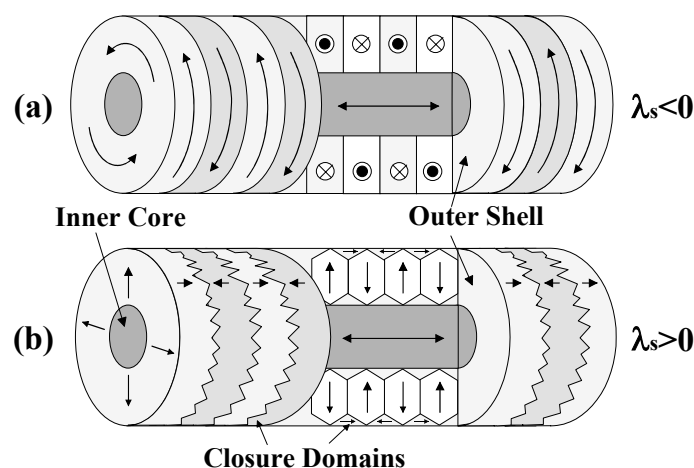


**Figure 6.2:** A simplified illustration of the domain structure for (a) negative magnetostriction, and (b) positive magnetostriction in amorphous melt-spun wires [Squire et al (1994)] of circular cross-section. The magnetoelastic coupling produces two different magnetic anisotropies, where the circumferential anisotropy (a) is more favourable than the radial (b) anisotropy for the MI effect in a circular wire.

associated with the coupling between the magnetostriction and the stresses induced by the rapid quenching process. For both positive and negative magnetostrictive wires, the domain structure consists of essentially two regions as shown in Figure 6.2. The core region for the two wires is a single domain, with the magnetisation running along the length of the wire, and the outer region is a multi-domain structure, where the magnetisation is oriented radially for a positively magnetostrictive wire (moments lie along the stress direction), and circumferentially for a negatively magnetostrictive wire. The magnetic field generated by the alternating current is of a solenoidal form, and one would therefore expect to see a much greater MI effect in the case of the amorphous wires which have a circumferential domain structure (Fig. 6.2a), compared to that of the radial domain structure (Fig. 6.2b). Experimentally this has been found to be the case by many authors, and this partly explains why the Co based amorphous wires show the greatest effect, because the negative magnetostriction induces a favourable magnetoelastic anisotropy. Also the Co based materials have much lower anisotropy constant giving them a larger effective susceptibility. A recent investigation of the MI effect on FeSiB amorphous wires by Takemura et al (1996) has shown that, by lightly annealing the amorphous wires, the radial domain structure (Fig. 6.2b) of the as-cast wire weakens, and gives way to a circumferential domain structure; this is due to surface crystallisation. This leads to an increase in the MI effect, which has also been reported by Atkinson et al (1995), and highlights the importance of the domain structure on the MI effect. It is only the Co based amorphous wires which exhibit nearly zero magnetostriction which show the largest MI effect. Not only does the sign of the magnetostriction control the type of magnetic anisotropy induced, but the magnitude of the magnetostriction also influences how large a coupling there is between the magnetisation and the stresses. Too large a coupling would reduce the effective susceptibility, because of the larger induced magnetoelastic anisotropy. It is generally found that the nearly zero magnetostrictive materials are magnetically much softer (smaller coercive fields  $< 1\text{A/m}$ ) as compared to those materials which have larger magnetostriction values, but the magnetostriction coupling is sufficient to induce a well defined magnetoelastic anisotropy. The same principles also apply to ribbons and thin films, where a uniaxial anisotropy of low magnitude is usually found to produce the maximum MI effect.

## 6.4 Sample preparation

The objective of this preliminary study into the MI effect, is to ascertain the potential use of thin films for MI sensors, and to correlate the magnetic properties with that of the impedance responses.

The experimental work carried out on the CoFeB thin films was a collaboration with David Garcia who was based at the Instituto de Magnetismo Aplicado in Madrid, under the Acciones Integradas program (HB95-0013). Two different compositions of magnetic thin films were investigated: FeSiBC films which were positively magnetostrictive, and CoFeB films which exhibited a slightly negative magnetostriction. The FeSiBC films were grown by RF magnetron sputter deposition at Sheffield, whereas the CoFeB thin films were grown in Madrid also by RF magnetron sputter deposition. The sputtering system used in Madrid is similar to the system described in Chapter 3. The CoFeB films were grown onto glass substrates from a solid, 20 mm thick target of composition  $\text{Co}_{76}\text{Fe}_4\text{B}_{20}$ . The base pressure was in the range of  $10^{-6}$  mTor, and the films were deposited at an argon pressure of  $5 \times 10^{-3}$  mTorr at a sputtering power of 300 W. The FeSiBC films were deposited using a sputtering power of 75 W at 4 mTorr of argon onto both glass and silicon substrates. The large difference in sputtering power is due to the very thick CoFeB target which dilutes the magnetron effect, and a much higher power is therefore needed to obtain a reasonable sputtering rate. The amorphous nature of the two types of films was confirmed by X-ray diffraction  $\theta$ - $2\theta$  scans using  $\text{Cu K}_\alpha$  radiation. The thickness of the single layered films ranged from 0.5  $\mu\text{m}$  to 4  $\mu\text{m}$ , whereas the thickness of the copper layer (see later for significance of the copper layer) used in the layered films ranged from 0.15  $\mu\text{m}$  to 2  $\mu\text{m}$ . The copper layer was deposited from a 5mm solid target which had purity of 99.99% using the same sputtering parameters as for the FeSiBC layers. The planar dimensions of the patterned films were controlled by two methods: the first method was by cutting the deposited films grown on the silicon or glass substrates using a conventional diamond tip scribe, and the second method involved photolithography techniques as described in Section 3.6. The patterned film structures which were obtained by photolithography techniques ensured that a sharp, geometrical definition was obtained. This also prevented the thicker films from suffering from any micro-tears from the breaking procedure which could give rise to edge effects. The magnetic anisotropy of the samples was controlled by stress annealing, as described in Section 5.8.3, and also by a number of conventional heat treatments, which will become apparent during the discussion of the results. The magnetic properties of the FeSiBC films were determined using MOKE (Chapter 2), with both point hysteresis loops and domain imaging. Bulk measurements were also made using the inductive magnetometer (MH-looper see Section 3.2). The magnetic measurements of the Co based films were carried out at Madrid where similar magnetic measurements were taken. The MI measurements were carried out in Madrid using an automated system which has been described in Section 3.5. Measurements were also performed on METGLAS<sup>®</sup> 2605SC ribbon strips which had been carefully sliced from the central portion of the target material, along with a number of VITROVAC<sup>®</sup> 6025 ribbon samples. Electrical contacts to all samples were made via high purity copper thin copper wires which were attached to the samples using silver paint. The silver paint was allowed to dry for 24 hours to ensure good electrical contact.

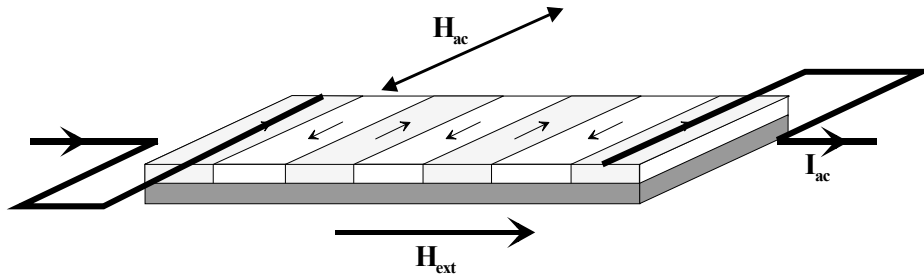


**Figure 6.3:** Geometry for MI in a magnetic film or ribbon.  $H_{ac}$  is the alternating magnetic field produced by the alternating current  $I_{ac}$  flowing along the sample and  $H_{ext}$  is the external biasing field. Ideally a transverse uniaxial anisotropy is required.

## 6.5 Results and Discussions

### 6.5.1 Ribbon samples

To achieve a large MI effect, an ideal sample should possess a magnetic anisotropy which is along the direction of the magnetic field produced by the current as discussed earlier for the case of amorphous wires. In the case of thin films or ribbons, this will be in the form of a transverse, uniaxial, magnetic anisotropy as shown in Figure 6.3. The easy axis is along the direction of the magnetic field generated by the current and this will ensure a large transverse susceptibility. Figure 6.4 represents the MI response as defined by equation (6.4)

$$\frac{\Delta Z}{Z}(H) = \frac{Z(H) - Z(H_{max})}{Z(H_{max})} \times 100 \quad (6.4)$$

as a function of an external bias field, for three Co-based ribbon samples (VITROVAC<sup>®</sup> 6025). This ribbon has a small negative magnetostriction ( $\lambda_s = -0.3 \times 10^{-6}$  [VAC (1993)]) compared to the METGLAS<sup>®</sup> ribbon, so one can compare how the responses differ in the two ribbon-based materials which have different magnetic characteristics. The MI curves for the as-cast, annealed and field annealed Co-based ribbons are compared in Figure 6.4. The MI response (23.5%) for the as-cast ribbon displays a maximum when no bias field is present, and decreases on the application of a field. Whereas the MI response (36%) of the annealed sample is of a double peak shape indicating that a uniaxial magnetic anisotropy exists which is not aligned along the length of the sample (i.e. Longitudinal). A double peak is good indication of a magnetisation rotation process. The annealing has relieved the as-cast stresses, and induced a weak transverse uniaxial magnetic anisotropy. The field annealed ribbon also indicates a transverse uniaxial magnetic anisotropy, but the MI response (22%) is much lower compared to the annealed sample. In both cases the MI peaks approximately coincide with the anisotropy field obtained from measurements along the length of the samples which seems to indicate a uniaxial magnetic anisotropy. Comparing the positions of the MI peaks for the annealed and field annealed samples, it is found that the field annealed MI peaks occur at a slightly higher value of field.

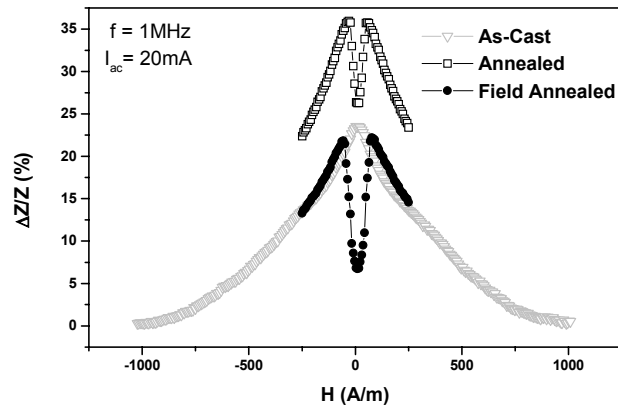


**Figure 6.4:** Magneto impedance ratios as a function of bias field, for three differently treated Co based ribbons. The dimensions of all Co based ribbon samples were 50mm in length, 5mm in width and 25  $\mu\text{m}$  in thickness. See Figure 6.5 for thermal treatment parameters.

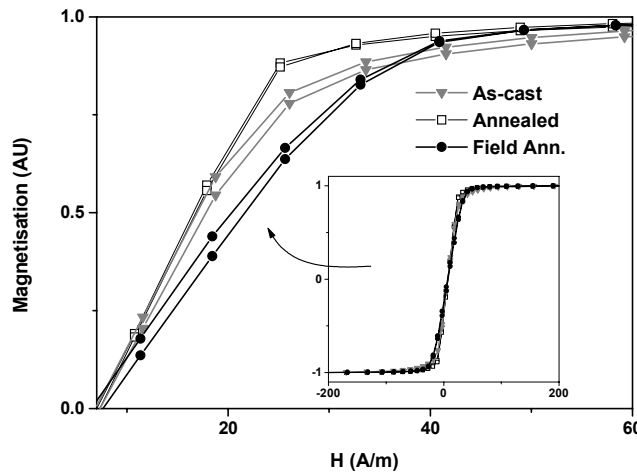


**Figure 6.5:** Longitudinal hysteresis loops for Co-based ribbons which have undergone different treatments. The thermal treatment used to relieve the growth induced stresses consisted of annealing the samples at 260 $^{\circ}\text{C}$  for 60 minutes under a low vacuum ( $10^{-2}$  Torr). The field annealing was performed with the same parameters, with a 0.3T magnetic field applied in the transverse direction.

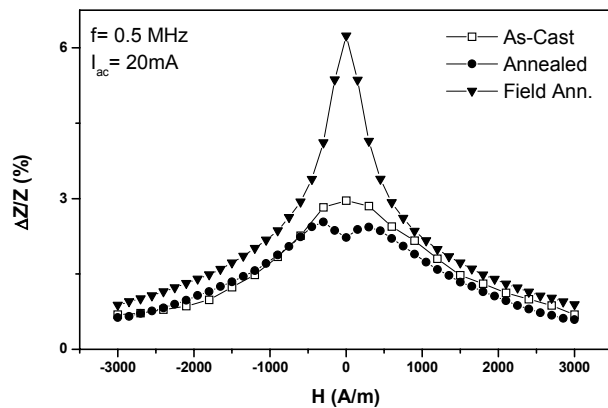


**Figure 6.6:** Magneto impedance ratios as a function of bias field, for three differently treated METGLAS<sup>®</sup> ribbons. The dimensions of the samples were 50mm in length, 5mm in width and 25  $\mu\text{m}$  in thickness. See Figure 6.7 for thermal treatment parameters.

This is confirmed by the longitudinal hysteresis loops taken along the length of sample (hard axis loop) which are shown in Figure 6.5. One can assume the slightly higher anisotropy has reduced the transverse susceptibility. The non-zero impedance change at the origin for the annealed and field annealed MI curves, indicates that the susceptibility is non-zero and is not totally due to the magnetisation oscillation process (domain rotation). These impedance curves have been obtained at a low 1 MHz frequency where contributions to the effective susceptibility are made up from domain wall movement and domain rotations. Figure 6.6 compares the MI responses obtained for the METGLAS<sup>®</sup> ribbon samples which were of the same dimensions as those of the Co based ribbon samples and were subjected to similar treatments. The first, most obvious, observation is that, the MI response is dramatically reduced in size. The as-cast sample displays a MI response of only 3%, and the annealed sample exhibits a response of 2.5% and shows a weak, double peak feature. The annealing procedure has the effect of reducing the as-cast stresses, which can be seen from examining Figure 6.7, were the longitudinal loops of the samples are shown. The MI response for the annealed sample seems to imply that, at this low frequency of 0.5 MHz, the domain wall susceptibility has been reduced and the susceptibility due to the domain rotation is becoming dominant.

Domain imaging which was found to be a very difficult process for the ribbon samples, mainly due to the dispersion of light because of the roughness of the ribbon surfaces, indicated no visible domain structure for the annealed samples. The MI response of the field annealed sample is 6%, and has a maximum response when no external field is applied. It has been shown that field annealing does produce a uniaxial anisotropy in METGLAS<sup>®</sup> ribbons [Thomas (1991)] and thin FeSiBC films [Ali et al (1998)]; this is shown in Figure 6.8, where a domain image was obtained for a field annealed METGLAS<sup>®</sup> ribbon sample. The image obtained is not as clear and sharp as other images presented in this thesis of its thin film counter parts due roughness of the surface, but it does show a uniaxial anisotropy. The image was obtained 10 mm from the end of the sample, and the domain walls appear to be curved, but this is an illusion caused by the sample not being flat. The hysteresis loop shown in Figure 6.7 displays a linear response which is typical for magnetisation rotation, with no visible

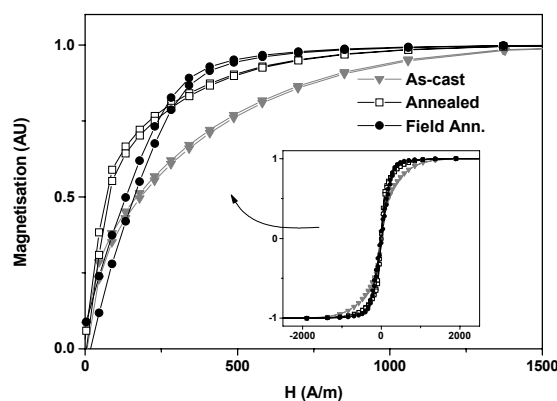


**Figure 6.7:** Longitudinal hysteresis loops for the METGLAS<sup>®</sup> ribbons which have undergone different heat treatments. The heat treatment used to relieve the growth induced anisotropy was to anneal the samples at 400°C for 60 minutes under a low vacuum ( $10^{-2}$  Torr). The field annealing was performed at the same parameters, with a 0.3T magnetic field applied in the transverse direction.

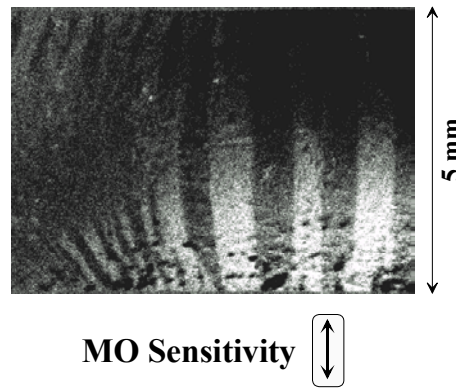


**Figure 6.8:** Domain image of a field annealed METGLAS<sup>®</sup> ribbon which displays a uniaxial anisotropy. Image obtained 10mm from end of sample. Note sample length 50mm.

hysteresis. Here it appears that the transverse susceptibility is being dominated by domain wall movement since no peaks due to rotational effects are seen. hysteresis.

The ribbon samples (METGLAS<sup>®</sup> 2605SC [ $M_s=1.61$  T] / VITROVAC<sup>®</sup> 6025 [ $M_s=0.55$  T]) were of the same dimensions which ensured that any shape-induced demagnetising factors were the same, but the internal demagnetising field was  $\sim 3$  times as large for the METGLAS<sup>®</sup> samples ( $H_d \propto M_s$ ); this will have the effect of reducing the susceptibility. The MI responses were obtained at virtually the same frequencies and the two materials have a similar resistivity of  $135 \mu\Omega\text{cm}$ , and therefore any skin effects should have been controlled by the effective susceptibility as indicated by equation 6.2.

The magnetic anisotropy of the METGLAS<sup>®</sup> ribbon samples was induced to maximise the transverse susceptibility by field annealing, but the MI response in comparison was poor. From examining Figure 6.9, where the respective loops for the METGLAS<sup>®</sup> and VITROVAC<sup>®</sup> ribbon samples are compared, it is clear that the METGLAS<sup>®</sup> samples are magnetically harder than the VITROVAC<sup>®</sup> samples, even after undergoing stress relief. The anisotropy field ( $H_k$ ) for the field annealed sample was  $320$  A/m for the METGLAS<sup>®</sup> and only  $27$  A/m for the VITROVAC<sup>®</sup>. The coercive field ( $H_c$ ) for the VITROVAC<sup>®</sup> samples were less than  $0.6$  A/m measured by the MH inductive magnetometer, whereas the METGLAS<sup>®</sup> samples had a coercive field of  $15$  A/m. It was found that field annealing the METGLAS<sup>®</sup> ribbon increased its coercive field from its annealed state of  $10$  A/m. It was not possible to obtain transverse hysteresis loops across the width of the samples, because of the limited size of the sensing

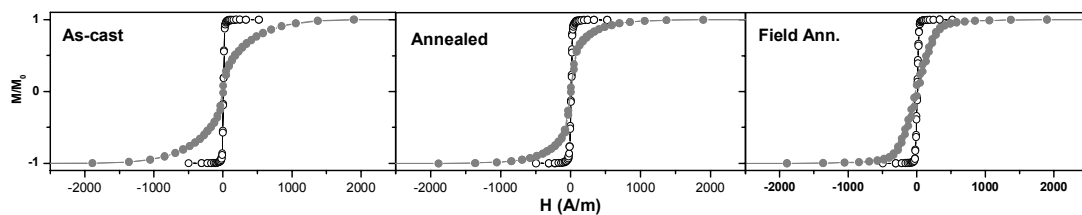


**Figure 6.9:** Comparison of METGLAS<sup>®</sup> (solid circles) and VITROVAC<sup>®</sup> (open circles) ribbon samples. Longitudinal loops taken for the three types of ribbon samples.

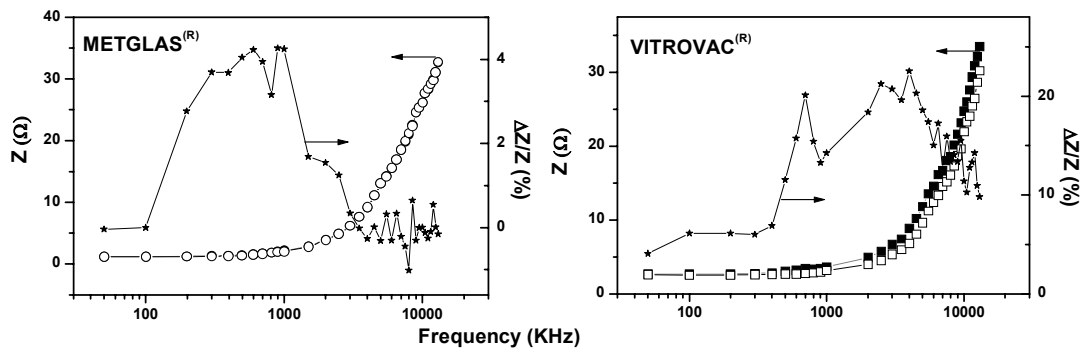


**Figure 6.10:** The impedance and MI response as a function of frequency, with no applied field (solid symbols), and with an applied field of 5000 A/m (open symbols). The MI response is shown by the solid star symbols for the two samples. Circles represent a field annealed METGLAS<sup>®</sup> ribbon sample, and the squares represent an annealed VITROVAC<sup>®</sup> ribbon sample. A current of 20 mA was used in both cases.

coils of the inductive magnetometer (Section 3.2). However from the MOKE measurements taken from the thin films it was generally found that the easy axis loops had slightly higher coercive fields. The higher coercive fields reduce the domain wall susceptibility, which explains the much lower MI responses for the METGLAS<sup>®</sup> ribbon samples. Generally it is found that the Co based amorphous alloys have larger permeabilities, lower coercive fields, and lower magnetostriction constants than the Fe based amorphous alloys. A frequency dependence of the MI response was carried out on the annealed VITROVAC<sup>®</sup> and field annealed METGLAS<sup>®</sup> samples and the curves are shown in Figure 6.10. The data here was obtained manually using a digital oscilloscope and a frequency generator and not by the automated system. Two frequency sweeps were performed: one with no external biasing field, and a second with biasing field of 5 kA/m. The external biasing field has an effect of reducing the effective transverse susceptibility, and hence the impedance response is reduced. The VITROVAC<sup>®</sup> sample shows a clear change in the impedance response with an applied field, whereas the METGLAS<sup>®</sup> sample indicates no visible change, but there is a difference in the MI ratio, as defined by equation 6.4, which shows that there is a small change in the MI on application of a field for the METGLAS<sup>®</sup> sample. For both samples the MI response increases before falling away with increasing frequency, the largest effect being in the VITROVAC<sup>®</sup> sample. The impedance response as a function of current was also investigated for the METGLAS<sup>®</sup> samples but there was no apparent dependency. Figure 6.11 shows a more detailed response of the MI as a function of frequency for an as cast METGLAS<sup>®</sup> sample. A maximum response of 3% is obtained at a frequency of 0.5 MHz, where the curve has a single peak located at the origin, and decreases to 0.5% at 8 MHz as the frequency is increased. In the process the single peak transforms into a double peak, indicating that the susceptibility due to domain wall movement is being reduced and the susceptibility due to rotational effects is becoming important. It appears that the damping of the domain wall movement occurs at the relatively low frequency of 1 MHz. A similar set of MI curves are obtained for the annealed samples. The MI curves for a field annealed sample is shown in Figure 6.12. Here again, a similar pattern is seen where the single peak becomes a double peak with increasing frequency, which indicates that the domain wall susceptibility is being reduced, and the susceptibility due to domain rotation is becoming dominant at higher frequencies. From the measurements performed on the METGLAS<sup>®</sup> ribbons, it

appears that the MI response is regulated by the susceptibility due to domain wall movement at low frequencies, and this contribution is reduced above a frequency of 1MHz. The above process has also been observed by Tejedor et al (1996), who have concluded that the decrease in MI maxima is a result of a decrease in the transverse susceptibility due to the increased frequency.

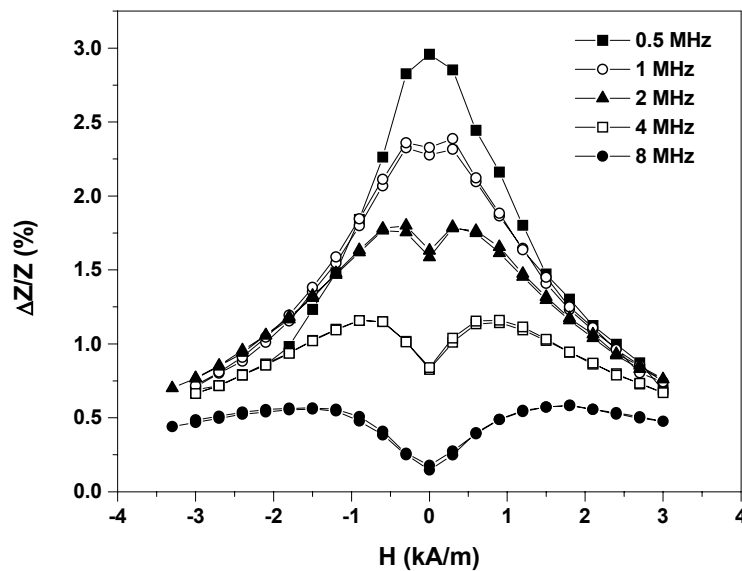


**Figure 6.11:** MI curves obtained at different driving frequencies for an as-cast METGLAS<sup>®</sup> 2605SC ribbon sample. The MI response decreases with increasing frequency. Measurements were taken using a current of 20 mA.

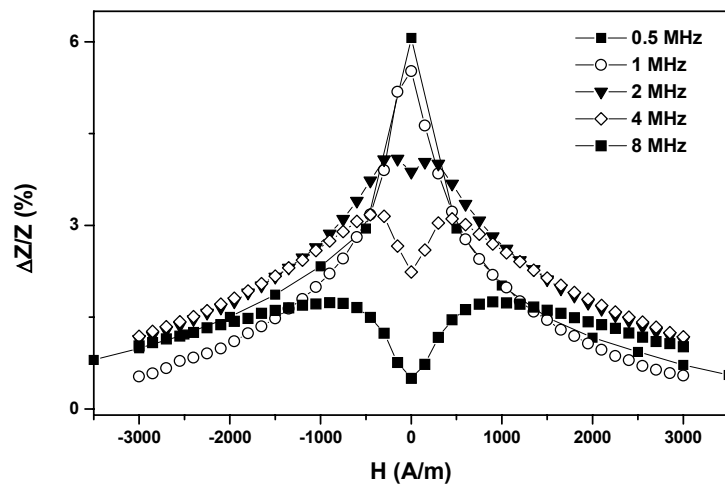


**Figure 6.12:** MI curves obtained at different driving frequencies for a field annealed METGLAS<sup>®</sup> ribbon sample. The MI response decreases with increasing frequency. Measurements were taken using a current of 20 mA.

## 6.5.2 Thin Film Samples

### 6.5.2.1 FeSiBC amorphous ferromagnetic films

The MI study of the FeSiBC single layered films were performed on four thicknesses (Fig. 6.13) of films which were deposited onto silicon substrates of dimensions 75×5 mm. Due to the limitation imposed by the MI apparatus at the time of these measurements (Section 3.6), the upper frequency limit of the MI analysis was limited to 10 MHz. Ideally, from the point of view of sensor applications it would be preferable if the thin films would operate at relatively low frequencies (1-15 MHz), since it simplifies the electronics needed for the sensor. It was found that the MI response (Fig. 6.13) increased as the thickness of the films increased, indicating that the inductive effect was dependent on the thickness of the film (cross-sectional area). This was verified by current-voltage measurements made by monitoring the voltage across the film and a series standard resistor using an oscilloscope. From Figure 6.13b, it is seen that the 500nm film exhibits a fraction of the inductive effective compared to the 2µm film over a range of frequencies. The susceptibility of the two films were the same, since the MOKE loops were similar and they both had similar coercive fields of 30 A/m. It was found that the largest MI responses appeared in the thicker films, and therefore most of the analysis presented here was carried out on 3µm thick films. The as-deposited films possessed the radial magnetic anisotropy [Ali et al (1998)] which is induced by the magnetron effect, and therefore the samples had to be thermally treated to remove, or induce, a uniform transverse uniaxial anisotropy. A number of samples were also examined in their deposited state.

As previously seen for the METGLAS<sup>®</sup> ribbon samples, two types of MI curves were obtained for the thin films; these are shown in Figure 6.14. The annealed samples display a single MI peak located at the origin, whereas the stress annealed and as-deposited samples display a double peak MI response. The maximum MI response was found to be approximately 1% for these samples. Surprisingly the field

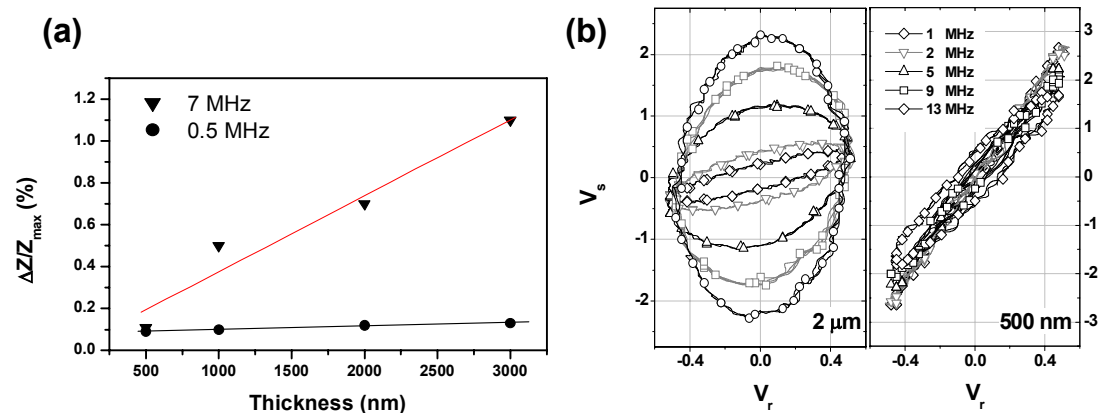


**Figure 6.13:** Figure (a) displays the MI response obtained from a variation in the thickness of the FeSiBC thin films at 0.5 MHz and 7 MHz. The solid lines are included as a guide only. (b) Current-voltage measurements over a range of frequencies.

annealed samples displayed a smaller response (0.4%) compared to the other three types of samples, and exhibited a weak double peak feature. From the results obtained from the ribbon material, it was expected that the field annealed samples would display the largest effect. The field annealed samples were obtained from the same deposition run as the other samples shown in Figure 6.14. This removed the possibility of the material being magnetically different, even though it has been shown that samples are very reproducible from consecutive deposition runs, and therefore some other mechanism is at work. Figure 6.15 represents the typical domain structures for the four types of samples used, in their remanent state, along with their corresponding hysteresis loops. For the as-grown, stress annealed, and field annealed samples, the domain images display a uniaxial anisotropy induced along the transverse direction (across the width), whereas the annealed samples have an easy axis along the longitudinal direction (along the length). The hysteresis loops for the annealed sample indicates a significant anisotropy has been induced. This has been attributed to two effects: the 15:1 aspect ratio of the samples creates a shape anisotropy which tries to align the moments along the length of the sample, and because no other agent is present which opposes this, during the annealing treatment, it creates an easy axis along the length of the samples. Secondly as described in Chapter 3, the samples are annealed in a solenoid observation furnace where a small field exists along the length of the coil, and which also prefers to align the magnetisation along the length of the samples. The curved domains are presumed to be the consequence of this AC field not being aligned perfectly along the axis of the samples. The uniaxial domain structure of the as-deposited samples is perpendicular to the long axis of the samples in the central region, but deviates away towards the ends of the samples as shown in Chapter 5. The anisotropy induced in the as-deposited and stress annealed samples is sufficiently large that it prevents the formation of closure domains, which would require the domain magnetisation to point along the hard axis. The energy of the system is minimised by the formation of reverse spike domains, and by the

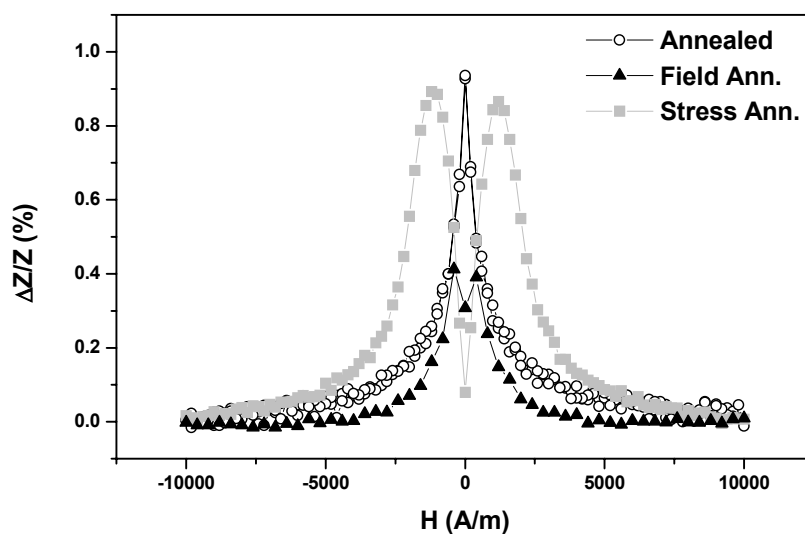


**Figure 6.14:** Magneto impedance ratios as a function of bias field for three differently treated FeSiBC films. The sample had dimensions of 75mm in length, 5mm in width and 3  $\mu\text{m}$  in thickness [Ali et al (1999)]. (7MHz).

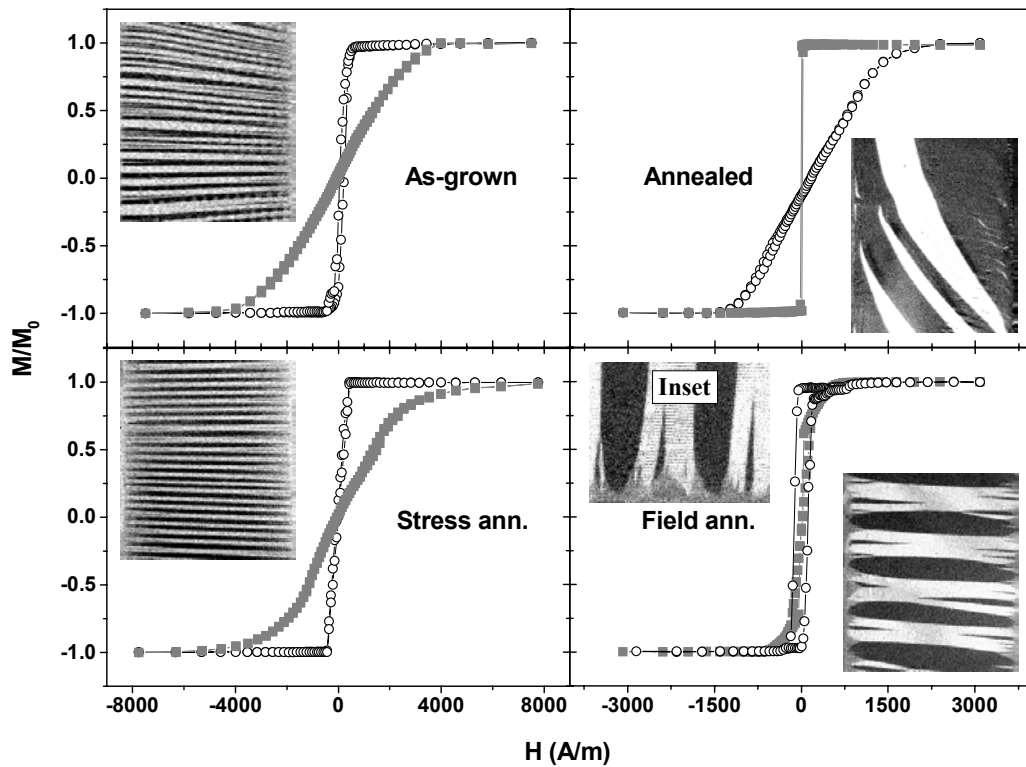


**Figure 6.15:** Domain images and their respective MOKE hysteresis loops for samples shown in Figure 6.14. MOKE loops were measured at the centres of each sample. The inset for the field annealed sample indicates that closure domains exist together with reverse spike domains.

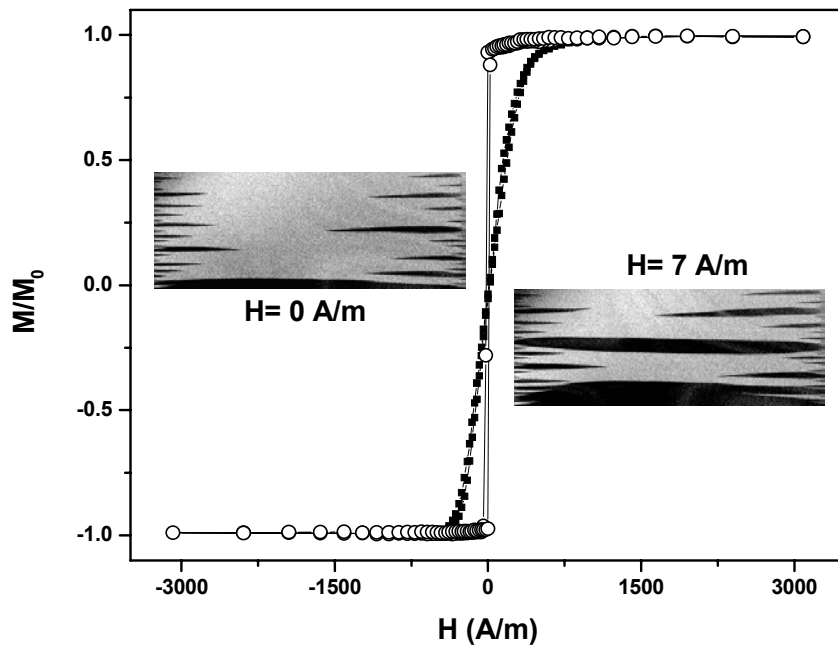


**Figure 6.16:** A FeSiBC thin film which was field annealed at the same time as the sample shown in Figure 6.15. This sample has an aspect ratio which is 3:1. In this case there are only reverse spike domains.

narrow domain widths, which reduce the demagnetising effects. The domain structure of the field annealed samples, is that of flux closure type where closure domains exist (see inset) at the edges together with reverse spike domains. In this case the anisotropy induced is relatively weak, and therefore much larger domains exist because of the formation of flux closure domains. It is assumed the closure domains are a consequence of the shape anisotropy, since Figure 6.16 shows the domain structure of a film on complete glass slide (aspect ratio 3:1) which was field annealed at the same time as the sample shown in Figure 6.15. Here the domain structure is uniaxial with reverse spike domains present only, and it therefore seems the closure domains are due to the shape anisotropy in the long narrow samples. We know from the samples which have undergone stress relief, that the shape anisotropy and the small magnetic field creates a significant anisotropy field of  $\sim 1500\text{A/m}$ . The easy axis coercive field, is notably larger ( $200\text{ A/m}$ ) in comparison to the other three sample types. It should be noted the larger coercive field appears to be due to the closure domains in combination with the reverse spike domains which seem to prevent the free movement of the main  $180^\circ$  degree domain walls.

Domain images have verified that the domain walls are pinned at the closure domains and do not move as freely as the  $180^\circ$  domain walls in the other samples. The higher coercive fields reduce the effective transverse susceptibility, especially the contribution from domain wall movement of the sample; this explains why the field annealed samples display a much lower MI response than the other thin film samples and the ribbon samples. The MI response was also investigated as a function of current amplitude for the four types of samples, but no significant dependence was found. Figure 6.17 shows the maximum MI response as function of frequency for a typical sample which has been annealed (stress relieved). The inset shows a number of selected MI curves from points on the main graph. The opposite effect is seen here, compared to that of the ribbon samples. The MI response for the annealed films increases with frequency, whereas it decreases for the ribbon samples. The effective

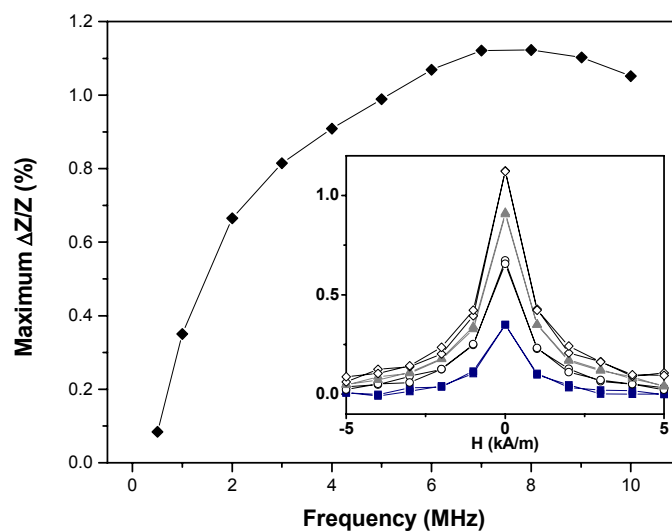


**Figure 6.17:** The maximum MI response a function of the current frequency for a  $3\mu\text{m}$  FeSiBC annealed (stress relieved) film. The inset shows the MI curves obtained at a number of frequencies. [1MHz $\Rightarrow$ solid squares, 2MHz $\Rightarrow$ open circles, 4MHz $\Rightarrow$ solid triangle, 8MHz $\Rightarrow$ open diamond].

susceptibility of the films is controlled by domain rotation and not by domain wall movement as in the case of the ribbon samples. The curve exhibits three regions: initially the MI increases rapidly - this is due to increasing rotational effects, it then increases linearly with frequency between the region 2-7 MHz (reactance  $\propto$  Freq), before decreasing. The shape of the MI curves is a single peak located at the  $H=0$  for all frequencies. This is what would be expected, since both hysteresis loops and domain images indicate that the easy axis is parallel to the current direction in these annealed samples, and therefore the DC axial field has the effect of increasing the field-imposed anisotropy, which reduces the transverse rotational susceptibility on the onset of the applied field. Similar responses were found for the as-deposited and stress annealed samples, and Figure 6.18 shows a typical response for a stress annealed sample as a function of frequency. The MI curves for these samples exhibit a double peak indicating domain rotation, since the magnetisation is no longer parallel to the applied field. The impedance increases to its maximum value, at the anisotropy field, because there is an increase in the rotational transverse susceptibility as the magnetisation is rotated towards the direction of the current by the external field. The decrease in the impedance with further increase of the external field is a result of the increasing field imposed anisotropy which reduces the transverse rotational susceptibility. An important result is obtained from the MI curves shown in the inset of Figure 6.18. When no external field is present, the MI response has a value of almost zero, at all frequencies (there is a slight decrease on increasing frequency). This indicates that the contribution to the transverse susceptibility from domain wall movement is very weak or negligible; this would be plausible since the easy axis coercive fields are higher. The finite value of the MI at  $H=0$  may be due to the easy axis not being aligned perfectly perpendicular to the current direction, or there is probably a distribution of the easy-axis orientation, which is a reasonable assumption; this would lead to a small domain rotation contribution to the susceptibility.

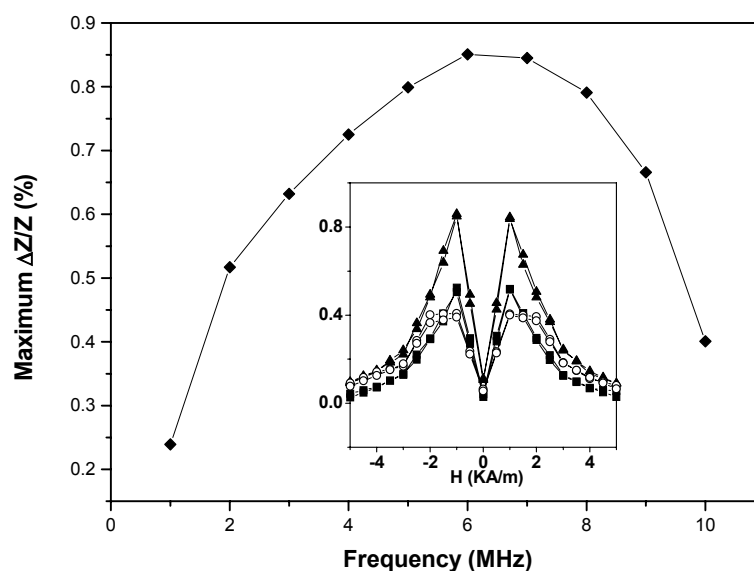


**Figure 6.18:** The maximum MI response a function of the current frequency for a  $3\mu\text{m}$  FeSiBC stress annealed film. The inset shows the MI curve obtained a number of frequencies. [1MHz $\Rightarrow$  solid squares, 6MHz $\Rightarrow$  solid triangle, 10MHz $\Rightarrow$  open circles].

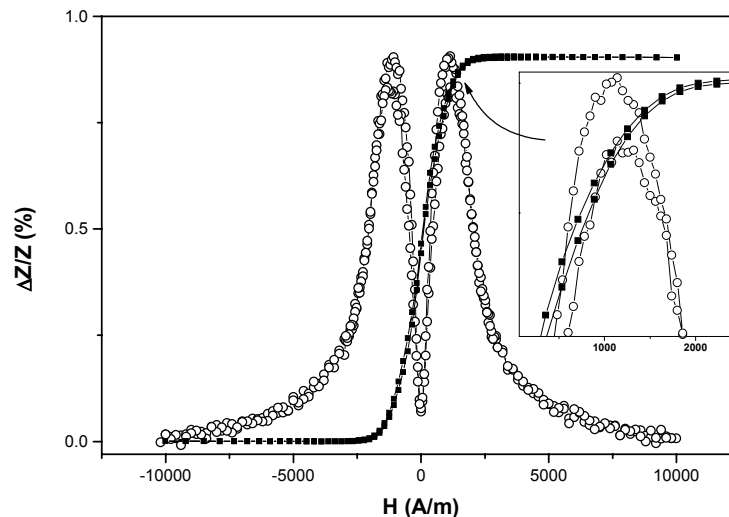


**Figure 6.19:** MI curve from a stress annealed FeSiBC film exhibiting hysteresis. The corresponding MH loop has been over-laid after being re-scaled, hence arbitrary units are used. Both the MI curve and MH loop indicate a magnetisation rotation process. The inset shows the hysteresis present around the anisotropy field. (Freq.=7MHz,  $I_{ac}$ =5mA) [Ali et al (1999)].

Comparing the MI curves to those of the METGLAS<sup>®</sup> ribbons shown in Figures 6.11 & 6.12, the MI response at  $H=0$  decreases to zero with increasing frequency as the contribution to the susceptibility from domain wall movement is restricted. This is in agreement with what is found in the present work for the FeSiBC films, where the response increases from zero due to the increasing rotational effects. The impedance response in these films is controlled by the process of domain rotation, which is a small effect in these samples. Figure 6.19 is the MI response of a stress annealed sample, along with its corresponding hard axis hysteresis loop. The shape of the hysteresis loop is that of a typical magnetisation rotation process, and the MI peaks coincide with the anisotropy field obtained from the hysteresis loop. The initial slopes of the MI curve are also linear, which indicates a rotational process. It is found that the MI effect is not hysteresis free, as shown by a recent publication by Sinnecker et al (1998)] where hysteresis effects are shown to be present in MI curves. It was found that the hysteresis effects in the MI curves coincided with the hysteresis observed in the magnetic hysteresis loops; this indicated that the hysteresis was a direct result of the magnetisation process. This is shown in the inset of Figure 6.19 where hysteresis effects were found in the MI curves obtained from the FeSiBC film samples. The hysteresis in the MI curves coincides with the magnetic hysteresis of the magnetic loops. The peaks for the positive field cycle are shown, where a small hysteresis effect can be observed. There was no significant difference found in the maximum MI response for either the transverse or longitudinal uniaxial anisotropy. The only difference between the two domain structures was the resulting shape of the magneto impedance curve. As shown in Figure 6.20, the typical MI response for an annealed sample was approximately 1% in an applied field of 10 kA/m, and the sensitivity to the magnetic response in the linear region is approximately 0.06%/Oe, which does not compare at all well with reported sensitivities of a few hundred percent per oertsed ( $1\text{Oe}=79.58\text{ A/m}$ ) for non-film based materials. Samples with transverse domain structures exhibited sensitivities of only 0.1%/Oe

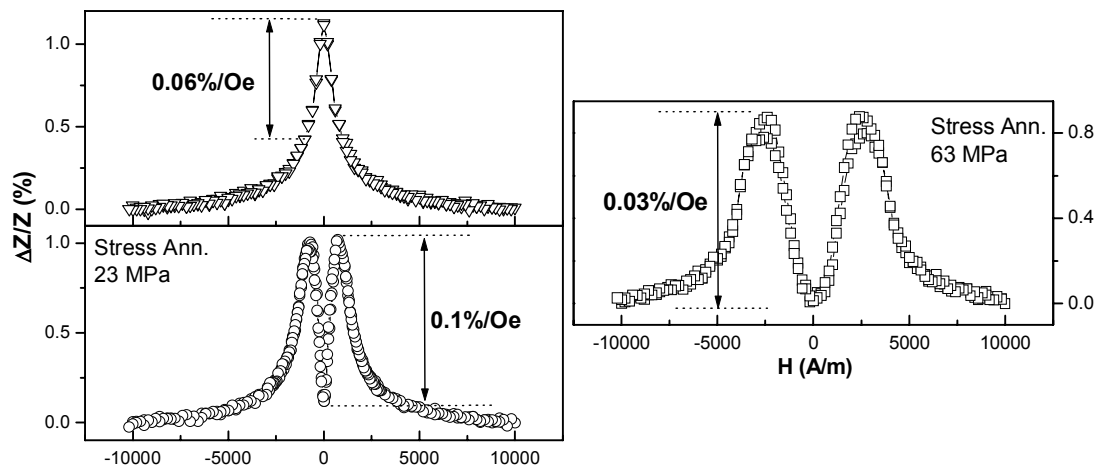


**Figure 6.20:** MI curves obtained from an annealed and two stress annealed FeSiBC films showing the sensitivity to the magnetic response. (Freq.=7MHz,  $I_{ac}$ =5mA). Notice that in the film which is stress annealed with a larger applied stress, the MI peaks occur at a higher field value.

depending upon how large an anisotropy had been induced. A larger anisotropy simply decreases the sensitivity, since a larger field is needed to obtain the same MI change. A positive and promising result from MI curves for samples with a transverse domain structure, is that the MI response is initially linear with field (Fig. 6.20) and therefore could be used as the basis of a field sensor, if the sensitivity could be increased. One possible option is to operate at a much higher driving frequency (>400MHz) where a skin effect would be present and the larger GMI effect could be used. The alternative method is to enhance the MI effect by using layered films as reported by Morikawa et al (1997) as discussed below.

In Chapter 5 it has been shown that the anisotropy field varies linearly with strain, and one can measure the resulting anisotropy field as a function of strain very accurately using MOKE; this therefore could be utilised as a stress sensor. A similar principle can be used here, using the MI effect instead of MOKE, to obtain the strain induced anisotropy. Figure 6.20 shows the MI response of two samples which were stress annealed with two different applied stresses and the MI peaks occur at two different fields. Unfortunately, the MI measurements were carried out in Madrid, where it was not possible to simultaneously vary the strain and to obtain MI measurements on the same sample. Instead a number of films with identical dimensions were stress annealed as described in Chapter 5 so as to create a range of strain induced anisotropies. The results are shown in Figure 6.21, where the anisotropy field ( $H_K^{MI}$ ), is obtained from the MI peaks. Since the MI effect is due to the magnetisation rotation process, the MI peaks can be taken to represent the stress induced anisotropy field. A domain rotation model for the susceptibility is discussed below where it is shown that the MI in the film samples is controlled by the magnetisation rotation process. The data obtained is not as linear as was expected, but considering that only one set of five samples was used, the data does look promising for future work. From the slope of the best fit line (see Chapter 5), one obtains a value for the magnetostriction constant of  $27 \pm 11.2$ ppm, which is lower than the expected value. When the measurements were carried out on these samples, it was over-looked at the time that the electrical contacts for MI measurements were made 5mm from the ends of the samples which were 75mm in

length. This meant the strain induced anisotropy was not linear between the two electrical contact points along the whole length of the samples as discussed in Section 5.8.3.3. This meant that the anisotropy field measured by the MI effect did not relate to the induced stress. The varying anisotropy causes the MI peaks to occur at lower fields because of an averaging effect. A more linear response would be expected if the contacts were made 10mm apart on the central region of the sample where the strain is approximately uniform, and if the stress was varied on the same sample. This would ensure that the anisotropy field measured by the MI could be correlated to the stress applied, which would produce a more linear response as shown in Section 5.8.

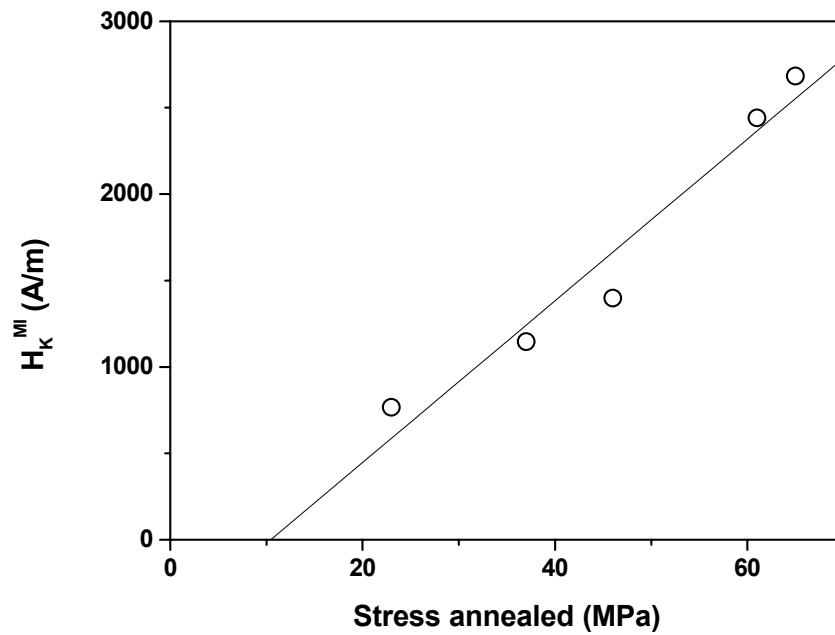


**Figure 6.21:** The anisotropy field obtained from MI measurements for samples which have been stress annealed with different applied stresses. (Freq.=7MHz,  $I_{ac}$ =5mA)

### 6.5.2.2 CoFeB amorphous ferromagnetic films

The thickness of the  $\text{Co}_{76}\text{Fe}_4\text{B}_{20}$  thin films which were deposited onto glass substrates ranged from 1.5 to 4.3  $\mu\text{m}$ . The anisotropies for these particular samples were induced by strained growth, AC and DC field annealing. In the case of the strained growth, the negative magnetostriction produced an easy axis along the length of the samples upon removal of the externally applied stress. In order to obtain a transverse domain structure, samples were then cut 2mm by 20mm in such a way that a transverse uniaxial anisotropy existed across the width of the final samples. Typical domain structures for the different induced anisotropies are shown in Figure 6.22. The strained growth and the DC field annealed samples all display a transverse uniaxial domain structure, with reverse spike domains at the edges. The as-deposited films exhibit a longitudinal anisotropy and this is attributed to the magnetron effect. The samples which underwent an AC field anneal, have a slightly different domain structure. Here the stripe domains have the form of an inverted “S” [Garcia et al (1998)], where the central region of the domain walls make an angle of approximately  $17^\circ$  with the transverse direction, and this increases further to approximately  $65^\circ$  towards the edges. The domain structure is determined by the net anisotropy between the AC field annealed, as-cast and shape-induced anisotropies.

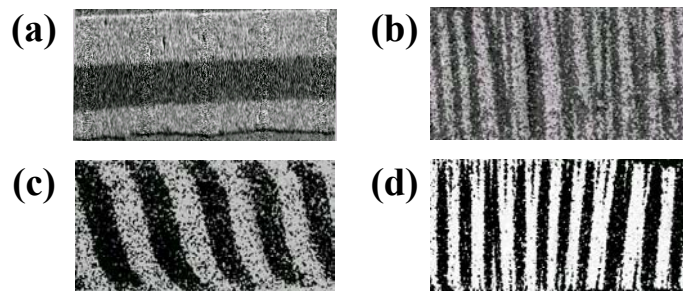


**Figure 6.22:** Domain structures for remanent state for an (a) as-deposited, (b) strained growth, (c) AC field annealed, (d) DC field annealed CoFeB thin film samples. Thermal treatments performed at  $300^\circ\text{C}$  at a field of 1.5kA/m (50 Hz) and 4kA/m respectively in an argon atmosphere for 1 hour. Domain images obtained in Madrid [Garcia et al (1999)].

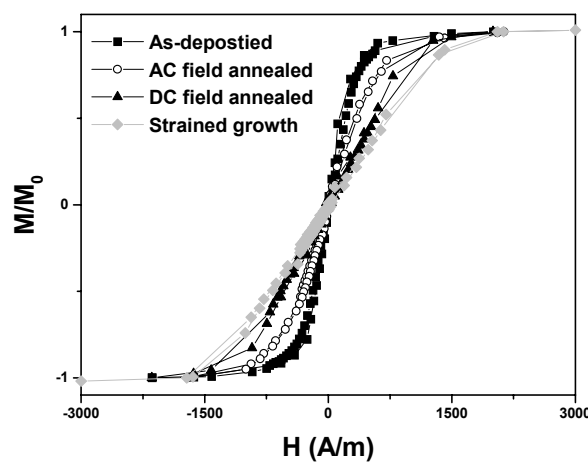


**Figure 6.23:** Longitudinal hysteresis loops obtained from the samples described using VSM. Measurements carried out on Madrid.

As shown in Figure 6.22a, the as-cast samples have a longitudinal domain structure, which the field annealing needs to overcome. Samples which were AC field annealed at a lower temperature of 250<sup>0</sup>C (50<sup>0</sup>C lower), were found to have a more pronounced curvature of the domain walls. In this case, the central region of the domain walls made an angle of 52<sup>0</sup>, indicating that the anisotropy induced by AC field annealing is much weaker at 250<sup>0</sup>C. From this one can infer that the “S” shaped domain structure is a result of the competing anisotropies. The “S” shaped domains also appear to remove the need for reverse spike domains, due to the curving domains towards the longitudinal direction as they approach the edges of the samples. The hysteresis loops for the four types of samples are shown in Figure 6.23. The samples have coercive fields in the range of 12 to 30 A/m. The strained growth and AC field annealed samples displayed smaller coercive fields compared to the other two types of samples. All samples displayed a small remanent magnetisation which correlated well with the remanent domain images shown in Figure 6.22, where approximately equal amounts of anti-parallel domains existed. As one would expect, the largest anisotropy was attained for the strained growth samples where anisotropy fields of approximately 1750 A/m were induced.

The DC and AC field annealed treatments induced anisotropy fields of 820 A/m and 1100 A/m respectively. Figure 6.24 shows the typical MI responses obtained from the AC field annealed and strained growth samples. No appreciable MI responses were found for the other samples over the range of frequencies and currents investigated. It was found that the largest MI response of 0.7% was measured from the AC field annealed samples, and a MI response of 0.4% from the stress annealed samples. The larger MI response for the AC annealed samples correlates to the lower coercive fields of the samples compared to the others. As with the FeSiBC films, it was found that the MI response is controlled by the process of magnetisation rotation, since the MI response increases with frequency. The MI curves exhibit a double peak which correlates with the transverse magnetic anisotropy and the peaks correspond to the anisotropy field, where the susceptibility due to magnetisation rotation is a maximum. So, it appears therefore that for both the FeSiBC and CoFeB thin films, the MI response is controlled by domain rotation.

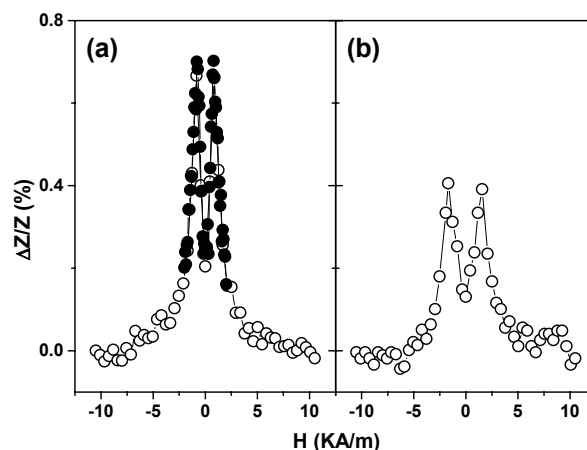


**Figure 6.24:** MI curves obtained from (a) AC field annealed, and (b) strained growth Fe Co<sub>76</sub>Fe<sub>4</sub>B<sub>20</sub> film samples (3 $\mu$ m). Measurements carried out at 5MHz at current amplitude of 5mA. [Garcia et al (1999)].

### 6.5.2.3 Layered FeSiBC amorphous ferromagnetic films with copper

Morikawa et al (1997) have demonstrated that by using multi-layered film structures, it is possible to increase the MI ratios of thin films without increasing the current frequency. MI ratios of 140% have been obtained at 1MHz, giving sensitivities of 15%/Oe, which have been shown to be three orders of magnitude larger than the respective single layered films of similar thicknesses. The sensitivity is further increased by a very modest increase in frequency to 10MHz to give sensitivities of 49%/Oe. The MI ratios and sensitivities obtained here are the largest values reported for thin films at these particularly low operating frequencies, and are comparable to sensitivities for some amorphous wires and ribbons. A schematic drawing of the MI element used by Morikawa et al is shown in Figure 6.25a. The MI element consists of a conductive non-magnetic core, which is surrounded by two layers of amorphous ferromagnetic material in which a transverse uniaxial anisotropy has been created. The magnetic material has a coercive field of 25A/m and a well defined transverse uniaxial anisotropy. Since the resistance of the conductive layer is much lower than the magnetic layers, the majority of the current flows through the conductive layer. The conductive layer also has the effect of reducing the resistance of the whole element. Typical results obtained by Morikawa et al are shown in Figure 6.25b, where the MI response as a function of frequency is shown for a single layered film of CoSiB, and a

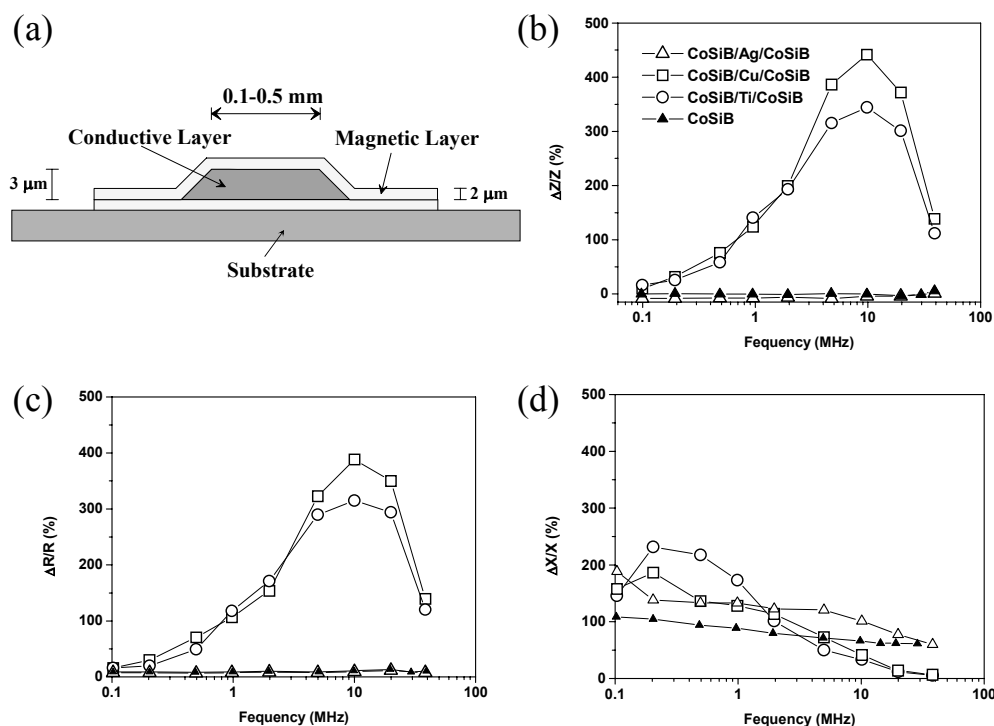


**Figure 6.25:** Layered films [Morikawa et al (1997)]. (a) Schematic-cross sectional view of the layered structure used for MI measurements. (b) MI dependence as a function of frequency for CoSiB film and layered films with conductive materials shown. (c) The dependence of the change in resistance as a function of frequency for the same samples as shown in Figure (b). (d) The corresponding reactance changes observed as a function of frequency. These results clearly indicate that the MI response appears to be dominated by the changes in the resistance, even though the skin effect is negligible at these low frequencies.

number of layered structures. The layered structures, except for the structure with titanium as the conductive layer, display a dramatic increase in the MI response compared to the single layered film. This increase is attributed to the insertion of the conductive layer, which enhances the resistance changes because the conductive layer reduces the resistance of the entire structure. Separate measurements carried out by Morikawa et al on the inductive and resistive components (shown in Fig. 6.25c,d) of the impedance have shown that very large resistance ratios ( $\Delta R/R$ ) exist for these structures at very low frequencies (1MHz), where there is no significant skin effect. These large resistance changes dominate the impedance changes, and have been shown to be a result of the difference between the resistivity of the conductive layer and the magnetic layer. The electrical resistivity of the CoSiB film is 30 times larger than that of the copper or silver and therefore most of the current flows through the inner conductive layer. Whereas the resistivity of the CoSiB compared to the titanium layer is only 2.5 times as large. Here the current is no longer confined to the titanium layer, and the whole structure is equivalent to the single layer film. It was therefore concluded by Morikawa that the difference between the resistivity of the inner and outer layers is the cause of these large resistance changes, which therefore appear in the impedance measurement.

To increase the MI response of the FeSiBC single layer films investigated in this thesis, a number of multi-layered structures were deposited by magnetron sputtering. The purpose of this was to ascertain if similar results could be obtained to those obtained by Morikawa et al (1997). This would then make the results obtained for the single layer films much more attractive for sensor applications because of the increased sensitivity. Figure 6.26 shows the structure and dimensions of the layered FeSiBC films which were deposited using copper as the conductive layer. The resistivity of the single layered FeSiBC films is equal to that of the CoSiB films, and therefore the difference in resistivity will be similar to the structures used by Morikawa. At the time, there was a problem with the masking procedure, which prevented the masking of layers during the growth deposition of the films; this restricted the structures and dimensions of the samples. Consequently the sputtered magnetic layers sputtered did not form a

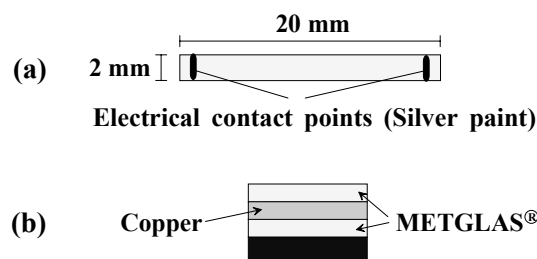


**Figure 6.26:** (a) Plan view of layered films used. (b) Schematic cross-sectional view of the layered structure which was fabricated for MI measurements.

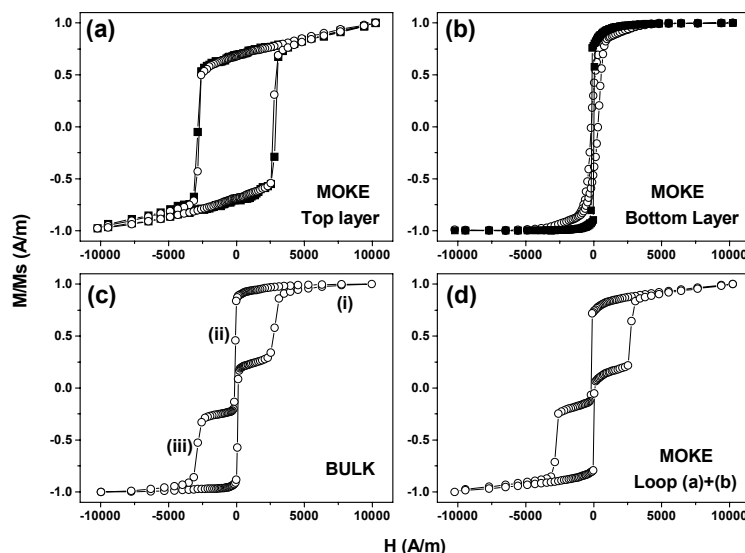
Sample set Ref.	FeSiBC/Cu/FeSiBC
SA1	1.5 $\mu$ m / 2 $\mu$ m / 1.5 $\mu$ m
SA2	400nm / 300nm / 400 nm
SA3	400nm / 150nm / 400 nm

**Table 6.1:** Layer thicknesses of the layered films.

closed magnetic structure as did the samples produced by Morikawa. For this preliminary investigation, the structures were simply layered as a sandwich structure as shown in Figure 6.26 where the magnetic layers were of equal thickness. Three sets of these layered films were deposited and are shown in Table 6.1.

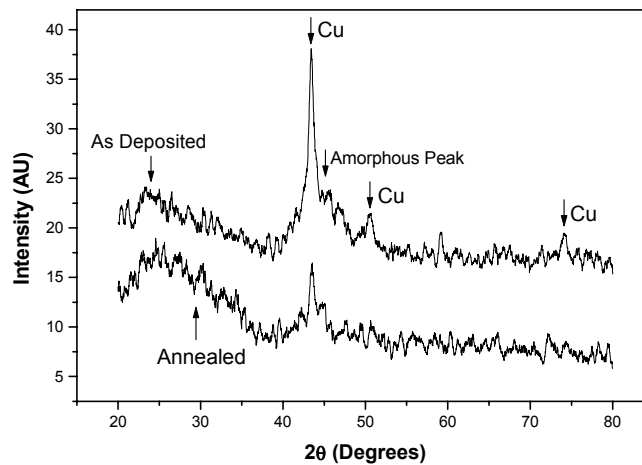
The as-deposited samples for all three sets of samples exhibited a two phase magnetic hysteresis loop, where the two FeSiBC layers were switching independently of each other. Figure 6.27 shows typical loops obtained from these samples. Figures 6.27a and 6.27b represent the MOKE loops obtained from the top and bottom FeSiBC layers. A number of samples were grown on Corning 7059<sup>®</sup> glass which allowed the characterisation of the bottom layer (see MOKE chapter). The MH curves clearly indicate that the two layers are magnetically different. The top layers were found to have coercive fields of approximately 2.5 kA/m, whereas for the bottom FeSiBC layers, the coercive fields were approximately 150 A/m. The high coercive field of the top layer is mainly attributed to the copper layer inducing stress into the FeSiBC film because of the different thermal expansion coefficients of the FeSiBC (5.9 ppm/<sup>0</sup>C) and the copper (1.8 ppm/<sup>0</sup>C). The effects of the copper surface itself should not be neglected since the top layer is no longer being deposited onto an amorphous substrate, and may introduce stress into the film. Annealing the sample relieves the stress since the coercive field of the top layer is dramatically reduced. (Fig. 6.29).

Figure 6.27c is the bulk hysteresis loop, which is sensitive to the average magnetisation of the layered structure. Here the MH loop switches at two distinct points which coincide with the coercive fields of the MOKE loops obtained from the top and bottom layer respectively. Figure 6.27d is the resultant MOKE loop obtained after combining the two respective MOKE loops of the top and bottom layer. The loop obtained is very similar to that of the bulk hysteresis loop, which indicates that the MOKE



**Figure 6.27:** Hysteresis loops from layered FeSiBC film as-deposited. (a) Orthogonal MOKE loops obtained from the top magnetic layer. (b) Orthogonal MOKE loops of the bottom magnetic layer obtained through the glass substrate. (c) Bulk hysteresis loop which is sensitive to both layers simultaneously. (d) Combination of MOKE loops (a)+(b).

loops are representative of each layer and the magnetisation processes in the two layers seem to occur independently. At saturation (i) the magnetisations in both layers are parallel to each other, while at some intermediate level (ii), the magnetisations of the lower layer switches and the magnetisation in the two layers are now anti-parallel. As the field is increased further (iii), the top layer switches and the magnetisations are now parallel in both layers. As mentioned earlier, equal thicknesses of the magnetic layers were deposited. This means therefore that the magnetisations in the two magnetic layers are different, since the magnetisations in each layer switches by different amounts ((ii),(iii)). It appears that the top layer, which is magnetically harder, has a lower magnetic moment than the lower layer. This is assumed to be due to the incorporation of more copper into the second layer. As discussed in Chapter 3, the sputtering process will remove material from all surfaces of the system which are in contact with the plasma, and such material will therefore be incorporated into the film which is being



**Figure 6.28:** X-ray diffraction  $\theta$ - $2\theta$  scans using  $\text{CuK}\alpha$  radiation before and after thermal stress relief treatment of FeSiBC layered films.

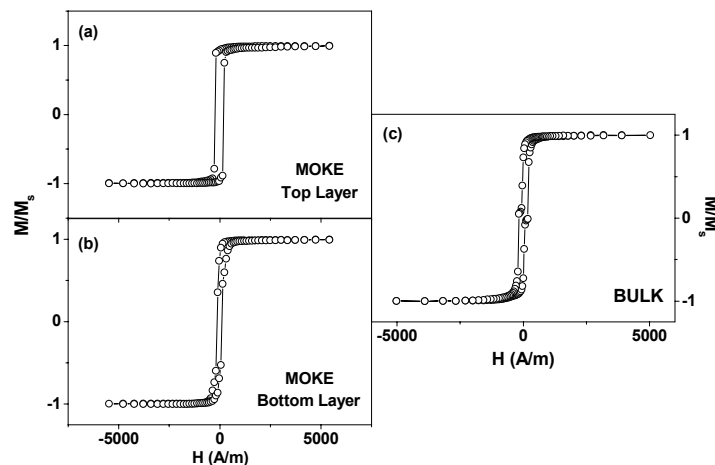


**Figure 6.29:** Hysteresis loops from a layered FeSiBC film after undergoing stress relief. (a) MOKE loop obtained from the top magnetic layer. (b) MOKE loop of the bottom magnetic layer obtained through the glass substrate. (c) Bulk hysteresis loop which is sensitive to both layers simultaneously. The two layers are now magnetically similar.

deposited. Since the structures were fabricated by depositing alternative layers of FeSiBC/copper/FeSiBC, this meant that copper was introduced into the FeSiBC. However this was unavoidable. X-ray analysis of these samples implied that the as-deposited FeSiBC layers were amorphous, and sharp copper peaks existed because of the copper layer. This is shown in Figure 6.28 where the peaks have been labelled. Upon annealing the samples, X-ray diffraction revealed that the copper peaks were now less intense; this seems to imply that the copper had diffused into the magnetic layers. The X-ray analyses were carried out in Madrid where  $\text{CuK}_\alpha$  radiation was used. This, unfortunately, gave a copper peak on top of the amorphous peak which masked the amorphous peak. However there appeared to be no real change after the annealing process, which seems to suggest that there has been no substantial change in the amorphous phase (FWHM). The annealing process relieved the stress, primarily in the top magnetic layer, which made the two layers magnetically similar after the treatment. This is shown in Figure 6.29, where MOKE and bulk hysteresis loops are shown. The MOKE loops show that the two magnetic layers are now similar and have coercive fields of 120 and 200 A/m. The bulk hysteresis loop is still sensitive to the small difference in the two layers, but they now both switch similarly. This is assumed to be due to the equal quantities of copper which has diffused into the two layers.

The samples were annealed and field annealed to ensure that the two magnetic layers were magnetically similar so that the magnetic properties were as favourable as possible for the MI measurements. The coercive fields were approximately three times larger for these layered structures than for the single layered films. Both MOKE and domain imaging indicated that field annealing did not produce a transverse uniaxial anisotropy. The domain studies on these particular samples for the as-deposited and annealed films did not reveal any domain structure. It was expected that the lower magnetic layer would display the radial anisotropy for the as-deposited structures, but no domains were visible. It is assumed

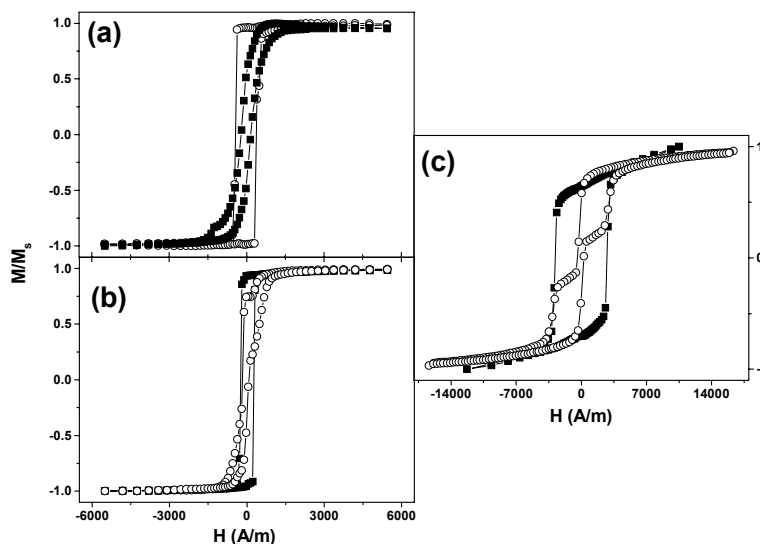


**Figure 6.30:** Typical hysteresis loops from layered FeSiBC films. (a) Transverse (open circles) and longitudinal (solid squares) MOKE loops for field annealed film. (b) Transverse (open circles) and longitudinal (solid squares) MOKE loops for an annealed film. (MOKE). (c) Transverse loops obtained by VSM (open circles), and MOKE (solid squares) from an as-deposited film.

that either the copper has diffused into the layers during the growth because of the substrate temperatures of around 100°C, or the differing thermal expansion coefficients of the two films and substrate, have induced residual stresses. Typical loops for the annealed, field annealed and as-deposited samples used for the MI measurements are shown in Figure 6.30.

The MI measurements carried out on these layered films did not display any MI response over a range of frequencies and current amplitudes. It is not clear why not even a small response was seen for the samples SA1, which were equivalent to a single layered 3µm thick film where changes of 1% were seen. A plausible argument is that this is due the copper which has diffused into the magnetic layers. The hysteresis loops show that the copper has the effect of increasing the coercive fields of the magnetic layers. The higher coercive fields will therefore reduce the effective transverse susceptibility of the material.

It seems likely that these preliminary investigations of layered structures for MI measurements have been impaired by the diffusion of the copper into the magnetic layers. This has two effects; one is that it degrades the magnetic properties, and secondly, it does not produce a distinct layered structure. The diffusion of the copper is also expected to decrease the difference in the resistivity of the two materials, on which the MI in the layered structures is shown to be dependent. Even though the magnetic layers used here do not form a closed magnetic loop for the flux as used by Morikawa et al, it was still anticipated that responses larger than one percent would be obtained. The problem of the copper diffusing into the magnetic layers needs to be addressed before one can conclude that the FeSiBC layered films are not viable for the MI effect as seen by Morikawa et al. It should be noted that Cu is insoluble in Co. An alternative conductive layer would be silver, which is known to have a very low solubility in most materials. Silver also has a lower resistivity than Cu, and from the results shown in Figure 6.22 it displays the largest MI changes for the layered structures.

## 6.6 Domain rotational model for the effective transverse susceptibility

From the results and discussions of the MI effect for the thin films, it appears that the MI behaviour is controlled by contributions to the susceptibility from the process of domain rotation. The higher coercive fields for the films has effectively suppressed the contribution from domain wall movement. At frequencies below 1 MHz there was found to be no substantial effect. On increasing the frequency, the MI effect rises from increases in the susceptibility due to increases in the process of magnetisation rotational effects. The increased frequency also has the effect of virtually damping [Panina et al (1995)] the domain wall movement due to eddy currents and therefore domain rotation becomes dominant.

A phenomenological model for the MI effect in soft ferromagnets, has been recently presented by Atkinson & Squire et al (1998,1997). The transverse susceptibility and MI response depends upon the domain structure and the magnetisation process. The model is an extension of a previous model of Squire (1995) for the magnetisation and magnetoelastic effects in amorphous ribbons. It was concluded the shape of the MI curve is dependent upon both the domain structure and magnetisation process which is contributing to the transverse susceptibility.

Here a special geometry is chosen consisting of a single domain to illustrate that the transverse susceptibility and therefore the MI response is due to domain rotation. Figure 6.31 shows schematically a simplified domain structure, where an ideal, uniaxial magnetic anisotropy exists, consisting only of anti-parallel domains with  $180^\circ$  domain walls. There are two components of magnetic field involved: the external dc field  $H_0$ , which is applied along the length of the film, and the high frequency transverse field  $H_{ac}$  which acts perpendicular to the field  $H_0$ . It is assumed here that there is no domain wall bowing, or domain wall movement on application of the field  $H_0$ . For simplicity it is assumed that

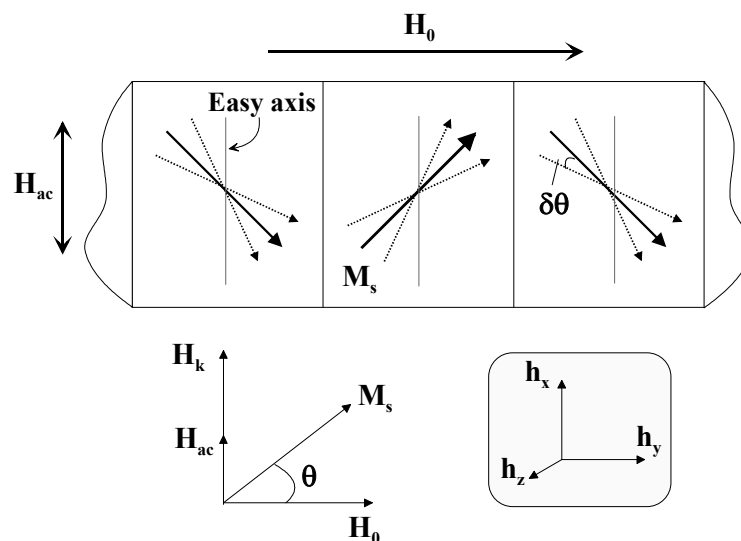


**Figure 6.31:** Simplified domain model used to illustrate the effective susceptibility for the magneto impedance effect in amorphous thin films. The solid arrows represents the domain magnetisation at equilibrium, and the dotted arrows represent the magnetisation rotated (oscillated) from its equilibrium position due to the field  $H_{ac}$ , from its equilibrium position.

the magnetisation process occurs purely by moment rotation. The longitudinal hysteresis loops (Fig. 6.19) for the samples which possess a uniaxial anisotropy indicate moment rotation, since the MI peaks coincide with the anisotropy field. The MI response is regulated by the transverse susceptibility which can be written as

$$\chi_t = \frac{\partial M_x}{\partial H_{ac}} \quad (6.5)$$

where the ac transverse magnetisation  $M_x$  is simply the oscillation of the component of the magnetisation vector  $M_s$ , in the transverse direction (x-axis), due to the field  $H_{ac}$ . The average angle  $\theta$  of the magnetisation vector  $M_s$  is determined by the balance between the field  $H_0$ , which tries to align  $M_s$  along the z-axis, and the magnetic anisotropy  $H_A$ , which tries to align  $M_s$  along the easy axis. The field  $H_{ac}$  causes  $M_s$  to oscillate with an amplitude  $\delta\theta$  about its equilibrium position  $\theta$ , as shown in Figure 6.31. The equilibrium angle  $\theta$ , can be determined by the standard method of minimising the free energy density of the system, from which the transverse susceptibility can be determined. The method used to determine the value of  $\theta$ , is to minimise the total energy for a given field  $H_0$  with the field  $H_{ac}$  equal to zero, and then to find changes in  $\theta$  for when a small applied field  $H_{ac}$  is applied. The energy of this system can be represented by the following free energy density expression

$$E(\theta) = E_{k_u}^x + E_H^x + E_H^z \quad (6.6)$$

where  $E_{k_u}^x$  is the uniaxial anisotropy density,  $E_H^x$  is the Zeeman energy due to the field  $H_{ac}$ , and  $E_H^z$  is the Zeeman energy due to the field  $H_0$ . In order to simplify the treatment, for simplification purposes the demagnetising effect has been neglected; this allows an analytical solution to be obtained. From Figure 6.31, and equation (6.6), the magnetic energy per unit volume of the system is

$$E(\theta) = -K_u \sin^2 \theta - \mu_0 M_s H_{ac} \sin \theta - \mu_0 M_s H_0 \cos \theta \quad (6.7)$$

Minimising equation (6.7) with respect to  $\theta$  we obtain the following expressions for (note  $\mu_0 M_s = 1$  here)

$$\frac{\partial E}{\partial \theta} = -2K_u \sin \theta \cos \theta + H_0 \sin \theta - H_{ac} \cos \theta = 0 \quad (6.8)$$

$$2K_u \sin \theta \cos \theta + H_{ac} \cos \theta = H_0 \sin \theta \quad (6.9)$$

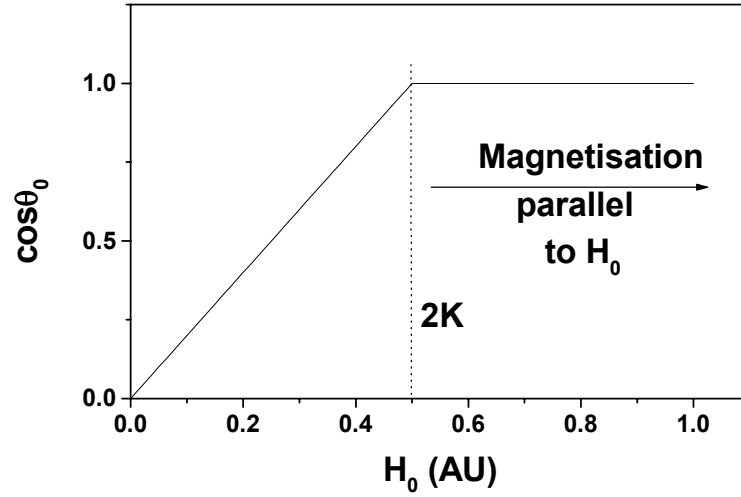


**Figure 6.32:** For the uniaxial domain structure considered, the equilibrium angle  $\theta$ , for the magnetisation depends on the balance between the field and the magnetic anisotropy as described by equation 6.12. When  $H_0=2K_u$ , then  $\theta=90^\circ$ .

When  $H_{ac}=0$ , the magnetisation will lie at some equilibrium angle  $\theta_0$  for a given field  $H_0$

$$\frac{\sin \theta_0}{\cos \theta_0} = \frac{2K_u \sin \theta_0}{H_0} \quad (6.10)$$

This is only satisfied when

$$\cos \theta_0 = \frac{H_0}{2K_u} \quad (6.11)$$

or

$$\sin \theta_0 = 0 \quad (6.12)$$

where equation (6.11) is the correct solution, since when  $H_0=2K_u$ , the magnetisation lies parallel to the field  $H_0$  (Fig. 6.32).

Now including the term  $H_{ac}$

$$\frac{\sin \theta_0}{\cos \theta_0} = \frac{2K_u \sin \theta_0 + H_{ac}}{H_0} \quad (6.13)$$

this will cause the magnetisation to oscillate by an amount  $\delta\theta$ .

$$\frac{\sin(\theta_0 + \delta\theta)}{\cos(\theta_0 + \delta\theta)} = \frac{2K_u \sin(\theta_0 + \delta\theta) + H_{ac}}{H_0} \quad (6.14)$$

Expanding in terms of  $\delta\theta$ , and after some algebraic manipulation (see Appendix 6.8) the following is obtained

$$\delta\theta \left[ 1 + \frac{\sin^2 \theta_0}{\cos^2 \theta_0} - \frac{2K_u \cos \theta_0}{H_0} \right] = \frac{H_{ac}}{H_0} \quad (6.15)$$

substituting  $\sin^2 \theta_0 = 1 - \cos^2 \theta_0$  and equation (6.11) into equation (6.15) gives  $\delta\theta$  to be

$$\delta\theta = \frac{H_{ac} H_0}{(2K_u)^2 - H_0^2} \quad (|H_0| < 2K_u) \quad (6.16)$$

The magnetisation  $M_x$  is given by

$$M_x = M_0 \sin \theta \quad (6.17)$$

and the transverse susceptibility is given by equation (6.5) as

$$\chi_t = \frac{\partial M_x}{\partial H_{ac}} = M_0 \cos \theta \frac{\partial \theta}{\partial H_{ac}} \quad (6.18)$$

Substitution of equation (6.16), leads to the transverse susceptibility due to the ac field  $H_{ac}$  for the condition when  $H_0 < 2K_u$ .

$$\chi_t = \frac{M_0 H_0^2}{2K_u(2K_u - H_0)(2K_u + H_0)} \quad (|H_0| < 2K_u) \quad (6.19)$$

To take account of the condition where  $H_0 > 2K_u$ , i.e. when the moments lie parallel to the field  $H_0$ ,  $\theta_0 = 0$  is substituted into equation (6.15), and the following expression is obtained for the transverse susceptibility.

$$\chi_t = \frac{M_0}{H_0 - 2K_u} \quad (H_0 > 2K_u) \quad (6.20)$$

Figure 6.33 shows typical MI responses, where the transverse susceptibility as calculated from equations (6.19) & (6.20), have also been plotted. Due to the simplicity of the model the susceptibility diverges as  $H_0$  converges on  $H_k$ , but it is clear that the MI response is controlled by the magnetisation process of domain rotation through the susceptibility. The non zero value of the MI at the origin from

the experimental data indicates the misalignment [Atkison & Squire (1997), Gehring (1998)] of the easy axis ( $\theta \approx 90^\circ$ ) or there is some domain wall contribution, giving rise to a finite susceptibility at  $H_0=0$ . The rounding of the peaks is a consequence of a distribution in the anisotropy constants and the easy axis [Atkison & Squire (1997), Gehring (1998)].

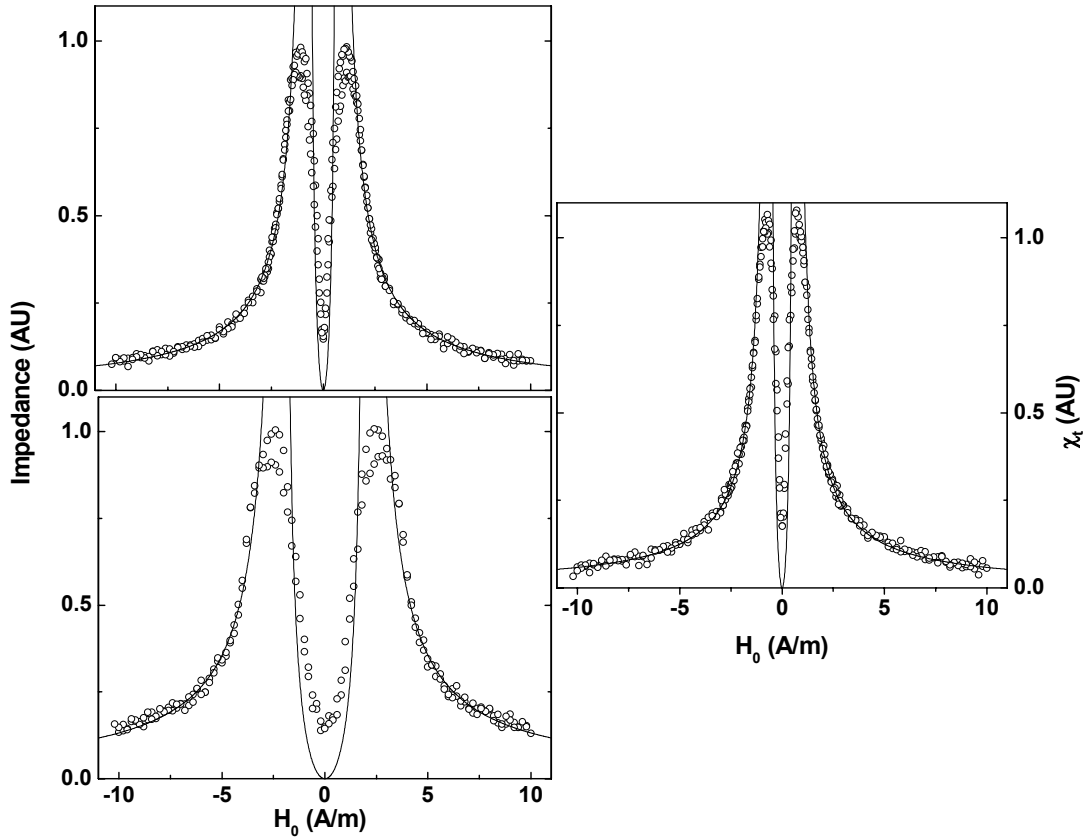


**Figure 6.33:** Comparison of the calculated transverse susceptibility with MI curves obtained by experiment. The initial value for  $2K_u$  was obtained from the experimental data which was adjusted in conjunction with a scaling constant. Both sets of data were normalised to illustrate that the transverse susceptibility has the same form as the MI response.

## 6.7 Conclusions

Preliminary investigations into the MI effect in magnetostrictive (FeSiBC) and non-magnetostrictive (CoFeB) thin films have shown that MI ratios of 1% are attainable at relatively low frequencies (5-7MHz). It has been demonstrated that the MI response is correlated to the domain structure and the magnetisation process.

For the ribbon samples investigated, it appears that the MI response below 1MHz is due to domain wall movement (oscillations), whereas above 1MHz, as with the deposited films, it is due to the oscillation of the domain magnetisation (domain rotation). This is as one would expect, since these commercially available ribbon based materials are used in low frequency (<1MHz) applications. A simplified rotational model was used to illustrate that the MI curves obtained by experiment were due to the process of domain rotation. Unfortunately the MI measurements carried out on the layered FeSiBC thin films were inconclusive. It seems likely that these preliminary investigations have been impaired by the diffusion of the copper into the magnetic layers and further work is necessary.

## 6.8 Appendix

Derivation of the transverse susceptibility due to domain rotation for the MI effect. See Section 6.6 for details.

The energy of the system

$$E(\theta) = E_{k_u}^x + E_H^x + E_H^z \quad (1)$$

$$E(\theta) = -K_u \sin^2 \theta - \mu_0 M_s H_{ac} \sin \theta - \mu_0 M_s H_0 \cos \theta \quad (2)$$

( $\mu_0 M_s = 1$  here)

$$E(\theta) = -K_u \sin^2 \theta - H_o \cos \theta - H_{ac} \sin \theta \quad (3)$$

Minimising equation 3 with respect to  $\theta$

$$\frac{\partial E}{\partial \theta} = -2K_u \sin \theta \cos \theta + H_o \sin \theta - H_{ac} \cos \theta = 0 \quad (4)$$

$$2K_u \sin \theta \cos \theta + H_{ac} \cos \theta = H_o \sin \theta \quad (5)$$

When  $H_{ac}=0$ ,  $M_s$  will lie at some angle  $\theta_0$ , for a given field  $H_o$ .

$$\frac{2K_u \sin \theta_0}{H_o} = \frac{\sin \theta_0}{\cos \theta_0} \quad (6)$$

This is only satisfied when

$$\cos \theta_0 = \frac{H_o}{2K_u} \quad (7)$$

or

$$\sin \theta_0 = 0 \quad (8)$$

Now including the  $H_{ac}$  term in equation (5)

$$\frac{\sin \theta_0}{\cos \theta_0} = \frac{2K_u \sin \theta_0 + H_{ac}}{H_o} \quad (9)$$

The magnetisation will oscillate by an amount  $\delta\theta$ .

$$\frac{\sin(\theta_0 + \delta\theta)}{\cos(\theta_0 + \delta\theta)} = \frac{2K_u \sin(\theta_0 + \delta\theta) + H_{ac}}{H_o} \quad (10)$$

Expanding in terms of  $\delta\theta$ ,

$$\frac{\sin \theta_0 \cos \delta\theta + \sin \delta\theta \cos \theta_0}{\cos \theta_0 \cos \delta\theta - \sin \theta_0 \sin \delta\theta} = \frac{2K_u [\sin \theta_0 \cos \delta\theta + \sin \delta\theta \cos \theta_0] + H_{ac}}{H_o} \quad (11)$$

Note:  $\sin \delta\theta = \delta\theta$ ,  $\cos \delta\theta = 1$

$$\frac{\sin \theta_0 + \delta\theta \cos \theta_0}{\cos \theta_0 - \delta\theta \sin \theta_0} = \frac{2K_u [\sin \theta_0 + \delta\theta \cos \theta_0] + H_{ac}}{H_o} \quad (12)$$

Now

$$\cos \theta_0 - \delta \theta \sin \theta_0 = \cos \theta_0 \left( 1 - \frac{\delta \theta \sin \theta_0}{\cos \theta_0} \right) \quad (13)$$

$$\frac{1}{\cos \theta_0 - \delta \theta \sin \theta} = \frac{1}{\cos \theta_0} \frac{1}{\left( 1 - \frac{\delta \theta \sin \theta_0}{\cos \theta_0} \right)} \quad (14)$$

Multiplying top and bottom by  $\left( 1 + \frac{\delta \theta \sin \theta_0}{\cos \theta_0} \right)$  and neglecting the  $\delta \theta^2$  term in equation (14)

$$\frac{1}{\cos \theta_0 - \delta \theta \sin \theta} = \frac{1}{\cos \theta_0} \left( 1 + \frac{\delta \theta \sin \theta_0}{\cos \theta_0} \right) \quad (15)$$

Now substituting equation (15) into equation (12)

$$\frac{(\sin \theta_0 + \delta \theta \cos \theta_0) \left( 1 + \frac{\delta \theta \sin \theta_0}{\cos \theta_0} \right)}{\cos \theta_0} = \frac{2K_u [\sin \theta_0 + \delta \theta \cos \theta_0] + H_{ac}}{H_0} \quad (16)$$

$$\frac{\sin \theta_0}{\cos \theta_0} + \frac{\delta \theta \sin^2 \theta_0}{\cos^2 \theta_0} + \delta \theta + \frac{\delta \theta^2 \sin \theta}{\cos \theta_0} = \frac{2K_u \sin \theta_0}{H_0} + 2 \frac{K_u \delta \theta \cos \theta_0}{H_0} + \frac{H_{ac}}{H_0} \quad (17)$$

Neglecting the  $\delta \theta^2$  term and substituting equation (6) into equation (17)

$$\frac{\delta \theta \sin^2 \theta_0}{\cos^2 \theta_0} + \delta \theta = \frac{2K_u \delta \theta \cos \theta_0}{H_0} + \frac{H_{ac}}{H_0} \quad (18)$$

$$\delta \theta \left[ 1 + \frac{\sin^2 \theta_0}{\cos^2 \theta_0} - \frac{2K_u \cos \theta_0}{H_0} \right] = \frac{H_{ac}}{H_0} \quad (19)$$

substituting  $\sin^2 \theta_0 = 1 - \cos^2 \theta_0$  into equation (7)

$$\delta \theta \left[ \frac{(2K_u)^2}{H_0^2} - 1 \right] = \frac{H_{ac}}{H_0} \quad (20)$$

$$\delta \theta = \frac{H_{ac} H_0}{(2K_u)^2 - H_0^2} \quad (|H_0| < 2K_u) \quad (21)$$

$$\frac{\partial \theta}{\partial H_{ac}} = \frac{H_0}{(2K_u)^2 - H_0^2} \quad (22)$$

The magnetisation  $M_x$

$$M_x = M_0 \sin \theta \quad (23)$$

$$\chi_t = \frac{\partial M_x}{\partial H_{ac}} = M_0 \cos \theta \frac{\partial \theta}{\partial H_{ac}} \quad (24)$$

Substituting equation (22) and (7), the transverse susceptibility due to the ac field  $H_{ac}$  is

$$\chi_t = \frac{H_0}{(2K_u)^2 - H_0^2} \frac{H_0}{2K_u} M_0 \quad (25)$$

$$\chi_t = \frac{M_0 H_0^2}{2K_u(2K_u - H_0)(2K_u + H_0)} \quad (|H_0| < 2K_u) \quad (26)$$

To take account of the condition when the moments lie parallel ( $H_0 > 2K_u$ ) to the field direction  $H_0$ , the following conditions ( $\theta_0 = 0$ ,  $\sin \theta_0 = 0$ ,  $\cos \theta_0 = 1$ ) are substituted into equation (19).

$$\delta\theta \left[ 1 - \frac{2K_u}{H_0} \right] = \frac{H_{ac}}{H_0} \quad (27)$$

$$\delta\theta = \frac{H_{ac}}{H_0 - 2K_u} \quad (28)$$

$$\frac{\partial\theta}{\partial H_{ac}} = \frac{1}{H_0 - 2K_u} \quad (29)$$

Now

$$M_x = M_0 \sin \theta \quad (30)$$

$$\chi_t = \frac{\partial M_x}{\partial H_{ac}} = M_0 \cos \theta \frac{\partial \theta}{\partial H_{ac}} \quad (31)$$

Substituting equation (29) and  $\cos \theta = 1$ , into equation (31), gives the transverse susceptibility when  $H_0 > 2K_u$  to be

$$\chi_t = \frac{M_0}{H_0 - 2K_u} \quad (|H_0| > 2K_u) \quad (32)$$

## 6.9 References

- Ali et al (1999) “Magneto impedance measurements in magnetostrictive FeSiBC thin films”, **M. Ali**, M.R.J. Gibbs, D. Garcia, M. Vazquez, In preparation for JMMM (1999).
- Ali et al (1998) “The use of stress for the control of magnetic anisotropy in amorphous FeSiBC thin films: a magneto-optic study”, **M. Ali**, R. Watts, W.J. Karl, M.R.J. Gibbs, J. Magn. Magn. Mater. 190(3) 199 (1998).
- Atkinson & Squire (1998) “Phenomenological model for magneto impedance in soft ferromagnets”, D. Atkinson, P.T. Squire, J. Appl. Phys. 83 (11) 6569 (1998).
- Atkinson & Squire(1997) “Experimental and Phenomenological investigation of the effect of stress on magneto impedance in amorphous alloys”, D. Atkinson, P.T. Squire, IEEE Trans. Mag-33 (5) 3364 (1997).
- Atkinson et al (1995) “Magneto-Impedance and  $\Delta E$  Measurements of iron- and Cobalt-Based Amorphous Wires”, D Atkinson, R.S Beach, P T Squire, C.L. Platt, S.N. Hogsdon, IEEE Trans. Mag-31(6) 3892 (1995).
- Beach et al (1994) “Giant magnetic-field dependent impedance of amorphous FeCoSiB wire”, R.S. Beach, A.E. Berkowitz, Appl. Phys. Lett. 64(26) 3652 (1994).
- Costa-Kramer et al(1995) “Influence of magnetostriction on magneto-impedance in amorphous soft ferromagnetic wires”, J.L. Costa-Kramer, K.V. Rao, IEEE Trans. Magn. MAG-31(2) 1153 (1995).
- Gehring (1998) Discussions with Prof. G.A. Gehring, Sheffield University (1998).
- Garcia et al (1998) “Magnetic domains and transverse induced anisotropy in magnetically soft CoFeB amorphous thin films.”, D. Garcia, J.L. Munoz, G. Kurlyandskaya, M. Vazquez, **M. Ali**, M.R.J. Gibbs, IEEE Trans. Magn. MAG-34(4) 1153 (1998).
- Garcia et al (1999) “Induced anisotropy, magnetic domain structure and magnetoimpedance effect in CoFeB amorphous thin films”, D.Garcia, J.L. Munoz, G. Kurlyandskaya, M. Vazquez, **M. Ali**, M.R.J. Gibbs, J. Magn. Magn. Mater. (191) 339 (1999).
- Mohri et al (1992) “Magneto-inductive effect (MI effect) in amorphous wires”, K. Mohri, T. Kohzawa, K. Kawashima, H. Yoshida, L.V. Panina, IEEE Trans. Magn. MAG-28(5) 3150 (1992).
- Mohri et al (1995) “Sensitive and quick response micro magnetic sensor utilizing magneto impedance in Co-rich amorphous wires”, K. Mohri, L.V. Panina, T. Uchiyama, K. Bushida, M. Noda, IEEE Trans. Magn. MAG-31(2) 1266 (1995).
- Morikawa et al (1995) “Thin film magnetic sensor with high sensitivity utilising magneto-impedance effect”, T Morikawa, Y Nishibe, H Yamadera, Y Nonomura, M Takeuhci, Y Taga, Tech. Digest of the 13<sup>th</sup> Sensor Symposium p93 (1995).

- Morikawa et al (1997) “Giant magneto-impedance effect in layered thin films”, T. Morikawa, Y. Nishibe, H. Yamadera, Y. Nonomura, M. Takeuchi, Y. Taga, IEEE Trans. Magn. MAG-33(5) 4367 (1997).
- Panina et al (1994) “Giant magneto-impedance and magneto-inductive effects in amorphous alloys”, L.V. Panina, K. Mohri, K. Bushida, M. Noda, J. Appl. Phys. 76(10) 6198 (1994).
- Panina et al (1995) “Giant magneto-impedance in Co-rich amorphous wires and films”, L.V. Panina, K. Mohri, T. Uchiyama, IEEE Trans. Magn. MAG-31(2) 1249 (1995).
- Panina et al (1996) “Effect on magnetic structure on giant magneto-impedance in Co-rich amorphous alloys”, L.V. Panina, K. Mohri, J. Magn. Magn. Mater. (157/158) 137 (1996).
- Rao et al (1994) “Very large magneto-impedance in amorphous soft ferromagnetic wires”, K.V. Rao, F.B. Humphrey, J.L. Costa-Kramer, J. Appl. Phys. 76 (10) 6204 (1994).
- Sinnecker et al (1998) “Hysteretic giant magneto impedance”, J.P. Sinnecker, P. Tiberto, G.V. Kurlyandskaia, E.H.C.P. Sinnecker, M. Vazquez, A. Hernando, J. Appl. Phys. 76 (10) 6204 (1994).
- Squire et al (1994) “Amorphous wires and their applications”, P.T. Squire, D. Atkinson, M.R.J. Gibbs, S. Atalay, J. Magn. Magn. Mater. (173) 10 (1994).
- Squire (1995) “Domain model for the magnetoelastic behaviour of uniaxial ferromagnets”, P.T. Squire, J. Magn. Magn. Mater. (140-144) 1829 (1995).
- Takemura et al (1996) “Dependence of magnetisation dynamics and magneto-impedance effect in FeSiB amorphous wire on annealing conditions”, T. Takemura, H. Tokuda, K. Komatsu, S. Masuda, T. Yamada, K. Kakuno, K. Saito, IEEE Trans. Mag-32 (5) 4947 (1996).
- Thomas (1991) “Magnetostriction in transition metal-metalloid metallic glasses A.P. Thomas, Ph.D Thesis, University of Bath, (1991).
- Tejedor et al (1996) “Influence of induced anisotropy on magneto-impedance in Co-rich metallic glasses ”, M. Tejedor, B. Hernando, M.L. Sanchez, A. Garcia-Arribas, J. Magn. Magn. Mater. (157/158) 141 (1996).
- Vazquez et al (1996) “A soft magnetic wire for sensor applications”, M. Vazquez, A. Hernando, J. Phys. D. Appl. Phys. (19) 939 (1996).
- Velazquez et al (1994) “Giant magnetoimpedance in nonmagnetostrictive amorphous wires”, J. Velazquez, M. Vazquez, D.X. Chen, A. Hernando, Phys. Rev.50 (22) 16737 (1994).
- Vac (1993) VAC Vacuumschmelze data sheets (1993).

## 7.0 Conclusions and Future work

In this thesis it has been demonstrated by the experimental results and discussions that FeSiBC films, deposited by RF magnetron sputtering can be produced with excellent soft magnetic properties; which are comparable with those exhibited by the METGLAS<sup>®</sup> 2605SC ribbon material from which the films were sputtered. The three main requirements for device quality films were satisfied: the correct composition was attained by sputtering from the correct compositional target, the microstructure was amorphous, and it has been shown that the magnetic anisotropy of the films is controllable. A summary of the main conclusions from the respective chapters is given below.

A MOKE magnetometer and a domain imaging system were constructed by the author in order to characterise the magnetic thin films utilising the Magneto Optical Kerr effect. The general principles of the Kerr effect have been discussed with a view to providing an insight into the implementation of the Kerr effect, and the interpretation of the domain images which are obtained using this effect. The two systems were used to investigate the in-plane anisotropy in the deposited amorphous FeSiBC films. The magnetometer was also used to interrogate the changes in the magnetic properties of a micro-machined membrane-type pressure sensor; this had been designed by Karl et al (1999 [2.8]).

Comparisons of hysteresis loops with measurements made at York University and with bulk hysteresis loops have shown that the results can be taken to be reliable.

MOKE was also utilised in a novel simple method of measuring the saturation magnetostriction of the FeSiBC films.

It has been shown that the deposition of films by sputtering is a complex process which is strongly dependent on many parameters. In this investigation, the sputtering process was mainly optimised by careful control of the sputtering pressure, since the sputtering power was chosen to give a reasonable deposition rate of approximately 5.5nm/min, and also to ensure that the temperature of the substrate was below 60°C. This avoided stresses being induced due to the different thermal expansion coefficients of the film and substrate. It was found that the use of a low sputtering power ensured that the sputtering kinetics could be moderated at low argon pressures. Higher sputtering powers would have increased the deposition rates, but this would have meant that higher pressures would have been required to moderate the sputtering process, and this would have increased any possible argon incorporation into the films. It has been demonstrated that, once the sputtering conditions have been carefully optimised (75W, 4mTorr), it is possible to deposit amorphous FeSiBC films by RF magnetron sputtering, which have excellent soft magnetic properties in the as-deposited state. Films have been deposited onto commercially important substrates such as GaAs, Si and Si<sub>3</sub>N<sub>4</sub>, which are compatible with the microelectronic fabrication technologies. This allows the fabrication of both the magnetic sensor and the electronic detection system on a single substrate, making it commercially more attractive. It also eliminates the problem of physically bonding the magnetostrictive material to the device.

Stress due to the sputtering process has been identified as the major factor in controlling the magnetic softness of the deposited films. Any factors which influence the sputtering dynamics will therefore have a direct effect on the stress induced in the films. At the sputtering conditions investigated (75W, 4mTorr) it appeared that the films were insensitive to oxygen contamination, but very sensitive to oil-based contaminants from the cleaning procedure and the diffusion pump. This contamination induced a state of compressive stress in the films, and it was also inferred that it altered the magnetic properties, since it was found that annealing did not produce the soft magnetic properties which were expected.

At the optimised sputtering parameters of 75W and 4mTorr, the as-deposited films had typical coercivities of 20-30 A/m; this was further reduced to ~10 A/m on annealing, which compares well with the values of 10 A/m for the annealed ribbons. The size of the anisotropy field of the as-deposited films at these parameters is highly dependent on the substrate position because of the radially induced anisotropy which is produced by the residual field from the magnetron source.

It has been shown that the as-deposited films display a significant, reproducible in-plane anisotropy, which is radial about a central point which corresponds to the centre of the magnetron sputtering source. This radial anisotropy has been shown to be a consequence of the small in-plane residual field present at the substrate platter. Its linear and symmetrical form could be utilised in the production of samples where a range of anisotropy fields and directions are needed.

The control of magnetic anisotropy in FeSiBC films by various treatments has been described. Field annealing is shown to be capable of producing a small transverse anisotropy. The use of stress induced anisotropy, either during the growth or subsequent annealing, has been shown to give rise to a well defined, strong anisotropy whose magnitude can be easily controlled by varying the applied stress.

A new, simple technique for the measurement of magnetostriction in thin films deposited onto fairly rigid thick substrates has been described. It has been applied to amorphous FeSiBC films sputter deposited onto microscope slides, Corning<sup>®</sup> glass and silicon substrates. For these systems, the error in the measurement of magnetostriction is determined almost entirely by the uncertainty in the Young's modulus. The technique has also been applied to an FeCo film deposited by sputtering onto a microscope slide. For both FeSiBC and FeCo, the values obtained are in good agreement with expected values.

The technique can be applied to a wide variety of different film/substrate combinations. If the Young's modulus of the film is known to a high accuracy, then the error in the value of  $\lambda_s$  obtained can be less than 5%, which compares well with other techniques. Such precise, quantitative values could be used to provide sample standards for use with other methods. The technique is not limited by film thickness, since the Magneto-Optical Kerr Effect can comfortably monitor the magnetisation down to a film thickness of 10nm. It overcomes the problem of non-uniform stresses by correlating the local stress with that of the local anisotropy field. No mechanical properties of the substrate are required, simplifying the calculation of  $\lambda_s$ . The equipment needed to implement the technique is inexpensive and commonly available; no special preparation of samples are required. This method gives a useful alternative to the conventional techniques and can be applied to films deposited onto moderately thick

substrates. This magnetostriction measurement may be applicable to films deposited onto a wide variety of commercially important substrates, for which there may be no alternative techniques.

Since magnetostriction is a fundamental physical property of magnetic materials, it is vital for high precision devices (such as magnetic information storage systems) that accurate quantification of its effects can be obtained.

The values of magnetostriction obtained in this study have been very reproducible from the three different methods used to strain the magnetic films. It has been found that the substrates have no significant influence on  $\lambda_s$ , and the magnetic softness (coercive fields), which is presumed to be caused by residual strains, also has little influence. These experiments also show that, in these strongly magnetostrictive materials,  $\lambda_s$  is independent of strain for the applied strains and also the residual strains caused by the substrate.

The technique of stress annealing to tailor the anisotropy field has been demonstrated to a high degree of precision on silicon and Corning<sup>®</sup> glass substrates. It provides an excellent means of inducing a given anisotropy field in thin film sensors. It also provides the means of inducing a well defined uniaxial domain structure, which simplifies the understanding of the magnetisation process for device applications.

Photolithographically patterned films display no adverse effects from the process, and it has been shown that the process of field annealing is still able to induce a weak uniaxial anisotropy in films with reduced lateral dimensions which is important for sensor devices.

Preliminary investigations into the MI effect in magnetostrictive (FeSiBC) and non-magnetostrictive (CoFeB) thin films have shown that MI ratios of 1% are attainable at relatively low frequencies (5-7MHz). It has been demonstrated that the MI response is correlated to the domain structure and the magnetisation process.

For the ribbon samples investigated, it appears that the MI response below 1MHz is due to domain wall movement (oscillations), whereas above 1MHz as with the deposited films, it is due to the oscillation of the domain magnetisation (domain rotation). A simplified rotational model was used to illustrate that the MI curves obtained by experiment, were due to the process of domain rotation.

MI measurements carried out on the layered FeSiBC thin films were inconclusive and it likely that these preliminary investigations were impaired by the diffusion of the copper into the magnetic layers.

It is believed that on further work, the problem of copper diffusion can be eliminated by the use of silver as the conductive core and thus be possible to reproduce similar results to those obtained by Morikawa et al (1997 [6.8]) on layered films. This increase in the MI ratio without an increase in the operating frequency would be more attractive in development of thin film sensors based on the MI effect. It has been discussed in chapter 5, that in the FeSiBC films the stress induced anisotropy scales linearly with stress, as ascertained by MOKE. A similar principle could also be applied using the MI effect to measure the variation of the stress induced anisotropy as function of stress and could therefore form a basis of stress sensor.

It has been demonstrated successfully that soft amorphous FeSiBC films can be attained by very careful optimisation of the sputtering parameters. The basic magnetic properties have been characterised, along with the as-deposited radially induced anisotropy. Typical values for the coercive fields for the as-deposited films were 20-30 A/m. However, at times, the as-deposited films exhibited easy axes coercive fields, as low as 2 A/m as shown in Figure 7.1. These were only obtainable for the first one or two depositions, immediately after the sputtering machine was thoroughly cleaned (external shot blasting). It was assumed that the sputtering environment was being minutely contaminated by oil vapour from the diffusion pump which therefore gave rise to a slight increase in the coercive fields to 20-30 A/m. It is, therefore, likely that improvements in the cleanness of the sputtering environment will allow the deposition of FeSiBC films with coercive fields in as-deposited state which are comparable or better than its ribbon counter part.

An absolute value of the saturation magnetisation was not ascertained during the study, nor was the exact composition of the as-deposited films. It is believed, however, that values are similar to those of the METGLAS<sup>®</sup> 2605SC ribbon, since the composition has an influence on the value of the saturation magnetostriction which was measured to be similar to that of the ribbon material. Further work on the effects of temperature on these FeSiBC films would be the obvious path to follow, especially if these types of highly magnetostrictive materials are intended to be utilised in micro-machined magnetic devices. Increases in temperature will be more significant in systems where the thermal expansion coefficients of the deposited film and substrate are different. This will introduce stress into the magnetic film and will obviously effect the magnetic properties of the film.

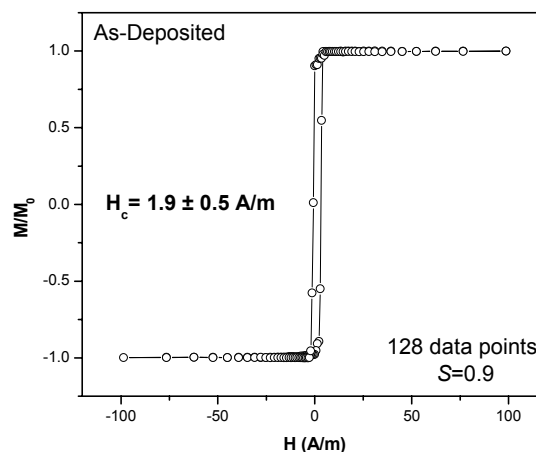


**Figure 7.1:** Easy axis MOKE loop from an as-deposited FeSiBC film obtained in a very clean environment. (75W,4mTorr).

## 8.0 Access To Thesis (Copyright Notice)

I, the author, agree to this thesis being made immediately available through the library for loan or consultation.

NAME: Mannan Ali  
ADDRESS: Department Of Physics & Astronomy  
The University Of Sheffield  
SIGNED: \_\_\_\_\_ DATE: (30/09/1999)

I, the author, give permission to the University of Sheffield and to the British Library to reproduce this thesis in whole or in part in order to supply single copies for the purpose of research or private study.

NAME: Mannan Ali  
ADDRESS: Mannan.ali@physics.org  
\_\_\_\_\_  
SIGNED: \_\_\_\_\_ DATE: (30/09/1999)

This work is subjected to copyright. All rights are reserved with the author, specifically the rights of the reuse of all illustrations, diagrams and figures in any form of publication without prior written permission from the author (Email: Mannan.Ali@physics.org or write to the above address). Violations are liable for prosecution under the UK Copyright Law.

Please note an Online version of this thesis is available (next page).

## 9.0 Online Version

An online version of this thesis can be found at the following Web addresses:

<http://members.xoom.com/MannansZone/thesis.html>

<http://study-on-line.co.uk/thesis.html> (Main Site)

<http://madasafish.com/~mannanali/thesis.html>

or the current Web address can be obtained by emailing the author.

Email: [Mannan.Ali@physics.org](mailto:Mannan.Ali@physics.org)

This work is subjected to copyright. All rights are reserved with the author, specifically the rights of the reuse of all illustrations, diagrams and figures in any form of publication without prior written permission from the author (Email: [Mannan.Ali@physics.org](mailto:Mannan.Ali@physics.org) or write to the above address). Violations are liable for prosecution under the UK Copyright Law.

## 10.0 Glossary

$E_a$	Anisotropy Energy Cubic System
$E_K$	Anisotropy Energy Uniaxial System
$E_{ms}$	Magnetostatic Anisotropy Energy
$E_\sigma$	Magnetoelastic Anisotropy Energy
$\varepsilon$	Strain
<b>H</b>	DC Magnetic Field
$H_{ac}$	AC Magnetic Field
$H_c$	Coercivity/Coercive Field
$H_d$	Demagnetising Field
$H_K$	Anisotropy Field
$K$	Anisotropy Constant Cubic System
$K_u$	Anisotropy Constant Uniaxial System
$K_{1,2,\dots}$	1 <sup>st</sup> , 2 <sup>nd</sup> , ... Anisotropy Constant's Cubic System
$K_{u1,u2,\dots}$	1 <sup>st</sup> , 2 <sup>nd</sup> , ... Anisotropy Constant's Uniaxial System
<b>METGLAS<sup>®</sup></b>	METGLAS <sup>®</sup> 2605SC (Fe <sub>81</sub> Si <sub>13.5</sub> B <sub>13.5</sub> C <sub>2</sub> )
$M$	Magnetisation
$M_s$	Saturation Magnetisation
<b>MI</b>	Magneto Impedance
<b>MO</b>	Magneto optical sensitivity
<b>MOKE</b>	Magneto Optical Kerr Effect
$N_d$	Demagnetising Factor
$\sigma$	Stress
$\lambda$	Magnetostriction
$\lambda_s$	Saturation Magnetostriction
$\chi$	Susceptibility
$\chi_t$	Transverse Susceptibility
<b>VSM</b>	Vibrating Sample Magnetometer
$Z$	Impedance